



DONOSTIA-SAN SEBASTIÁN

APRIL 2020

CLICK CHEMISTRY: AN EFFICIENT TOOLBOX FOR THE DESIGN OF CHITOSAN-BASED HYDROGELS FOR BIOMEDICINE

OLATZ GUARESTI LARREA

eman ta zabal zazu



Universidad
del País Vasco

Euskal Herriko
Unibertsitatea

ENGINEERING SCHOOL OF GIPUZKOA

DEPARTMENT OF CHEMICAL AND ENVIRONMENTAL ENGINEERING

'MATERIALS + TECHNOLOGIES' GROUP



GIPUZKOAKO
INGENIARITZA
ESKOLA
ESCUELA
DE INGENIERÍA
DE GIPUZKOA

CLICK CHEMISTRY: AN EFFICIENT TOOLBOX FOR THE DESIGN OF CHITOSAN–BASED HYDROGELS FOR BIOMEDICINE

PhD Dissertation presented by

OLATZ GUARESTI LARREA

Under the supervision of

Dr. M^a ARANZAZU ECEIZA MENDIGUREN

Dr. NAGORE GABILONDO LÓPEZ

Donostia–San Sebastián, April 2020

'Imagination is more important than knowledge'
Albert Einstein

'To live is to face one problem after another. The way you face them makes
the difference'
Benjamin Franklin

Zuentzat.

Acknowledgements

Después de 4 años, ha llegado el momento de poner el punto final a esta etapa y puedo decir que sí, que ha merecido la pena. Me quedo con el esfuerzo, la constancia, la disciplina y la formación adquirida, pero sobre todo con la experiencia, la satisfacción, la curiosidad y el entusiasmo. Porque no importa lo duro o largo que sea el camino, sino lo que está al final. Sé que no hubiera sido posible sin toda la gente que me ha acompañado durante este tiempo, tanto los que lleváis toda una vida a mi lado, como los que he tenido la suerte de encontrarme.

En primer lugar, dar las gracias a mis directoras Nagore Gabilondo y Arantxa Eceiza, por confiar en mí y darme la oportunidad de iniciarme en el mundo de la investigación. Por haber hecho posible la realización de este trabajo, por vuestro conocimiento, experiencia y apoyo durante estos años.

Me gustaría agradecer a la Universidad del País Vasco tanto por la beca predoctoral concedida dentro del programa de Formación del Personal Investigador (PIF15/092) que ha permitido la realización de este proyecto, así como por la beca de movilidad para la realización de la estancia en el extranjero. Gracias también a los Servicios Generales (SGIker) de la UPV/EHU por su apoyo técnico. En especial a Loli Martín por su ayuda y disponibilidad todo este tiempo.

I would also like to acknowledge Dr. Ljiljana Fruk, head of the Bionano Engineering Group at the Department of Chemical Engineering and Biotechnology of the University of Cambridge, for giving me the opportunity to learn from her cool and amazing chemistry world, and for her advice and support during my stay at CEB, to the point of returning. Thank you to all the people from the group and the department for making me feel part of the team from the first day and for helping me always when needed. Special thanks to Sam and Leander for making my stay in Cambridge one of my best experiences.

Por supuesto, muchas gracias a todos mis compañeros del Grupo 'Materiales + Tecnologías' (GMT) y del Departamento de Ingeniería Química y del Medio

Ambiente. A los que siguen, a los que están o han estado de paso y a los que ya se han ido. A mis vecinos del laboratorio, por las risas y las infinitas e intensas horas de trabajo juntos. Hemos sabido arreglárnoslas para ayudarnos y no acabar desquiciados entre todos, dando color (y tragos) a los días grises. Habéis hecho que acabe cogiendo cariño a Donosti y alrededores, ¡y eso es decir mucho! Y en especial a vosotros, ya sabéis quienes, por vuestro apoyo durante estos años. Por convertirnos en amigos, por haber sido el paréntesis de calma en medio de la locura de cada día.

A Clara, por acogerme desde el primer día, por estar siempre dispuesta a ayudarme y por hacerme sentir que puedo contar contigo para lo que sea, incluso en la distancia. También quiero darle las gracias a Sheila, por tu ayuda en el área de la nanotecnología y esos emails infinitos. A Janire, por tu amistad y por haberte quedado a formar parte de mi vida, por nuestros planes improvisados.

A mi amiga Leire, milesker, por tanto. Porque no hubiese llegado hasta aquí sin tenerte a mi lado. Y a vosotras chicas, porque os quiero infinito, por vuestro apoyo incondicional y vuestra paciencia, por vuestras risas, consejos, planes y poteos, por encontrar juntas el sentido de la vida y seguir yendo a contracorriente.

Y por último quiero agradecer a toda mi familia por su apoyo constante. A mi aita y mi ama, por estar a mi lado durante esta etapa tan importante en mi vida, por creer en mí y siempre desearme lo mejor. Y en especial a mi amama, por estar siempre, aun sin entender nada, pero compartiendo mi ilusión en los buenos momentos y mis miedos en los malos. ¡Casi has sufrido más que yo! A mi prima, porque la distancia se soluciona con infinitos e interminables audios de horas que conectan nuestras vidas. Gracias Ane por escucharme, entenderme y compartir cada momento.

Guztioi, eskerrik asko!

Summary

The present thesis was focused on the development of novel chitosan-based hydrogels chemically cross-linked by applying the bases of click chemistry with enhanced stimuli-response properties.

The use of natural occurring polymers to obtain hydrogels acquires great importance in the field of biomedicine mainly due to its renewable character. At the same time, click chemistry is a formidable candidate for the synthesis of this type of biomaterials, since it includes high efficiency reactions, complete selectivity, orthogonality, mild reaction conditions and absence of secondary reactions. The combination of both concepts leads to the origin of this thesis.

Chitosan is particularly interesting for biological activities and applications due to its adaptable character and excellent properties. Hence, it was endowed with specific functionalities, after the controlled insertion of furan, maleimide, thiol or tetrazole groups in the main chain of the biopolymer, through the formation of amide bonds. Subsequently, hydrogels with different size and molecular structure were developed by means of click type cross-linking reactions (Diels-Alder, thiol-Michael addition and NITEC).

Hydrogels developed from biopolymers offer high hydrophilicity, stiffness and resistance properties close to natural tissues and the ability to accommodate biomolecules, characteristics that are crucial for uses such as drug release or tissue engineering. For that reason and in view of the future applicability of the synthesized biomaterials in the field of biomedicine, relevant properties were studied along with drug release experiments of a model antibiotic drug, mucoadhesive tests and short-term cytotoxicity assays.

INDEX

CHAPTER I

I. INTRODUCTION	3
I.1. MOTIVATION	3
I.2. CHITOSAN	5
I.2.1. Origin and structure	5
I.2.2. General properties	8
I.2.3. Preparation techniques and applications	11
I.3. BIOPOLYMER–BASED HYDROGELS	14
I.3.1. General characteristics	14
I.3.1.1. Cross–linking strategies	17
I.3.2. Chitosan–based hydrogels	18
I.4. CLICK CHEMISTRY FOR HYDROGEL DESIGN	20
I.5. GENERAL OBJECTIVES	25
REFERENCES	29

CHAPTER II

II. MATERIALS AND CHARACTERIZATION	49
TECHNIQUES AND METHODS	
II.1. MATERIALS	49
II.2. CHARACTERIZATION TECHNIQUES AND	52
METHODS	
II.2.1. Characterization of chitosan	52
II.2.2. Physico–chemical characterization	54
II.2.2.1. Fourier transformed infrared spectroscopy	54
II.2.2.2. Nuclear magnetic resonance spectroscopy	55
II.2.2.2.1. Liquid–state ¹ H NMR measurements	55
II.2.2.2.2. Solid–state ¹³ C NMR measurements	56

II.2.2.3. X–ray diffraction	56
II.2.3. Light–based characterization	57
II.2.3.1. Ultraviolet–visible spectroscopy	57
II.2.3.1.1. Monitorization of the click reactions	57
II.2.3.1.2. Ninhydrin assay for thiol–functionalized chitosan	58
II.2.3.1.3. Ellman´s test for thiol–functionalized chitosan	59
II.2.3.2. Fluorescence spectroscopy	59
II.2.3.3. Nanoparticle analyser	60
II.2.3.3.1. Dynamic light scattering	60
II.2.3.3.2. Zeta potential	61
II.2.4. Thermogravimetric analysis	61
II.2.5. Morphological and dimensional characterization	61
II.2.5.1. Scanning electron microscopy	61
II.2.5.2. Transmission electron microscopy	62
II.2.5.3. Atomic force microscopy	62
II.2.5.3.1. Roughness	62
II.2.5.3.2. Morphology of nanogels	63
II.2.6. Swelling capacity	63
II.2.6.1. Swelling parameters	64
II.2.6.2. pH–sensitivity	64
II.2.7. Gel fraction	64
II.2.8. Enzymatic and hydrolytic degradation studies	65
II.2.9. Rheological characterization	66
II.2.9.1. Gelation time	66
II.2.9.2. Frequency sweep test	66
II.2.9.2.1. Network parameters	67
II.2.9.3. Shear thinning	67
II.2.9.4. Yield point	68
II.2.9.5. Self–healing ability	68
II.2.10. Specific characterization	69

II.2.10.1. Drug delivery measurements	69
II.2.10.2. Mucoadhesion capacity	70
II.2.10.3. Antibacterial activity	71
II.2.10.4. <i>In vitro</i> cell response evaluation	72
II.2.10.4.1. Cytotoxicity	72
II.2.10.4.2. Cell adhesion and viability	73
REFERENCES	74

CHAPTER III

III. CHITOSAN DERIVATIVES READY FOR CLICK REACTIONS	81
III.1. INTRODUCTION AND OBJECTIVE	81
III.2. SYNTHESIS OF FURAN-FUNCTIONALIZED CHITOSAN (CsFu)	83
III.2.1. Experimental part	83
III.2.2. Results and discussion	85
III.3. SYNTHESIS OF MALEIMIDE- FUNCTIONALIZED CHITOSAN (CsAMI)	89
III.3.1. Synthesis of 3-(2,5-dioxo-2H-pyrrol-1(5H)-yl) propanoic acid (AMI)	89
III.3.2. Experimental part	90
III.3.3. Results and discussion	91
III.4. SYNTHESIS OF THIOL-FUNCTIONALIZED CHITOSAN (CsSH)	97
III.4.1. Experimental part	97
III.4.2. Results and discussion	99
III.5. SYNTHESIS OF TETRAZOLE- FUNCTIONALIZED CHITOSAN (CsTZ)	107
III.5.1. Synthesis of (4-(2-(4-methoxyphenyl)-2H-tetrazol-5- -yl)benzoic acid (TBA)	107

III.5.2. Experimental part	108
III.5.3. Results and discussion	109
III.6. CONCLUSIONS	113
REFERENCES	116

CHAPTER IV

IV. HYDROGELS FOR DRUG DELIVERY	127
THROUGH THE DIELS–ALDER REACTION	
IV.1. INTRODUCTION AND OBJECTIVE	127
IV.2. FURAN/MALEIMIDE CHITOSAN–BASED	129
HYDROGEL FORMATION (CsFu/CsAMI)	
IV.2.1. Experimental part	129
IV.2.2. Results and discussion	130
IV.2.2.1. Physico–chemical characterization	130
IV.2.2.2. Rheological behaviour	131
IV.2.2.3. Morphological analysis	134
IV.2.2.4. Swelling and degradation studies	135
IV.2.2.5. Drug delivery study	139
IV.2.2.6. Antimicrobial activity	140
IV.2.2.7. Biocompatibility	141
IV.3. FURAN–FUNCTIONALIZED CHITOSAN AND	143
POLYETHERAMINE–BASED BISMALIMIDE	
HYDROGELS FORMATION (CsFu/BMI)	
IV.3.1. Experimental part	143
IV.3.2. Results and discussion	145
IV.3.2.1. Physico–chemical characterization	145
IV.3.2.2. Rheological behaviour	147
IV.3.2.3. Morphological analysis	151
IV.3.2.4. Swelling, pH sensitivity studies	156
IV.3.2.5. Drug delivery study	161

IV.4. CONCLUSIONS	163
REFERENCES	166

CHAPTER V

V. THE THIOL–MICHAEL ADDITION FOR <i>IN SITU</i> FORMING HYDROGELS	177
V.1. INTRODUCTION AND OBJECTIVE	177
V.2. THIOL–FUNCTIONALIZED CHITOSAN AND POLYETHERAMINE–BASED BISMALIMIDE HYDROGELS FORMATION (CsSH/BMI)	179
V.2.1. Experimental part	179
V.2.2. Results and discussion	180
V.2.2.1. Rheological behaviour	181
V.2.2.2. Morphological analysis	184
V.2.2.3. Swelling study	185
V.2.2.4. Biocompatibility	187
V.3. CONCLUSIONS	188
REFERENCES	191

CHAPTER VI

VI. DEVELOPING FLUORESCENT HYDROGELS BY THE NITEC REACTION	199
VI.1. INTRODUCTION AND OBJECTIVE	199
VI.2. TETRAZOLE/MALEIMIDE CHITOSAN–BASED HYDROGELS FORMATION (CsTZ/CsAMI)	201
VI.2.1. Experimental part	201
VI.2.2. Results and discussion	203
VI.2.2.1. Physico–chemical characterization	204
VI.2.2.2. Rheological behaviour	207

VI.2.2.3. Morphological analysis	214
VI.2.2.4. Swelling, pH sensitivity and degradation studies	216
VI.2.2.5. Biocompatibility	220
VI.3. CONCLUSIONS	221
REFERENCES	223

CHAPTER VII

VII. NANOGELS DESIGN FOR TARGETED DELIVERY	229
VII.1. INTRODUCTION AND OBJECTIVE	229
VII.2. THIOLATED CHITOSAN-BASED NANOGELS FORMATION (CS₂SH/PEGBCOOH)	233
VII.2.1. Experimental part	233
VII.2.2. Results and discussion	235
VII.2.2.1. Physico-chemical characterization	236
VII.2.2.2. Thermal behaviour	238
VII.2.2.3. pH-responsive swelling properties	239
VII.2.2.4. Size and morphological analysis	243
VII.2.2.5. Mucoadhesion property	245
VII.2.2.6. Assessment as potential nanocarriers for drug delivery by click chemistry	250
VII.2.2.6.1. Experimental part	251
VII.2.2.6.2. Results and discussion	251
VII.3. CONCLUSIONS	254
REFERENCES	257

CHAPTER VIII

VIII. GENERAL CONCLUSIONS, FUTURE WORK AND PUBLICATIONS	265
VIII.1. GENERAL CONCLUSIONS	265
VIII.2. FUTURE WORK	271
VIII.3. LIST OF PUBLICATIONS AND COMMUNICATIONS	273
VIII.3.1. List of publications	274
VIII.3.2. List of communications	278
REFERENCES	287

ANNEXES

LIST OF FIGURES	293
LIST OF SCHEMES	302
LIST OF TABLES	304
LIST OF ABBREVIATIONS	308
LIST OF SYMBOLS	311

CHAPTER I

INTRODUCTION

I.1. MOTIVATION	3
I.2. CHITOSAN	5
I.2.1. ORIGIN AND STRUCTURE	5
I.2.2. GENERAL PROPERTIES	8
I.2.3. PREPARATION TECHNIQUES AND APPLICATIONS	11
I.3. BIOPOLYMER-BASED HYDROGELS	14
I.3.1. GENERAL CHARACTERISTICS	14
I.3.1.1. Cross-linking strategies	17
I.3.2. CHITOSAN-BASED HYDROGELS	18
I.4. CLICK CHEMISTRY FOR HYDROGEL DESIGN	20
I.5. GENERAL OBJECTIVES	25
REFERENCES	29

I. INTRODUCTION

I.1. MOTIVATION

The research works for developing new biomaterials continue being a very important issue in both academic and industrial fields due to their application in several technologies. This is proved by the impressive number of investigations and international scientific publications focused on this scope in the past decades. Specifically, the interest in the development of hydrogels, microgels or nanogels for biomedicine is greatly high nowadays, since the newest manufacture technologies offer magnificent possibilities in disciplines such as controlled release of drugs or biomolecules and tissue engineering, among others. Traditionally, materials for biomedical purposes have been developed using synthetic polymers, which are generally synthesized by traditional radical polymerization reactions. Nevertheless, nowadays biopolymers and their derivatives are the ones that attract the attention among the research community.

The use of polymers of natural origin, especially polysaccharides, is interesting in any field of research, mainly due to their renewable character but it is in the field of biomedicine where it acquires, if possible, greater relevance. This interest is driven not only by the outstanding properties of the natural polymers in terms of biocompatibility and tissue similarity but also by the growing interest in replacing synthetic petrochemicals by renewable raw materials. Indeed, hydrogels developed from biopolymers offer high hydrophilicity, stiffness and resistance properties close to those of natural tissues, as well as the ability to accommodate biomolecules, characteristics that are crucial for uses such as carriers in sustained drug release systems or scaffolds in tissue engineering¹. Within the last years, extensive research focused on gelatin²⁻⁶, cellulose⁷⁻⁹, alginate¹⁰⁻¹³, starch¹⁴⁻¹⁷, collagen¹⁸⁻²⁰, hyaluronic acid²¹⁻²³ or chitosan²⁴⁻²⁷-based hydrogels have been reported. Among them, chitosan is gaining increasing interest due to its unique

properties and its suitability in multiple biomedical applications, therefore, it has been chosen as the starting point of this thesis.

On the other hand, hydrogels can be classified into three main categories based on their major size: macroscopic hydrogels, microgels and nanogels²⁸. Microgels and nanogels are particular hydrogels with dimensions on the order of micrometres and nanometres, respectively, while the size of macroscopic hydrogels is typically on the order of millimetres to centimetres. New technologies of fabrication are being applied in numerous fields of study, in which the most satisfactory way to create novel devices is investigated by means of very diverse methods, usually with associated activity, to develop materials with certain stimulus–response behaviour²⁹. The fusion of both concepts leads to design hydrogels of any shape and size from biopolymers that, without dissolving or losing their structure, are capable of absorbing large amounts of water or biological fluids due to physical entanglement and/or chemical cross–linking³⁰. Chemical cross–linking between the hydrogel forming macromolecules, even if not essential, is desirable since physical hydrogels tend to show poorer stability in service. However, it could be a particularly delicate task in the biomedical field, since undesired contaminating substances must be avoided or minimized.

In this regards, the click chemistry is an excellent tool for the synthesis of hydrogels, since it includes high–efficiency reactions, complete selectivity, orthogonality, mild reaction conditions, no potentially toxic catalysts and absence of secondary reactions³¹. Strain–promoted azide–alkyne cycloaddition (SPAAC), radical mediated thiol–ene chemistry, Diels–Alder cycloaddition, Michael addition or tetrazole–alkene chemistry, among others, are currently under study for the development of biomaterials³¹, such as intelligent devices for transporting biomolecules, cells or drugs^{32,33}, patterned surfaces with precise control over the number and nature of functional groups³⁴ or interpenetrated networks³⁵.

Therefore, in this thesis, the development of new gel-type biomaterials from chitosan with excellent stimuli-responsive properties using different click chemistry reactions was proposed. To this end, in the first place, chitosan was endowed with specific functionalities, after the controlled insertion of furan, maleimide, thiol or tetrazole groups in the main chain of the biopolymer, maintaining its original biocompatible character. Hereafter, hydrogels with different size and molecular structures were synthesized by means of click type cross-linking reactions (Diels–Alder, thiol–Michael addition or nitrile imine-mediated tetrazole–ene cycloaddition). The final physico-chemical, swelling, viscoelastic and morphological properties of the different hydrogel systems were studied. So that the new developed biomaterials would be competent in the biomedical field biodegradability studies under specific enzymes, controlled drug release assays, mucoadhesion experiments with mucin, antibacterial studies against *Escherichia coli* and *Staphylococcus aureus* and short-term cytotoxicity assays were conducted, depending on the intended final application.

I.2. CHITOSAN

I.2.1. Origin and structure

Chitin is the most abundant organic substance in nature after cellulose³⁶. It is usually a white and nitrogenous polysaccharide, part of the structural components of numerous living organisms, such as arthropods (crustaceans and insects), molluscs, yeast and fungi, and, thus, it has become the object of study of a large number of investigations worldwide. It is a linear biopolymer, highly insoluble in water given its crystallinity as a result of the formation of intra/intermolecular hydrogen bonds³⁷. This features of chitin makes any chemical modification and application of the polymer difficult, being also insoluble in acids and organic media and, hence, causing a low chemical reactivity^{38,39}.

Although chitin is biosynthesized by more than 10^6 species in three polymorphic configurations (α , β and γ), at present, it is mainly obtained from the exoskeleton of industrially processed crustaceans, particularly lobsters, crabs and shrimps⁴⁰. Therefore, it can be presented in different crystal structures, according to its biological function and its natural source; these polymorphic forms are differentiated depending on the arrangement of the carbohydrate chains⁴¹. The α form has chains arranged alternately antiparallel, the β form has all chains in parallel and the γ -chitin has two chains in one direction with an additional inverted chain^{42–45}, being a variant of the α family and rarely studied^{42,46}. Figure I.1 shows the polymorphic configuration of the three different crystal allomorphs designated as α , β and γ -chitin. The α -chitin is the most common and abundant form and has higher thermodynamic stability, probably due to the hydrogen interactions between chains, whereas the β -chitin has weaker intermolecular interactions between the strands (lower density) while is more reactive and shows higher affinity for solvents³⁹. Chitin found in crab and shrimp shell wastes is in α form⁴⁷.

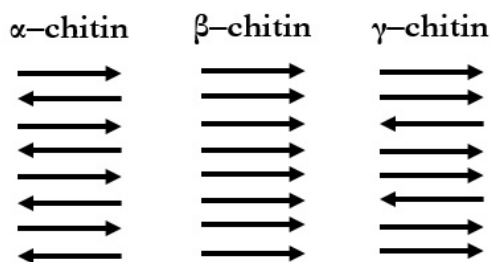


Figure I.1. Schematic disposal of chitin chains in α , β and γ -chitin.

The worldwide total production rate of chitin has been estimated to be approximately 10^{11} tons annually^{39,48}. The increasing use of chitin, as well as its derivatives, has been motivated by the fact that, unlike oil derivatives, it is obtained from the by-products of several industries, mainly from fisheries. More concretely, the total production of aquatic products (aquaculture plus fishing) in

the European Union in 2017 was of 7,034,104 tons, suffering an increase of 7.3 % compared to the previous year (APROMAR report). It is worth noting that the 75–85 % of the life-weight of the seafood processing industry (prawns, crabs, etc.) is waste (shells, heads and legs), which pollutes the environment and becomes an economic burden for the processing industries due to its problematic and expensive elimination, turning it in a highly solid waste generator⁴⁹. Considering this, it is of great relevance to search for technological alternatives for the processing of these wastes and their conversion into useful products such as chitin. These residues generally contain 14–35 % of chitin associated with proteins (30–40 %), lipids, pigments and calcium deposits (30–50 %), estimating therefore, an annual world production of chitin in this kind of wastes of about 120,000 tons.

In industrial processing, chitin is extracted by acid treatment to dissolve the calcium carbonate followed by alkaline solution to dissolve proteins. In addition, a decolourization step is often added in order to remove pigments and obtain a colourless pure chitin. All those treatments must be adapted to chitin source, owing to differences in the ultrastructure of the raw material, to produce first a high-quality chitin³⁸.

As explained, being a highly insoluble and chemically rather unreactive material, chitin has more applications while transforming to chitosan. Thus, chitosan (Cs) is obtained from chitin by partial deacetylation under alkaline conditions, leaving the amino group of carbon 2 (C₂) free. This process never reaches 100 %, being the chitosan a random copolymer with a molar fraction DAc (degree of acetylation) of β -(1→4)-*N*-acetyl-D-glucosamine (GlcNAc) and a fraction (1–DAc, DDC) (degree of deacetylation) of β -(1→4)-D-glucosamine (GlcN) (Figure I.2).

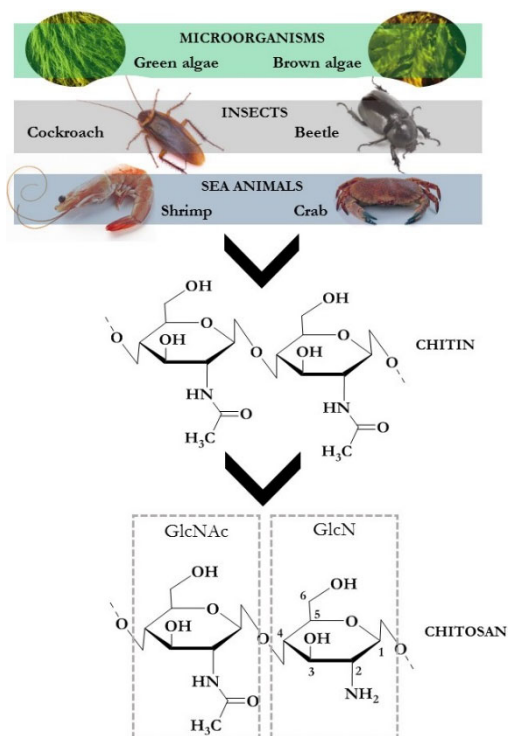


Figure I.2. Chemical structure of chitin and chitosan as integral structural components of different living organisms.

I.2.2. General properties

Chitosan is particularly interesting for biological activities and applications due to its adaptable character, especially in medicine, pharmaceuticals, cosmetics, biotechnology, food and agriculture^{50–52}. It has received a great deal of attention due to its well–documented renewability, biocompatibility, biodegradability by human enzymes, adsorption properties and the presence of lots of hydroxyl and amino groups on its surface^{53–55}. As a unique positively charged polysaccharide, the primary amines in the chitosan main chain are responsible for properties such as mucoadhesion (adheres to negatively charged mucus surfaces), *in situ* gelation, antimicrobial activity, permeation enhancement, etc.^{52,56,57}. Consequently, it

promotes attachment, proliferation and viability of cells, being considered a very interesting biomaterial.

The average molecular weight (M_w) and the degree of deacetylation (DDc) are the main physico-chemical properties of chitosan that determine its functional and biological properties, without neglecting other parameters like the crystallinity index (CI^{XRD}) or the polydispersity (PDI). In fact, chitosan with very different molecular weight (20–2000 kDa), viscosity (1 % chitosan in 1 % aqueous acetic acid (HAc), < 2000 mPa·s) and degree of deacetylation (40–98 %) can be found⁴³. Thus, depending on the source of natural chitin and the conditions of its production, chitosan can differ in size (average molecular weight), DDc and other physicochemical properties³⁹.

The degree of deacetylation (DDc) is the percentage of amino groups that remain free in the chitosan and is characterized as a percentage of acetylation (100–DAc %), which is closely related with its solubility. As a consequence of the hydrolysis of the *N*-acetyl group, the hydrophilic character of chitosan increases and become soluble in dilute acid solutions (acetic, formic, chloric, among others) since the pKa of the primary amino group of chitosan is ~ 6.5 ⁵⁸. Thus, chitosan is soluble in acidic solutions but insoluble at $pH > 6.5$ and in most organic solvents. The protonation of these groups in acidic medium gives to the chitosan a highly reactive character. Namely, it can be readily functionalized by the attachment of new pendant moieties to the main chain, providing it with specific reactivity and the ability to respond to particular purposes. Thus, the free amino groups of chitosan not only are responsible for most of the distinct properties attributed to it⁵⁹, but also serve as reactive sites for the synthesis of new chitosan derivatives. Thus, novel modified chitosan can exhibit new properties, displaying controlled responses to one or several stimuli⁶⁰. Thereby, the chemical functional groups can be modified to achieve specific goals, making it a polymer with tremendous range of potential applications.

On the other hand, chitosan is formed by repeated units of D-glucosamine, so the length of the chain and, therefore, its molecular weight, is an important characteristic of the compound. A good approximation to determine the viscosity-average can be obtained using viscometry methods⁶¹.

The effect of average molecular weight and degree of deacetylation on the physico-chemical and biological properties of chitosan has been intensively investigated to date^{52,62-64}. Selected relationships between the structural DDC and M_w parameters and the physico-chemical and biological properties are presented in Table I.1.

In general terms, physico-chemical properties are mostly affected by the degree of deacetylation, even if the biodegradability of chitosan in living organism depends at the same time on the molecular weight of the polymer. On the other hand, biological properties are greatly enhanced when the degree of deacetylation is higher, confirming the suitability of chitosan against chitin. On the other hand, various studies indicate that low M_w chitosans have a greatly enhanced biological activity when compared to the high M_w polymers⁶¹. In fact, low M_w chitosans, in the order of several tens of kDa, exhibit more pronounced antimicrobial and antifungal effects^{65,66}.

Table I.1. Influence of the degree of deacetylation (DDc) and molecular weight (M_w) on the physico–chemical and biological properties of chitosan samples (↑ directly proportional to the property; ↓ inversely proportional to the property)³⁹.

	Properties	DDc	M_w
Physico–chemical	Solubility	↑	
	Crystallinity	↓	
	Viscosity	↑	
	Biodegradability	↓	↓
	Biocompatibility	↑	
Biological	Antimicrobial	↑	↓
	Analgesic	↑	
	Antioxidant	↑	↓
	Haemostatic	↑	
	Mucoadhesive	↑	↑
	Permeation enhancing effect	↑	↑
	Antitumor		↓

I.2.3. Preparation techniques and applications

Chitosan displays great diversity and can be moulded into required shape and physical form for use in a wide range of applications. It can be easily processed into various products⁵⁶, including hydrogels⁶⁷, membranes^{68,69}, fibres^{70,71}, beads⁷², conjugates⁷³, microspheres^{74,75}, nanoparticles^{58,76}, scaffolds^{77,78}, etc. depending on the function and final purpose. Figure I.3 represents various chitosan–based end products according to the fabrication technique they follow.

As mentioned previously, the selection of the physical form depends mainly on the system configuration to be used for particular applications. Table I.2 summarizes the main applications of chitosan as a biomaterial, showing the wide variety of choices.

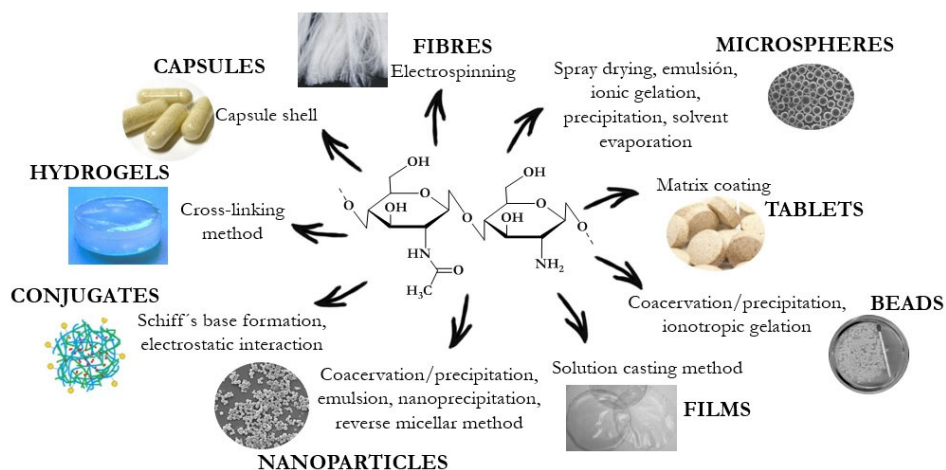


Figure I.3. Chitosan-based systems and their preparation techniques⁵⁶.

Even if most of the materials produced from chitosan are intended for applications in the biomedical sector (Table I.2), other potential areas cannot be ignored. Thereby, the antimicrobial properties and biodegradability make chitosan a suitable material for plant and seed protection, stimulation of its growth and controlled release of fertilizers in agriculture⁷⁹; as well as an interesting natural preservative for the food industry⁸⁰. Furthermore, chitosan is used in various cosmetics applications, especially in the treatment of skin, hair and teeth as it maintains skin moisture, improves elasticity and reduces the static electricity in hair⁷⁹. It also has the ability to act as a natural chelate, which makes this polymer suitable for wastewater treatments as it binds to metal anions, such as copper, lead, mercury and uranium⁸¹. Hence, it has been used to remove negatively charged dyes and solids from water streams and processing media.

Table I.2. Main applications of chitosan as a biomaterial⁵⁸.

Form	Application
Capsules	Delivery vehicle
Microspheres	Surface modification/microcarrier
Tables	Compressed diluent/Disintegrating agent
Beads	Drug delivery/Enzyme immobilization
Films	Wound care/Dialysis membrane
Nanoparticles	Encapsulation of proteins/Sustained release
Conjugates	Ligand
Hydrogels	Delivery vehicle/Implants, coatings/Tissue engineering
(nano)Fibres	Medical textiles/Sutures
Powder	Adsorbent for pharmaceutical and medical devices/Surgical glove powder/Enzyme immobilization
Solutions	Cosmetics/Anticoagulants/Bacteriostatic, haemostatic, anti-tumour agent

In particular, during the last years hydrogels derived from chitosan have received a great deal of attention⁵³, being imposing the number of procedures for preparing hydrogels from this biopolymer^{82,83}. Softness, smartness and the capacity to store water make hydrogels unique materials. Specifically, chitosan-based hydrogels are intended to be the materials that mimic better the natural extracellular matrix (ECM) in terms of composition, structural characteristics and mechanical properties, as well as potential carriers for delivery of different drug molecules or cell transplantation and tissue regeneration.

I.3. BIOPOLYMER-BASED HYDROGELS

I.3.1. General characteristics

Hydrogels are three dimensional, hydrophilic, polymeric networks which can absorb large amount of water, biological fluids and/or bioactive compounds (up to thousands times their dry weight) while maintaining their 3D structure^{35,84}. The ability of hydrogels to absorb water arises from the hydrophilic functional groups attached to the polymer backbone while their resistance to dissolution arises from cross-links and entanglements between the macromolecular chains. Considering the advantages that natural polymers provide in terms of biodegradability and low cost, along with their matrix complexion, they can provide structural integrity to tissue constructions, drug control and protein delivery to tissues and cultures, and serve as adhesives or barriers between tissue and material surfaces since they resemble to the extracellular matrix⁸⁵.

The gel is a state that is neither completely liquid nor completely solid. These half liquid-like and half solid-like properties cause many interesting relaxation behaviours that they are not found in either a pure solid or a pure liquid. Thereby, from the point of view of their mechanical properties, hydrogels are characterized by a viscous modulus which is considerably smaller than the elastic modulus in the plateau region⁸⁶.

The suitability of the hydrogels as biomedical materials and their performance in a particular application depend to a large extent on their structure. There are features in hydrogels with length scales spanning from centimetres to sub-nanometres (Figure I.4). The macroscopic design of hydrogels includes the size and porous structure, which largely determines the routes by which hydrogels can be introduced into the human body. Hydrogels can be either non-porous or contain macroscopic pores of 10–500 μm , which will dramatically affect the overall properties. On the nanometric scale, the space between cross-linked polymeric

chains in the network (mesh size) is tunable from around 5 to 100 nm, which will govern how biomolecules in general diffuse inside the hydrogel network. Finally, at the molecular scale, chemical interactions between molecules may occur. This multiscale architecture enables the ad-hoc design of hydrogels, which can serve as versatile platforms to meet specific application-based requirements²⁸.

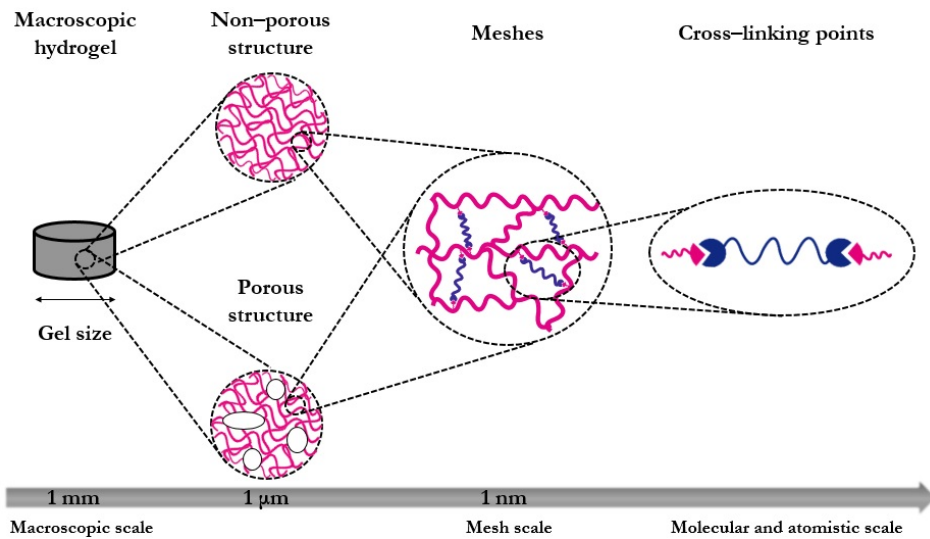


Figure I.4. Multiscale properties of hydrogels.

In fact, the so-called ‘smart’ hydrogels have emerged as a most versatile and viable platform for sustained protein release, targeted drug delivery and tissue engineering since they present a microporous structure with tuneable porosities and pore sizes and dimensions spanning from those of human organs, cells to viruses³¹. At the same time, the resulting 3D microstructure of the hydrogels would also be a determining factor for the control of the swelling/shrinking ability and kinetics⁸⁷. Pores homogeneously distributed within the hydrogel are expected to result in fast-responsive materials, turning the response-rate into a direct function of the microstructure.

In the same line, 'smart' hydrogels may exhibit drastic volume changes in response to specific external stimuli, such as temperature, solvent, pH, electric field, etc. Depending on the design of the hydrogel matrices, this volume change may occur continuously over a range of stimulus level or discontinuously at a critical stimulus level⁸⁶. Indeed, the design of scaffolds exhibiting environment-responsive faculties is crucial in many potential application areas of 3D materials. Thus, these flexible polymeric structures can be considered as the future biomaterials in biomedicine.

Other relevant parameters related with the inner microstructure of the hydrogels that are used to characterize their network structure include the molecular weight of the polymer chains between two neighbouring cross-links (M_c), the corresponding mesh size (ξ) and the effective network density (n_c). These structural parameters are inter-related and can be determined by applying the rubber-elasticity theory based on rheology studies^{1,88,89}.

On the other hand, hydrogels can be formed into practically any shape and size, depending on the requirements of the route of incorporation into the human body. Thus, hydrogels can be synthesized in the form of macroscopic networks or confined to smaller dimensions such as microgels or nanogels. Microgels and nanogels have tunable size from nanometres to several micrometres and a large surface area for multivalent bioconjugation⁹⁰. Figure I.5 shows a schematic representation of the most commonly used procedures for the implantation of different size hydrogels into the human body. Namely, macroporous hydrogels are generally used for transepithelial delivery and placement inside the body for guided cell growth and tissue regeneration. Besides, hydrogels of this size can also be introduced by local injection in the case of *in situ* gelling hydrogels, shear-thinning hydrogels and hydrogels that can undergo reversible dramatic volumetric changes. In addition, microgels are suitable for oral, pulmonary and intrabony

sustained delivery or 3D cell culture, whereas nanogels are suitable for systemic administration of molecules or drugs^{28,31}.

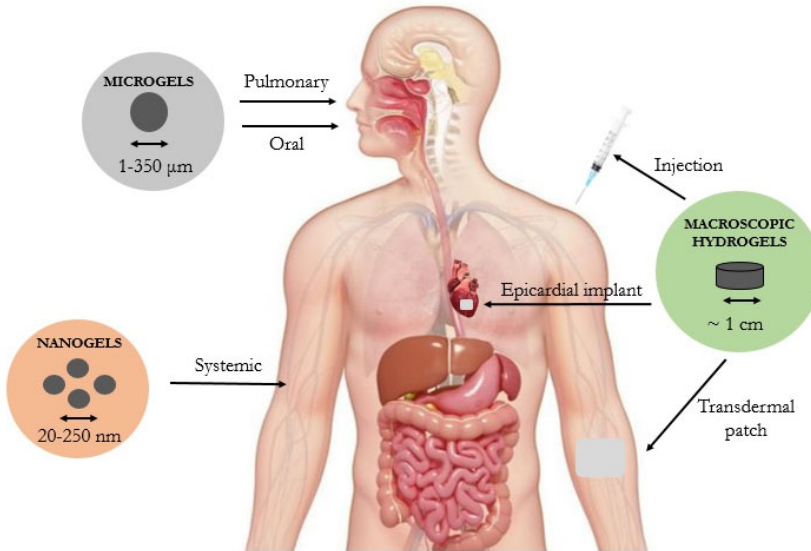


Figure I.5. Implantation route for hydrogels of different size.

I.3.1.1. Cross-linking strategies

In the past decade, various physical and chemical cross-linking strategies have been developed to fabricate gel-type materials^{90–92}. Physical hydrogels (reversible hydrogels) are generally cross-linked by non-covalent bonds such as hydrophobic interactions^{93–95}, electrostatic interactions⁹⁶, hydrogen bonds⁹⁷, metal coordination^{98,99}, stereocomplex crystallization¹⁰⁰ or even through changes in environmental conditions (i.e. thermosensitive hydrogels)^{101,102}. Even if they are formed under particularly mild conditions, physically cross-linked networks are typically weak and exhibit poor long-term stability (uncontrolled dissolution may occur), difficult control of pore size and low mechanical properties^{67,92,103,104}. In contrast, chemically cross-linked hydrogels (permanent hydrogels), which can be obtained by free radical polymerization^{105,106}, irradiation^{107,108} or enzymatic cross-

linking^{109–111}, are generally characterized by better stability, durability and mechanical properties³¹, due to the irreversible bonds formed during the covalent cross-linking. Moreover, hydrogels based on reversible covalent bonds also represent an attractive topic for research at both academic and industrial level. The molecular reversibility can be achieved either by making use of equilibrium reactions or through dynamic exchange reactions, such as cycloadditions, redox reactions, imine and enamine formation, acylhydrazone or borax acid reaction with hydroxyls¹¹². The general idea is that the use of dynamic covalent bonds allows the polymeric network to adjust itself as a result of an external stimulus. Nevertheless, regardless the type, traditional chemical procedures often require the use of an initiator or catalyst or organic solvents that might introduce potential toxicity concerns¹¹³.

I.3.2. Chitosan-based hydrogels

Numerous investigations have been performed to prepare hydrogels based on chitosan or its derivatives, mainly in order to design novel and more efficient materials that maintain the biomedical properties of the original polymer. The intermolecular forces between the polysaccharide chains of chitosan are hydrogen bonding, hydrophobic and ionic interactions, which are influenced by the average molecular weight and ionic strength¹¹⁴. It should be mentioned that chitosan is capable of self-aggregation and can form gel-like structures in aqueous medium due to these intra and intermacromolecular secondary interactions, mainly to decrease interfacial energy¹¹⁵. In addition, as a natural pH-sensitive polymer, chitosan is soluble at acidic pH but can form itself 3D networks at neutral pH¹¹⁶. However, both systems result highly unstable.

Therefore, chitosan-based hydrogels have been developed mainly by ionic cross-linking based on ionotropic gelation, which consists on the ionic interaction between negatively charged polyanionic molecules (i.e. tripolyphosphate, TPP)

with chitosan, due to the cationic character of the polymer caused by the protonation of the amino pending groups^{117,118}. On the other hand, in the last decade, increasing attention has been attracted from natural biopolymer-based polyelectrolyte complexes (PEC), formed by electrostatic interactions between two oppositely charged biopolymers as shown in Figure I.6. Thus, natural anionic polyelectrolytes including alginate, hyaluronic acid, pectin, carrageenan, chondroitin sulfate, xanthan gum, gellan gum, gum arabic and carboxymethyl cellulose have been successfully employed to create chitosan-based PEC systems¹¹⁹. Indeed, Barroso et al. design self-healing materials in form of multilayers due to the dynamic nature of the electrostatic interactions between the carboxylate ($-\text{COO}^-$) groups of hyaluronic acid and the amino ($-\text{NH}_3^+$) groups of chitosan at pH 5 where the ionization of both polyelectrolytes was maximum¹²⁰.

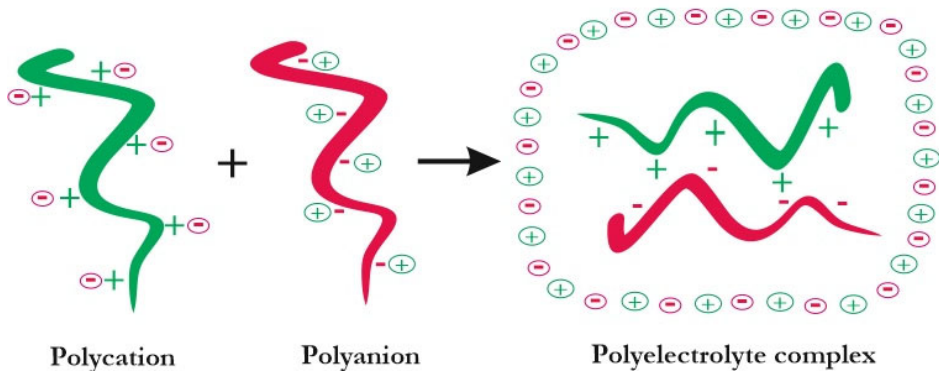


Figure I.6. Structure of polyelectrolyte complexes (PEC).

Nevertheless, as already mentioned, covalent cross-linking of hydrogels present significant advantages over those secondary interactions. Therefore, covalent cross-linking of chitosan-based hydrogels have also been extensively investigated by the reaction between chitosan and suitable bifunctional cross-linkers. To date, the most common cross-linkers used to obtain chitosan hydrogels are di-

aldehydes, such as glutaraldehyde^{121,122}, formaldehyde^{123,124} and glyoxal¹²⁵, or other compounds as genipin^{126–131}, oxalic acid¹³² or ethylene glycol di-glycidyl ether (EGDE)¹³³.

Furthermore, photo cross-linking reactions in the presence of ultraviolet (UV) light and a chemical photo initiator have also been applied as an approach to cross-link chitosan^{134,135}. Alternatively, enzymatic cross-linking has been also employed to prepare injectable chitosan hydrogels^{111,136}.

Regardless of the cross-linking procedure used for the formation of chitosan-based hydrogels, the high number of amine groups on the chitosan backbone confer pH-sensitivity to the final materials even after reaction. This particular behaviour makes chitosan-based hydrogels suitable as targeted drug carriers or tissue regeneration materials, due to their ability to release drugs or act at specific infected sites or tissues of the body by conveniently changing their volume at different pH values¹³⁷.

As mentioned previously, all these strategies lead to chemically cross-linked hydrogel networks with superior mechanical properties and structural integrity; however, the high risk of toxicity that traditional techniques can generate raises on a current need to find new biocompatible technologies for the preparation of hydrogels.

I.4. CLICK CHEMISTRY FOR HYDROGEL DESIGN

In order to avoid the drawbacks of conventional chemistry, click chemistry has emerged as a green, quick and reliable way to develop new biomaterials in the absence of catalysts and under mild reaction conditions^{138–141}. Over the past decade, click chemistry has gained significant attention in a broad range of applications, mainly for the chemical synthesis of small molecules, polymers, dendrimers, biomacromolecules and bioconjugation¹⁴².

Click chemistry occurs essentially through the chemical reaction between complementary functional groups considering the principal basis of biomedical applications, where the chemical reactions employed in cross-linked hydrogels should be achievable in aqueous solutions without generating toxic by-products¹⁴³. This promising strategy offers high reactivity, excellent selectivity and mild reaction conditions to prepare hydrogels with varying dimensions and patterns³¹. Besides, the unique bioorthogonality of click reactions renders thus formed hydrogels highly compatible with encapsulated bioactives including living cells, proteins and drugs.

The most used click reaction that can fulfil these conditions is the Cu^I-catalysed azide/alkyne cycloaddition (CuAAC), given the facility to be carried out and its wide applicability^{144,145}. Indeed, it is unaffected by a variety of functional groups and can be achieved with many sources of Cu^I catalysts and solvents, including aqueous¹⁴³. Furthermore, hydrogels from natural sources have been synthesized by the 1,3-dipolar cycloaddition reaction catalysed by Cu^I^{146,147}. However, to avoid the toxicity of copper, metal-free chemistry has been developed to eliminate heavy metal residues in hydrogel matrix¹³⁹. There has been a strong interest in other click reactions which proceed without the need for a copper catalyst, in particular, strain-promoted azide/alkyne cycloaddition (SPAAC), Diels–Alder reaction, radical mediated thiol–ene chemistry, Michael addition or tetrazole–alkene chemistry. Therewith, the most common click reactions are listed in Table I.3 and are described in more detail down below.

The strain-promoted azide/alkyne cycloaddition (SPAAC) involves the reaction between a cyclooctyne moiety and azides under mild reaction conditions. Due to the ring strain and the electron-withdrawing, the alkyne functionality is greatly activated for a cycloaddition without a catalyst¹⁴⁸. This reaction has been shown to be very efficient with high chemoselectivity even for *in vivo* applications, making it suitable for *in situ* cross-linking hydrogels. However, it is worth noticing

that the cross-linking of azide and alkyne functionalized polymers with metal-free click reactions is normally too slow to be used in most *in situ* applications¹⁴⁹. In order for this cross-linking strategy to be useful, the gelation kinetics needs to be improved by increasing the electron deficiency of alkynes and electron density of azide structures.

The Diels–Alder (DA) cycloaddition reaction is a highly selective [4+2] cycloaddition between a diene and a dienophile to form an adduct. It is a robust cross-linking strategy greatly employed for biopolymer-based hydrogels of different nature such as alginate¹³, gelatin^{5,33}, chitosan^{150,151} or starch¹⁴, as it is rapid, efficient, versatile and selective. Moreover, it is greatly accelerated when using water as solvent due to increased hydrophobic effects³¹. Indeed, apart from being an environmentally benign solvent, water has special properties that are essentially unique, related to what is called the ‘hydrophobic effect’, where hydrocarbons or molecules with hydrocarbon components avoid contact with water and associate instead with other hydrocarbon species in this medium¹⁵². Moreover, the reversible nature of the DA reaction is an attractive feature especially when dynamic materials are targeted. Thus, adduct formation is predominant near 65 °C with reasonable reaction rates, whereas the reverse reaction (retro-DA) takes place around 110 °C, leading to the initial precursors and opening the way to controlled depolymerisation or reversible cross-linking¹⁵³.

The thiol–ene click reaction proceeds through a radical-mediated mechanism which involves the addition of a thiol to a double bond, under the presence of an initiator at room temperature and in aqueous conditions even in the presence of biological molecules such as proteins or cells, making it a good technique for poly(ethylene glycol) (PEG)-based hydrogel cross-linking to a great extent^{31,154,155}. Unlike the traditional free radical polymerization, the radical thiol–ene reactions are relatively not oxygen sensitive¹⁵⁶, which is efficient, high yielding

and tolerant of different functional groups¹⁵⁷. It is well known that the radical thiol–ene reaction can be initiated by a variety of techniques including thermal or oxidation–reduction processes¹⁵⁸, even if the most commonly employed method is based on photochemical reactions¹⁵⁹.

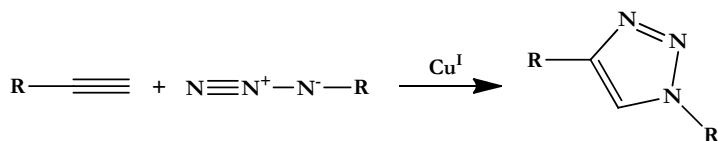
Michael addition (MA) is a 1,4–addition of nucleophiles to α,β –unsaturated ketones or esters. The cross–linking kinetics of Michael addition depends greatly on the electron deficiency of the alkenes. It occurs in high efficiency under aqueous conditions without any side products, making it a suitable approach for cross–linking in hydrogel synthesis. Indeed, hyaluronic acid/ poly(amidoamine) dendrimers hybrid hydrogels¹⁶⁰, dextran–based hydrogels for 3D cell encapsulation¹⁶¹ or *in situ* synthesized collagen/hyaluronan hydrogels¹⁶² have been developed through Michael addition reaction. On the other hand, surfactants can be used to promote the kinetics of the Michael addition reaction when the nucleophilic and the electrophilic macromolecules exhibit significant differences in hydrophilicity.

Tetrazole–alkene photo–click chemistry inherits the great features of click chemistry such as high specificity and quantitative conversion. Moreover, it has also unique advantages of photopolymerization including excellent spatial and temporal control over the reaction but without the use of possible toxic photo initiator. Furthermore, nitrile imine dipoles, which are formed from a UV activated tetrazole by releasing molecular nitrogen gas, readily react with alkenes, leading to fluorescent pyrazoline cycloadducts. Thus, the light–induced nitrile imine–mediated tetrazole–ene cycloaddition (NITEC) reaction provides intrinsically fluorescent hydrogels, which could be used to monitor the hydrogel formation and can facilitate the study of hydrogel fate *in vitro* and *in vivo*. *In situ* forming PEG hydrogels were prepared through this photo–click approach¹⁶³.

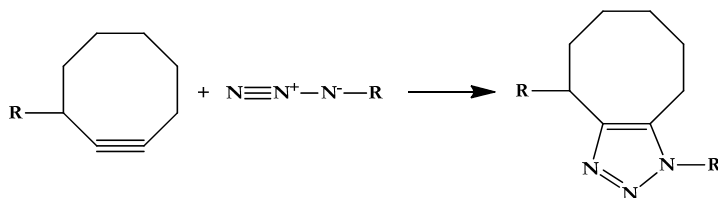
Table I.3. Schemes of the click chemistry reactions.

CLICK CHEMISTRY REACTIONS

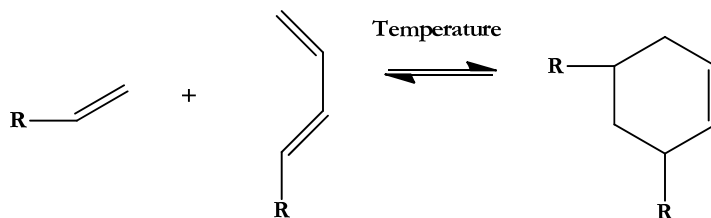
Cu^I-catalysed azide/alkyne cycloaddition (CuAAC)



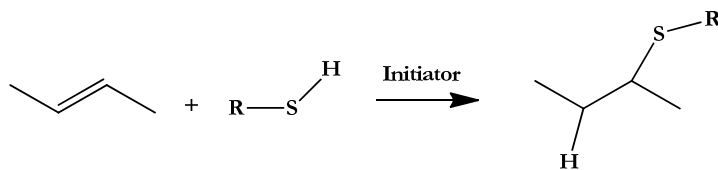
Strain-promoted azide/alkyne cycloaddition (SPAAC)



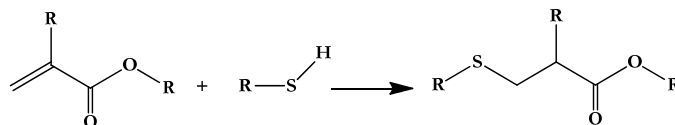
Diels-Alder reaction (DA)



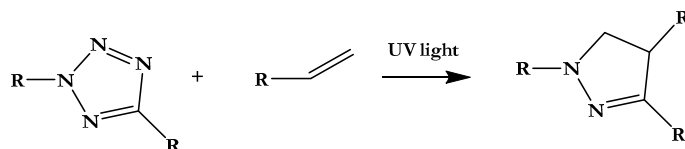
Radical mediated thiol-ene chemistry



Michael addition (MA)



Tetrazole–alkene chemistry (NITEC)



Accordingly, click chemistry has been widely used in cross-linking hydrogels due to its high selectivity and efficiency without generating by-products in aqueous conditions, plus the bioorthogonality of the components without interaction with the environment of biological or biomedical systems¹⁶⁴. As reported, to date, click reactions of different versions have been developed not only to build materials that are biologically compatible, highly functional and organized in structure, but also to produce highly complex patterns of biofunctionalities within in a single cellular scaffold¹⁶⁵. Therefore, according to the needs, conditions and final purpose of each specific case, the most appropriate click-inspired method will be implemented.

I.5. GENERAL OBJECTIVES

The main goal of this thesis was to develop gel-type biomaterials of different sizes from chitosan through novel synthetic strategies based on click chemistry reactions. Indeed, by the valorisation of seafood processing industry wastes, biodegradable and non-toxic hydrogels with well-defined properties in service were synthesized. All the chemical cross-linking pathways were found to be efficient technologies for the formation of stable biomaterials of different sizes intended for biomedical applications. Figure I.7 shows the general scheme of the work done in this thesis.

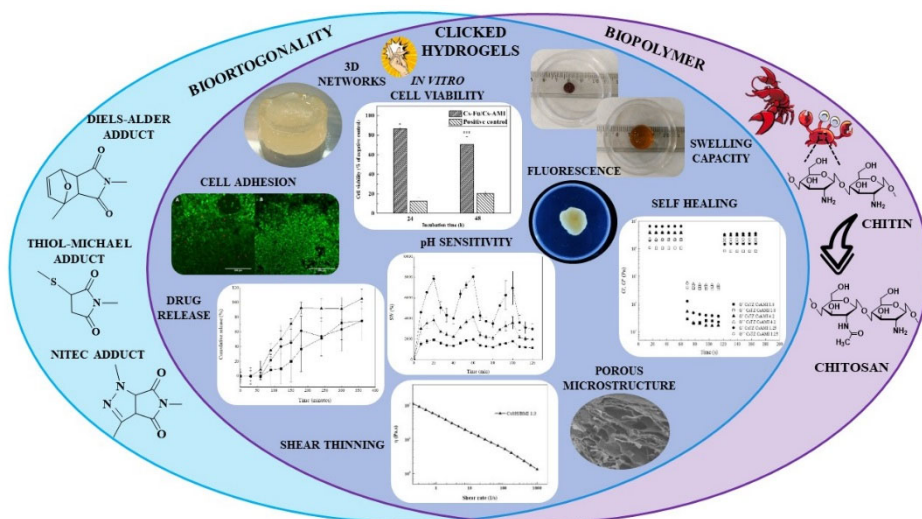


Figure I.7. Schematic representation of this thesis.

The present document summarizes the most important results and conclusions achieved during the development of the thesis structured in different chapters in order to make it more comprehensible.

- ❖ Chapter I consists of an introduction to focus the topic of the research and gives a general overview of the work, including the most important aspects of chitosan, hydrogels and click chemistry reactions.
- ❖ Chapter II describes the materials and methods used for the synthesis and characterization of hydrogels.
- ❖ Chapter III is based on the controlled endow of specific functionalities into the chitosan that are intended to be used in the final hydrogels. The biocompatible character of chitosan was maintained while new characteristics were attributed to the biopolymer. The new functionalized chitosan samples were characterized in detail and subsequently cross-linked by means of click reactions, either through the reaction between complementary chitosan derivates or through the use of cross-linking agents

endowed with complementary functional groups that were previously synthesized.

- ❖ Chapter IV is focused on the development of different furan/maleimide systems by Diels–Alder reaction, which greatly facilitate the formation of drug delivery systems. The effect of using complementary chitosans or a bifunctional cross–linker for hydrogel synthesis, as well as the influence of the amount of cross–linker used in the final properties of the materials was studied.
- ❖ Chapter V contains the results obtained for the synthesis and characterization of *in situ* cross–linked hydrogels via thiol–Michael addition reaction between thiol–modified chitosan and a properly synthesized bismaleimide under physiological conditions. The effectiveness of the cross–linking was proved to be influenced by the thiol/maleimide ratio and so, different cross–linker amounts were used in order to analyse its influence on the properties of the ensuing materials.
- ❖ Chapter VI shows the synthesis of fluorescent hydrogels through the covalent cross–linking of two complementary chitosan derivatives by the nitrile imine–mediated tetrazole–ene cycloaddition reaction. The addition of different amounts of tetrazole–functionalized chitosan into a maleimide–functionalized chitosan matrix was shown to affect the final behaviour of the hydrogels.
- ❖ Chapter VII depicts the preparation of thiolated chitosan nanogels cross–linked with a dicarboxylic acid by reverse nanoemulsion method. It was found that the incorporation of thiol groups improved certain properties of the nanogels.
- ❖ Chapter VIII summarizes the general conclusions of this work and proposes future challenges as well as it contains the publications and contributions to conferences as a result of this thesis.

- ❖ Finally, an annexe includes several lists of figures, schemes, tables, abbreviations and symbols that have been used throughout the text.

This thesis had a multidisciplinary aspect and it demanded the collaboration and continuous communication with researchers and companies from different scientific branches and research groups. There have to be highlighted the following collaborations with:

- i. Dr. Ljiljana Fruk, lecturer in Bionanotechnology and leader of the Bionano Engineering Group at the Department of Chemical Engineering and Biotechnology of the University of Cambridge, with whom I worked in the design of photo-activated fluorescent biopolymeric hydrogels cross-linked under UV light.
- ii. Dr. Leyre Perez from the Macromolecular Chemistry Research Group at the Department of Physical Chemistry of the Faculty of Science and Technology of the University of the Basque Country (UPV/EHU), with whom I learned about the synthesis of chitosan-based nanogels by reverse microemulsion method.
- iii. Professor Ana Alonso and Dr. Teodoro Palomares from the Tissue Engineering Group at the Department of Cell Biology and Histology of the Faculty of Medicine and Dentistry of the University of the Basque Country (UPV/EHU). They oversaw the biocompatibility tests that allowed the evaluation of the behaviour of materials in different cellular systems *in vitro* through cytotoxicity and cell adhesion studies according to ISO-10993-5.

REFERENCES

- (1) Van Vlierberghe, S.; Dubruel, P.; Schacht, E. Biopolymer-Based Hydrogels as Scaffolds for Tissue Engineering Applications: A Review. *Biomacromolecules* **2011**, *12* (5), 1387–1408. <https://doi.org/10.1021/bm200083n>.
- (2) Inoo, K.; Bando, H.; Tabata, Y. Enhanced Survival and Insulin Secretion of Insulinoma Cell Aggregates by Incorporating Gelatin Hydrogel Microspheres. *Regen. Ther.* **2018**, *8*, 29–37. <https://doi.org/10.1016/J.RETH.2017.12.002>.
- (3) Gritsch, L.; Motta, F. L.; Contessi Negrini, N.; Yahia, L.; Farè, S. Crosslinked Gelatin Hydrogels as Carriers for Controlled Heparin Release. *Mater. Lett.* **2018**, *228*, 375–378. <https://doi.org/10.1016/J.MATLET.2018.06.047>.
- (4) García-Astrain, C.; Guaresti, O.; González, K.; Santamaria-Echart, A.; Eceiza, A.; Corcuera, M. A.; Gabilondo, N. Click Gelatin Hydrogels: Characterization and Drug Release Behaviour. *Mater. Lett.* **2016**, *182*. <https://doi.org/10.1016/j.matlet.2016.06.115>.
- (5) García-Astrain, C.; Gandini, A.; Peña, C.; Algar, I.; Eceiza, A.; Corcuera, M.; Gabilondo, N. Diels-Alder “Click” Chemistry for the Cross-Linking of Furfuryl-Gelatin-Polyetheramine Hydrogels. *RSC Adv.* **2014**, *4* (67), 35578–35587. <https://doi.org/10.1039/c4ra06122e>.
- (6) García-Astrain, C.; Peña-Rodríguez, C.; Retegi, A.; Eceiza, A.; Corcuera, M. A.; Gabilondo, N. Green Chemistry for the Cross-Linking of Photo-Sensitive Furan Modified Gelatin. *Mater. Lett.* **2015**, *160*, 142–145. <https://doi.org/10.1016/j.matlet.2015.07.096>.
- (7) Chen, N.; Wang, H.; Ling, C.; Vermerris, W.; Wang, B.; Tong, Z. Cellulose-Based Injectable Hydrogel Composite for PH-Responsive and Controllable Drug Delivery. *Carbohydr. Polym.* **2019**, *225*, 115207. <https://doi.org/10.1016/J.CARBPOL.2019.115207>.
- (8) Liu, D.; Cao, Y.; Qu, R.; Gao, G.; Chen, S.; Zhang, Y.; Wu, M.; Ma, T.; Li, G. Production of Bacterial Cellulose Hydrogels with Tailored Crystallinity from Enterobacter Sp. FY-07 by the Controlled Expression of Colanic Acid Synthetic Genes. *Carbohydr. Polym.* **2019**, *207*, 563–570. <https://doi.org/10.1016/J.CARBPOL.2018.12.014>.
- (9) Teow, Y. H.; Kam, L. M.; Mohammad, A. W. Synthesis of Cellulose Hydrogel for Copper (II) Ions Adsorption. *J. Environ. Chem. Eng.* **2018**, *6* (4), 4588–4597. <https://doi.org/10.1016/J.JECE.2018.07.010>.

- (10) Zhao, X.; Xia, Y.; Zhang, X.; Lin, X.; Wang, L. Design of Mechanically Strong and Tough Alginate Hydrogels Based on a Soft-Brittle Transition. *Int. J. Biol. Macromol.* **2019**, *139*, 850–857. <https://doi.org/10.1016/j.IJBIOMAC.2019.08.057>.
- (11) Doderò, A.; Pianella, L.; Vicini, S.; Alloisio, M.; Ottonelli, M.; Castellano, M. Alginate-Based Hydrogels Prepared via Ionic Gelation: An Experimental Design Approach to Predict the Crosslinking Degree. *Eur. Polym. J.* **2019**, *118*, 586–594. <https://doi.org/10.1016/j.EURPOLYMJ.2019.06.028>.
- (12) García-Astrain, C.; Avérous, L. Synthesis and Behavior of Click Cross-Linked Alginate Hydrogels: Effect of Cross-Linker Length and Functionality. *Int. J. Biol. Macromol.* **2019**, *137*, 612–619. <https://doi.org/10.1016/j.IJBIOMAC.2019.07.010>.
- (13) García-Astrain, C.; Avérous, L. Synthesis and Evaluation of Functional Alginate Hydrogels Based on Click Chemistry for Drug Delivery Applications. *Carbohydr. Polym.* **2018**, *190*, 271–280. <https://doi.org/10.1016/j.carbpol.2018.02.086>.
- (14) González, K.; García-Astrain, C.; Santamaria-Echart, A.; Ugarte, L.; Avérous, L.; Eceiza, A.; Gabilondo, N. Starch/Graphene Hydrogels via Click Chemistry with Relevant Electrical and Antibacterial Properties. *Carbohydr. Polym.* **2018**, *202*, 372–381. <https://doi.org/10.1016/j.carbpol.2018.09.007>.
- (15) Tangsrianugul, N.; Suphantharika, M.; McClements, D. J. Simulated Gastrointestinal Fate of Lipids Encapsulated in Starch Hydrogels: Impact of Normal and High Amylose Corn Starch. *Food Res. Int.* **2015**, *78*, 79–87. <https://doi.org/10.1016/j.FOODRES.2015.11.004>.
- (16) Torres, M. D.; Moreira, R. Production of Hydrogels with Different Mechanical Properties by Starch Roasting: A Valorization of Industrial Chestnut by-Products. *Ind. Crops Prod.* **2019**, *128*, 377–384. <https://doi.org/10.1016/j.INDCROP.2018.11.035>.
- (17) Biduski, B.; Silva, W. M. F. da; Colussi, R.; Halal, S. L. de M. El; Lim, L.-T.; Dias, Á. R. G.; Zavareze, E. da R. Starch Hydrogels: The Influence of the Amylose Content and Gelatinization Method. *Int. J. Biol. Macromol.* **2018**, *113*, 443–449. <https://doi.org/10.1016/j.IJBIOMAC.2018.02.144>.
- (18) Norris, E. G.; Dalecki, D.; Hocking, D. C. Acoustic Modification of Collagen Hydrogels Facilitates Cellular Remodeling. *Mater. Today Bio* **2019**, *3*, 100018. <https://doi.org/10.1016/j.MTBIO.2019.100018>.

- (19) Zhang, T.; Chen, H.; Zhang, Y.; Zan, Y.; Ni, T.; Liu, M.; Pei, R. Photo-Crosslinkable, Bone Marrow-Derived Mesenchymal Stem Cells-Encapsulating Hydrogel Based on Collagen for Osteogenic Differentiation. *Colloids Surfaces B Biointerfaces* **2019**, *174*, 528–535. <https://doi.org/10.1016/J.COLSURFB.2018.11.050>.
- (20) Mas-Vinyals, A.; Gilabert-Porres, J.; Figueras-Esteve, L.; Borrós, S. Improving Linking Interface between Collagen-Based Hydrogels and Bone-like Substrates. *Colloids Surfaces B Biointerfaces* **2019**, *181*, 864–871. <https://doi.org/10.1016/J.COLSURFB.2019.06.046>.
- (21) Koivusalo, L.; Kauppila, M.; Samanta, S.; Parihar, V. S.; Ilmarinen, T.; Miettinen, S.; Oommen, O. P.; Skottman, H. Tissue Adhesive Hyaluronic Acid Hydrogels for Sutureless Stem Cell Delivery and Regeneration of Corneal Epithelium and Stroma. *Biomaterials* **2019**, *225*, 119516. <https://doi.org/10.1016/J.BIOMATERIALS.2019.119516>.
- (22) Haridas, N.; Rosemary, M. J. Effect of Steam Sterilization and Biocompatibility Studies of Hyaluronic Acid Hydrogel for Viscosupplementation. *Polym. Degrad. Stab.* **2019**, *163*, 220–227. <https://doi.org/10.1016/J.POLYMDEGRADSTAB.2019.03.019>.
- (23) Suo, A.; Xu, W.; Wang, Y.; Sun, T.; Ji, L.; Qian, J. Dual-Degradable and Injectable Hyaluronic Acid Hydrogel Mimicking Extracellular Matrix for 3D Culture of Breast Cancer MCF-7 Cells. *Carbohydr. Polym.* **2019**, *211*, 336–348. <https://doi.org/10.1016/J.CARBPOL.2019.01.115>.
- (24) Saekhor, K.; Udomsinprasert, W.; Honsawek, S.; Tachaboonyakiat, W. Preparation of an Injectable Modified Chitosan-Based Hydrogel Approaching for Bone Tissue Engineering. *Int. J. Biol. Macromol.* **2019**, *123*, 167–173. <https://doi.org/10.1016/J.IJBIOMAC.2018.11.041>.
- (25) Adibnia, V.; Mirbagheri, M.; Latreille, P.-L.; Faivre, J.; Cécyre, B.; Robert, J.; Bouchard, J.-F.; Martinez, V. A.; Delair, T.; David, L.; et al. Chitosan Hydrogel Micro-Bio-Devices with Complex Capillary Patterns via Reactive-Diffusive Self-Assembly. *Acta Biomater.* **2019**. <https://doi.org/10.1016/j.actbio.2019.08.037>.
- (26) Heim buck, A. M.; Priddy-Arrington, T. R.; Sawyer, B. J.; Caldorera-Moore, M. E. Effects of Post-Processing Methods on Chitosan-Genipin Hydrogel Properties. *Mater. Sci. Eng. C* **2019**, *98*, 612–618. <https://doi.org/10.1016/J.MSEC.2018.12.119>.
- (27) Ahn, J.; Ryu, J.; Song, G.; Whang, M.; Kim, J. Network Structure and Enzymatic Degradation of Chitosan Hydrogels Determined by Crosslinking

- Methods. *Carbohydr. Polym.* **2019**, *217*, 160–167. <https://doi.org/10.1016/J.CARBPOL.2019.04.055>.
- (28) Li, J.; Mooney, D. J. Designing Hydrogels for Controlled Drug Delivery. *Nat. Rev. Mater.* **2016**, *1* (12), 1–38. <https://doi.org/10.1038/natrevmats.2016.71>.
- (29) Daniel-Da-Silva, A. L.; Salgueiro, A. M.; Trindade, T. Effects of Au Nanoparticles on Thermoresponsive Genipin-Crosslinked Gelatin Hydrogels. *Gold Bull.* **2013**, *46* (1), 25–33. <https://doi.org/10.1007/s13404-012-0078-1>.
- (30) Schacht, E. H. Polymer Chemistry and Hydrogel Systems. *J. Phys. Conf. Ser.* **2004**, *3*, 22–28. <https://doi.org/10.1088/1742-6596/3/1/004>.
- (31) Jiang, Y.; Chen, J.; Deng, C.; Suuronen, E. J.; Zhong, Z. Click Hydrogels, Microgels and Nanogels: Emerging Platforms for Drug Delivery and Tissue Engineering. *Biomaterials* **2014**, *35* (18), 4969–4985. <https://doi.org/10.1016/J.BIOMATERIALS.2014.03.001>.
- (32) García-Astrain, C.; Ahmed, I.; Kendziora, D.; Guaresti, O.; Eceiza, A.; Fruk, L.; Corcuera, M. A.; Gabilondo, N. Effect of Maleimide-Functionalized Gold Nanoparticles on Hybrid Biohydrogels Properties. *RSC Adv.* **2015**, *5* (62). <https://doi.org/10.1039/c5ra06806a>.
- (33) García-Astrain, C.; Chen, C.; Burón, M.; Palomares, T.; Eceiza, A.; Fruk, L.; Corcuera, M. A.; Gabilondo, N. Biocompatible Hydrogel Nanocomposite with Covalently Embedded Silver Nanoparticles. *Biomacromolecules* **2015**, *16* (4), 1301–1310. <https://doi.org/10.1021/acs.biomac.5b00101>.
- (34) Iha, R. K.; Wooley, K. L.; Nyström, A. M.; Burked, D. J.; Kade, M. J.; Hawker, C. J. Applications of Orthogonal “Click” Chemistries in the Synthesis of Functional Soft Materials. *Chem. Rev.* **2009**, *109* (11), 5620–5686. <https://doi.org/10.1021/cr900138t>.
- (35) Dragan, E. S. Design and Applications of Interpenetrating Polymer Network Hydrogels. A Review. *Chem. Eng. J.* **2014**, *243*, 572–590. <https://doi.org/10.1016/j.cej.2014.01.065>.
- (36) Daraghmeh, N. H.; Chowdhry, B. Z.; Leharne, S. A.; Al Omari, M. M.; Badwan, A. A. Chitin. *Profiles Drug Subst. Excipients Relat. Methodol.* **2011**, *36*, 35–102. <https://doi.org/10.1016/B978-0-12-387667-6.00002-6>.
- (37) Pillai, C. K. S.; Paul, W.; Sharma, C. P. Chitin and Chitosan Polymers: Chemistry, Solubility and Fiber Formation. *Prog. Polym. Sci.* **2009**, *34* (7), 641–678. <https://doi.org/10.1016/j.progpolymsci.2009.04.001>.

- (38) Younes, I.; Rinaudo, M. Chitin and Chitosan Preparation from Marine Sources. Structure, Properties and Applications. *Mar. Drugs* **2015**, *13* (3), 1133–1174. <https://doi.org/10.3390/md13031133>.
- (39) Kumirska, J.; Weinhold, M. X.; Thöming, J.; Stepnowski, P. Biomedical Activity of Chitin/Chitosan Based Materials—Influence of Physicochemical Properties Apart from Molecular Weight and Degree of N-Acetylation. *Polymers (Basel)*. **2011**, *3* (4), 1875–1901. <https://doi.org/10.3390/polym3041875>.
- (40) Tolaimate, A.; Desbrieres, J.; Rhazi, M.; Alagui, A. Contribution to the Preparation of Chitins and Chitosans with Controlled Physico-Chemical Properties. *Polymer* **2003**, *44* (26), 7939–7952. <https://doi.org/10.1016/J.POLYMER.2003.10.025>.
- (41) Faria, R. R.; Guerra, R. F.; De Sousa Neto, L. R.; Motta, L. F.; Franca, E. D. F. Computational Study of Polymorphic Structures of α - And β - Chitin and Chitosan in Aqueous Solution. *J. Mol. Graph. Model.* **2016**, *63*, 78–84. <https://doi.org/10.1016/j.jmglm.2015.11.001>.
- (42) Guo, Z.; Xing, R.; Liu, S.; Zhong, Z.; Ji, X.; Wang, L.; Li, P. The Influence of Molecular Weight of Quaternized Chitosan on Antifungal Activity. *Carbohydr. Polym.* **2008**, *71* (4), 694–697. <https://doi.org/10.1016/J.CARBPOL.2007.06.027>.
- (43) Kurita, K. Controlled Functionalization of the Polysaccharide Chitin. *Prog. Polym. Sci.* **2001**, *26* (9), 1921–1971. [https://doi.org/10.1016/S0079-6700\(01\)00007-7](https://doi.org/10.1016/S0079-6700(01)00007-7).
- (44) Atkins, E. Conformations in Polysaccharides and Complex Carbohydrates. *J. Biosci.* **1985**, *8* (1–2), 375–387. <https://doi.org/10.1007/BF02703990>.
- (45) Mincea, M.; Negrulescu, A.; Ostafe, V. Preparation, Modification, and Applications of Chitin Nanowhiskers: A Review. *Rev. Adv. Mater. Sci.* **2012**, *30* (3), 225–242.
- (46) Jang, M. K.; Kong, B. G.; Jeong, Y. Il; Lee, C. H.; Nah, J. W. Physicochemical Characterization of α -Chitin, β -Chitin, and γ -Chitin Separated from Natural Resources. *J. Polym. Sci. Part A Polym. Chem.* **2004**, *42* (14), 3423–3432. <https://doi.org/10.1002/pola.20176>.
- (47) Raut, A. V.; Satvekar, R. K.; Rohiwal, S. S.; Tiwari, A. P.; Gnanamani, A.; Pushpavanam, S.; Nanaware, S. G.; Pawar, S. H. In Vitro Biocompatibility and Antimicrobial Activity of Chitin Monomer Obtain from Hollow Fiber Membrane. *Des. Monomers Polym.* **2016**, *19* (5), 445–455.

- <https://doi.org/10.1080/15685551.2016.1169379>.
- (48) Hoell, I. A.; Vaaje-Kolstad, G.; Eijsink, V. G. H. Structure and Function of Enzymes Acting on Chitin and Chitosan. *Biotechnol. Genet. Eng. Rev.* **2010**, *27* (1), 331–366. <https://doi.org/10.1080/02648725.2010.10648156>.
- (49) Gildberg, A.; Stenberg, E. A New Process for Advanced Utilisation of Shrimp Waste. *Process Biochem.* **2001**, *36* (8–9), 809–812. [https://doi.org/10.1016/S0032-9592\(00\)00278-8](https://doi.org/10.1016/S0032-9592(00)00278-8).
- (50) Wang, Y.; Wang, J.; Yuan, Z.; Han, H.; Li, T.; Li, L.; Guo, X. Chitosan Cross-Linked Poly(Acrylic Acid) Hydrogels: Drug Release Control and Mechanism. *Colloids Surfaces B Biointerfaces* **2017**, *152*, 252–259. <https://doi.org/10.1016/J.COLSURFB.2017.01.008>.
- (51) Libio, I. C.; Demori, R.; Ferrão, M. F.; Lionzo, M. I. Z.; da Silveira, N. P. Films Based on Neutralized Chitosan Citrate as Innovative Composition for Cosmetic Application. *Mater. Sci. Eng. C* **2016**, *67*, 115–124. <https://doi.org/10.1016/J.MSEC.2016.05.009>.
- (52) Dash, M.; Chiellini, F.; Ottenbrite, R. M.; Chiellini, E. Chitosan—A Versatile Semi-Synthetic Polymer in Biomedical Applications. *Prog. Polym. Sci.* **2011**, *36* (8), 981–1014. <https://doi.org/10.1016/J.PROGPOLYMSCI.2011.02.001>.
- (53) Hu, L.; Sun, Y.; Wu, Y. Advances in Chitosan-Based Drug Delivery Vehicles. *Nanoscale* **2013**, *5* (8), 3103–3111. <https://doi.org/10.1039/c3nr00338h>.
- (54) Kean, T.; Thanou, M. Biodegradation, Biodistribution and Toxicity of Chitosan. *Adv. Drug Deliv. Rev.* **2010**, *62* (1), 3–11. <https://doi.org/10.1016/j.addr.2009.09.004>.
- (55) Bagheri-Khoulenjani, S.; Taghizadeh, S. M.; Mirzadeh, H. An Investigation on the Short-Term Biodegradability of Chitosan with Various Molecular Weights and Degrees of Deacetylation. *Carbohydr. Polym.* **2009**, *78* (4), 773–778. <https://doi.org/10.1016/J.CARBPOL.2009.06.020>.
- (56) Ali, A.; Ahmed, S. A Review on Chitosan and Its Nanocomposites in Drug Delivery. *Int. J. Biol. Macromol.* **2018**, *109*, 273–286. <https://doi.org/10.1016/j.ijbiomac.2017.12.078>.
- (57) Amidi, M.; Mastrobattista, E.; Jiskoot, W.; Hennink, W. E. Chitosan-Based Delivery Systems for Protein Therapeutics and Antigens. *Adv. Drug Deliv. Rev.* **2010**, *62* (1), 59–82. <https://doi.org/10.1016/J.ADDR.2009.11.009>.
- (58) Mohammed, M. A.; Syeda, J. T. M.; Wasan, K. M.; Wasan, E. K. An

- Overview of Chitosan Nanoparticles and Its Application in Non-Parenteral Drug Delivery. *Pharmaceutics* **2017**, *9* (4). <https://doi.org/10.3390/pharmaceutics9040053>.
- (59) Croisier, F.; Jérôme, C. Chitosan-Based Biomaterials for Tissue Engineering. *Eur. Polym. J.* **2013**, *49* (4), 780–792. <https://doi.org/10.1016/J.EURPOLYMJ.2012.12.009>.
- (60) Recillas, M.; Silva, L. L.; Peniche, C.; Goycoolea, F. M.; Rinaudo, M.; Argüelles-Monal, W. M. Thermoresponsive Behavior of Chitosan-g-N-Isopropylacrylamide Copolymer Solutions. *Biomacromolecules* **2009**, *10* (6), 1633–1641. <https://doi.org/10.1021/bm9002317>.
- (61) Czechowska-Biskup, R.; Wach, R. A.; Rosiak, J. M.; Ulański, P. Procedure for Determination of the Molecular Weight of Chitosan by Viscometry. *Prog. Chem. Appl. Chitin its Deriv.* **2018**, *23*, 45–54. <https://doi.org/10.15259/PCACD.23.04>.
- (62) Aranaz, I.; Mengibar, M.; Harris, R.; Panos, I.; Miralles, B.; Acosta, N.; Galed, G.; Heras, A.; Aranaz, I.; Mengibar, M.; Harris, R.; Paños, I.; Miralles, B.; Acosta, N.; Galed, G.; Heras, A. Functional Characterization of Chitin and Chitosan. *Curr. Chem. Biol.* **2009**, *3* (2), 203–230.
- (63) Tsao, C. T.; Chang, C. H.; Lin, Y. Y.; Wu, M. F.; Wang, J.-L.; Han, J. L.; Hsieh, K. H. Antibacterial Activity and Biocompatibility of a Chitosan- γ -Poly(Glutamic Acid) Polyelectrolyte Complex Hydrogel. *Carbohydr. Res.* **2010**, *345* (12), 1774–1780. <https://doi.org/10.1016/J.CARRES.2010.06.002>.
- (64) Kong, M.; Chen, X. G.; Xing, K.; Park, H. J. Antimicrobial Properties of Chitosan and Mode of Action: A State of the Art Review. *Int. J. Food Microbiol.* **2010**, *144* (1), 51–63. <https://doi.org/10.1016/J.IJFOODMICRO.2010.09.012>.
- (65) Kulikov, S. N.; Lisovskaya, S. A.; Zelenikhin, P. V.; Bezrodnykh, E. A.; Shakirova, D. R.; Blagodatskikh, I. V.; Tikhonov, V. E. Antifungal Activity of Oligochitosans (Short Chain Chitosans) against Some Candida Species and Clinical Isolates of Candida Albicans: Molecular Weight–Activity Relationship. *Eur. J. Med. Chem.* **2014**, *74*, 169–178. <https://doi.org/10.1016/J.EJMECH.2013.12.017>.
- (66) Liu, N.; Chen, X.-G.; Park, H.-J.; Liu, C.-G.; Liu, C.-S.; Meng, X.-H.; Yu, L.-J. Effect of MW and Concentration of Chitosan on Antibacterial Activity of Escherichia Coli. *Carbohydr. Polym.* **2006**, *64* (1), 60–65. <https://doi.org/10.1016/J.CARBPOL.2005.10.028>.

- (67) Hamed, H.; Moradi, S.; Hudson, S. M.; Tonelli, A. E. Chitosan Based Hydrogels and Their Applications for Drug Delivery in Wound Dressings: A Review. *Carbohydr. Polym.* **2018**, *199*, 445–460. <https://doi.org/10.1016/J.CARBPOL.2018.06.114>.
- (68) Marreco, P. R.; Da Luz Moreira, P.; Genari, S. C.; Moraes, Â. M. Effects of Different Sterilization Methods on the Morphology, Mechanical Properties, and Cytotoxicity of Chitosan Membranes Used as Wound Dressings. *J. Biomed. Mater. Res. - Part B Appl. Biomater.* **2004**, *71* (2), 268–277. <https://doi.org/10.1002/jbm.b.30081>.
- (69) Madhumathi, K.; Binulal, N. S.; Nagahama, H.; Tamura, H.; Shalumon, K. T.; Selvamurugan, N.; Nair, S. V.; Jayakumar, R. Preparation and Characterization of Novel β -Chitin–Hydroxyapatite Composite Membranes for Tissue Engineering Applications. *Int. J. Biol. Macromol.* **2009**, *44* (1), 1–5. <https://doi.org/10.1016/J.IJBIOMAC.2008.09.013>.
- (70) Qasim, S. B.; Najeeb, S.; Delaine-Smith, R. M.; Rawlinson, A.; Ur Rehman, I. Potential of Electrospun Chitosan Fibers as a Surface Layer in Functionally Graded GTR Membrane for Periodontal Regeneration. *Dent. Mater.* **2017**, *33* (1), 71–83. <https://doi.org/10.1016/J.DENTAL.2016.10.003>.
- (71) Li, L.; Yuan, B.; Liu, S.; Yu, S.; Xie, C.; Liu, F.; Guo, X.; Pei, L.; Zhang, B. Preparation of High Strength Chitosan Fibers by Using Ionic Liquid as Spinning Solution. *J. Mater. Chem.* **2012**, *22* (17), 8585–8593. <https://doi.org/10.1039/c2jm30555k>.
- (72) Nitsae, M.; Madjid, A.; Hakim, L.; Sabarudin, A. Preparation of Chitosan Beads Using Tripolyphosphate and Ethylene Glycol Diglycidyl Ether as Crosslinker for Cr(VI) Adsorption. *Chem. Chem. Technol.* **2016**, *10* (1), 105–114. <https://doi.org/10.23939/chcht10.01.105>.
- (73) Saranya, T. S.; Rajan, V. K.; Biswas, R.; Jayakumar, R.; Sathianarayanan, S. Synthesis, Characterisation and Biomedical Applications of Curcumin Conjugated Chitosan Microspheres. *Int. J. Biol. Macromol.* **2018**, *110*, 227–233. <https://doi.org/10.1016/J.IJBIOMAC.2017.12.044>.
- (74) Zhai, L.; Bai, Z.; Zhu, Y.; Wang, B.; Luo, W. Fabrication of Chitosan Microspheres for Efficient Adsorption of Methyl Orange. *Chinese J. Chem. Eng.* **2018**, *26* (3), 657–666. <https://doi.org/10.1016/J.CJCHE.2017.08.015>.
- (75) Pan, M.; Tang, Z.; Tu, J.; Wang, Z.; Chen, Q.; Xiao, R.; Liu, H. Porous Chitosan Microspheres Containing Zinc Ion for Enhanced Thrombosis and Hemostasis. *Mater. Sci. Eng. C* **2018**, *85*, 27–36. <https://doi.org/10.1016/J.MSEC.2017.12.015>.

- (76) Grenha, A. Chitosan Nanoparticles: A Survey of Preparation Methods. *J. Drug Target.* **2012**, *20* (4), 291–300. <https://doi.org/10.3109/1061186X.2011.654121>.
- (77) Bergonzi, C.; Di Natale, A.; Zimetti, F.; Marchi, C.; Bianchera, A.; Bernini, F.; Silvestri, M.; Bettini, R.; Elviri, L. Study of 3D-Printed Chitosan Scaffold Features after Different Post-Printing Gelation Processes. *Sci. Rep.* **2019**, *9* (1), 1–11. <https://doi.org/10.1038/s41598-018-36613-8>.
- (78) Lan Levengood, S.; Zhang, M. Chitosan-Based Scaffolds for Bone Tissue Engineering. *J Mater Chem B Mater Biol Med.* **2015**, *2* (21), 3161–3184. <https://doi.org/10.1039/C4TB00027G>. Chitosan-based.
- (79) Rinaudo, M. Chitin and Chitosan: Properties and Applications. *Prog. Polym. Sci.* **2006**, *31* (7), 603–632. <https://doi.org/10.1016/J.PROGPOLYMSCI.2006.06.001>.
- (80) Dutta, J.; Tripathi, S.; Dutta, P. K. *Progress in Antimicrobial Activities of Chitin, Chitosan and Its Oligosaccharides: A Systematic Study Needs for Food Applications*; 2012; Vol. 18. <https://doi.org/10.1177/1082013211399195>.
- (81) Urbina, L.; Guaresti, O.; Requies, J.; Gabilondo, N.; Eceiza, A.; Corcuera, M. A.; Retegi, A. Design of Reusable Novel Membranes Based on Bacterial Cellulose and Chitosan for the Filtration of Copper in Wastewaters. *Carbohydr. Polym.* **2018**, *193* (November 2017), 362–372. <https://doi.org/10.1016/j.carbpol.2018.04.007>.
- (82) Berger, J.; Reist, M.; Mayer, J. M.; Felt, O.; Gurny, R. Structure and Interactions in Chitosan Hydrogels Formed by Complexation or Aggregation for Biomedical Applications. *Eur. J. Pharm. Biopharm.* **2004**, *57* (1), 35–52. [https://doi.org/10.1016/S0939-6411\(03\)00160-7](https://doi.org/10.1016/S0939-6411(03)00160-7).
- (83) Berger, J.; Reist, M.; Mayer, J. M.; Felt, O.; Peppas, N. A.; Gurny, R. Structure and Interactions in Covalently and Ionically Crosslinked Chitosan Hydrogels for Biomedical Applications. *Eur. J. Pharm. Biopharm.* **2004**, *57* (1), 19–34. [https://doi.org/10.1016/S0939-6411\(03\)00161-9](https://doi.org/10.1016/S0939-6411(03)00161-9).
- (84) Ullah, F.; Othman, M. B. H.; Javed, F.; Ahmad, Z.; Akil, H. M. Classification, Processing and Application of Hydrogels: A Review. *Mater. Sci. Eng. C* **2015**, *57*, 414–433. <https://doi.org/10.1016/J.MSEC.2015.07.053>.
- (85) Slaughter, B. V.; Khurshid, S. S.; Fisher, O. Z.; Khademhosseini, A.; Peppas, N. A. Hydrogels in Regenerative Medicine. *Adv. Mater.* **2009**, *21*, 3307–3329. <https://doi.org/10.1002/adma.200802106>.

- (86) Gerlach, G.; Arndt, K. Hydrogel Sensors and Actuators Volume. *Springer Ser. Chem. Sensors Biosens.* **2013**, *6*, 1–272. <https://doi.org/10.1007/978-3-540-75645-3>.
- (87) Xu, H.; Matysiak, S. Effect of PH on Chitosan Hydrogel Polymer Network Structure. *Chem. Commun.* **2017**, *53* (53), 7373–7376. <https://doi.org/10.1039/c7cc01826f>.
- (88) Kloczkowski, A. Application of Statistical Mechanics to the Analysis of Various Physical Properties of Elastomeric Networks — a Review. *Polymer* **2002**, *43* (4), 1503–1525. [https://doi.org/10.1016/S0032-3861\(01\)00588-2](https://doi.org/10.1016/S0032-3861(01)00588-2).
- (89) Karvinen, J.; Ihalainen, T. O.; Calejo, M. T.; Jönkkäri, I.; Kellomäki, M. Characterization of the Microstructure of Hydrzone Crosslinked Polysaccharide-Based Hydrogels through Rheological and Diffusion Studies. *Mater. Sci. Eng. C* **2019**, *94* (April 2018), 1056–1066. <https://doi.org/10.1016/j.msec.2018.10.048>.
- (90) Oh, J. K.; Drumright, R.; Siegwart, D. J.; Matyjaszewski, K. The Development of Microgels/Nanogels for Drug Delivery Applications. *Prog. Polym. Sci.* **2008**, *33* (4), 448–477. <https://doi.org/10.1016/J.PROGPOLYMSCI.2008.01.002>.
- (91) Van Tomme, S. R.; Storm, G.; Hennink, W. E. In Situ Gelling Hydrogels for Pharmaceutical and Biomedical Applications. *Int. J. Pharm.* **2008**, *355* (1–2), 1–18. <https://doi.org/10.1016/J.IJPHARM.2008.01.057>.
- (92) Hoare, T. R.; Kohane, D. S. Hydrogels in Drug Delivery: Progress and Challenges. *Polymer* **2008**, *49* (8), 1993–2007. <https://doi.org/10.1016/J.POLYMER.2008.01.027>.
- (93) Tuncaboylu, D. C.; Sari, M.; Oppermann, W.; Okay, O. Tough and Self-Healing Hydrogels Formed via Hydrophobic Interactions. *Macromolecules* **2011**, *44* (12), 4997–5005. <https://doi.org/10.1021/ma200579v>.
- (94) Chang, X.; Geng, Y.; Cao, H.; Zhou, J.; Tian, Y.; Shan, G.; Bao, Y.; Wu, Z. L.; Pan, P. Dual-Crosslink Physical Hydrogels with High Toughness Based on Synergistic Hydrogen Bonding and Hydrophobic Interactions. *Macromol. Rapid Commun.* **2018**, *39* (14), 1–7. <https://doi.org/10.1002/marc.201700806>.
- (95) Hao, J.; Weiss, R. A. Viscoelastic and Mechanical Behavior of Hydrophobically Modified Hydrogels. *Macromolecules* **2011**, *44* (23), 9390–9398. <https://doi.org/10.1021/ma202130u>.

- (96) Sun, T. L.; Kurokawa, T.; Kuroda, S.; Ihsan, A. Bin; Akasaki, T.; Sato, K.; Haque, M. A.; Nakajima, T.; Gong, J. P. Physical Hydrogels Composed of Polyampholytes Demonstrate High Toughness and Viscoelasticity. *Nat. Mater.* **2013**, *12* (10), 932–937. <https://doi.org/10.1038/nmat3713>.
- (97) Cui, J.; Campo, A. Del. Multivalent H-Bonds for Self-Healing Hydrogels. *Chem. Commun.* **2012**, *48* (74), 9302–9304. <https://doi.org/10.1039/c2cc34701f>.
- (98) Lin, P.; Ma, S.; Wang, X.; Zhou, F. Molecularly Engineered Dual-Crosslinked Hydrogel with Ultrahigh Mechanical Strength, Toughness, and Good Self-Recovery. *Adv. Mater.* **2015**, *27* (12), 2054–2059. <https://doi.org/10.1002/adma.201405022>.
- (99) Jeon, I.; Cui, J.; Illeperuma, W. R. K.; Aizenberg, J.; Vlassak, J. J. Extremely Stretchable and Fast Self-Healing Hydrogels. *Adv. Mater.* **2016**, *28*, 4678–4683. <https://doi.org/10.1002/adma.201600480>.
- (100) Cao, H.; Chang, X.; Mao, H.; Zhou, J.; Wu, Z. L.; Shan, G.; Bao, Y.; Pan, P. Stereocomplexed Physical Hydrogels with High Strength and Tunable Crystallizability. *Soft Matter* **2017**, *13* (45), 8502–8510. <https://doi.org/10.1039/c7sm01491k>.
- (101) Jung, Y.; Park, W.; Park, H.; Lee, D.-K.; Na, K. Thermo-Sensitive Injectable Hydrogel Based on the Physical Mixing of Hyaluronic Acid and Pluronic F-127 for Sustained NSAID Delivery. *Carbohydr. Polym.* **2017**, *156*, 403–408. <https://doi.org/10.1016/J.CARBPOL.2016.08.068>.
- (102) Barros, S. C.; da Silva, A. A.; Costa, D. B.; Cesarino, I.; Costa, C. M.; Lanceros-Méndez, S.; Pawlicka, A.; Silva, M. M. Thermo-Sensitive Chitosan–Cellulose Derivative Hydrogels: Swelling Behaviour and Morphologic Studies. *Cellulose* **2014**, *21* (6), 4531–4544. <https://doi.org/10.1007/s10570-014-0442-9>.
- (103) Hiemstra, C.; Zhou, W.; Zhong, Z.; Wouters, M.; Feijen, J. Rapidly in Situ Forming Biodegradable Robust Hydrogels by Combining Stereocomplexation and Photopolymerization. *J. Am. Chem. Soc.* **2007**, *129* (32), 9918–9926. <https://doi.org/10.1021/ja072113p>.
- (104) Lim, D. W.; Nettles, D. L.; Setton, L. A.; Chilkoti, A. Rapid Cross-Linking of Elastin-like Polypeptides with (Hydroxymethyl)Phosphines in Aqueous Solution. *Biomacromolecules* **2007**, *8* (5), 1463–1470. <https://doi.org/10.1021/bm061059m>.
- (105) Matyjaszewski, K.; Spanswick, J. Controlled/Living Radical Polymerization.

- Mater. Today* **2005**, *8* (3), 26–33. [https://doi.org/10.1016/S1369-7021\(05\)00745-5](https://doi.org/10.1016/S1369-7021(05)00745-5).
- (106) Ahmed, E. M. Hydrogel: Preparation, Characterization, and Applications: A Review. *J. Adv. Res.* **2015**, *6* (2), 105–121. <https://doi.org/10.1016/J.JARE.2013.07.006>.
- (107) Wang, Y. C.; Wu, J.; Li, Y.; Du, J. Z.; Yuan, Y. Y.; Wang, J. Engineering Nanoscopic Hydrogels via Photo-Crosslinking Salt-Induced Polymer Assembly for Targeted Drug Delivery. *Chem. Commun.* **2010**, *46* (20), 3520–3522. <https://doi.org/10.1039/c002620d>.
- (108) Zhang, M.; Cheng, Z.; Zhao, T.; Liu, M.; Hu, M.; Li, J. Synthesis, Characterization, and Swelling Behaviors of Salt-Sensitive Maize Bran-Poly(Acrylic Acid) Superabsorbent Hydrogel. *J. Agric. Food Chem.* **2014**, *62* (35), 8867–8874. <https://doi.org/10.1021/jf5021279>.
- (109) Bode, F.; Da Silva, M. A.; Drake, A. F.; Ross-Murphy, S. B.; Dreiss, C. A. Enzymatically Cross-Linked Tilapia Gelatin Hydrogels: Physical, Chemical, and Hybrid Networks. *Biomacromolecules* **2011**, *12* (10), 3741–3752. <https://doi.org/10.1021/bm2009894>.
- (110) Zhang, Y.; Fan, Z.; Xu, C.; Fang, S.; Liu, X.; Li, X. Tough Biohydrogels with Interpenetrating Network Structure by Biezymatic Crosslinking Approach. *Eur. Polym. J.* **2015**, *72*, 717–725. <https://doi.org/10.1016/J.EURPOLYMJ.2014.12.038>.
- (111) Moreira Teixeira, L. S.; Feijen, J.; van Blitterswijk, C. A.; Dijkstra, P. J.; Karperien, M. Enzyme-Catalyzed Crosslinkable Hydrogels: Emerging Strategies for Tissue Engineering. *Biomaterials* **2012**, *33* (5), 1281–1290. <https://doi.org/10.1016/J.BIOMATERIALS.2011.10.067>.
- (112) Picchioni, F.; Muljana, H. Hydrogels Based on Dynamic Covalent and Non Covalent Bonds: A Chemistry Perspective. *Gels* **2018**, *4* (1), 21. <https://doi.org/10.3390/gels4010021>.
- (113) Annabi, N.; Tamayol, A.; Uquillas, J. A.; Akbari, M.; Bertassoni, L. E.; Cha, C.; Camci-Unal, G.; Dokmeci, M. R.; Peppas, N. A.; Khademhosseini, A. 25th Anniversary Article: Rational Design and Applications of Hydrogels in Regenerative Medicine. *Adv. Mater.* **2014**, *26* (1), 85–124. <https://doi.org/10.1002/adma.201303233>.
- (114) Qun, G.; Ajun, W. Effects of Molecular Weight, Degree of Acetylation and Ionic Strength on Surface Tension of Chitosan in Dilute Solution. *Carbohydr. Polym.* **2006**, *64* (1), 29–36.

<https://doi.org/10.1016/J.CARBPOL.2005.10.026>.

- (115) Hwang, H.-Y.; Kim, I.-S.; Kwon, I. C.; Kim, Y.-H. Tumor Targetability and Antitumor Effect of Docetaxel-Loaded Hydrophobically Modified Glycol Chitosan Nanoparticles. *J. Control. Release* **2008**, *128* (1), 23–31. <https://doi.org/10.1016/J.JCONREL.2008.02.003>.
- (116) Strehin, I.; Nahas, Z.; Arora, K.; Nguyen, T.; Elisseeff, J. A Versatile PH Sensitive Chondroitin Sulfate–PEG Tissue Adhesive and Hydrogel. *Biomaterials* **2010**, *31* (10), 2788–2797. <https://doi.org/10.1016/J.BIOMATERIALS.2009.12.033>.
- (117) Low, W.; Kenward, M. A.; Amin, M.; Martin, C. Ionically Crosslinked Chitosan Hydrogels for the Controlled Release of Antimicrobial Essential Oils and Metal Ions for Wound Management Applications. *Medicines* **2016**, *3* (1), 8. <https://doi.org/10.3390/medicines3010008>.
- (118) Gierszewska, M.; Ostrowska-Czubenko, J. Chitosan-Based Membranes with Different Ionic Crosslinking Density for Pharmaceutical and Industrial Applications. *Carbohydr. Polym.* **2016**, *153*, 501–511. <https://doi.org/10.1016/J.CARBPOL.2016.07.126>.
- (119) Luo, Y.; Wang, Q. Recent Development of Chitosan-Based Polyelectrolyte Complexes with Natural Polysaccharides for Drug Delivery. *Int. J. Biol. Macromol.* **2014**, *64*, 353–367. <https://doi.org/10.1016/J.IJBIOMAC.2013.12.017>.
- (120) Barroso, N.; Guaresti, O.; Pérez-Álvarez, L.; Ruiz-Rubio, L.; Gabilondo, N.; Vilas-Vilela, J. L. Self-Healable Hyaluronic Acid/Chitosan Polyelectrolyte Complex Hydrogels and Multilayers. *Eur. Polym. J.* **2019**, *120* (April), 109268. <https://doi.org/10.1016/j.eurpolymj.2019.109268>.
- (121) Tahtat, D.; Mahlous, M.; Benamer, S.; Khodja, A. N.; Oussedik-Oumehdi, H.; Laraba-Djebari, F. Oral Delivery of Insulin from Alginate/Chitosan Crosslinked by Glutaraldehyde. *Int. J. Biol. Macromol.* **2013**, *58*, 160–168. <https://doi.org/10.1016/j.ijbiomac.2013.03.064>.
- (122) Gonçalves, J. O.; Santos, J. P.; Rios, E. C.; Crispim, M. M.; Dotto, G. L.; Pinto, L. A. A. Development of Chitosan Based Hybrid Hydrogels for Dyes Removal from Aqueous Binary System. *J. Mol. Liq.* **2017**, *225*, 265–270. <https://doi.org/10.1016/J.MOLLIQ.2016.11.067>.
- (123) Singh, A.; Narvi, S. S.; Dutta, P. K.; Pandey, N. D. External Stimuli Response on a Novel Chitosan Hydrogel Crosslinked with Formaldehyde. *Bull. Mater. Sci.* **2006**, *29* (3), 233–238. <https://doi.org/10.1007/BF02706490>.

- (124) Sadeghi, M.; Hanifpour, F.; Taheri, R.; Javadian, H.; Ghasemi, M. Comparison of Using Formaldehyde and Carboxy Methyl Chitosan in Preparation of Fe₃O₄ Superparamagnetic Nanoparticles-Chitosan Hydrogel Network: Sorption Behavior toward Bovine Serum Albumin. *Process Saf. Environ. Prot.* **2016**, *102*, 119–128. <https://doi.org/10.1016/j.psep.2016.03.005>.
- (125) Wang, L.; Stegemann, J. P. Glyoxal Crosslinking of Cell-Seeded Chitosan/Collagen Hydrogels for Bone Regeneration. *Acta Biomater.* **2011**, *7* (6), 2410–2417. <https://doi.org/10.1016/j.ACTBIO.2011.02.029>.
- (126) Dimida, S.; Demitri, C.; De Benedictis, V. M.; Scalera, F.; Gervaso, F.; Sannino, A. Genipin-Cross-Linked Chitosan-Based Hydrogels: Reaction Kinetics and Structure-Related Characteristics. *J. Appl. Polym. Sci.* **2015**, *132* (28), 1–8. <https://doi.org/10.1002/app.42256>.
- (127) Gao, L.; Gan, H.; Meng, Z.; Gu, R.; Wu, Z.; Zhang, L.; Zhu, X.; Sun, W.; Li, J.; Zheng, Y.; et al. Effects of Genipin Cross-Linking of Chitosan Hydrogels on Cellular Adhesion and Viability. *Colloids Surfaces B Biointerfaces* **2014**, *117*, 398–405. <https://doi.org/10.1016/j.colsurfb.2014.03.002>.
- (128) Yuan, Y.; Chesnutt, B. M.; Utturkar, G.; Haggard, W. O.; Yang, Y.; Ong, J. L.; Bumgardner, J. D. The Effect of Cross-Linking of Chitosan Microspheres with Genipin on Protein Release. *Carbohydr. Polym.* **2007**, *68* (3), 561–567. <https://doi.org/10.1016/j.carbpol.2006.10.023>.
- (129) Artech Pujana, M.; Pérez-Álvarez, L.; Cesteros Iturbe, L. C.; Katime, I. Biodegradable Chitosan Nanogels Crosslinked with Genipin. *Carbohydr. Polym.* **2013**, *94* (2), 836–842. <https://doi.org/10.1016/j.carbpol.2013.01.082>.
- (130) Delmar, K.; Bianco-Peled, H. Composite Chitosan Hydrogels for Extended Release of Hydrophobic Drugs. *Carbohydr. Polym.* **2016**, *136*, 570–580. <https://doi.org/10.1016/J.CARBPOL.2015.09.072>.
- (131) Gao, L.; Gan, H.; Meng, Z.; Gu, R.; Wu, Z.; Zhu, X.; Sun, W.; Li, J.; Zheng, Y.; Sun, T.; et al. Evaluation of Genipin-Crosslinked Chitosan Hydrogels as a Potential Carrier for Silver Sulfadiazine Nanocrystals. *Colloids Surfaces B Biointerfaces* **2016**, *148*, 343–353. <https://doi.org/10.1016/J.COLSURFB.2016.06.016>.
- (132) Fadzallah, I. A.; Majid, S. R.; Careem, M. A.; Arof, A. K. A Study on Ionic Interactions in Chitosan–Oxalic Acid Polymer Electrolyte Membranes. *J. Memb. Sci.* **2014**, *463*, 65–72. <https://doi.org/10.1016/J.MEMSCI.2014.03.044>.

- (133) Liu, R.; Xu, X.; Zhuang, X.; Cheng, B. Solution Blowing of Chitosan/PVA Hydrogel Nanofiber Mats. *Carbohydr. Polym.* **2014**, *101*, 1116–1121. <https://doi.org/10.1016/J.CARBPOL.2013.10.056>.
- (134) Cho, I. S.; Cho, M. O.; Li, Z.; Nurunnabi, M.; Park, S. Y.; Kang, S.-W.; Huh, K. M. Synthesis and Characterization of a New Photo-Crosslinkable Glycol Chitosan Thermogel for Biomedical Applications. *Carbohydr. Polym.* **2016**, *144*, 59–67. <https://doi.org/10.1016/J.CARBPOL.2016.02.029>.
- (135) Rickett, T. A.; Amoozgar, Z.; Tucheck, C. A.; Park, J.; Yeo, Y.; Shi, R. Rapidly Photo-Cross-Linkable Chitosan Hydrogel for Peripheral Neurosurgeries. *Biomacromolecules* **2011**, *12* (1), 57–65. <https://doi.org/10.1021/bm101004r>.
- (136) Jin, R.; Moreira Teixeira, L. S.; Dijkstra, P. J.; Karperien, M.; van Blitterswijk, C. A.; Zhong, Z. Y.; Feijen, J. Injectable Chitosan-Based Hydrogels for Cartilage Tissue Engineering. *Biomaterials* **2009**, *30* (13), 2544–2551. <https://doi.org/10.1016/j.biomaterials.2009.01.020>.
- (137) Wang, K.; Fu, Q.; Chen, X.; Gao, Y.; Dong, K. Preparation and Characterization of PH-Sensitive Hydrogel for Drug Delivery System. *RSC Adv.* **2012**, *2* (20), 7772–7780. <https://doi.org/10.1039/c2ra20989f>.
- (138) Delaittre, G.; Guimard, N. K.; Barner-Kowollik, C. Cycloadditions in Modern Polymer Chemistry. *Acc. Chem. Res.* **2015**, *48* (5), 1296–1307. <https://doi.org/10.1021/acs.accounts.5b00075>.
- (139) Anseth, K. S.; Klok, H. A. Click Chemistry in Biomaterials, Nanomedicine, and Drug Delivery. *Biomacromolecules* **2016**, *17* (1), 1–3. <https://doi.org/10.1021/acs.biomac.5b01660>.
- (140) Espeel, P.; Du Prez, F. E. “click”-Inspired Chemistry in Macromolecular Science: Matching Recent Progress and User Expectations. *Macromolecules* **2015**, *48* (1), 2–14. <https://doi.org/10.1021/ma501386v>.
- (141) Meng, X.; Edgar, K. J. “Click” Reactions in Polysaccharide Modification. *Prog. Polym. Sci.* **2016**, *53*, 52–85. <https://doi.org/10.1016/j.progpolymsci.2015.07.006>.
- (142) Ado, O. L. O. R. Sequential Click Reactions for Synthesizing and Patterning Hydrogels Sequential Click Reactions for Synthesizing and Patterning Hydrogels. *Biomacromolecules* **2009**, *8* (8), 1–2.
- (143) Liang, L.; Astruc, D. The Copper(I)-Catalyzed Alkyne-Azide Cycloaddition (CuAAC) “Click” Reaction and Its Applications. An Overview. *Coord. Chem. Rev.* **2011**, *255* (23–24), 2933–2945.

<https://doi.org/10.1016/J.CCR.2011.06.028>.

- (144) Mullen, D. G.; McNerny, D. Q.; Desai, A.; Cheng, X. M.; Dimaggio, S. C.; Kotlyar, A.; Zhong, Y.; Qin, S.; Kelly, C. V.; Thomas, T. P.; et al. Design, Synthesis, and Biological Functionality of a Dendrimer-Based Modular Drug Delivery Platform. *Bioconjug. Chem.* **2011**, *22* (4), 679–689. <https://doi.org/10.1021/bc100360v>.
- (145) Mansfeld, U.; Pietsch, C.; Hoogenboom, R.; Becer, C. R.; Schubert, U. S. Clickable Initiators, Monomers and Polymers in Controlled Radical Polymerizations - A Prospective Combination in Polymer Science. *Polym. Chem.* **2010**, *1* (10), 1560–1598. <https://doi.org/10.1039/c0py00168f>.
- (146) Hu, X.; Li, D.; Zhou, F.; Gao, C. Biological Hydrogel Synthesized from Hyaluronic Acid, Gelatin and Chondroitin Sulfate by Click Chemistry. *Acta Biomater.* **2011**, *7* (4), 1618–1626. <https://doi.org/10.1016/J.ACTBIO.2010.12.005>.
- (147) Crescenzi, V.; Cornelio, L.; Di Meo, C.; Nardecchia, S.; Lamanna, R. Novel Hydrogels via Click Chemistry: Synthesis and Potential Biomedical Applications. *Biomacromolecules* **2007**, *8* (6), 1844–1850. <https://doi.org/10.1021/bm0700800>.
- (148) Codelli, J. A.; Baskin, J. M.; Agard, N. J.; Bertozzi, C. R. Second-Generation Difluorinated Cyclooctynes for Copper-Free Click Chemistry. *J. Am. Chem. Soc.* **2008**, *130* (34), 11486–11493. <https://doi.org/10.1021/ja803086r>.
- (149) Uliniuc, A.; Popa, M.; Hamaide, T.; Dobromir, M. New Approaches in Hydrogel Synthesis - Click Chemistry: A Review. *Cellul. Chem. Technol.* **2012**, *46* (1–2), 1–11.
- (150) Montiel-Herrera, M.; Gandini, A.; Goycoolea, F. M.; Jacobsen, N. E.; Lizardi-Mendoza, J.; Recillas-Mota, M.; Argüelles-Monal, W. M. N-(Furfural) Chitosan Hydrogels Based on Diels-Alder Cycloadditions and Application as Microspheres for Controlled Drug Release. *Carbohydr. Polym.* **2015**, *128*, 6–12. <https://doi.org/10.1016/j.carbpol.2015.03.052>.
- (151) Zhang, M.; Wang, J.; Jin, Z. Supramolecular Hydrogel Formation between Chitosan and Hydroxypropyl β -Cyclodextrin via Diels-Alder Reaction and Its Drug Delivery. *Int. J. Biol. Macromol.* **2018**, *114*, 381–391. <https://doi.org/10.1016/J.IJBIOMAC.2018.03.106>.
- (152) Meijer, A.; Otto, S.; Engberts, J. B. F. N. Effects of the Hydrophobicity of the Reactants on Diels-Alder Reactions in Water. *J. Org. Chem.* **1998**, *63* (24), 8989–8994. <https://doi.org/10.1021/jo981359x>.

- (153) Kotha, S.; Banerjee, S. Recent Developments in the Retro-Diels-Alder Reaction. *RSC Adv.* **2013**, *3* (21), 7642–7666. <https://doi.org/10.1039/c3ra22762f>.
- (154) Arslan, M.; Gevrek, T. N.; Sanyal, A.; Sanyal, R. Cyclodextrin Mediated Polymer Coupling via Thiol-Maleimide Conjugation: Facile Access to Functionalizable Hydrogels. *RSC Adv.* **2014**, *4* (101), 57834–57841. <https://doi.org/10.1039/c4ra12408a>.
- (155) Arslan, M.; Aydin, D.; Degirmenci, A.; Sanyal, A.; Sanyal, R. Embedding Well-Defined Responsive Hydrogels with Nanocontainers: Tunable Materials from Telechelic Polymers and Cyclodextrins. *ACS Omega* **2017**, *2* (10), 6658–6667. <https://doi.org/10.1021/acsomega.7b00787>.
- (156) Hoyle, C. E.; Bowman, C. N. Polymer Chemistry Thiol – Ene Click Chemistry ^{**} *Angewandte.* **2010**, 1540–1573. <https://doi.org/10.1002/anie.200903924>.
- (157) Campos, L. M.; Killops, K. L.; Sakai, R.; Paulusse, J. M. J.; Damiron, D.; Drockenmuller, E.; Messmore, B. W.; Hawker, C. J. Development of Thermal and Photochemical Strategies for Thiol-Ene Click Polymer Functionalization. *Macromolecules* **2008**, *41* (19), 7063–7070. <https://doi.org/10.1021/ma801630n>.
- (158) Hoyle, C. E.; Lowe, A. B.; Bowman, C. N. Thiol-Click Chemistry: A Multifaceted Toolbox for Small Molecule and Polymer Synthesis. *Chem. Soc. Rev.* **2010**, *39* (4), 1355–1387. <https://doi.org/10.1039/b901979k>.
- (159) Lowe, A. B. Thiol-Ene “Click” Reactions and Recent Applications in Polymer and Materials Synthesis: A First Update. *Polym. Chem.* **2014**, *5* (17), 4820–4870. <https://doi.org/10.1039/c4py00339j>.
- (160) Bi, X.; Liang, A.; Tan, Y.; Maturavongsadit, P.; Higginbotham, A.; Gado, T.; Gramling, A.; Bahn, H.; Wang, Q. Thiol-Ene Crosslinking Polyamidoamine Dendrimer-Hyaluronic Acid Hydrogel System for Biomedical Applications. *J. Biomater. Sci. Polym. Ed.* **2016**, *27* (8), 743–757. <https://doi.org/10.1080/09205063.2016.1159473>.
- (161) Liu, Z. Q.; Wei, Z.; Zhu, X. L.; Huang, G. Y.; Xu, F.; Yang, J. H.; Osada, Y.; Zrínyi, M.; Li, J. H.; Chen, Y. M. Dextran-Based Hydrogel Formed by Thiol-Michael Addition Reaction for 3D Cell Encapsulation. *Colloids Surfaces B Biointerfaces* **2015**, *128*, 140–148. <https://doi.org/10.1016/J.COLSURFB.2015.02.005>.
- (162) Li, R.; Cai, Z.; Li, Z.; Zhang, Q.; Zhang, S.; Deng, L.; Lu, L.; Li, L.; Zhou, C.

- Synthesis of In-Situ Formable Hydrogels with Collagen and Hyaluronan through Facile Michael Addition. *Mater. Sci. Eng. C* **2017**, *77*, 1035–1043. <https://doi.org/10.1016/j.msec.2017.04.046>.
- (163) Fan, Y.; Deng, C.; Cheng, R.; Meng, F.; Zhong, Z. In Situ Forming Hydrogels via Catalyst-Free and Bioorthogonal “Tetrazole-Alkene” Photo-Click Chemistry. *Biomacromolecules* **2013**, *14* (8), 2814–2821. <https://doi.org/10.1021/bm400637s>.
- (164) Jirawutthiwongchai, J.; Krause, A.; Draeger, G.; Chirachanchai, S. Chitosan-Oxanorbornadiene: A Convenient Chitosan Derivative for Click Chemistry without Metal Catalyst Problem. *ACS Macro Lett.* **2013**, *2* (3), 177–180. <https://doi.org/10.1021/mz400006j>.
- (165) Piluso, S.; Hiebl, B.; Gorb, S. N.; Kovalev, A.; Lendlein, A.; Neffe, A. T. Hyaluronic Acid-Based Hydrogels Crosslinked by Copper-Catalyzed Azide-Alkyne Cycloaddition with Tailorable Mechanical Properties. *Int. J. Artif. Organs* **2011**, *34* (2), 192–197. <https://doi.org/10.5301/IJAO.2011.6394>.

CHAPTER II

MATERIALS AND CHARACTERIZATION TECHNIQUES AND METHODS

II.1. MATERIALS	49
II.2. CHARACTERIZATION TECHNIQUES AND METHODS	52
II.2.1. CHARACTERIZATION OF CHITOSAN	52
II.2.2. PHYSICO-CHEMICAL CHARACTERIZATION	54
II.2.2.1. Fourier transformed infrared spectroscopy	54
II.2.2.2. Nuclear magnetic resonance spectroscopy	55
II.2.2.2.1. Liquid-state ^1H NMR measurements	55
II.2.2.2.2. Solid-state ^{13}C NMR measurements	56
II.2.2.3. X-ray diffraction	56
II.2.3. LIGHT-BASED CHARACTERIZATION TECHNIQUES	57
II.2.3.1. Ultraviolet-visible spectrophotometry	57
II.2.3.1.1. Monitorization of the click reactions	57
II.2.3.1.2. Ninhydrin assay for thiol-functionalized chitosan	58
II.2.3.1.3. Ellman's test for thiol-functionalized chitosan	59
II.2.3.2. Fluorescence spectrophotometry	59
II.2.3.3. Nanoparticle analyser	60
II.2.3.3.1. Dynamic light scattering	60
II.2.3.3.2. Zeta Potential	61
II.2.4. THERMOGRAVIMETRIC ANALYSIS	61
II.2.5. MORPHOLOGICAL AND DIMENSIONAL CHARACTERIZATION	61
II.2.5.1. Scanning electron microscopy	61
II.2.5.2. Transmission electron microscopy	62
II.2.5.3. Atomic force microscopy	62
II.2.5.3.1. Roughness	62
II.2.5.3.2. Morphology of nanogels	63
II.2.6. SWELLING CAPACITY	63
II.2.6.1. Swelling parameters	64

II.2.6.2. pH-sensitivity	64
II.2.7. GEL FRACTION	64
II.2.8. ENZYMATIC AND HYDROLYTIC DEGRADATION STUDIES	65
II.2.9. RHEOLOGICAL CHARACTERIZATION	66
II.2.9.1. Gelation time	66
II.2.9.2. Frequency sweep test	66
II.2.9.2.1. Network parameters	67
II.2.9.3. Shear thinning	67
II.2.9.4. Yield point	68
II.2.9.5. Self-healing ability	68
II.2.10. SPECIFIC CHARACTERIZATION	69
II.2.10.1. Drug delivery measurements	69
II.2.10.2. Mucoadhesion capacity	70
II.2.10.3. Antibacterial activity	71
II.2.10.4. <i>In vitro</i> cell response evaluation	72
II.2.10.4.1. Cytotoxicity	72
II.2.10.4.2. Cell adhesion and viability	73
REFERENCES	74

II. MATERIALS AND CHARACTERIZATION TECHNIQUES AND METHODS

Hereafter, the compounds used for hydrogel synthesis and the description of the characterization techniques and methods used during the development of this thesis are presented, as well as the conditions of analysis used and the preparation of the samples. Thereby, physico-chemical, thermal, morphological, rheological and other specific properties are detailed. Moreover, the procedures employed for swelling, degradation, drug delivery and mucoadhesion studies, as well as the protocol employed for the *in vitro* cell response evaluation are presented. Physico-chemical properties were mostly related to the chitosan derivatives, while the remaining characterization was focused of the synthesized chitosan-based hydrogels and nanogels.

II.1. MATERIALS

The principal polymer used in this thesis was chitosan (Cs). Different batches were employed throughout the thesis; all of them were purchased from Sigma-Aldrich. Chitosan was modified by the reaction of its free amino groups in aqueous solution following different pathways.

Regarding Diels-Alder clicked hydrogels, for the functionalization of chitosan with furan groups (CsFu), furfural (Fu, 99 %, Sigma-Aldrich) and sodium borohydride (NaBH_4 , ≥ 99 %, Sigma-Aldrich) were used; whereas for the maleimide-functionalized chitosan (CsAMI), β -alanine (99 %, Sigma-Aldrich) and maleic anhydride (98 %, Panreac) were employed to develop a maleimide-based acid (AMI)¹. In the case of the thiol-Michael addition reaction, the functionalization of chitosan with thiol groups (CsSH) was carried out using thiolactic acid (TLA, 95 %, Sigma-Aldrich). For the incorporation of tetrazole groups into the main chain of chitosan (CsTZ), 4-formylbenzoic acid (98 %, Alfa), *p*-toluenesulfonyl hydrazide (98 %, Alfa), *p*-Anisidine (≥ 99 %, Sigma-

Aldrich), sodium nitrite (NaNO_2 , 98 %, Merck) and pyridine (99.5 %, Acros) were used in order to synthesized a tetrazole-based acid (TBA)².

Bismaleimide (BMI) acted as a cross-linker in both Diels–Alder and thiol–Michael addition reactions. This bifunctional cross-linker was prepared from Jeffamine[®] ED 900 polyetheramine (900 g mol^{-1} average molar mass, Huntsman). The ED Jeffamine[®] series are water-soluble aliphatic polyether diamines composed by poly(propylene oxide)–poly(ethylene oxide)–poly(propylene oxide) (PPO–PEO–PPO) in this case that have been shown to be biocompatible and could impart amphiphilic and thermoresponsive properties to the hydrogels³. The BMI was synthesized by the modification of Jeffamine[®] with maleic anhydride (98 %, PanReac) using triethylamine (Et_3N), sodium acetate trihydrate (CH_3COONa , ≥ 99 %, Sigma–Aldrich) and acetic anhydride (Ac_2O , PanReac) following a two-step procedure^{3,4}, in order to obtain the necessary dienophiles for hydrogel formation.

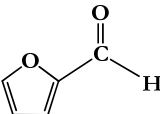
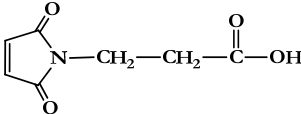
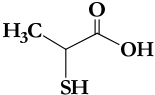
Thiolated nanogels were prepared by reverse nanoemulsion technique after cross-linking with a biocompatible cross-linking agent, namely, PEGBCOOH (poly(ethylene glycol)bis(carboxymethyl)ether, 600 g mol^{-1} average molar mass, Sigma–Aldrich) using Triton X-100 (Sigma–Aldrich) as emulsifying agent, cyclohexane (for synthesis 98 %, PanReac) as oleic phase and hexanol (for synthesis 98 %, Sigma–Aldrich) as co-surfactant. The functionalization of the nanogels with folate moieties was carried out via thiol–Michael addition reaction between the localized thiol groups on nanogels surface and the maleimide groups present on Folate–PEG–Mal compound (Folate–poly(ethylene glycol)–Maleimide, 2000 g mol^{-1} average molar mass, Nanosoft Biotechnology).

Several common solvents and reagents were employed during the thesis, either to prepare solutions for further characterization, as reaction media or for dialysis: glacial acetic acid (HAc, PanReac), sodium hydroxide solution (NaOH , 1M,

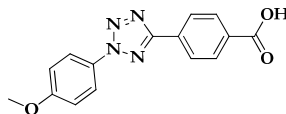
PanReac), sodium hydroxide pellets (98 %, PanReac), hydrochloric acid solution (HCl, for analysis 37 %, PanReac), dichloromethane (DCM, for HPLC, Lab Scan Analytical Sciences), ethyl acetate (for analysis, PanReac), chloroform (Lab Scan Analytical Sciences), acetone (Oppac S.A.), ethanol (for analysis 96 % v/v extra pore, Scharlau), phosphate buffered saline tablets (PBS, pH = 7.4, PanReac), sodium chloride (NaCl, PanReac), anhydrous N,N-dimethylformamide (DMF, Acros), dimethyl sulfoxide (DMSO, VWR), N-hydroxysuccinimide (NHS, 98 %, Sigma-Aldrich) and N-(3-dimethylaminopropyl)-N'-ethylcarbodiimide hydrochloride (EDC, purum \geq 98 %, Sigma-Aldrich). Deuterium oxide (deuterium degree 99.96 %, Merck) was used for ^1H NMR analysis. Deionized water was employed as solvent. The commercially available compounds and solvents were employed as received, without further purification.

Table II.1 shows the chemical structure of the most relevant compounds used throughout this work.

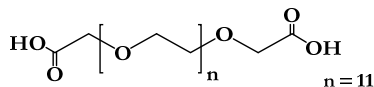
Table II.1. Chemical structure of some of the compounds used in this thesis.

Compound	Chemical structure
Furfural (Fu)	
3-(2,5-dioxo-2H-pyrrol-1(5H)-yl)propanoic acid (AMI)	
Thiolactic acid (TLA)	

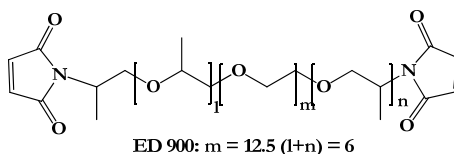
4-(2-(4-methoxyphenyl)-2H-tetrazol-5-yl)benzoic acid (TBA)



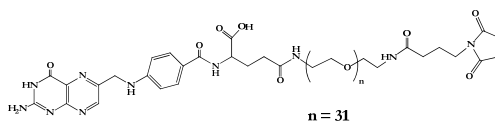
Poly(ethylene glycol)bis(carboxymethyl)ether (PEGBCOOH)



Bismaleimide (BMI)



Folate-poly(ethylene glycol)-Maleimide (Folate-PEG-Mal)



II.2. CHARACTERIZATION TECHNIQUES AND METHODS

II.2.1. Characterization of chitosan

The final behaviour of the obtained hydrogels strongly depend on the characteristics of the original biopolymer. Therefore, it was of great relevance to deepen on the properties of neat chitosan. Different batches of chitosan were used for the synthesis of hydrogels, each of them with individual degree of deacetylation (DDc) and average molecular weight (M_w).

The degree of acetylation (DAc) of the different chitosan batches was calculated from the ^1H NMR spectrum of each sample, from the ratio between the area (A) of the signal corresponding to the protons of the methyl group (3) and the sum of the areas of the protons related to the carbons 2 to 6 ($\text{H}_2\text{--H}_6$) from the chitosan ring structure (6) according to Equation II.1⁵. The degree of deacetylation (DDc) was then calculated as the difference with DAc.

$$\text{DAc (\%)} = \left(\frac{2 \cdot A_{\text{CH}_3}}{A_{\text{H}_2-\text{H}_6}} \right) \cdot 100 \quad (\text{II.1})$$

The average molecular weight (M_w) of the different chitosan batches used for the development of the clicked hydrogels was estimated by a general viscosimetry method following Mark–Houwink–Sakurada equation (Equation II.2), which represents the relationship between the intrinsic viscosity $[\eta]$ and the average molecular weight^{6,7}. Thus, the above–mentioned procedure is based on the measurements of the intrinsic viscosity of chitosan in a common solvent. A solution of 0.3 M acetic acid (HAc)/0.2 M sodium acetate trihydrate was used as solvent, being one of the best solvents with respect to the molecular dissolution of chitosan and prevention of aggregation. Viscosity measurements were carried out using an automated capillary viscometer equipped with a jacket to control the temperature and was maintained at 25 °C. The intrinsic viscosity depends on the specific volume of the polymer, which is related to its molecular weight and the polymer–solvent interactions.

$$[\eta] = K \cdot M_w^\alpha \quad (\text{II.2})$$

where K and α are constants that are characteristic for a particular polymer–solvent system at a specific temperature and $[\eta]$ is the intrinsic viscosity of the polymer in that solution. Constants K and α are dependent on the temperature and deacetylation degree of chitosan and are valid for a certain range of molecular weights, being tabulated for common polymer–solvent pairs⁷. For chitosans in study, with respect to DDC, molecular weight and solvent of acetic acid/sodium acetate, the K and α parameters were 0.03466 mL g⁻¹ and 0.845, respectively.

Therefore, the principal properties of the employed chitosan batches are summarized in Table II.2. The value of the molecular weight took special relevance in the present thesis due to the strong relationship with the ability to form robust

hydrogels. Indeed, it is the main parameter to be considered in the first place and will determine the consistency of the final materials. Regarding the degree of deacetylation, the corresponding values are in general high in all the samples and can be considered to affect the hydrogels in the same way.

Table II.2. Physico-chemical properties (molecular weight (M_w) and degree of deacetylation (DDc)) of the employed chitosan batches.

Reaction	Chitosan derivative	Molecular weight range	M_w (kDa)	DDc (%)
Diels-Alder (Chapter IV)	CsFu/CsAMI	Medium	58	81
Michael addition (Chapter V)	CsSH	Medium	680	77
NITEC reaction (Chapter VI)	CsTZ/CsAMI	Low	67	80
Thiolated nanogels (Chapter VII)	CsSH	Low	39	73

Moreover, the degree of deacetylation directly influences the degree of crystallinity of the chitosan: the higher the DDc, the lower the degree of crystallinity. Accordingly, the crystallinity index was calculated from the Equation II.6 (detailed below) and it was found that the values ranged from 0.66 to 0.77 for the different chitosan batches, coinciding the highest values with the least deacetylated samples. The resulting values were in agreement with reported literature, where the crystallinity index of chitosan samples can vary within a wide range from 0.4 to 0.88⁹.

II.2.2. Physico-chemical characterization

II.2.2.1. Fourier transformed infrared spectroscopy

Fourier transformed infrared (FTIR) spectroscopy was used to identify the characteristic functional groups and hydrogen bonding interactions of the samples. This technique is based on irradiating the sample with an infrared light source. In

this way, the light absorbed by the freeze-dried sample is reflected in the spectrum at different wavenumbers. Spectra were recorded at room temperature using a Nicoler Nexus spectrophotometer provided with a Specac MKII Golden Gate accessory equipped with a diamond crystal at a nominal incident angle of 45° and ZnSe lens. Measurements were run after averaging 32 scans with a resolution of 4 cm⁻¹ in the range from 4000 to 600 cm⁻¹.

II.2.2.2. Nuclear magnetic resonance spectroscopy

The chemical structure of the neat chitosan samples and the presence of specific reactive groups grafted into the biopolymer chain after modification were investigated using proton and carbon nuclear magnetic resonance (¹H and ¹³C NMR). This technique is based on the application of an electromagnetic field and the analysis of the variation in the frequencies of proton or carbon nucleus.

II.2.2.2.1. Liquid-state ¹H NMR measurements

Liquid-state ¹H NMR measurements were conducted with an Avance Bruker 500 spectrometer equipped with a BBO probe with gradient in Z axis, at a frequency of 500 MHz, number of scans 64, spectral window of 5000 Hz and recovery delay of 1 s. A mixture of D₂O/HCl (0.5 M) in 1:10 (v/v) ratio at 80 °C was employed as solvent.

Furthermore, nuclear magnetic resonance spectroscopy spectra (¹H NMR) were also employed to calculate the degrees of substitution (DS) of both the furan and the maleimide modified chitosan derivatives (Chapter IV). Thus, the degree of substitution of each derivative was calculated from the areas (A) of the proton signals corresponding to the furan or maleimide ring and those of the glucosamine repeating unit from the carbons that were not affected by the functionalization (3 to 6), with a 5/3 and 5/2 ratio between them, respectively.

Namely, Equation II.3 and II.4 were applied based on a previously reported procedure¹⁰.

$$DS_{CsFu}(\%) = \left(\frac{5 \cdot A_{Fu}}{3 \cdot A_{Cs}} \right) \cdot 100 \quad (\text{II.3})$$

$$DS_{CsAMI}(\%) = \left(\frac{5 \cdot A_{AMI}}{2 \cdot A_{Cs}} \right) \cdot 100 \quad (\text{II.4})$$

II.2.2.2.2. Solid–state ¹³C NMR measurements

Solid–state ¹³C NMR measurement was conducted for tetrazole–functionalized chitosan due to solubility limitations. Solid–state spectra were recorded on a Bruker AVANCE III, 9.4 T equipped with a MASDVT BL4 X//H Probe head at a spinning rate of 10 kHz. ¹³C chemical shifts were calibrated indirectly with glycine. The spectra were recorded with a delay between scans of 15 s and the number of scans were 10240.

For the tetrazole–functionalized chitosan (¹³C NMR) (Chapter VI) the DS was determined by the integration of the areas of the carbon signals of the glucosamine units and those of the tetrazole unit that were not affected (3 to 5), with a 3/11 ratio between them. Calculations were made using Equation II.5.

$$DS_{CsTZ}(\%) = \left(\frac{3 \cdot A_{TZ}}{11 \cdot A_{Cs}} \right) \cdot 100 \quad (\text{II.5})$$

II.2.2.3. X–ray diffraction

All neat chitosan samples and their derivatives were analysed by X–ray diffraction (XRD) in order to assess the effect of the functionalization on the crystalline structure of original biopolymer. The XRD patterns were measured using

PHILIPS X'Pert Pro automatic diffractometer, in theta–theta configuration secondary monochromator with Cu K α radiation ($\lambda = 0.154$ nm) and a PIXcel solid state detector (active length in $2\theta = 3.347^\circ$), operating at 40 kV with a filament of 40 mA. The diffractograms were collected in the region $2\theta = 5^\circ$ to 80° , where θ is the angle of incidence of the X–ray beam on the sample. The crystallinity index (CI^{XRD}) was calculated using Equation II.6.

$$CI^{XRD} = \frac{I_{110} - I_{am}}{I_{110}} \quad (II.6)$$

where I_{110} is the maximum intensity (arbitrary units) of the (110) diffraction peak at $2\theta = 20^\circ$ and I_{am} is the intensity of the amorphous diffraction signal at $2\theta = 16^\circ$ ^{8,11–13}.

II.2.3. Light–based characterization techniques

II.2.3.1. Ultraviolet–visible spectrophotometry

UV–vis spectrophotometry refers to absorption spectroscopy using light in the visible and adjacent ranges for the quantitative determination of different analytes. The spectrophotometer used was the UV–3600/3100 from Shimadzu.

II.2.3.1.1. Monitorization of the click reactions

The UV–vis spectrophotometry was used to monitorize different reactions involving maleimide groups. Namely, either the DA cycloaddition between furan–functionalized chitosan and maleimide–functionalized chitosan or bismaleimide cross–linker (Chapter IV) and the incorporation of Folate–PEG–Mal into the surface of thiolated nanogels through MA reaction (Chapter VII) were confirmed by this technique. In both cases the consumption of the maleimide groups when reacting was measured. For the DA cycloadditions, the spectrometer was equipped with a thermoelectric cell holder at 65°C , operating

in a scan range of 200–600 nm with a 0.1 mm optical path quartz cuvette, where gel-like state samples were placed. UV spectra were taken every 30 min for 24 h. In the case of the thiol–Michael addition between thiolated nanogels and Folate–PEG–Mal, diluted samples were analysed in a scan range of 200–600 nm in a 10 mm optical path quartz cuvette every hour for 24 h.

Unfortunately, the thiol–Michael addition reaction between the thiolated chitosan and the maleimide (Chapter V) resulted too fast and it was not possible to follow it by this technique. In the case of the NITEC reaction between tetrazole/maleimide groups (Chapter VI), the presence of several chromophore groups in both precursors can interfere in the measurement, being unreliable for this particular case.

II.2.3.1.2. Ninhydrin assay for thiol-functionalized chitosan

The extent of amine substitution was quantitatively determined by using UV–vis spectroscopy for the thiol-functionalized chitosan sample (Chapter V) following the mathematical model proposed by Shitrit and Bianco–Peled¹⁴ and the method proposed by Mahmood et al. with several modifications¹⁵. Thus, in order to quantify the thiolation degree, ninhydrin reagent was reacted with the primary free amino groups of chitosan to form a coloured reaction product that show an absorbance signal at 570 nm. From starting solutions of chitosan and thiol-functionalized chitosan at a concentration of 0.15 % (w/v) in a mixture of 2 % (v/v) acetic acid, 1 % (w/v) acetic acid/acetate buffer (pH 5.5) and ninhydrin reagent solution (2 % solution, Sigma–Aldrich), a set of solutions at different concentrations (0.1–0.03 mg mL⁻¹) was prepared. The final mixtures were incubated at 100 °C for 20 min. Samples were cooled down in an ice bath and the absorbance was measured. The degree of substitution (DS) was determined by Equation II.7, taking into account the slope (*m*) of absorption vs. concentration

curves, which was empirically found to be proportional to the percentage of free amino groups.

$$DS_{CsSH}(\%) = \left(1 - \frac{m_{CsSH}}{m_{Cs}} \right) \cdot 100 \quad (II.7)$$

where m_{CsSH} is the value of the slope of the modified polymer curve and m_{Cs} is the value of the slope of the neat polymer curve.

II.2.3.1.3. Ellman's test for thiol-functionalized chitosan

The amount of thiol groups immobilized on CsSH (Chapter V) was also quantified photometrically by Ellman's test. In brief, 250 μ L of 0.1 % (w/v) CsSH in 1 Mm EDTA/0.1 M sodium phosphate buffer (pH 8) were reacted with 50 μ L of Ellman's buffer ((5,5'-Dithiobis(2-nitrobenzoic acid)), \geq 98 %, Sigma-Aldrich) at a 0.4 % (w/v) concentration, and mixed to a final volume of 2.8 mL. After an incubation of 4 h at room temperature in dark, the absorbance of the sample was measured at 420 nm. The amount of immobilized thiol moieties was calculated using a standard curve obtained from an increasing concentration of thiolactic acid.

II.2.3.2. Fluorescence spectroscopy

Fluorescence spectroscopy is used to analyse the fluorescence properties of a sample by determining the concentration of an analyte in a sample when passing a light of a specific wavelength. Therefore, this technique involves the use of a beam of light, commonly ultraviolet light, that excites electrons in certain molecules or atoms and causes the emission of, typically but not necessarily, visible light. The amount of light that is absorbed by the sample (excitation spectrum) and the amount of light that is emitted by the sample (emission spectrum) can be quantified. Fluorescence emission spectra were recorded on a

Cary Eclipse Fluorescence Spectrophotometer (Agilent Technologies) at an excitation wavelength of 396 nm for the tetrazole/maleimide hydrogels and both chitosan derivatives separately as reference (Chapter VI). The influence of the irradiation time (after 1 and 2 hours of reaction) and the solvent (HCl and PBS) on the fluorescent properties of the tetrazole/maleimide hydrogels was studied. Thin dried samples were placed in a micro quartz cuvette of 200 μL in a 45° angle, which was placed in the sample holder. The spectra were recorded from 380 nm to 700 nm at an excitation slit width of 5 nm, an emission slit width of 5 nm, a resolution of 1 nm and a scan rate of 600 nm min^{-1} .

II.2.3.3. Nanoparticle analyser

A pH sensitivity study was performed measuring at the same time the size variation of the swollen nanogels based on the pH and the zeta potential of the nanogels at the different pH values (Chapter VII). Both the hydrodynamic radius in dynamic light scattering (DLS) and the zeta potential were measured at room temperature with a Zetasizer Nano Z (Malvern Instruments Ltd.). The synthesized nanogels were dispersed with a concentration of 0.04 mg mL^{-1} in an aqueous solution of HAc (1% v/v) and were kept under constant magnetic stirring for one week. After that time, samples were measured. The pH of the medium was varied by the dropwise addition of different NaOH solutions with different molarities depending on the pH to be achieved. Data were obtained from the average of at least ten measurements in specialized cells from Malvern Instruments (DTS1070). The uncertainties of the measurements represented the standard deviation of the mean of the replicate runs.

II.2.3.3.1. Dynamic light scattering

The dynamic light scattering (DLS) technique was used to determine the hydrodynamic radius of the synthesized nanogels in their swollen state. DLS method determines the size of extremely small particles in the submicron range, which are found in Brownian motion in suspension. Interference occurs within the light which

is scattered by the different particles. The interference changes over time and leads to variation of the scattered light intensity. Therefore, the time dependency of the scattered light intensity depends on the motion speed of the particles and, thus, on the particle size, which is usually analysed via autocorrelation. The scattering light was recorded at 90 ° angle to the incident laser light.

II.2.3.3.2. Zeta Potential

The zeta potential (ζ -potential) provides information on the distribution of the surface charge at the solid/water interface. Namely, when a solid surface is immersed in a polar liquid medium, electric charge can be generated at the solid/liquid interface. When a dispersion is subjected to the laser diffraction process while controlling the electric field that is applied, the diffracted light will be related to the applied field. By measuring the frequency change in diffracted light, the zeta potential analyzers determine the charge on the particles, which favours their dispersibility.

II.2.4. Thermogravimetric analysis

The thermal degradation process of the sample is controlled by measuring the mass of the sample in a microbalance during a heating scan. Thereby, the evolution of the mass loss regarding the initial mass of the sample can be quantified. Measurements were performed by using a TGA/DSC3+ Mettler Toledo analyser. Samples of about 5 mg were submitted to a 10 °C min⁻¹ heating rate from 25 to 800 °C under nitrogen atmosphere in order to prevent the thermoxidative degradation.

II.2.5. Morphological and dimensional characterization

II.2.5.1. Scanning electron microscopy

Scanning electron microscopy (SEM) consists on irradiating the surface of the samples with a high-energy electron beam, in order to analyse the different signals

obtained from the electron-sample interactions. The microstructure of all the different hydrogels was studied and the pore size distribution was obtained. Prior to SEM assay, samples were fractured in order to expose the cross-section and coated with approximately 20 nm of chromium using a Quorum Q150 TES metallizer. SEM experiments were performed by a JEOL JSM-6400 with a wolframium filament operating at an accelerated voltage of 20 kV and at a working distance of 15 mm.

II.2.5.2. Transmission electron microscopy

Transmission electron microscopy (TEM) employs an electron beam to visualise the sample in transmission mode. In order to study the morphology and size, TEM analysis of the nanogels was performed using a transmission electron microscope Philips CM120 Biofilter operating at 120 kW. A solution drop of acidic aqueous (HAc, 1 % v/v) dispersion of nanogels (0.04 mg mL^{-1}) was settled on a carbon-coated TEM grid and it was dried and glow-discharged in a high vacuum chamber.

II.2.5.3. Atomic force microscopy

Atomic force microscopy (AFM) is based on the quality of the interactions between the tip and the sample. Namely, the attractive-repulsion forces between the tip and the sample create a deflection in the tip, creating images by mapping the deflections in each point.

II.2.5.3.1. Roughness

AFM was used to characterize the topographic features in order to study the surface roughness of the final hydrogels. Images were obtained in a Bruker Dimension ICON scanning probe microscope equipped with a Nanoscope V controller, operating in peak force tapping mode. An integrated silicon nitride tip/cantilever frequency of around 70 kHz and a spring constant of 0.4 N/m was

used, performing measurements at a scan rate of 0.5 Hz s^{-1} with 512 scan lines. A sharp-edged tool was used to obtain a smooth surface of the samples.

II.2.5.3.2. Morphology of nanogels

AFM imaging was also used to characterize the size and the morphology of the nanogels (Chapter VII). Images were obtained at room temperature with a Bruker Dimension ICON scanning probe microscope equipped with a Nanoscope V controller, operating in tapping mode using silicon TESP-V2 tips having a resonance frequency at approximately 320 kHz and a cantilever spring constant about 42 N/m. A solution drop of acidic aqueous (HAc, 2% v/v) of nanogels ($5 \cdot 10^{-4} \text{ mg mL}^{-1}$) dispersed during 7 days was settled on a mica disk and it was dried at ambient temperature.

II.2.6. Swelling capacity

The swelling capacity of freeze-dried hydrogels was studied by a general gravimetric method. Samples were immersed in different medium, PBS (pH 7.4) and 0.1 M HCl (pH 1), simulating intestinal and gastric fluids, respectively) at 37°C . At selected time intervals after immersion (15 min, 30 min, 1 h, 2 h, 24 h or 48 h), the swollen samples were removed, weighed once the excess of liquid was withdrawn with filter paper and again freeze-dried. The equilibrium swelling was considered to be achieved when the weight of the hydrogels no longer increased. The swelling ratio (SR) was calculated using the following Equation II.8.

$$\text{SR (\%)} = \left(\frac{W_s - W_d}{W_d} \right) \cdot 100 \quad (\text{II.8})$$

where W_s and W_d are the weight of the swollen and final freeze-dried hydrogel samples, respectively. The assay was conducted in triplicate.

II.2.6.1. Swelling parameters

The swelling kinetics of the hydrogels was adjusted following a previously reported method for this type of materials, which is based on Equation II.9¹⁶.

$$\frac{t}{SR} = \frac{1}{SR_{\max}^2 \cdot k_s} + \frac{1}{SR_{\max}} \cdot t \quad (\text{II.9})$$

where SR is the swelling degree at time t, SR_{\max} the maximum swelling value and k_s ($\text{g}_{\text{hydrogel}} \text{g}_{\text{solution}}^{-1} \text{s}^{-1}$) the swelling constant rate. The initial swelling rate (r_0 , $\text{g}_{\text{solution}} \text{g}_{\text{hydrogel}}^{-1} \text{s}^{-1}$) was obtained from $1/(SR_{\max}^2 \cdot k_s) = 1/(dSR/dt)_0$. The swelling process in all cases followed second order kinetics with correlation coefficients above 0.99.

II.2.6.2. pH-sensitivity

The response of hydrogels to the environmental pH was studied by performing pulsatile swelling tests at 37 °C in NaOH 0.01 M (pH 12) and HCl 0.01 M (pH 2). Freeze-dried samples were first swollen in the HCl solution for 20 minutes and their swollen weight was monitored every 7 minutes. Subsequently, the samples were transferred to the NaOH solution and the swelling was monitored following the same procedure. Finally, the swelling capacity of the samples in study at each pH was measured according to the Equation II.8 after freeze-drying. The alternative immersion was repeated three times so that an extreme swelling/shrinking behaviour was ensured. The pH-dependency of the swelling was studied in a total period of 2 h of incubation in both media. The assay was conducted in triplicate.

II.2.7. Gel fraction

The insoluble fraction of the cross-linked materials was estimated as the gel fraction (%). The hydrogels were immersed in PBS at 37 °C for 3 h, based on the

equilibrium swelling time from previous swelling studies which was independent of the nature of each system. The sol–gel ratio of the hydrogels was determined by Equation II.10.

$$\text{Gel (\%)} = \frac{W_t}{W_0} \cdot 100 \quad (\text{II.10})$$

where W_0 and W_t are the initial and final weights of the hydrogel sample referred to the dry state.

II.2.8. Enzymatic and hydrolytic degradation studies

Degradation studies were carried out by gravimetric analysis according to a method described elsewhere^{16–19}. Dried samples (4–10 mg) were weighed (W_0) and immersed in PBS for prescribed days at 37 °C with 1 mg mL⁻¹ lysozyme (≥ 40000 units mg⁻¹ protein from chicken egg white). Samples were removed at fixed time intervals (2, 7, 14, 21 and 28 days) and washed out with deionized water to eliminate any superficial buffer and lysozyme traces. Samples were finally dried and weighed until constant value (W_t). Hydrolytic degradation was also studied as the control reference by incubation in lysozyme–free PBS solution at the same conditions. The measurements were performed in triplicate and the weight loss of the samples was calculated using Equation II.11.

$$\text{Degradation (\%)} = \left(\frac{W_0 - W_t}{W_0} \right) \cdot 100 \quad (\text{II.11})$$

where W_0 and W_t are the dried weights of the samples at initial and final time, respectively.

II.2.9. Rheological characterization

II.2.9.1. Gelation time

The gel point was considered as the time where the curves of storage (G') and loss (G'') modulus crossover at a fixed temperature and frequency^{20,21}. The gelation time was studied by dynamic oscillatory viscoelastic measurements performed in a Haake Viscotester IQ using the parallel plate geometry (titanium upper plate of 35 mm and steel lower plate of 60 mm) at 65 °C or 37 °C, depending on the reaction conditions. The viscometer was equipped with a Peltier cooling system for the better temperature and humidity control and a solvent trap. Additionally, solvent evaporation was prevented by applying low-viscosity oil to the periphery of the sample holder. The evolution of storage (G') and loss (G'') modulus was measured in the linear viscoelastic region (LVR), at constant temperature and a shear strain of 1 % (determined by previous stress sweep experiments) at 1 Hz.

II.2.9.2. Frequency sweep test

The dynamic rheological behaviour of the synthesized hydrogels was studied by frequency sweep tests. Thereby, the storage modulus (G'), loss modulus (G'') and the damping factor ($\tan \delta$) of the final hydrogels were calculated by oscillatory rheometry using a Rheometric Scientific Advanced Rheometric Expansion System (ARES) and parallel plate geometry (diameter 25 mm) as described, in oscillation mode at 37 °C. After the determination of the linear viscoelastic region (LVR) from stress sweep study, frequency sweep analyzes were evaluated from 0.1 to 500 rad s⁻¹ at a fixed strain of 1 % for DA and NITEC-based hydrogels or 10 % for the MA hydrogels. The damping factor describes the ratio between the two portions of the viscoelastic behaviour (G' and G''), i.e. for ideally elastic behaviour $\tan \delta = 0$ whereas $\tan \delta = 1$ for ideally viscous behaviour.

II.2.9.2.1. Network parameters

Based on the rheological results, the structural parameters of the developed chitosan-based hydrogels were determined. The average mesh size (ξ , nm), the cross-linking density (n_e , mol m⁻³) and the average molecular weight between neighbouring cross-links (M_c , kg mol⁻¹), were calculated based on the so-called rubber elastic theory (RET) from Equation II.12, II.13 and II.14, respectively²².

$$\xi = \left(\frac{G' \cdot N_A}{RT} \right)^{-1/3} \quad (\text{II.12})$$

$$n_e = \frac{G_e}{RT} \quad (\text{II.13})$$

$$M_c = \frac{c\rho RT}{G_e} \quad (\text{II.14})$$

where G' is the storage modulus, N_A is the Avogadro constant ($6.022 \cdot 10^{23}$), R is the gas constant ($8.314 \text{ J K}^{-1} \text{ mol}^{-1}$), T is the temperature (310 K), G_e represents the plateau value of storage modulus measured by frequency sweep test (being equal to the value of G' for covalently cross-linked hydrogels), c is the polymer concentration in the hydrogels (% w/v, which varies according to the hydrogel system on study) and ρ is the density of water at 310 K (993 kg/m^3).

II.2.9.3. Shear thinning

Shear-thinning is the decrease in the polymer viscosity with increased shear rate, resulting from the alignment of polymer molecules during processing, and describes a typical non-Newtonian pseudoplastic fluid behavior. The shear-thinning was analysed in a Haake Viscotester IQ using the parallel plate geometry. The viscosity of the hydrogels was measured under steady shear strain measurements in the range of 0.1 to 1000 s⁻¹ in rotatory mode.

II.2.9.4. Yield point

The yield point marks the transition from predominant elastic to viscous behaviour. Oscillatory stress sweep experiments were carried out in order to estimate the yield point. Below the critical stress amplitude (LVR), the material responds as a solid ($G' > G''$) and G' and G'' are independent of the applied stress. At higher stress values, G' decreases and G' and G'' cross. From this point onwards, the viscous character of the material will dominate²³. The yield point was studied by recording the evolution of storage and loss moduli at a given frequency of 1 Hz in a shear stress (τ) range from 1 to 1000 Pa at 20 °C in a Haake Viscotester IQ using the parallel plate geometry. The crossover point will determine the yield point.

II.2.9.5. Self-healing ability

Materials with self-healing ability present the built-in capacity to automatically repair damage to themselves without any external intervention. The self-healing ability measurements were conducted in a Haake Viscotester IQ using the parallel plate geometry and was assessed by registering the variation of the storage and loss moduli in step-strain measurements at a fixed frequency of 1 Hz at 20 °C. Samples were treated for 60 seconds under very low strain (0.1 %), which is substantially under the deformation limit. Subsequently, the strain was increased above the critical region (50 %) for 60 seconds and afterwards, the cycle was completed by descending again the applied strain (0.1 %).

All the rheological tests were conducted in triplicate.

II.2.10. Specific characterization

II.2.10.1. Drug delivery measurements

For drug delivery studies, chloramphenicol antibiotic (CIPh, $\geq 98\%$ (TLC) Sigma–Aldrich) was used as a model drug, namely due to its water–solubility and its wide antibacterial spectrum²⁴, for *in vitro* release studies in a simulated intestinal medium for the Diels–Alder hydrogels. The drug solution was prepared by dissolving CIPh in aqueous solution at a concentration of 0.5 mg mL^{-1} at $25\text{ }^{\circ}\text{C}$. Based on the equilibrium swelling times from the swelling studies, dried hydrogel samples were maintained in the drug solution for 3 h. After that time, samples were removed from the solution and dried at ambient temperature until constant weight. The amount of drug loaded was determined from the amount of drug solution absorbed by the hydrogels, calculating the difference between the initial dried weight of the samples and the final swollen weight after loading. The release experiments were carried out by stirring the dried loaded hydrogel samples (kept in a metallic perforated container) in 80 mL of 0.01 M PBS at $37\text{ }^{\circ}\text{C}$. At predetermined time intervals, an aliquot of 1 mL of the release medium was withdrawn and analysed by UV–vis spectroscopy to determine the amount of drug released at each time point, returning the aliquot to the beaker once analysed. The amount of CIPh released was quantified by comparing the absorbance at 275 nm (maximum absorbance of CIPh) with a standard calibration curve prepared for pure drug solutions in the appropriate concentration regions. The cumulative drug release was calculated using Equation II.15.

$$\text{Cumulative Release (\%)} = \frac{M_t}{M_0} \cdot 100 \quad (\text{II.15})$$

where M_t is the cumulative mass of CIPh released at time t and M_0 is the total amount of CIPh loaded.

In order to study the mechanisms that govern the chloramphenicol release from the as-prepared Diels–Alder based hydrogel systems; the release data were fitted into the so-called power law (Equation II.16), which was reported by Siepmann and Peppas for polymeric systems²⁵ and has been applied to deduce the release mechanism of various drugs from biopolymeric hydrogels of different nature^{26–28}.

$$\frac{M_t}{M_\infty} = k \cdot t^n \quad (\text{II.16})$$

where M_t and M_∞ are the amount of drug released at time t and infinite time (4 h for CsFu/CsAMI hydrogel and 6 h for CsFu/BMI hydrogels), respectively, k is a constant incorporating structural and geometric characteristics of the sample and n is the release exponent, indicative of the mechanism of drug release. When the exponent n takes a value of 1, the release is controlled by swelling mechanism (case II transport), whereas if n takes a value of 0.50 the diffusion is the controlling step in the drug release (Fickian transport). If n lies in between, both phenomena take place simultaneously and the transport is considered to be anomalous.

II.2.10.2. Mucoadhesion capacity

Thiomers exhibit much stronger mucoadhesive properties than the corresponding unmodified polymers, thus, thiol-functionalized chitosan was evaluated in order to compare the presented mucoadhesion regarding neat chitosan and the nanogels obtained therefrom (Chapter III and Chapter VII). The mucoadhesion capacity was assessed by turbidimetric measurements using mucin from porcine stomach (Type II, Sigma–Aldrich). Hence, different mixtures were prepared and polymer/mucin interactions were measured spectrophotometrically with a UV–3600/3100 from Shimadzu at 500 nm. The influence of the pH and the concentration of mucin was studied for the different systems at 1, 2, and 5 h.

Firstly, solutions of neat chitosan, thiol–functionalized chitosan and nanogels (0.25 mg mL^{-1}), as well as mucin solutions at tested concentrations (0.25 , 0.50 , 1.25 and 1.50 mg mL^{-1}) were prepared as controls in both media, namely, water (pH 6) and acid aqueous environment ($0.5\% \text{ v/v}$ HAc, pH 3). In order to ensure the homogeneity of the solutions, controls were left in dark at room temperature under constant magnetic stirring overnight.

Mixtures of polymer/mucin solutions were then prepared in both media keeping the polymer (neat chitosan, thiol–functionalized chitosan and nanogels) concentration constant (0.25 mg mL^{-1}) while varying mucin concentration (0.25 , 0.50 , 1.25 and 1.50 mg mL^{-1}), being the polymer:mucin ratio (w/w) of 1:1, 1:2, 1:5 and 1:6 in the samples. After 1, 2 and 5 h under magnetic stirring at room temperature, samples were analyzed.

The absorbances of the individual polymers ($[\text{Abs}]_{\text{polym}}$) and mucin ($[\text{Abs}]_{\text{mucin}}$) samples were recorded as controls, where neither of the components in solution state barely absorbed. The algebraic sum ($[\text{Abs}]_{\text{theoretical}}$) of the absorbance of individual samples was used to give the theoretical values of a non–interacting system (Equation II.17)²⁹.

$$[\text{Abs}]_{\text{theoretical}} = [\text{Abs}]_{\text{polym}} + [\text{Abs}]_{\text{mucin}} \quad (\text{II.17})$$

In case of an interaction, absorbance of mixture samples ($[\text{Abs}]_{\text{exp}}$) increases. Consequently, the difference of absorbance ($\Delta[\text{Abs}]$) reflecting the occurrence of an interaction was calculated following Equation II.18²⁹.

$$\text{Interaction} = \Delta[\text{Abs}] = [\text{Abs}]_{\text{exp}} - [\text{Abs}]_{\text{theoretical}} \quad (\text{II.18})$$

II.2.10.3. Antibacterial activity

The antimicrobial activity of hydrogel extracts was studied against two pathogenic bacterial strains, namely *Escherichia coli* CECT 405 (Gram–negative) and

Staphylococcus aureus CECT 239 (Gram-positive). The microbial activity test of the final biomaterial was performed by the technique of disc-plate antibiogram. The sterilized hydrogel sample was placed on the agar surface of a petri dish, previously inoculated with the microorganism of interest. After the deposition of the hydrogel on the inoculated plate with the microorganism to be tested, the sample was incubated at 37 °C for 24 h. Even if there is no standard range for zone inhibition, 4–8 mm zone diameters are considered 'resistant'. Indeed, Manjumeena et al. considered no activity for any inhibition zone below 8 mm³⁰. Each measurement was repeated twice to ensure the reproducibility of the results.

II.2.10.4. *In vitro* cell response evaluation

II.2.10.4.1. Cytotoxicity

To assess *in vitro* cell response of the materials, a short-term cytotoxicity assay was performed, in order to evaluate the presence and/or release of toxic degradation products, following ISO 10993 recommendations. Cytotoxicity was assessed by PrestoBlue® (Invitrogen, USA), a resazurin-based solution that functions as a colorimetric cell viability indicator. Briefly, murine fibroblasts (L929 cells) were seeded into 96-well plates at a density of $4 \cdot 10^3$ cells/well in 100 µL of complete standard culture medium (Dulbecco's modified Eagle's medium, DMEM, Gibco, EEUU) that was supplemented with 10 % fetal bovine serum, 1 % of non essential aminoacids, 1 mM sodium pyruvate and 1 % penicillin/streptomycin. After 24 h, the medium was replaced with 100 µL of negative control (complete medium), positive control (10:1 ratio of complete medium:DMSO) or sterilized biomaterial extractive media and a 10 % of PrestoBlue® was added. The optical density was measured at 570 nm in a spectrophotometer (Biotek, HT Synergy, USA) at different time points (0, 24 and 48 h). The viability of the cells was calculated following the Equation II.19.

$$\text{Viability (\%)} = \frac{[\text{Abs}]_{\text{sample}}}{[\text{Abs}]_{\text{negative control}}} \cdot 100 \quad (\text{II.19})$$

where $[\text{Abs}]_{\text{sample}}$ is the absorbance of the sample cells and $[\text{Abs}]_{\text{negative control}}$ is the absorbance of the negative control cells. All assays were conducted in triplicate and average values and standard deviations were estimated.

II.2.10.4.2. Cell adhesion and viability

Live/Dead viability staining was used to test the adhesion and viability of L929 murine fibroblasts after 3 and 7 days in culture. Sterilized squared shaped samples of 0.5 cm² (n = 3) were sterilized with UV light irradiation for 30 min and placed on 24-well ultra-low attachment culture plates (Corning, NY, USA) to prehumidified with complete medium. They were incubated under standard culture conditions for 24 hours. Subsequently, PBS was added in the adjacent wells in order to avoid evaporation of the culture medium during the seeding of 5·10⁴ cells/well in 15 μL of complete medium on the materials. After incubating the cell suspensions for 90 minutes under standard conditions to ensure adhesion, 500 μL of complete medium were added to each sample.

Evaluation of the adhesion and viability of the L929 fibroblasts after 3 and 7 days was carried out by marking with 4 μM calcein-AM (Sigma-Aldrich, St Louis, MO, USA) and 5 μM propidium iodide (Molecular Probes, Eugene, Oregon, USA) on PBS. In living cells, calcein-AM acquires green fluorescence ($\lambda_{\text{ex}}/\lambda_{\text{em}} = 495/515$ nm) after hydrolysis of acetoxymethyl ester by intracellular esterases. The propidium iodide indicates the loss of the integrity of the plasma membrane since, when binding to nucleic acids with great affinity, it shows red fluorescence ($\lambda_{\text{ex}}/\lambda_{\text{em}} = 528/617$ nm)³¹. Samples were observed with the Olympus LV500 confocal microscope (Olympus, Japan).

REFERENCES

- (1) Mantovani, G.; Lecolley, F.; Tao, L.; Haddleton, D. M.; Clerx, J.; Cornelissen, J. J. L. M.; Velonia, K. Design and Synthesis of N-Maleimido-Functionalized Hydrophilic Polymers via Copper-Mediated Living Radical Polymerization: A Suitable Alternative to Pegylation Chemistry. *J. Am. Chem. Soc.* **2005**, *127* (9), 2966–2973. <https://doi.org/10.1021/ja0430999>.
- (2) Rodriguez-Emmenegger, C.; Preuss, C. M.; Yameen, B.; Pop-Georgievski, O.; Bachmann, M.; Mueller, J. O.; Bruns, M.; Goldmann, A. S.; Bastmeyer, M.; Barner-Kowollik, C. Controlled Cell Adhesion on Poly(Dopamine) Interfaces Photopatterned with Non-Fouling Brushes. *Adv. Mater.* **2013**, *25* (42), 6123–6127. <https://doi.org/10.1002/adma.201302492>.
- (3) García-Astrain, C.; Algar, I.; Gandini, A.; Eceiza, A.; Corcuera, M. Á.; Gabilondo, N. Hydrogel Synthesis by Aqueous Diels-Alder Reaction between Furan Modified Methacrylate and Polyetheramine-Based Bismaleimides. *J. Polym. Sci. Part A Polym. Chem.* **2015**, *53* (5), 699–708. <https://doi.org/10.1002/pola.27495>.
- (4) García-Astrain, C.; Gandini, A.; Peña, C.; Algar, I.; Eceiza, A.; Corcuera, M.; Gabilondo, N. Diels-Alder “Click” Chemistry for the Cross-Linking of Furfuryl-Gelatin-Polyetheramine Hydrogels. *RSC Adv.* **2014**, *4* (67), 35578–35587. <https://doi.org/10.1039/c4ra06122e>.
- (5) Kasai, M. R. Determination of the Degree of N-Acetylation for Chitin and Chitosan by Various NMR Spectroscopy Techniques: A Review. *Carbohydr. Polym.* **2010**, *79* (4), 801–810. <https://doi.org/10.1016/J.CARBPOL.2009.10.051>.
- (6) Czechowska-Biskup, R.; Wach, R. A.; Rosiak, J. M.; Ulański, P. Procedure for Determination of the Molecular Weight of Chitosan by Viscometry. *Prog. Chem. Appl. Chitin its Deriv.* **2018**, *23*, 45–54. <https://doi.org/10.15259/PCACD.23.04>.
- (7) Kasai, M. R. Calculation of Mark-Houwink-Sakurada (MHS) Equation Viscometric Constants for Chitosan in Any Solvent-Temperature System Using Experimental Reported Viscometric Constants Data. *Carbohydr. Polym.* **2007**, *68* (3), 477–488. <https://doi.org/10.1016/j.carbpol.2006.11.006>.
- (8) Yuan, Y.; Chesnutt, B. M.; Haggard, W. O.; Bumgardner, J. D. Deacetylation of Chitosan: Material Characterization and in Vitro Evaluation via Albumin Adsorption and Pre-Osteoblastic Cell Cultures. *Materials (Basel)*. **2011**, *4* (8), 1399–1416. <https://doi.org/10.3390/ma4081399>.
- (9) Pires, C. T. G. V. M. T.; Vilela, J. A. P.; Airoidi, C. The Effect of Chitin Alkaline Deacetylation at Different Condition on Particle Properties. *Procedia Chem.* **2014**, *9*, 220–225. <https://doi.org/10.1016/j.proche.2014.05.026>.

- (10) García-Astrain, C.; Gandini, A.; Coelho, D.; Mondragon, I.; Retegi, A.; Eceiza, A.; Corcuera, M. A.; Gabilondo, N. Green Chemistry for the Synthesis of Methacrylate-Based Hydrogels Crosslinked through Diels-Alder Reaction. *Eur. Polym. J.* **2013**, *49* (12), 3998–4007. <https://doi.org/10.1016/j.eurpolymj.2013.09.004>.
- (11) Chesnutt, B. M.; Viano, A. M.; Yuan, Y.; Yang, Y.; Guda, T.; Appleford, M. R.; Ong, J. L.; Haggard, W. O.; Bumgardner, J. D. Design and Characterization of a Novel Chitosan/Nanocrystalline Calcium Phosphate Composite Scaffold for Bone Regeneration. *J. Biomed. Mater. Res. - Part A* **2009**, *88* (2), 491–502. <https://doi.org/10.1002/jbm.a.31878>.
- (12) Ahmad, L. O.; Permana, D.; Wahab; Sabarwati, S. H.; Ramadhan, L. O. A. N.; Rianse, U. Improved Chitosan Production from Tiger Shrimp Shell Waste (*Penaeus Monodon*) by Multistage Deacetylation Method and Effect of Bleaching 2 Materials and Methods. *Adv. Environ. Geol. Sci. Eng.* **2015**, 373–378.
- (13) Raut, A. V.; Satvekar, R. K.; Rohiwal, S. S.; Tiwari, A. P.; Gnanamani, A.; Pushpavanam, S.; Nanaware, S. G.; Pawar, S. H. In Vitro Biocompatibility and Antimicrobial Activity of Chitin Monomer Obtain from Hollow Fiber Membrane. *Des. Monomers Polym.* **2016**, *19* (5), 445–455. <https://doi.org/10.1080/15685551.2016.1169379>.
- (14) Shitrit, Y.; Bianco-Peled, H. Acrylated Chitosan for Mucoadhesive Drug Delivery Systems. *Int. J. Pharm.* **2017**, *517* (1–2), 247–255. <https://doi.org/10.1016/j.ijpharm.2016.12.023>.
- (15) Mahmood, A.; Lanthaler, M.; Laffleur, F.; Huck, C. W.; Bernkop-Schnürch, A. Thiolated Chitosan Micelles: Highly Mucoadhesive Drug Carriers. *Carbohydr. Polym.* **2017**, *167*, 250–258. <https://doi.org/10.1016/j.carbpol.2017.03.019>.
- (16) Altinisik, A.; Yurdakoc, K. Chitosan/Poly(Vinyl Alcohol) Hydrogels for Amoxicillin Release. *Polym. Bull.* **2014**, *71* (3), 759–774. <https://doi.org/10.1007/s00289-013-1090-1>.
- (17) Badhe, R. V.; Bijukumar, D.; Chejara, D. R.; Mabrouk, M.; Choonara, Y. E.; Kumar, P.; du Toit, L. C.; Kondiah, P. P. D.; Pillay, V. A Composite Chitosan-Gelatin Bi-Layered, Biomimetic Macroporous Scaffold for Blood Vessel Tissue Engineering. *Carbohydr. Polym.* **2017**, *157*, 1215–1225. <https://doi.org/10.1016/j.carbpol.2016.09.095>.
- (18) Fan, M.; Ma, Y.; Mao, J.; Zhang, Z.; Tan, H. Cytocompatible in Situ Forming Chitosan/Hyaluronan Hydrogels via a Metal-Free Click Chemistry for Soft Tissue Engineering. *Acta Biomater.* **2015**, *20*, 60–68. <https://doi.org/10.1016/j.actbio.2015.03.033>.
- (19) Saravanan, S.; Chawla, A.; Vairamani, M.; Sastry, T. P.; Subramanian, K. S.;

- Selvamurugan, N. Scaffolds Containing Chitosan, Gelatin and Graphene Oxide for Bone Tissue Regeneration in Vitro and in Vivo. *Int. J. Biol. Macromol.* **2017**, *104*, 1975–1985. <https://doi.org/10.1016/J.IJBIOMAC.2017.01.034>.
- (20) Hsiao, M. H.; Larsson, M.; Larsson, A.; Evenbratt, H.; Chen, Y. Y.; Chen, Y. Y.; Liu, D. M. Design and Characterization of a Novel Amphiphilic Chitosan Nanocapsule-Based Thermo-Gelling Biogel with Sustained in Vivo Release of the Hydrophilic Anti-Epilepsy Drug Ethosuximide. *J. Control. Release* **2012**, *161* (3), 942–948. <https://doi.org/10.1016/j.jconrel.2012.05.038>.
- (21) Chen, F.; Song, S.; Wang, H.; Zhang, W.; Lin, C.; Ma, S.; Ye, T.; Zhang, L.; Yang, X.; Qin, X.; et al. Injectable Chitosan Thermogels for Sustained and Localized Delivery of Pingyangmycin in Vascular Malformations. *Int. J. Pharm.* **2014**, *476* (1–2), 232–240. <https://doi.org/10.1016/J.IJPHARM.2014.09.058>.
- (22) Karvinen, J.; Ihalainen, T. O.; Calejo, M. T.; Jönkkäri, I.; Kellomäki, M. Characterization of the Microstructure of Hydrazone Crosslinked Polysaccharide-Based Hydrogels through Rheological and Diffusion Studies. *Mater. Sci. Eng. C* **2019**, *94*, 1056–1066. <https://doi.org/10.1016/j.msec.2018.10.048>.
- (23) Cyriac, F.; Lugt, P. M.; Bosman, R. On a New Method to Determine the Yield Stress in Lubricating Grease. *Tribol. Trans.* **2015**, *58* (6), 1021–1030. <https://doi.org/10.1080/10402004.2015.1035414>.
- (24) García-Astrain, C.; Chen, C.; Burón, M.; Palomares, T.; Eceiza, A.; Fruk, L.; Corcuera, M. Á.; Gabilondo, N. Biocompatible Hydrogel Nanocomposite with Covalently Embedded Silver Nanoparticles. *Biomacromolecules* **2015**, *16* (4), 1301–1310. <https://doi.org/10.1021/acs.biomac.5b00101>.
- (25) Siepmann, J.; Peppas, N. . Modeling of Drug Release from Delivery Systems Based on Hydroxypropyl Methylcellulose (HPMC). *Adv. Drug Deliv. Rev.* **2001**, *48* (2–3), 139–157. [https://doi.org/10.1016/S0169-409X\(01\)00112-0](https://doi.org/10.1016/S0169-409X(01)00112-0).
- (26) García-Astrain, C.; Guaresti, O.; González, K.; Santamaria-Echart, A.; Eceiza, A.; Corcuera, M. A.; Gabilondo, N. Click Gelatin Hydrogels: Characterization and Drug Release Behaviour. *Mater. Lett.* **2016**, *182*. <https://doi.org/10.1016/j.matlet.2016.06.115>.
- (27) García-Astrain, C.; Avérous, L. Synthesis and Behavior of Click Cross-Linked Alginate Hydrogels: Effect of Cross-Linker Length and Functionality. *Int. J. Biol. Macromol.* **2019**, *137*, 612–619. <https://doi.org/10.1016/J.IJBIOMAC.2019.07.010>.
- (28) Martínez-Ruvalcaba, A.; Sánchez-Díaz, J. C.; Becerra, F.; Cruz-Barba, L. E.; González-Álvarez, A. Swelling Characterization and Drug Delivery Kinetics of Polyacrylamide-Co-Itaconic Acid/Chitosan Hydrogels. *Express Polym.*

- Lett.* **2009**, *3* (1), 25–32. <https://doi.org/10.3144/expresspolymlett.2009.5>.
- (29) Hsein, H.; Garrait, G.; Beyssac, E.; Hoffart, V. Whey Protein Mucoadhesive Properties for Oral Drug Delivery: Mucin-Whey Protein Interaction and Mucoadhesive Bond Strength. *Colloids Surfaces B Biointerfaces* **2015**, *136*, 799–808. <https://doi.org/10.1016/j.colsurfb.2015.10.016>.
- (30) Manjumeena, R.; Venkatesan, R.; Duraibabu, D.; Sudha, J.; Rajendran, N.; Kalaichelvan, P. T. Green Nanosilver as Reinforcing Eco-Friendly Additive to Epoxy Coating for Augmented Anticorrosive and Antimicrobial Behavior. *Silicon* **2016**, *8* (2), 277–298. <https://doi.org/10.1007/s12633-015-9327-2>.
- (31) Althouse, G. C.; Hopkins, S. M. Assessment of Boar Sperm Viability Using a Combination of Two Fluorophores. *Theriogenology* **1995**, *43* (3), 595–603. [https://doi.org/10.1016/0093-691X\(94\)00065-3](https://doi.org/10.1016/0093-691X(94)00065-3).

CHAPTER III

CHITOSAN DERIVATIVES READY FOR CLICK REACTIONS

III.1. INTRODUCTION AND OBJECTIVE	81
III.2. SYNTHESIS OF FURAN-FUNCTIONALIZED CHITOSAN (CsFu)	83
III.2.1. EXPERIMENTAL PART	83
III.2.2. RESULTS AND DISCUSSION	85
III.3. SYNTHESIS OF MALEIMIDE-FUNCTIONALIZED CHITOSAN (CsAMI)	89
III.3.1. SYNTHESIS OF 3-(2,5-DIOXO-2H-PYRROL-1(5H)-YL)PROPANOIC ACID (AMI)	89
III.3.2. EXPERIMENTAL PART	90
III.3.3. RESULTS AND DISCUSSION	91
III.4. SYNTHESIS OF THIOL-FUNCTIONALIZED CHITOSAN (CsSH)	97
III.4.1. EXPERIMENTAL PART	97
III.4.2. RESULTS AND DISCUSSION	99
III.5. SYNTHESIS OF TETRAZOLE-FUNCTIONALIZED CHITOSAN (CsTZ)	107
III.5.1. SYNTHESIS OF 4-(2-(4-METHOXYPHENYL)-2H-TETRAZOLE-5-YL)BENZOIC ACID (TBA)	107
III.5.2. EXPERIMENTAL PART	108
III.5.3. RESULTS AND DISCUSSION	109
III.6. CONCLUSIONS	113
REFERENCES	116

III. CHITOSAN DERIVATIVES READY FOR CLICK REACTIONS

III.1. INTRODUCTION AND OBJECTIVE

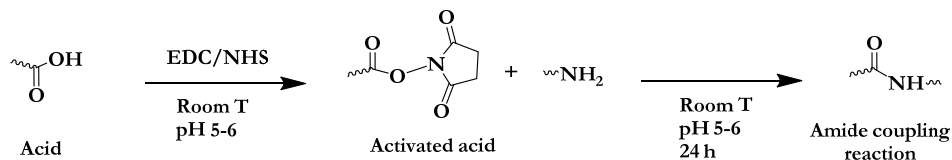
Some of the commonly used techniques for preparing chitosan-based polymers include blending, grafting and cross-linking¹. Among all them, the chemical modification of chitosan has been shown to be a promising method for the generation of new functional materials, which would not further change the fundamental backbone of neat chitosan, while maintaining the original biological properties of the polymer. Both the $-NH_2$ and $-OH$ groups of chitosan backbone can act as active sites for modification in order to alter properties such as solubility, mucoadhesion and stability for specific applications. Therefore, the nature of the attached group could bring new properties into the original chitosan, i.e., the incorporation of thiol containing compounds contributes to solve the impediment of water solubility, since $-SH$ groups are highly hydrophilic^{2,3} and, at the same time, enhance the mucoadhesivity of the original polymer⁴; the addition of maleimide groups brings extra biocompatible nature⁵ and a greater capacity to adapt under different environments due to their reactivity towards different biomolecules⁶; in the case of furan grafted groups, the renewable nature is promoted whereas reactions are favoured in terms of yield and kinetics due to their pronounced dienic character⁶; while tetrazole groups exhibit a very rich photochemistry turning the chitosan into an excellent precursor for light triggered reactions^{7,8}. Therefore, the chemical modification affords a wide range of derivatives with modified properties for specific end use applications in diversified areas mainly of pharmaceutical, biomedical and biotechnological fields. The versatility in possible modifications and applications of chitosan derivatives presents a great challenge to scientific community and industry.

Accordingly, modification can take place by several ways, which include chemical, radiation-mediated, photochemical, plasma-induced and enzymatic grafting

methods¹. Thus, the main objective of this chapter was to develop novel chitosan derivatives following two chemical routes where the biopolymer was modified with different functional groups by means of the primary amines as a preliminary step for developing novel biomaterials.

On the one hand, based on the well-documented reaction of aldehydes with chitosan⁹, furfural was used to incorporate diene character moieties into the biopolymer chain. The primary amines of chitosan undergo Schiff reaction with aldehydes to form the corresponding imines, which are then converted to N-alkyl derivatives on hydrogenation with borohydride¹⁰.

Another viable and easy route to covalently attached functional groups into chitosan is the one based on the formation of amide bonds¹¹, which was also used throughout this thesis. Herein, the functionalization of the biopolymer was achieved by amide coupling conjugation between the primary amines of the polymer and the carboxylic acid groups of the corresponding acid modifier (based on maleimide, thiol or tetrazole-containing compounds), some of them having been previously synthesized, in the presence of the double system of coupling agents (EDC/NHS) as shown in Scheme III.1. According to literature, the pKa of the primary amino group of chitosan is ~ 6.5 ¹². For this reason, chitosan was previously dissolved at acid pH in order to ensure the availability of the protonated amino groups for the modification reaction and afterwards, the pH reaction media was raised to 5–6 since amide coupling reaction selectivity is higher at this pH.



Scheme III.1. General representation for the acid activation mechanism prior to the amide coupling cross-linking reaction.

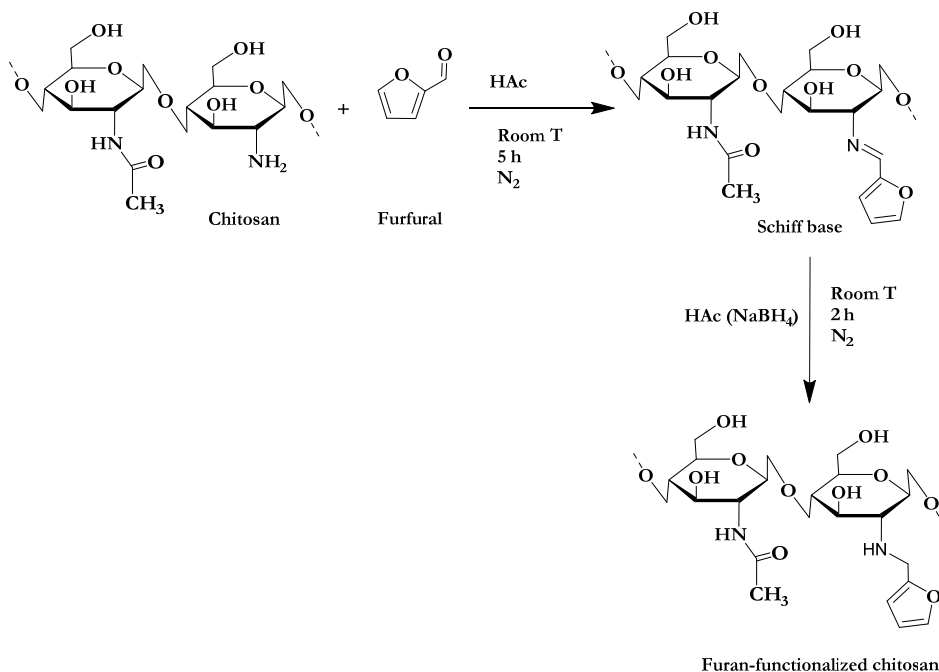
The functionalization of chitosan was confirmed by the determination of the amine substitution degree (DS) following different strategies based on the derivative. FTIR and NMR spectroscopy were used in order to compare the chemical structures before and after the functionalizations. Furthermore, the effect of the modifications on the crystalline structure of the biopolymer was evaluated by XRD. The thermal stability of the precursors was studied by thermogravimetric analysis in order to study the influence of grafting different reactive compounds to the chitosan main chain. Thus, similar characterization was performed for the four derivatives, which followed a similar tendency based on the spectra of original chitosans for each of the assays.

III.2. SYNTHESIS OF FURAN-FUNCTIONALIZED CHITOSAN (CsFu)

III.2.1. Experimental part

Furan-functionalized chitosan was prepared according to a method described elsewhere¹³. The diene was obtained by the modification of chitosan with furfural through the formation of imine groups (Schiff base) between the aldehyde and the amino group of chitosan. The synthetic strategy of the furanic chitosan derivative is shown in Scheme III.2. Chitosan (1 g; $5 \cdot 10^{-3}$ eq. NH_2) was dissolved in 100 mL of 2 % v/v aqueous acetic acid solution. Furfural (675 μL) was added dropwise in a 1.6:1 equivalent ratio with respect to chitosan under magnetic stirring to ensure significant modification of the polymer and the mixture was

allowed to react for 5 h at room temperature. In order to avoid subsequent interferences of the formed imine groups ($-\text{CH}=\text{N}-$), an excess of NaBH_4 was added to reduce the Schiff base. To prevent small bubbles generation due to the reduction process, the reaction was maintained under nitrogen atmosphere for 2 hours. The pH of the solution was close to 3 during all the process. The polymer was then precipitated in 1 M NaOH , filtered using a polyamide membrane filter of $0.2 \mu\text{m}$ pore size (Sartorius Stedim Biotech) and successively washed with water-ethanol-water. The solid was removed and purified by dialysis against deionized water for 24 hours using a Spectra/Por[®] 2 Dialysis Membrane, MWCO: 12–14 kD (Spectrum Laboratories, Inc.). CsFu was recovered as a solid material (60 % w/w yield) after drying in an oven at $60 \text{ }^\circ\text{C}$.



Scheme III.2. Synthesis of CsFu through the reaction of chitosan and furfural.

III.2.2. Results and discussion

Furan-functionalized chitosan was characterized by FTIR spectroscopy. The FTIR spectra of original chitosan and CsFu are shown in Figure III.1. The success of the modification could be confirmed by the appearance of the signals related to the new functional group in the chitosan chain attributed to the diene.

As it can be observed for the neat chitosan spectrum, four strong bands belonging to the saccharide structure appeared at 1150, 1064, 1023 and 897 cm^{-1} . Furthermore, amide I and amide II bands were also observed at 1644 and 1555 cm^{-1} , respectively^{14,15}. The amide I band corresponded to the $\text{C}=\text{O}$ stretching vibration, whereas the amide II band was associated with the $\text{N}-\text{H}$ bending vibration and the $\text{C}-\text{N}$ stretching vibration¹⁶. Furthermore, the spectrum of unmodified chitosan shows a strong broad absorption band with two peaks at 3358 and 3282 cm^{-1} , which were assigned to the stretching vibrations of $\text{O}-\text{H}$ and $\text{N}-\text{H}$ groups¹⁷, while the band at 2873 cm^{-1} was attributed to $\text{C}-\text{H}$ stretching vibrations of hydrocarbons. All these results were in good agreement with other authors^{15,18,19}. Even if the characteristic bands of the polysaccharide main chain remained unchanged after modification, new absorption signals appeared due to the insertion of furan groups in the chitosan backbone. The stretching vibration of the furan ring showed up at 1480 cm^{-1} ^{19,20}. Moreover, the presence of the grafted furan groups was appreciated at 934 and 884 cm^{-1} ^{6,13}. On the other hand, it is worth noting that the intensity of the band assigned to the amide II of the chitosan at 1555 cm^{-1} decreased, evidencing the partial modification of the -NH_2 groups of the original polymer with the furfural molecules²¹⁻²³.

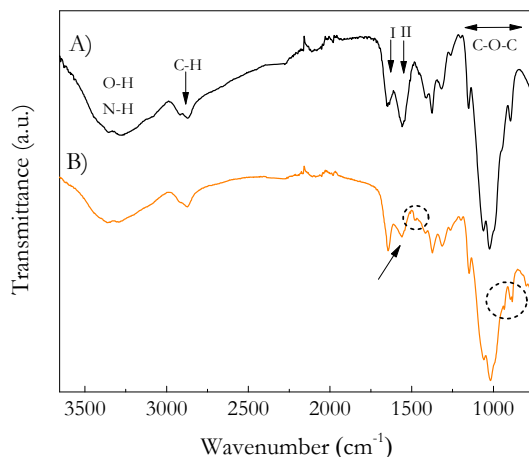


Figure III.1. FTIR spectra of A) chitosan and B) furan-functionalized chitosan (CsFu).

The chemical structure and the degree of substitution (DS) of furan modified chitosan were confirmed by ^1H NMR spectroscopy and the spectra of chitosan and CsFu are shown in Figure III.2. The characteristic proton signals of the glucosamine unit appeared in the range of 4.50–2.50 ppm (1–6)^{24,25}. The peak close to 1.90 ppm was attributed to the proton signal of the methyl group of the acetamido moiety. In the ^1H NMR spectrum of the furan modified sample the distinctive peaks of the furan ring could be observed at 7.43 (–OCH=, c), 6.48 and 6.32 (–CH=, a–b) ppm²⁶. Unreacted furfural moieties that prevail in the sample before purification are shown with an asterisk¹³. The degree of substitution of the furanic derivative was determined by the Equation II.3 and was found to be 29 %.

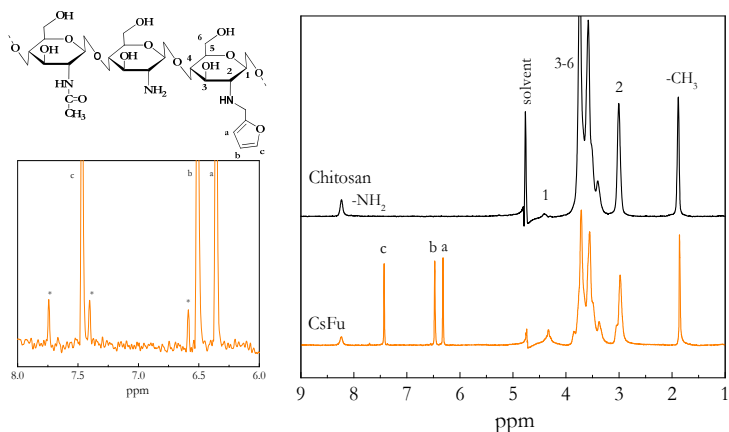


Figure III.2. Liquid-state ¹H NMR spectra and chemical structure of chitosan and furan-functionalized chitosan (CsFu).

Additionally, the crystallinity of the neat chitosan and the furanic sample was analysed by X-ray diffraction. XRD patterns are shown in Figure III.3. As it has been explained in Chapter I and II, chitosan is less crystalline than chitin and therefore, shows lower crystallinity indexes. It exhibited three characteristic peaks at 2θ about $10\text{--}10.5^\circ$, 16° and $20\text{--}20.5^\circ$. In agreement with previous reports, the strongest peak at 2θ about 20° is assigned to crystal forms II from (110) planes, whereas the peak at 2θ about 10° corresponds to crystal forms I from (020) planes and the one at 2θ about 16° to the amorphous phase^{27–29}. The XRD patterns of α and β -chitin expose clear differences due to the different arrangements adopted by these polymorphs as detailed in Chapter I. The XRD profile of the α -chitin exhibits well-resolved and intense peaks, while a broad diffuse scattering and less intense peaks are found for the β -chitin at 10° and 20° ^{30,31}. This behaviour indicates that α -chitin is a more crystalline polymorph because of its antiparallel compact structure. Therefore, from the XRD spectra obtained for the chitosans under study (shown throughout this chapter), it could

be deduced that chitosans came from α -chitin. Moreover, the crystallinity index (CI^{XRD}) of CsFu was calculated using the Equation II.6 and was found to be 0.29. As expected, after the functionalization process, the degree of crystallinity decreased^{32,33}. In addition, distortions could be observed in the crystalline network of the modified polymer in comparison with the original one, probably due to the preparation methodology, which altered the crystalline structure of the chitosan. Nevertheless, the crystallinity index was not influenced by this fact.

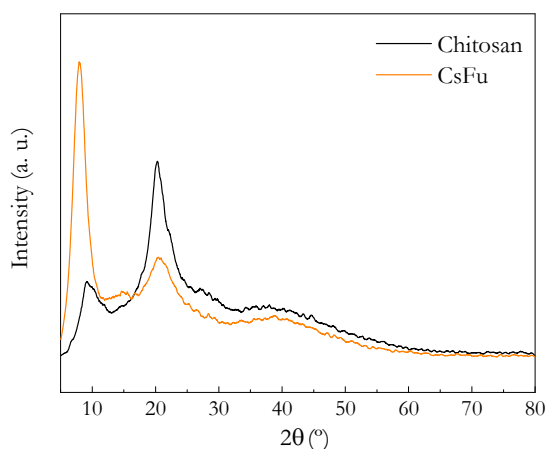


Figure III.3. X-ray diffractograms of chitosan and furan-functionalized chitosan (CsFu).

The thermal behaviour of the synthesized furanic chitosan was analysed by TGA and the thermograms (TGA) and derivative curves (dTGA) of chitosan and furan-functionalized chitosan can be observed in Figure III.4. Thermogravimetric analysis was performed between 25 and 800 °C in order to assess the thermal stability of CsFu. According to the measurements, weight loss of chitosan took place in two stages. The first event was observed at 60 °C, which was assigned to the release of sorbed water. The second stage started near 230 °C and corresponded to the decomposition of the chitosan main chain^{27,34,35}. As it has been previously reported by several authors, substituted polymers usually

show lower thermal stability due to the disruption of the ordered structure of the neat polymer by the grafted molecule^{27,36}. This is the case of the furanic chitosan derivative, which degradation started earlier after the modification with furan groups and which degradation peak observed in the dTGA curve shifted to lower temperatures. This trend has been already reported for other furan derivatives^{6,37}.

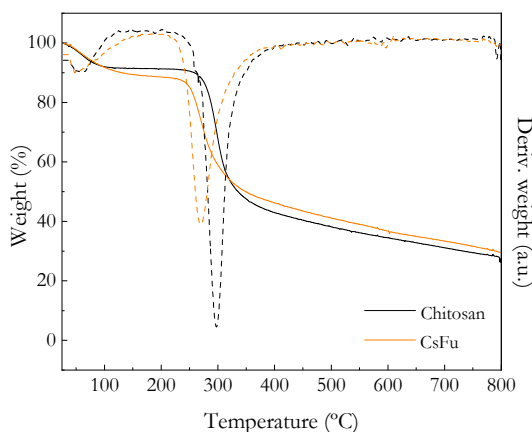


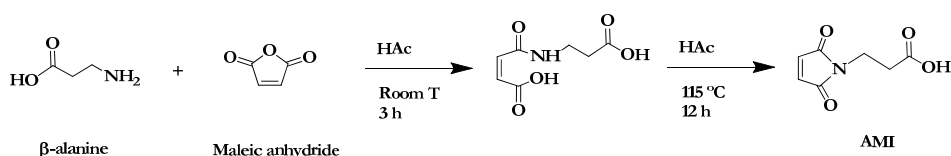
Figure III.4. TGA (left axis, solid line) and dTGA (right axis, dash line) curves of chitosan and furan-functionalized chitosan (CsFu) under inert atmosphere.

III.3. SYNTHESIS OF MALEIMIDE-FUNCTIONALIZED CHITOSAN (CsAMI)

III.3.1. Synthesis of 3-(2,5-dioxo-2H-pyrrol-1(5H)-yl)propanoic acid (AMI)

A maleimide-end acid (AMI) was firstly synthesized in a two step procedure (Scheme III.3) following a reported method with some modifications³⁸ and was then used to functionalize the chitosan. This synthesized acid was previously assess as effective modifier of cellulose nanocrystals to be used as cross-linkers for bionanocomposite hydrogels. Therefore, for the AMI synthesis, an acetic acid solution containing maleic anhydride at 10 % w/v (5 g in 50 mL) was added

dropwise to an acetic acid solution with β -alanine at 9 % w/v (4.54 g in 50 mL). The mixture was stirred for 3 h at room temperature and a white suspension was obtained. After that period, 70 mL of HAc were added, while the temperature was raised until 115 °C and the mixture was stirred overnight. After one hour of reaction a limpid colourless solution was observed. At the end of the whole process, an orange oil was obtained. The solvent excess was removed under reduced pressure and the product was washed with 30 mL of toluene for three consecutive times, which was also removed under reduced pressure. The product was then purified by flash chromatography using a silica column (DCM/ethyl acetate 9:1). Finally, a white solid (AMI) was obtained (30 % w/w yield).

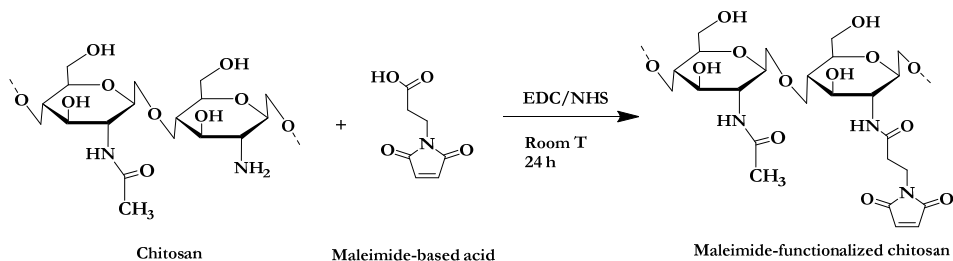


Scheme III.3. AMI synthesis from β -alanine and maleic anhydride.

III.3.2. Experimental part

Chitosan was modified by the reaction of its amino groups with the previously synthesized acid precursor containing maleimide groups (AMI) in aqueous solution, through amide coupling reaction. The synthetic strategy of the chitosan derivative (CsAMI) is shown in Scheme III.4. An aqueous solution of AMI (0.042 g mL⁻¹) was activated by stirring for 1 hour with EDC and NHS in 1:1 and 1:1.1 molar ratios, respectively. At the same time, chitosan (0.3 g) was dissolved in 30 mL of 2 % v/v aqueous acetic acid solution and the pH of the solution was increased from 3 to 5–6 with 1 M NaOH. An equivalent ratio of 1:2 for amine-to-carboxylic acid was established. Subsequently, the activated AMI solution was added dropwise to the chitosan solution and the reactive mixture was left 24 hours at room temperature and under magnetic stirring. The polymer was precipitated

in 1 M NaOH, filtered using a polyamide membrane filter of 0.2 μm pore size (Sartorius Stedim Biotech) and successively washed with water–ethanol–water. The final material (gel-like appearance) was removed and purified by dialysis against deionized water for 72 hours using a Spectra/Por® 2 Dialysis Membrane, MWCO: 12–14 kD (Spectrum Laboratories, Inc.). The pH of the final product was maintained at 5 after the purification step. The polymer was treated differently depending on the end use; thus, CsAMI was recovered as a solid material after drying in an oven at 60 $^{\circ}\text{C}$ or stored in the freezer as a gel-like matrix until further use.



Scheme III.4. Synthesis of CsAMI through the reaction of chitosan and AMI modifier.

III.3.3. Results and discussion

The FTIR spectrum of the modified chitosan is shown in Figure III.5, along with the one corresponding to the neat chitosan. Significant differences between both spectra could be detected, although the characteristics bands of the chitosan polymer indicated in Section III.2.2. were still observed. When modifying the chitosan with AMI (B), the band assigned to the amide II significantly increased, since this modification led to the formation of new amide groups. Besides, the new band located at 1724 cm^{-1} , corresponding to the carbonyl groups ($-\text{C}=\text{O}$) of the grafted maleimide ring, could be noticed. Additionally, the functionalization was also confirmed by the presence of other distinctive peaks of the AMI molecule, as the ones at 1109 and 836 cm^{-1} , which appeared slightly displaced because of the modification and could be related to the C–N and C–C bonds of the maleimide

ring and the $-\text{CH}_2$ groups of the AMI molecule chain. On the other hand, the double peak of the chitosan at 3358 and 3282 cm^{-1} turned into a broad single peak, due to the modification³⁹.

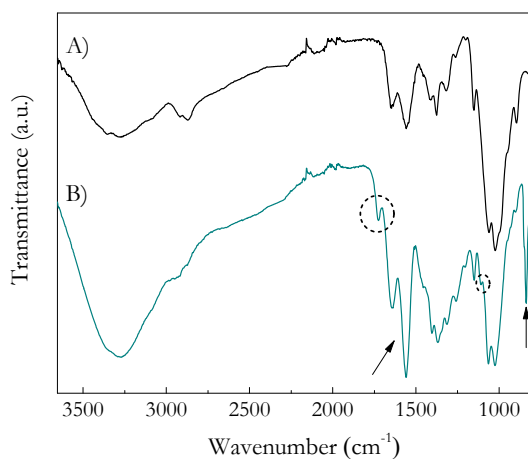


Figure III.5. FTIR spectra of A) chitosan and B) maleimide-functionalized chitosan (CsAMI).

The presence of specific reactive groups grafted to the chitosan chain was also confirmed by ^1H NMR spectroscopy. Figure III.6 shows the ^1H NMR spectra of neat chitosan and CsAMI. The insertion of the maleimide ring into the polymer structure could be confirmed by the peak at 6.27 ppm (d) corresponding to the protons of the double bond of the ring $-\text{CH}=\text{CH}-$ ²⁶. The degree of substitution was calculated from the Equation II.4 and was found to be 27% .

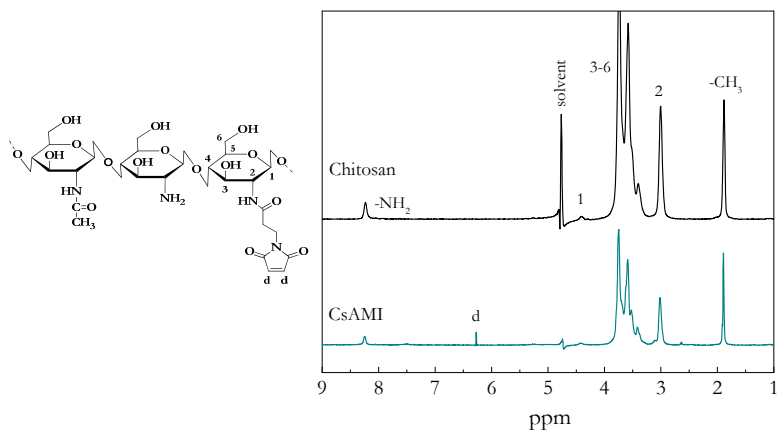


Figure III.6. Liquid–state ¹H NMR spectra and chemical structure of chitosan and maleimide–functionalized chitosan (CsAMI).

The effect of the functionalization on the crystalline structure of the chitosan was evaluated by XRD. The X–ray diffraction pattern indicates that no changes on the crystalline structure occurred after the functionalization of chitosan since, same spectrum profile could be observed on both diffraction patterns. However, in the case of CsAMI, the peak at $2\theta \approx 10^\circ$ almost disappeared and the one at $2\theta \approx 20^\circ$ became wider and weaker, being in great agreement with other results where it was observed the same trend after the chitosan modification⁴⁰. Additionally, the crystallinity index, calculated from XRD data according to the Equation II.6, decreased considerably after the modification, being 0.18. These results indicated that the crystallinity of the chitosan decreased after the modification, supporting the success of the functionalization reaction⁴¹.

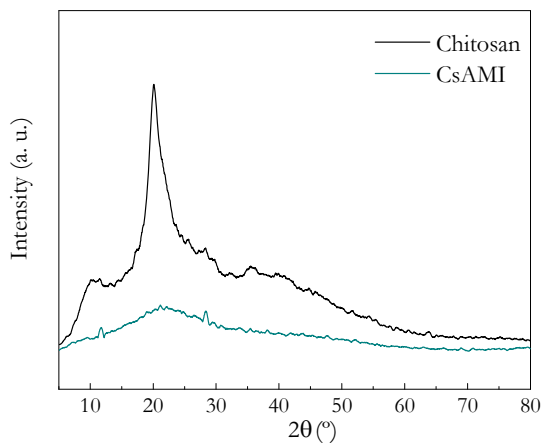


Figure III.7. X-ray patterns of chitosan and maleimide-functionalized chitosan (CsAMI).

The neat chitosan and the modified chitosan:maleimide precursor were characterized in terms of their thermal behaviour as shown in Figure III.8. Following the same trend of the substituted precursors as described in the previous section, the degradation of CsAMI started earlier due to the presence of the dienophile components in the polymer structure. Namely, the degradation of maleimide-functionalized chitosan occurred at 260 °C while chitosan degraded at almost 300 °C as shown in the dTGA curve.

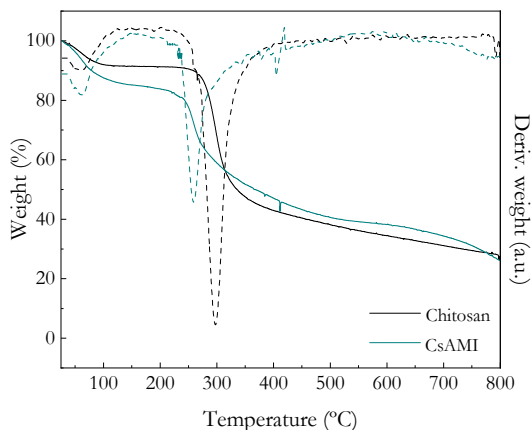


Figure III.8. TGA (left axis, solid line) and dTGA (right axis, dash line) curves of chitosan and maleimide–functionalized chitosan (CsAMI) under inert atmosphere.

To test the potential of this precursor to be applied as matrix of a final material with future biomedical applicability, preliminary *in vitro* cytotoxicity assays were performed investigating material extracts and direct cell–material interactions with L929 murine fibroblast cells following the procedure reported in Chapter II. As expected, these preliminary studies confirmed the favourable cytocompatibility of CsAMI.

Figure III.9A shows the absorbance versus incubation time for the positive and negative controls, as well as for CsAMI sample. The positive control showed a notably toxic effect where the L929 murine fibroblasts were not able to proliferate. On the contrary, CsAMI displayed non–toxic cell growth, similar to the negative control. The cell proliferation with respect to the negative control as a function of the incubation time is represented in Figure III.9B. It was observed that the viability of the L929 cells cultured in the extracted medium was significantly higher than the established acceptance limit of 70 % with respect to the negative control.

In addition, long-term cell adhesion test was carried out by Live/Dead assay. Figure III.9C shows the fluorescence confocal microscopy images (x100) where calcein-AM shows cell viability (green) and propidium iodide non-viable cells (red). For direct cell-material contact, cells were seeded onto the modified chitosan sample. As it can be observed, the sample showed a high level of cell survival since the big majority of cells fluoresced green and very few dead cells were observed. The culture reached the monolayer in 3 days, showing adhesion and stable growth until day 7. Therefore, cytotoxicity and cell viability studies revealed that the as-prepared maleimide-functionalized chitosan was a good candidate for biomedical applications.

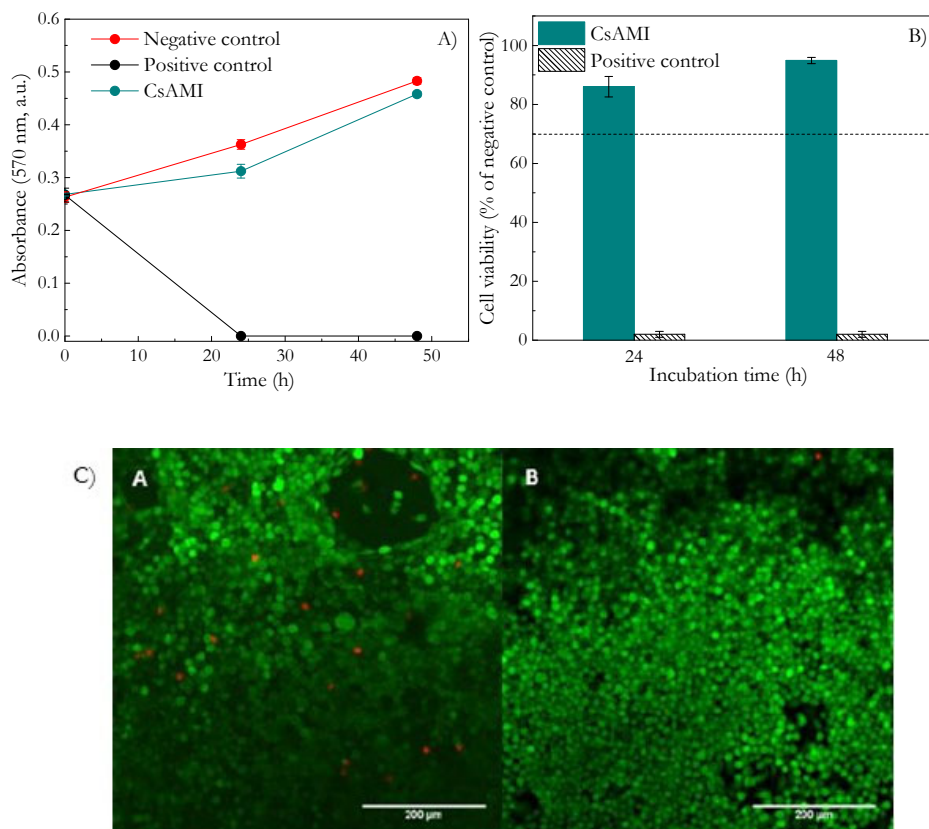


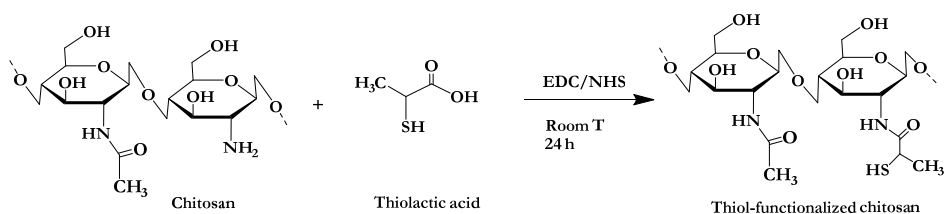
Figure III.9. A) Cell proliferation of murine fibroblasts L929 in contact with the CsAMI material as a function of time (the viability data represented were obtained from PrestoBlue® at 570 nm), B) viability of L929 murine fibroblast cell line with respect to the negative control at 24 and 48 h and C) adhesion and viability of L929 cells on CsAMI at 3 (A) and 7 (B) days of incubation, where live cells appear in green and dead cells in red (images obtained by confocal microscopy (100x)).

III.4. SYNTHESIS OF THIOL-FUNCTIONALIZED CHITOSAN (CsSH)

III.4.1. Experimental part

The thiol functionalization of chitosan (CsSH) was achieved by amide coupling conjugation with thiolactic acid (TLA), following a reported procedure that was

consequently modified⁴². A schematic representation of the reaction between chitosan and thiolactic acid is shown in Scheme III.5. Chitosan was dissolved in 2 % v/v aqueous acetic acid to a final concentration of 0.5 % w/v. Thiolactic acid, EDC and NHS were then added to the solution while adjusting the pH to 5–6 using 1 M NaOH and the mixture was stirred 24 hours in dark at room temperature. The pH of the surrounding medium will influence on the concentration of thiolate anions since the thiol groups could loss their proton and react to disulphide bridges ($-S-S-$)⁴³. Therefore, in order to avoid the formation of disulphide bonds between the polymeric chains, the synthesis was performed at pH 5–6. At that pH, the amount of thiol groups in the oxidized form is low and the formation of disulphide bonds can be minimized^{2,44}. The molar ratio of amine-to-carboxylic acid used was 1:1 and the thiolactic acid (120 μ L) was activated with EDC and NHS in 1:1 and 1:1.1 molar ratios, respectively. The product was dialyzed in cellulose membranes (molecular weight cutt-off of 12–14 kDa) for 72 hours against 5 mM HCl, then once against the same medium but containing 1 % w/v NaCl to reduce the ionic interactions between the cationic polymer and the anionic sulfhydryl groups, and finally, once against 5 mM HCl for 48 h. The dialysis was done in dark at 4 °C for avoiding the oxidation of sulfhydryl groups⁴⁴. CsSH was lyophilized (88 % w/w yield) and stored at 4 °C in dark until needed for further use.



Scheme III.5. Synthesis of CsSH through the reaction of chitosan and thiolactic acid.

III.4.2. Results and discussion

FTIR spectroscopy was used for the comparison of the chemical structures of chitosan before and after the modification of the polymer. Figure III.10 illustrates the FTIR spectra of both neat and thiol modified chitosan. As in the previous sections, the common bands belonging to the saccharide structure could be identified in both spectra. However, significant differences were observed by comparing both spectra due to the grafting of thiol groups into the chitosan chain via amide-mediated reaction. As it could be observed, in the spectrum of the CsSH derivative (B), the characteristic double peak at high wavenumbers disappeared and a single peak around 3294 cm^{-1} appeared, supporting the fact that the $-\text{NH}_2$ group reacted with the thiolactic acid in this case^{17,45}. Moreover, the functionalization led to the insertion of new C–H linkages in the polymeric structure, resulting in the differentiation of two bands at 2920 and 2851 cm^{-1} , which corresponded to the stretching vibrations of CH_3 and CH_2 , respectively⁴⁶, and the appearance of a new band at 1458 cm^{-1} ^{14,47}. Besides, amide I and II bands appeared slightly displaced in the CsSH derivative (1628 and 1518 cm^{-1} , respectively), which could be related to the addition of a new group after the amide bond formation^{14,28}. Furthermore, the intensity of the band assigned to the amide II of the chitosan, which is associated to the C–N stretching vibration, was significantly stronger, suggesting that the grafting occurred at the chitosan amine site⁴⁷. In fact, the thiolation of chitosan was also qualitatively confirmed by the appearance of some other new bands as the signal of sulfur-based groups at 796 cm^{-1} (S–C) and the characteristic band of the carbonyl groups ($-\text{C}=\text{O}$) of the grafted thiol ended molecule at 1742 cm^{-1} confirming the success of the modification¹⁴.

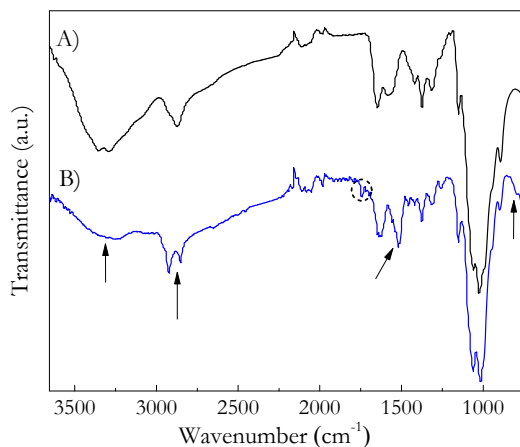


Figure III.10. FTIR spectra of A) chitosan and B) thiol-functionalized chitosan (CsSH).

The thiol functionalization of the chitosan was confirmed by the determination of the amine substitution degree (DS). Indeed, the ninhydrin assay (Equation II.7) was used to determine the remaining free amine groups of the thiolated chitosan derivative, calculating the DS value of 26 %. Moreover, the amount of thiol groups determined by Ellman's test was found to be $2162 \mu\text{mol g}^{-1}$ of polymer. The amount of thiol immobilized in native chitosan was enough to avoid the insolubility problems and was found to be highly adequate for the subsequent cross-linking reaction. Furthermore, it has been recently observed that the *in situ* gelling properties of chitosan significantly improve after thiolation⁴⁸.

To confirm the influence of the modification on the crystallinity of chitosan, X-ray diffraction patterns of unmodified and modified samples were compared (Figure III.11). The signal of the most intense peak ($2\theta \approx 20^\circ$) almost disappeared in the CsSH pattern, indicating the existence of new intermolecular interactions that influenced the regularity of the chitosan ordered structure^{27,49,50}. The crystallinity index of the thiolated chitosan was calculated from the Equation II.6 and was found to reduce to 0.14. The amorphous form of the chitosan derivative

could present certain advantages for being used in biomedical applications^{51,52}. Indeed, the showed water solubility of the CsSH derivative was likely attributed to the new stable amorphous form, enhancing both the drug release capacity and subsequent absorption and bioavailability⁵³ and also the biodegradability and mucoadhesive properties of the polymer²⁸.

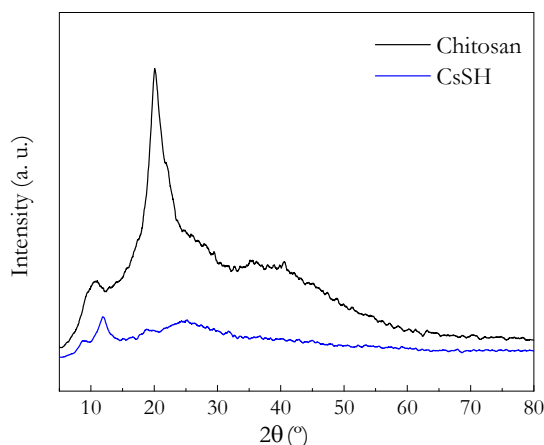


Figure III.11. X-ray patterns of chitosan and thiol-functionalized chitosan (CsSH).

The thermal stability was studied by thermogravimetric analysis and the thermograms and dTGA curves of pure chitosan and thiol-grafted chitosan are shown in Figure III.12. Compared to chitosan, for the thiolated derivative the degradation of the backbone started significantly earlier, indicating that the presence of the thiol groups grafted to the polymer main chain decreased the thermal stability of the polysaccharide. After a progressive loss of water up to 135 °C, which depends on the initial moisture content of the samples⁵⁴, the modified polymer decomposition reaction was observed to start at 180 °C. The incorporation of thiol groups decreased the decomposition temperature and, at the same time, a small shoulder in the dTGA curve indicated two-stage decomposition pattern in the case of the modified chitosan, in contrast to the single peak registered for the pure chitosan, which could be an indicative of the

incorporation of a new compound into the polymer main chain³⁶, verifying the successful functionalization of chitosan. Indeed, the resistance to thermal degradation was reduced in a greater extent in this case, which could be related to the increase in the amorphous form of the precursor.

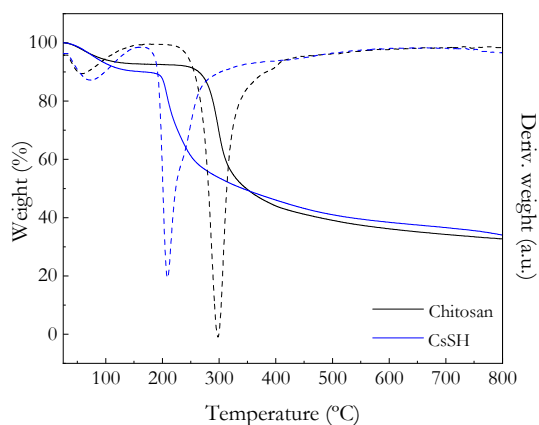


Figure III.12. TGA (left axis, solid line) and dTGA (right axis, dash line) curves of chitosan and thiolated chitosan (CsSH) under inert atmosphere.

Mucoadhesion is a complex process that involves interaction (chemical and physical) between the mucin epithelial layer and polymers with mucoadhesive potential. Therefore, mucoadhesive polymers can adhere to mucus membranes in different parts of the body (intestinal, oral or gastric mucosa)⁴⁸. As it was remarked in Chapter I, chitosan shows mucoadhesive properties as it has been shown to interact with mucin^{55–57}, even if the nature of the interactions between chitosan and mucin remains poorly weak based on electrostatic interactions. In fact, it has been demonstrated that polymers capable of forming covalent bonds with the mucus layer display more pronounced mucoadhesive properties, where thiolated chitosans based on disulphide bonds are greatly highlighted^{58,59}.

Thus, the mucoadhesion capacity of the new chitosan thiolated derivative was evaluated. The influence of the pH and the concentration of mucin was studied for different polymer/mucin mixtures after 1, 2, and 5 h of interaction under magnetic stirring at room temperature. As described in Chapter II, mixtures of polymer/mucin solutions were prepared in water (pH 6) and acid aqueous environment (0.5% v/v HAc, pH 3). The polymer (neat chitosan and thiol-functionalized chitosan) concentration was kept constant (0.25 mg mL^{-1}) while the mucin concentration was varied ($0.25, 0.50, 1.25$ and 1.50 mg mL^{-1}). Results obtained after applying the Equation II.17 and II.18 were represented on Figure III.13 and III.14 in both media.

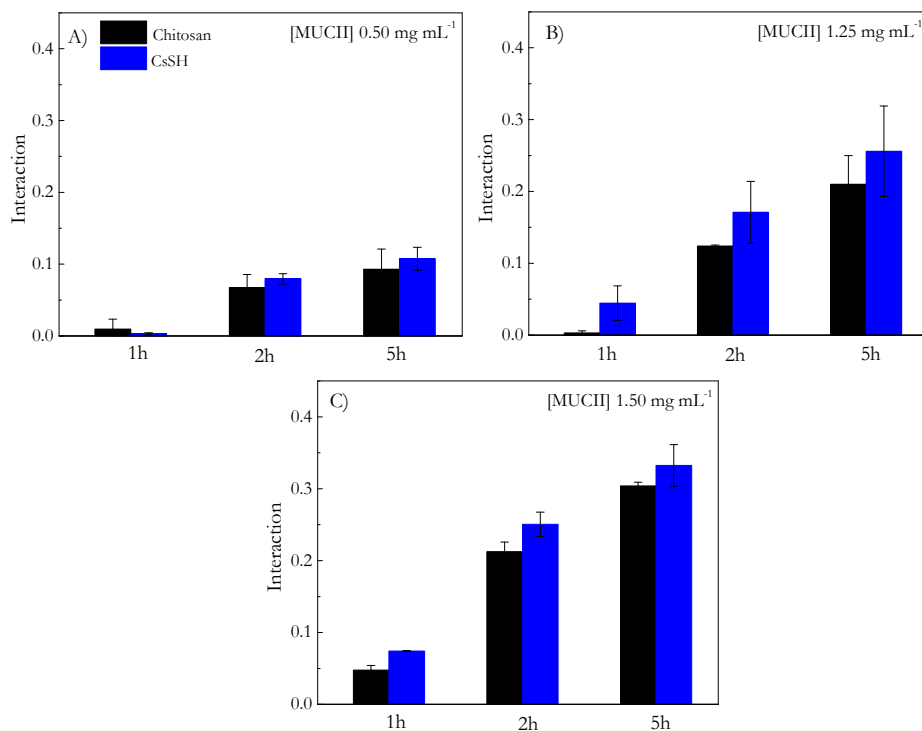


Figure III.13. Influence of mucin concentration on chitosan and thiolated chitosan as a function of interaction time for: A) 0.50, B) 1.25 and C) 1.50 mg mL^{-1} mucin concentrations at pH 3.

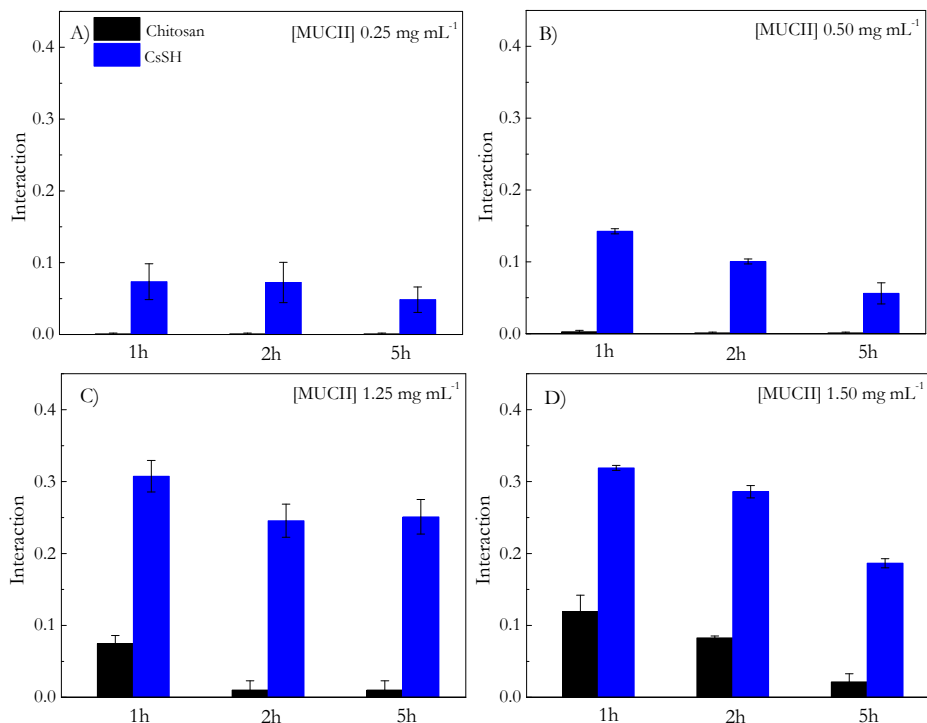


Figure III.14. Influence of mucin concentration on chitosan and thiolated chitosan as a function of interaction time for: A) 0.25, B) 0.50, C) 1.25 and D) 1.50 mg mL⁻¹ mucin concentrations at pH 6.

As previously mentioned, it has been widely reported the mucoadhesive nature of chitosan based on numerous works. Thereby, the primary interactive strength of adhesion between chitosan and mucus layer was found to be electrostatic, being these interactions higher in acid environment in accordance with other studies⁶⁰. This behaviour was clearly observed in Figure III.13, where the mucoadhesion property of the neat polymer showed the highest values, especially when increasing the contact time with the mucus layer. Additionally, modifying mucoadhesive polymers commonly leads to significantly improved mucoadhesion properties, leading to develop novel polymers⁵. Thereby, the presence of free thiol groups allowed the establishment of covalent disulphide bridges that could lead to boost

mucoadhesive properties. Therefore, the adhesion of thiolated chitosan to the stomach and intestine mucus was significantly higher than chitosan, being highly relevant in the case of neutral pH. Under these conditions, the thiol groups maximized the mucoadhesive nature of the original polymer, since the formation of inter and intramolecular disulphide bonds occurs at $\text{pH} > 5$ in the presence of oxidants, such as oxygen⁴.

On the other hand, the time factor acquired greater relevance under acidic conditions, where the polymer/mucin interactions significantly increased from 1 h to 5 h of contact with mucin for both samples, regardless the mucin concentration in study. Moreover, no adhesion was detected for none of the materials in stomachal conditions (pH 3) for 0.25 mg mL^{-1} mucin concentration, which indicated that this concentration was not enough for the creation of detectable interactions under these conditions. If at pH 3 the contact time was highlighted, under basic environment, where the chitosan/mucin interactions were observed to be quite poor, the mucin concentration played an important role. Namely, at higher concentrations of mucin, the mucoadhesive properties of both the chitosan and the thiolated derivative were enhanced.

Finally, *in vitro* cytotoxicity assay was also performed to evaluate the non-toxicity of the thiolated chitosan derivative since it was intended to be used as a precursor in the development of biomaterials. *In vitro* viability and proliferation of cells was studied by short-term assays evaluating changes in cellular growth, incubating L929 mouse fibroblast cells for 24 and 48 h in CsSH sample as described in Chapter II. The obtained results are shown in Figure III.15.

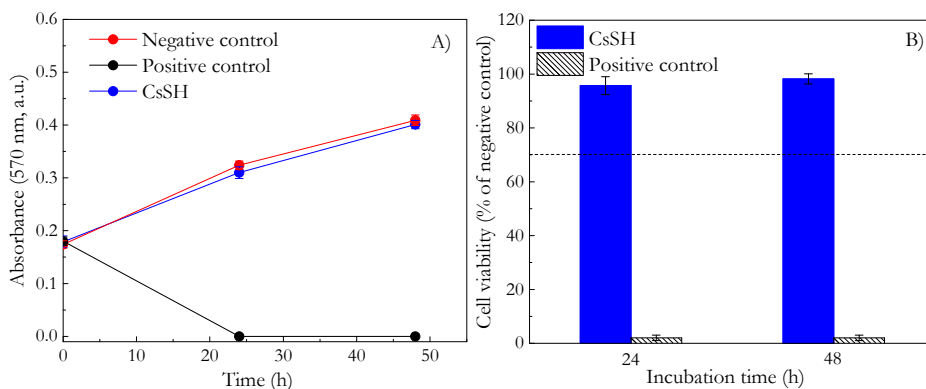


Figure III.15. A) Cell proliferation of murine fibroblasts L929 in contact with the CsSH material as a function of time (the viability data represented were obtained from PrestoBlue[®] at 570 nm) and B) viability of L929 murine fibroblast cell line with respect to the negative control at 24 and 48 h.

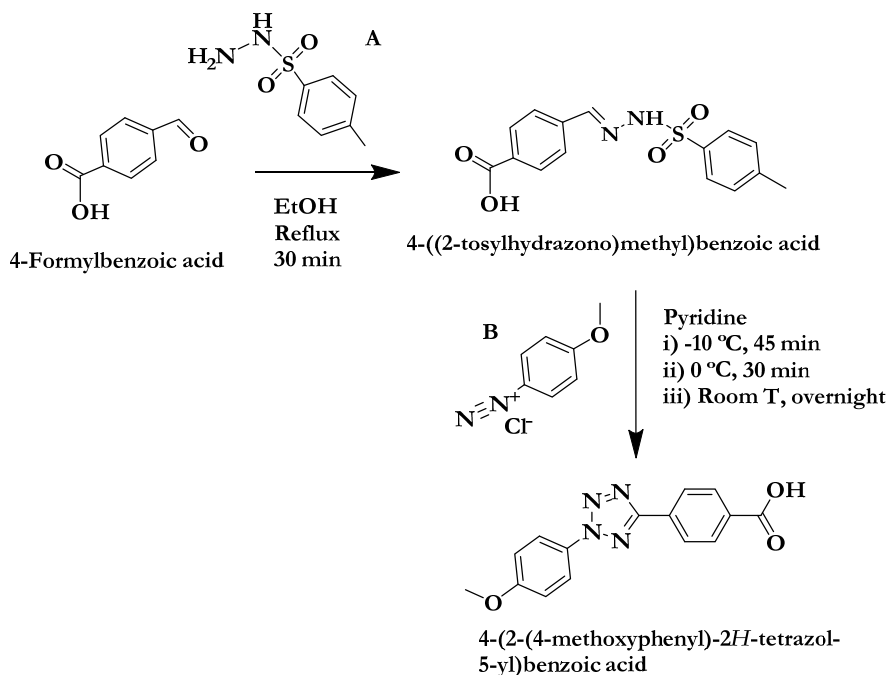
Preliminary viability results showed that the thiolated chitosan precursor presented non-toxic behaviour and allowed cell growth. The proliferation curve of hydrogels (Figure III.15A) showed the same increasing pattern of the negative control, whereas the positive control presented a decreasing slope for the proliferation curve. As mentioned, the cell viability was measured at 24 and 48 h in cells cultured in extracted medium from CsSH (Figure III.15B), showing cell viability values higher than the acceptance limit of 70 % (compared with the negative control) as established by ISO 10993 standards, which were close to 100 %. Therefore, the CsSH material guarantees cell proliferation, reaching cell viability values above the level of acceptance. The possible cytotoxicity is completely ruled out, being a biocompatible material.

III.5. SYNTHESIS OF TETRAZOLE-FUNCTIONALIZED CHITOSAN (CsTZ)

III.5.1. Synthesis of 4-(2-(4-methoxyphenyl)-2H-tetrazol-5-yl)benzoic acid (TBA)

An acid precursor containing tetrazole groups was first synthesized following a reported method in the literature⁶¹ (Scheme III.6) for later functionalization of chitosan. Thus, the desired molecule (4-(2-(4-methoxyphenyl)-2H-tetrazol-5-yl)benzoic acid, TBA) was obtained by two-step procedure. Namely, a mixture of 4-formylbenzoic acid (6.558 g, 43.7 mmol) and *p*-toluenesulfonyl hydrazide (8.138 g, 43.7 mmol) (A) in 100 mL of ethanol was heated to reflux for 30 min in a 1:1 equivalent ratio. The solution was diluted with 100 mL of water and the precipitate was filtered off. The solid (4-((2-tosylhydrazono)methyl)benzoic acid) was washed with 100 mL of aqueous ethanol (98 % w/w yield).

Subsequently, *p*-Anisidine (4 g, 32.5 mmol) was dissolved in a mixture of 8.46 mL of concentrated HCl, 26.9 mL of H₂O and 26.9 mL of EtOH and cooled to 0 °C. A cooled solution of NaNO₂ (2.241 g, 32.5 mmol) in 13.45 mL of H₂O was added dropwise and stirred for 10 min at 0 °C, being 1:1 the equivalent ratio of *p*-Anisidine to NaNO₂. The *in situ* generated diazonium salt solution (B) was added dropwise to a solution of (4-((2-tosylhydrazono)methyl)benzoic acid) (10.34 g, 32.5 mmol) in 200 mL of pyridine at 1:1 equivalent ratio at -10 °C – -5 °C over a period of 45 min. After complete addition, the solution was stirred at 0 °C for 30 min and then, at ambient temperature overnight. The turbid solution was poured into 500 mL of 10 % v/v aqueous HCl solution and the precipitate (TBA) was filtered off and washed with 250 mL of EtOH (65 % w/w yield).

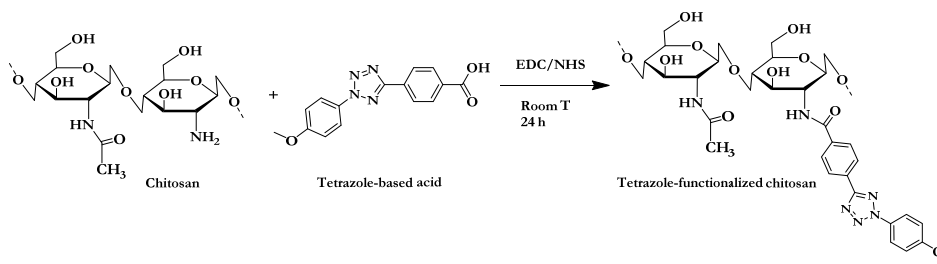


Scheme III.6. Synthesis of 4-(2-(4-methoxyphenyl)-2H-tetrazol-5-yl)benzoic acid.

III.5.2. Experimental part

The tetrazole-functionalized chitosan (CsTZ) was prepared via carbodiimide conjugation in DMF and under argon atmosphere. An equivalent ratio of 1:1.5 for amine-to-carboxylic acid was fixed in this case. Scheme III.7 shows the reaction between TBA and chitosan. Firstly, 0.3 g of chitosan were dissolved in 1 % v/v aqueous acetic acid to a final concentration of 1 % w/v, while the pH of the solution was adjusted to 5–6 using 1 M NaOH. At the same time, TBA (0.066 g mL⁻¹) was activated in DMF for 1 hour with EDC and NHS in 1:1 and 1:1.1 molar ratios, respectively. The activated acid was added dropwise to the chitosan solution and the mixture was stirred overnight under magnetic stirring in dark at ambient temperature under argon atmosphere. The product was precipitated in acetone, washed with methanol and DMSO and centrifuged several times against

deionized water (4200 rpm, 20 °C and 15 min per cycle (x4)). Finally, CsTZ was lyophilized (64 % w/w yield) and stored in dark at 4 °C until further use.



Scheme III.7. Synthesis of CsTZ through the reaction of chitosan and TBA modifier.

III.5.3. Results and discussion

Chitosan was modified with TBA in order to obtain photo-reactive precursor for the subsequent formation of fluorescent hydrogels once reacted with the appropriate complementary chitosan derivative. CsTZ was chemically characterized by FTIR and ^{13}C NMR spectroscopies to confirm the success of the functionalization reaction.

The FTIR spectra of the original chitosan and the tetrazole-functionalized chitosan (CsTZ) are shown in Figure III.14. Significant differences were observed by comparing the chemical structures before and after the functionalization of chitosan with TBA. Apart from the characteristic bands of the polysaccharide backbone that have been detailed in the previous sections of this chapter, in the CsTZ spectrum significant differences existed, most notably from 1800 cm^{-1} onwards still maintaining the bands related to the backbone of the original biopolymer. Accordingly, the presence of the grafted tetrazole moieties on the chitosan could be confirmed by the bands at 1517, 835 and 742 cm^{-1} , which are mainly related to the stretches in the aromatic ring ($-\text{C}=\text{C}-$) of the TBA acid. Moreover, the appearance of two new bands at 1766 and 1735 cm^{-1} could be

assigned to the carbonyl groups ($-C=O$) of the remains of the modifier that could be presented and to the new formed amide groups, respectively.

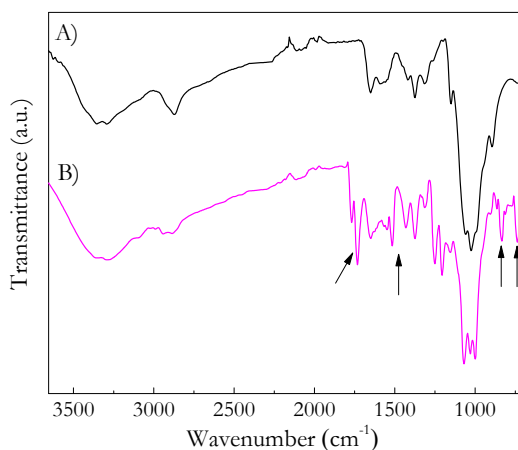


Figure III.14. FTIR spectra of A) chitosan and B) tetrazole-functionalized chitosan (CsTZ).

The chemical structure of the new derivative as well as the degree of substitution (DS) were also confirmed by solid-state ^{13}C NMR spectroscopy (Figure III.15). As it could be observed, specific reactive groups corresponding to the tetrazole group grafted to the chitosan backbone clearly manifested in the spectrum of the chitosan derivative. The ^{13}C NMR spectrum of chitosan is characterized by the presence of one signal corresponding to the anomeric carbon (C_1) at 104.5 ppm and a second signal containing multiple peaks in the 90–45 ppm region, associated to the rest of carbons of the deacetylated glucosamine unit (C_{2-6}). Finally, the signals of the carbons of carbonyl and methyl groups of the acetamido moiety appear at 172.9 and 23.0 ppm, respectively^{62–65}. The incorporation of the tetrazole ring into the polymeric structure could be confirmed by the signals in the range between 166–156 ppm ($\text{C}_{\text{e,i}}$) and 136–107 ppm ($\text{C}_{\text{g-h}}$), which corresponded to the carbons of the grafted molecule⁶¹. Furthermore, as the grafting of the tetrazole

groups into the chitosan led to the formation of new amide groups, the signal located at 172.1 ppm corresponding to the carboxyl groups, was transformed due to the functionalization.

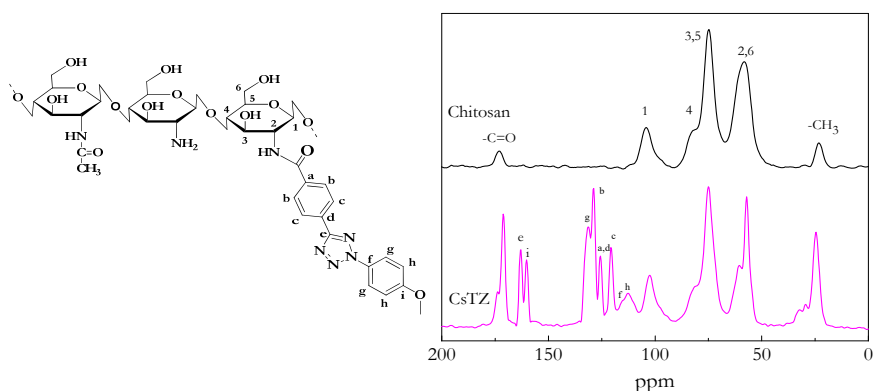


Figure III.15. Solid-state ^{13}C NMR spectra and chemical structure of chitosan and tetrazole-functionalized chitosan (CsTZ).

The DS was determined by the integration of the areas of the carbon signals of the glucosamine units and those of the tetrazole unit that were not affected. Calculations were made using the Equation II.5, where A_{TZ} corresponds to the area of tetrazole carbon signals in the range of 136–107 ppm and A_{Cs} to that of the glucosamine carbon units (C_{3-5}). The DS for the tetrazole-containing chitosan was 29 %.

Figure III.16 shows the XRD patterns for the original chitosan and the tetrazole-functionalized chitosan. The same trend as in the previous cases was observed this time. Namely, in the CsTZ spectrum both peaks decreased and the peak at $2\theta = 20^\circ$ became broader and weaker, suggesting a higher amorphous form in the modified sample⁵¹. After applying the Equation II.6, chitosan derivative presented a crystallinity index of 0.39.

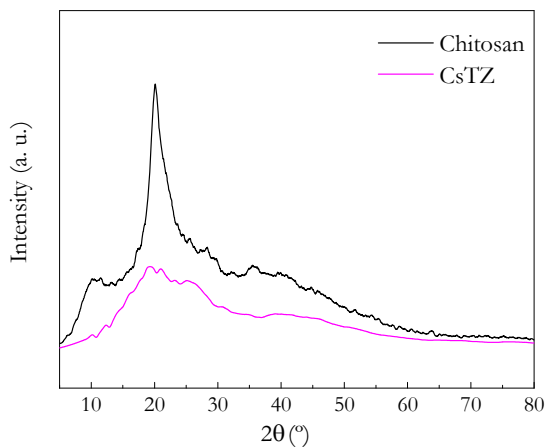


Figure III.16. X-ray patterns of chitosan and tetrazole-functionalized chitosan (CsTZ).

The thermal degradation behaviour and dTGA curves of neat chitosan and tetrazole-functionalized chitosan are shown in Figure III.17. The observed tendency was in agreement with the results showed in the previous sections of this chapter, where substituted polymers usually show lower thermal stability. For the tetrazole-functionalized chitosan the degradation took place at 191 °C after the initial loss of water, being the decomposition of the sample highly influenced by the presence of the new groups in the main chain of the biopolymer. Therefore, the dTGA curve of CsTZ displayed two significant degradation peaks at 225 and 262 °C with a consecutive shoulder at 304 °C, which could be related to the degradation of TBA and the decomposition of the chitosan derivative main chain, respectively. Furthermore, the degradation pattern of CsTZ registered another peak at higher temperatures (563 °C) due to the presence of new fragments in the polymer main chain related to the TBA, which might be due to the overlap of different concomitant degradation processes.

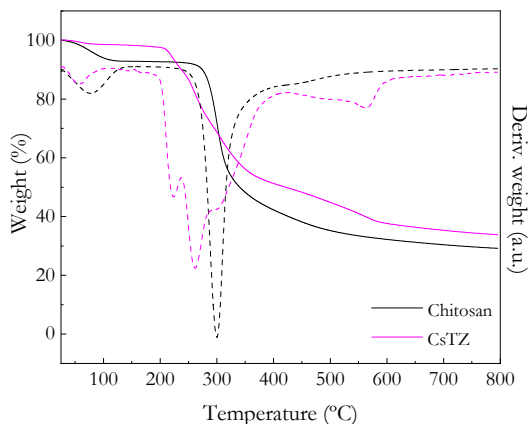


Figure III.17. TGA (left axis, solid line) and dTGA (right axis, dash line) curves of chitosan and tetrazole–functionalized chitosan (CsTZ) under inert atmosphere.

III.6. CONCLUSIONS

The physico–chemical and biological properties of chitosan could be tailored by grafting new molecules into the chitosan backbone. Therefore, chitosan was functionalized by the attachment of new pendant moieties to the main chain, proving it with specific reactivity and the ability to respond to particular purposes. Chitosan–based precursors were successfully synthesized following two different chemical strategies. In any case, the free amino groups of the biopolymer served as reactive sites for the synthesis of novel chitosan derivatives after reacting with aldehyde or carboxylic acid groups.

Four complementary chitosan derivatives were developed in order to use them as precursors in subsequent click reactions for the formation of three–dimensional structures. Namely, furan, maleimide, thiol and tetrazole–containing chitosans were prepared and suitably characterized in terms of physico–chemical properties, thermal behaviour and crystallinity. Table III.1 shows the most relevant properties of the synthesized chitosan derivatives. These modifications

further enhanced the primary features of native chitosans, making them more suitable as precursors for further design of biomedical devices via click chemistry.

Table III.1. Main properties of the synthesized chitosan derivatives.

Chitosan functionalization	Eq. ratio amine-to-aldehyde/acid	Degree of substitution (DS, %)	Crystallinity index (CI)	Degradation temperature (°C)
CsFu (Chapter IV)	1:1.6	29 ^a	0.29	270
CsAMI (Chapter IV and VI)	1:2	27 ^a / 10 ^a	0.18	258
CsSH (Chapter V and VII)	1:1	26 ^b / 11 ^b	0.14	208
CsTZ (Chapter VI)	1:1.5	29 ^c	0.39	262/304

^a DS calculated from liquid-state ¹H NMR

^b DS calculated from ninhydrin assay

^c DS calculated from solid-state ¹³C NMR

The reaction conditions were optimized in order to obtain the maximum substitution that would preserve required solubility of the polymer. Thereby, modifiers were added in excess, except in the case of the thiolactic acid since higher ratios of amine-to-carboxylic acid groups did not result in a greater number of substituted amines. The functionalization of chitosan was confirmed by the determination of the amine substitution degree (DS) in all the cases. The percentages of specific units grafted in the chitosan were found to be similar in all cases, regardless of the employed technique to calculate them, chosen by the modifier and the nature of the resulted precursor. Therefore, a significant number of distinctive groups were immobilized in native chitosan in all the cases, being the DS highly adequate for the subsequent cross-linking click reactions.

The success of the modifications was demonstrated by means of FTIR and NMR spectroscopy. The chemical structure of the chitosan before and after the functionalization was compared and the presence of the specific reactive groups grafted to the chitosan chains were observed in all the spectra.

The effect of the functionalizations on the crystalline structure of chitosan was evaluated by XRD. The crystallinity index of the precursors tended to decrease after the functionalization process in all the cases (Table III.1). Even if different oriented patterns were observed in the diffractograms of the chitosan precursors depending on the sample preparation, the crystallinity indexes were not influenced by this fact.

Furthermore, results showed that the thermal degradation of chitosan-based precursors was influenced by the presence of grafted molecules on the main chain of the biopolymer. Accordingly, the stability of neat chitosan was diminished in all the cases, registering lower degradation temperatures in the case of the precursors. Above 600 °C, the thermal decomposition of the samples was complete, where only 30 % of char remained. Nevertheless, all modified samples were stable and no degradation occurred within the required temperature range for biomedical applications.

It is worth noting that the synthesized CsSH precursor exhibited good solubility in water, solving the mayor impediment that conditions this biopolymer. On the other hand, the thiolated chitosan derivative further improved the mucoadhesive properties of the native biopolymer by forming disulphide bonds with mucin, particularly at pH 6. Therefore, the results confirmed the exposed theory, where upon thiol modification, the mucoadhesive properties of chitosan were significantly improved. Finally, short-term cytotoxicity assays demonstrated *in vitro* cell viability and proliferation in chitosan samples, resulting in non-toxic precursors, which made them good candidates in view of being part of materials for biomedical applications.

REFERENCES

- (1) Shukla, S. K.; Mishra, A. K.; Arotiba, O. A.; Mamba, B. B. Chitosan-Based Nanomaterials: A State-of-the-Art Review. *Int. J. Biol. Macromol.* **2013**, *59*, 46–58. <https://doi.org/10.1016/j.ijbiomac.2013.04.043>.
- (2) Anitha, A.; Deepa, N.; Chennazhi, K. P.; Nair, S. V.; Tamura, H.; Jayakumar, R. Development of Mucoadhesive Thiolated Chitosan Nanoparticles for Biomedical Applications. *Carbohydr. Polym.* **2011**, *83* (1), 66–73. <https://doi.org/10.1016/j.carbpol.2010.07.028>.
- (3) Zhang, H.; Qadeer, A.; Chen, W. In Situ Gelable Interpenetrating Double Network Hydrogel Formulated from Binary Components: Thiolated Chitosan and Oxidized Dextran. *Biomacromolecules* **2011**, *12* (5), 1428–1437. <https://doi.org/10.1021/bm101192b>.
- (4) Bonengel, S.; Bernkop-Schnürch, A. Thiomers - From Bench to Market. *J. Control. Release* **2014**, *195*, 120–129. <https://doi.org/10.1016/j.jconrel.2014.06.047>.
- (5) Shtenberg, Y.; Goldfeder, M.; Schroeder, A.; Bianco-Peled, H. Alginate Modified with Maleimide-Terminated PEG as Drug Carriers with Enhanced Mucoadhesion. *Carbohydr. Polym.* **2017**, *175*, 337–346. <https://doi.org/10.1016/j.carbpol.2017.07.076>.
- (6) García-Astrain, C.; Gandini, A.; Coelho, D.; Mondragon, I.; Retegi, A.; Eceiza, A.; Corcuera, M. A.; Gabilondo, N. Green Chemistry for the Synthesis of Methacrylate-Based Hydrogels Crosslinked through Diels-Alder Reaction. *Eur. Polym. J.* **2013**, *49* (12), 3998–4007. <https://doi.org/10.1016/j.eurpolymj.2013.09.004>.
- (7) Estupiñán, D.; Gegenhuber, T.; Blinco, J. P.; Barner-Kowollik, C.; Barner, L. Self-Reporting Fluorescent Step-Growth Raft Polymers Based on Nitrile Imine-Mediated Tetrazole-Ene Cycloaddition Chemistry. *ACS Macro Lett.* **2017**, *6* (3), 229–234. <https://doi.org/10.1021/acsmacrolett.7b00024>.
- (8) Fan, Y.; Deng, C.; Cheng, R.; Meng, F.; Zhong, Z. In Situ Forming Hydrogels via Catalyst-Free and Bioorthogonal “Tetrazole-Alkene” Photo-Click Chemistry. *Biomacromolecules* **2013**, *14* (8), 2814–2821. <https://doi.org/10.1021/bm400637s>.
- (9) Hamedí, H.; Moradi, S.; Hudson, S. M.; Tonelli, A. E. Chitosan Based Hydrogels and Their Applications for Drug Delivery in Wound Dressings: A Review. *Carbohydr. Polym.* **2018**, *199*, 445–460. <https://doi.org/10.1016/J.CARBPOL.2018.06.114>.

- (10) Jain, A.; Gulbake, A.; Shilpi, S.; Jain, A.; Hurkat, P.; Jain, S. K. A New Horizon in Modifications of Chitosan: Syntheses and Applications. *Crit. Rev. Ther. Drug Carrier Syst.* **2013**, *30* (2), 91–181. <https://doi.org/10.1615/CritRevTherDrugCarrierSyst.2013005678>.
- (11) Ways, T. M. M.; Lau, W. M.; Khutoryanskiy, V. V. Chitosan and Its Derivatives for Application in Mucoadhesive Drug Delivery Systems. *Polymers* **2018**, *10* (3). <https://doi.org/10.3390/polym10030267>.
- (12) Mohammed, M. A.; Syeda, J. T. M.; Wasan, K. M.; Wasan, E. K. An Overview of Chitosan Nanoparticles and Its Application in Non-Parenteral Drug Delivery. *Pharmaceutics* **2017**, *9* (4). <https://doi.org/10.3390/pharmaceutics9040053>.
- (13) Montiel-Herrera, M.; Gandini, A.; Goycoolea, F. M.; Jacobsen, N. E.; Lizardi-Mendoza, J.; Recillas-Mota, M.; Argüelles-Monal, W. M. N-(Furfural) Chitosan Hydrogels Based on Diels-Alder Cycloadditions and Application as Microspheres for Controlled Drug Release. *Carbohydr. Polym.* **2015**, *128*, 6–12. <https://doi.org/10.1016/j.carbpol.2015.03.052>.
- (14) Medeiros Borsagli, F. G. L.; Carvalho, I. C.; Mansur, H. S. Amino Acid-Grafted and N-Acylated Chitosan Thiomers: Construction of 3D Bio-Scaffolds for Potential Cartilage Repair Applications. *Int. J. Biol. Macromol.* **2018**, *114*, 270–282. <https://doi.org/10.1016/J.IJBIOMAC.2018.03.133>.
- (15) Ruiz Matute, A. I.; Cardelle-Cobas, A.; García-Bermejo, A. B.; Montilla, A.; Olano, A.; Corzo, N. Synthesis, Characterization and Functional Properties of Galactosylated Derivatives of Chitosan through Amide Formation. *Food Hydrocoll.* **2013**, *33* (2), 245–255. <https://doi.org/10.1016/j.foodhyd.2013.03.016>.
- (16) Farris, S.; Song, J.; Huang, Q. Alternative Reaction Mechanism for the Cross-Linking of Gelatin with Glutaraldehyde. *J. Agric. Food Chem.* **2010**, *58* (2), 998–1003. <https://doi.org/10.1021/jf9031603>.
- (17) Mohamed, N. A.; Fahmy, M. M. Synthesis and Antimicrobial Activity of Some Novel Cross-Linked Chitosan Hydrogels. *Int. J. Mol. Sci.* **2012**, *13* (9), 11194–11209. <https://doi.org/10.3390/ijms130911194>.
- (18) Chen, X.; Chew, S. L.; Kerton, F. M.; Yan, N. Direct Conversion of Chitin into a N-Containing Furan Derivative. *Green Chem.* **2014**, *16* (4), 2204–2212. <https://doi.org/10.1039/c3gc42436g>.
- (19) Kumirska, J.; Czerwicka, M.; Kaczyński, Z.; Bychowska, A.; Brzozowski, K.; Thöming, J.; Stepnowski, P. Application of Spectroscopic Methods for

- Structural Analysis of Chitin and Chitosan. *Mar. Drugs* **2010**, *8* (5), 1567–1636. <https://doi.org/10.3390/md8051567>.
- (20) Nimmo, C. M.; Owen, S. C.; Shoichet, M. S. Diels-Alder Click Cross-Linked Hyaluronic Acid Hydrogels for Tissue Engineering. *Biomacromolecules* **2011**, *12* (3), 824–830. <https://doi.org/10.1021/bm101446k>.
- (21) Qu, X.; Wirsén, A.; Albertsson, A. C. Novel PH-Sensitive Chitosan Hydrogels: Swelling Behavior and States of Water. *Polymer* **2000**, *41* (12), 4589–4598. [https://doi.org/10.1016/S0032-3861\(99\)00685-0](https://doi.org/10.1016/S0032-3861(99)00685-0).
- (22) Bhattarai, N.; Ramay, H. R.; Gunn, J.; Matsen, F. A.; Zhang, M. PEG-Grafted Chitosan as an Injectable Thermosensitive Hydrogel for Sustained Protein Release. *J. Control. Release* **2005**, *103* (3), 609–624. <https://doi.org/10.1016/J.JCONREL.2004.12.019>.
- (23) Kurita, O.; Murakami, K.; Fujiwara, T. Chemical Modification of Polysaccharides by the Use of Intramolecular Associations in Polar Organic Solvents. *Polym. Bull.* **2010**, *65* (5), 443–454. <https://doi.org/10.1007/s00289-009-0219-8>.
- (24) Pereira, A. G. B.; Muniz, E. C.; Hsieh, Y. Lo. 1H NMR and 1H-13C HSQC Surface Characterization of Chitosan-Chitin Sheath-Core Nanowhiskers. *Carbohydr. Polym.* **2015**, *123*, 46–52. <https://doi.org/10.1016/j.carbpol.2015.01.017>.
- (25) Ramasamy, P.; Subhadrappa, N.; Thinesh, T.; Selvin, J.; Selvan, K. M.; Shanmugam, V.; Shanmugam, A. Characterization of Bioactive Chitosan and Sulfated Chitosan from *Doryteuthis Singhalensis* (Ortmann, 1891). *Int. J. Biol. Macromol.* **2017**, *99*, 682–691. <https://doi.org/10.1016/J.IJBIOMAC.2017.03.041>.
- (26) Gandini, A.; Coelho, D.; Silvestre, A. J. D. Reversible Click Chemistry at the Service of Macromolecular Materials. Part 1: Kinetics of the Diels-Alder Reaction Applied to Furan-Maleimide Model Compounds and Linear Polymerizations. *Eur. Polym. J.* **2008**, *44* (12), 4029–4036. <https://doi.org/10.1016/j.eurpolymj.2008.09.026>.
- (27) Jiang, M.; Wang, K.; Kennedy, J. F.; Nie, J.; Yu, Q.; Ma, G. Preparation and Characterization of Water-Soluble Chitosan Derivative by Michael Addition Reaction. *Int. J. Biol. Macromol.* **2010**, *47* (5), 696–699. <https://doi.org/10.1016/j.ijbiomac.2010.09.002>.
- (28) Prabakaran, M.; Gong, S. Novel Thiolated Carboxymethyl Chitosan-g- β -Cyclodextrin as Mucoadhesive Hydrophobic Drug Delivery Carriers.

- Carbohydr. Polym.* **2008**, *73* (1), 117–125.
<https://doi.org/10.1016/J.CARBPOL.2007.11.005>.
- (29) Raut, A. V.; Satvekar, R. K.; Rohiwal, S. S.; Tiwari, A. P.; Gnanamani, A.; Pushpavanam, S.; Nanaware, S. G.; Pawar, S. H. In Vitro Biocompatibility and Antimicrobial Activity of Chitin Monomer Obtain from Hollow Fiber Membrane. *Des. Monomers Polym.* **2016**, *19* (5), 445–455.
<https://doi.org/10.1080/15685551.2016.1169379>.
- (30) Jang, M. K.; Kong, B. G.; Jeong, Y. Il; Lee, C. H.; Nah, J. W. Physicochemical Characterization of α -Chitin, β -Chitin, and γ -Chitin Separated from Natural Resources. *J. Polym. Sci. Part A Polym. Chem.* **2004**, *42* (14), 3423–3432.
<https://doi.org/10.1002/pola.20176>.
- (31) Sagheer, F. A. A.; Al-Sughayer, M. A.; Muslim, S.; Elsabee, M. Z. Extraction and Characterization of Chitin and Chitosan from Marine Sources in Arabian Gulf. *Carbohydr. Polym.* **2009**, *77* (2), 410–419.
<https://doi.org/10.1016/j.carbpol.2009.01.032>.
- (32) Feng, F.; Liu, Y.; Zhao, B.; Hu, K. Characterization of Half N-Acetylated Chitosan Powders and Films. *Procedia Eng.* **2012**, *27* (2011), 718–732.
<https://doi.org/10.1016/j.proeng.2011.12.511>.
- (33) Gokila, S.; Gomathi, T.; Sudha, P. N.; Anil, S. Removal of the Heavy Metal Ion Chromium(VI) Using Chitosan and Alginate Nanocomposites. *Int. J. Biol. Macromol.* **2017**, *104* (May), 1459–1468.
<https://doi.org/10.1016/j.ijbiomac.2017.05.117>.
- (34) Pereira, F. S.; Da Silva Agostini, D. L.; Job, A. E.; González, E. R. P. Thermal Studies of Chitin-Chitosan Derivatives. *J. Therm. Anal. Calorim.* **2013**, *114* (1), 321–327. <https://doi.org/10.1007/s10973-012-2835-z>.
- (35) Neto, C. G. T.; Giacometti, J. A.; Job, A. E.; Ferreira, F. C.; Fonseca, J. L. C.; Pereira, M. R. Thermal Analysis of Chitosan Based Networks. *Carbohydr. Polym.* **2005**, *62* (2), 97–103. <https://doi.org/10.1016/j.carbpol.2005.02.022>.
- (36) Nanaki, S.; Tseklina, M.; Christodoulou, E.; Triantafyllidis, K.; Kostoglou, M.; Bikiaris, D. N. Thiolated Chitosan Masked Polymeric Microspheres with Incorporated Mesocellular Silica Foam (MCF) for Intranasal Delivery of Paliperidone. *Polymers* **2017**, *9* (11). <https://doi.org/10.3390/polym9110617>.
- (37) García-Astrain, C.; Avérous, L. Synthesis and Evaluation of Functional Alginate Hydrogels Based on Click Chemistry for Drug Delivery Applications. *Carbohydr. Polym.* **2018**, *190* (February), 271–280.
<https://doi.org/10.1016/j.carbpol.2018.02.086>.

- (38) Mantovani, G.; Lecolley, F.; Tao, L.; Haddleton, D. M.; Clerx, J.; Cornelissen, J. J. L. M.; Velonia, K. Design and Synthesis of N-Maleimido-Functionalized Hydrophilic Polymers via Copper-Mediated Living Radical Polymerization: A Suitable Alternative to Pegylation Chemistry. *J. Am. Chem. Soc.* **2005**, *127* (9), 2966–2973. <https://doi.org/10.1021/ja0430999>.
- (39) Jabeen, S.; Kausar, A.; Saeed, S.; Muhammad, B.; Gul, S.; Farooq, M. Crosslinking of Alginic Acid/Chitosan Matrices Using Bis Phenol-F-Diglycidyl Ether: Mechanical, Thermal and Water Absorption Investigation. *Int. J. Plast. Technol.* **2016**, *20* (1), 159–174. <https://doi.org/10.1007/s12588-016-9143-6>.
- (40) Ostrowska-Czubenko, J.; Pierog, M.; Gierszewska-Druzynska, M. State of Water in Noncrosslinked and Crosslinked Hydrogel Chitosan Membranes–DSC Studies. In *Progress on Chemistry and Application of chitin and its derivatives*; Poland, 2011; Vol. XVI, pp 147–156.
- (41) Govindan, S.; Nivethaa, E. A. K.; Saravanan, R.; Narayanan, V.; Stephen, A. Synthesis and Characterization of Chitosan–Silver Nanocomposite. *Appl. Nanosci.* **2012**, *2* (3), 299–303. <https://doi.org/10.1007/s13204-012-0109-5>.
- (42) Shitrit, Y.; Bianco-Peled, H. Acrylated Chitosan for Mucoadhesive Drug Delivery Systems. *Int. J. Pharm.* **2017**, *517* (1–2), 247–255. <https://doi.org/10.1016/j.ijpharm.2016.12.023>.
- (43) Bernkop-Schnürch, A. Thiomers: A New Generation of Mucoadhesive Polymers. *Adv. Drug Deliv. Rev.* **2005**, *57* (11), 1569–1582. <https://doi.org/10.1016/J.ADDR.2005.07.002>.
- (44) Bernkop-Schnürch, A.; Hornof, M.; Guggi, D. Thiolated Chitosans. *Eur. J. Pharm. Biopharm.* **2004**, *57* (1), 9–17. [https://doi.org/10.1016/S0939-6411\(03\)00147-4](https://doi.org/10.1016/S0939-6411(03)00147-4).
- (45) Chesnutt, B. M.; Viano, A. M.; Yuan, Y.; Yang, Y.; Guda, T.; Appleford, M. R.; Ong, J. L.; Haggard, W. O.; Bumgardner, J. D. Design and Characterization of a Novel Chitosan/Nanocrystalline Calcium Phosphate Composite Scaffold for Bone Regeneration. *J. Biomed. Mater. Res. - Part A* **2009**, *88* (2), 491–502. <https://doi.org/10.1002/jbm.a.31878>.
- (46) Zhang, J.; Tan, W.; Zhang, Z.; Song, Y.; Li, Q.; Dong, F.; Guo, Z. Synthesis, Characterization, and the Antifungal Activity of Chitosan Derivatives Containing Urea Groups. *Int. J. Biol. Macromol.* **2018**, *109*, 1061–1067. <https://doi.org/10.1016/J.IJBIOMAC.2017.11.092>.
- (47) Radhakumary, C.; Antonty, M.; Sreenivasan, K. Drug Loaded

- Thermoresponsive and Cytocompatible Chitosan Based Hydrogel as a Potential Wound Dressing. *Carbohydr. Polym.* **2011**, *83* (2), 705–713. <https://doi.org/10.1016/j.carbpol.2010.08.042>.
- (48) Tekade, M.; Maheshwari, N.; Youngren-Ortiz, S. R.; Pandey, V.; Chourasiya, Y.; Soni, V.; Deb, P. K.; Sharma, M. C. Thiolated-Chitosan: A Novel Mucoadhesive Polymer for Better-Targeted Drug Delivery. *Biomater. Bionanotechnol.* **2019**, 459–493. <https://doi.org/10.1016/B978-0-12-814427-5.00013-5>.
- (49) Abdelgawad, A. M.; El-Naggar, M. E.; Hudson, S. M.; Rojas, O. J. Fabrication and Characterization of Bactericidal Thiol-Chitosan and Chitosan Iodoacetamide Nanofibres. *Int. J. Biol. Macromol.* **2017**, *94*, 96–105. <https://doi.org/10.1016/j.ijbiomac.2016.07.061>.
- (50) Li, Y.; Xu, J.; Xu, Y.; Huang, L.; Wang, J.; Cheng, X. Synthesis and Characterization of Fluorescent Chitosan-ZnSe/ZnS Nanoparticles for Potential Drug Carriers. *RSC Adv.* **2015**, *5* (49), 38810–38817. <https://doi.org/10.1039/c5ra02933c>.
- (51) Kumar, S.; Koh, J. Physicochemical, Optical and Biological Activity of Chitosan-Chromone Derivative for Biomedical Applications. *Int. J. Mol. Sci.* **2012**, *13* (5), 6103–6116. <https://doi.org/10.3390/ijms13056102>.
- (52) Artech Pujana, M.; Perez-Alvarez, L.; Cesteros Iturbe, L. C.; Katime, I. PH-Sensitive Chitosan-Folate Nanogels Crosslinked with Biocompatible Dicarboxylic Acids. *Eur. Polym. J.* **2014**, *61*, 215–225. <https://doi.org/10.1016/j.eurpolymj.2014.10.007>.
- (53) Boateng, J.; Areago, D. Composite Sodium Alginate and Chitosan Based Wafers for Buccal Delivery of Macromolecules. *Austin J. Anal. Pharm. Chem.* **2014**, *1* (5), 1–7.
- (54) Olivas-Armendáriz, I.; Santos-Rodríguez, E.; Correa-Espinoza, S.; Domínguez-Domínguez, D.-S.; Márquez-Méndez, I.; Mendoza-Duarte, M.; Chavarría-Gaytán, M.-C.; Martel-Estrada, S.-A. Evaluation of Mechanical and Thermophysical Properties of Chitosan/Poly(DL-Lactide-Co-Glycolide)/Multiwalled Carbon Nanotubes for Tissue Engineering. *Am. J. Mater. Sci.* **2015**, *5* (1), 9–16. <https://doi.org/10.5923/j.materials.20150501.02>.
- (55) Wittaya-Areekul, S.; Krueenate, J.; Praharn, C. Preparation and in Vitro Evaluation of Mucoadhesive Properties of Alginate/Chitosan Microparticles Containing Prednisolone. *Int. J. Pharm.* **2006**, *312* (1–2), 113–118. <https://doi.org/10.1016/j.ijpharm.2006.01.003>.

- (56) Silva, C. A.; Nobre, T. M.; Pavinatto, F. J.; Oliveira, O. N. Interaction of Chitosan and Mucin in a Biomembrane Model Environment. *J. Colloid Interface Sci.* **2012**, *376* (1), 289–295. <https://doi.org/10.1016/j.jcis.2012.03.027>.
- (57) Sogias, I. A.; Williams, A. C.; Khutoryanskiy, V. V. Why Is Chitosan Mucoadhesive? *Biomacromolecules* **2008**, *9* (7), 1837–1842. <https://doi.org/10.1021/bm800276d>.
- (58) Dhawan, S.; Singla, A. K.; Sinha, V. R. Evaluation of Mucoadhesive Properties of Chitosan Microspheres Prepared by Different Methods. *AAPS PharmSciTech* **2004**, *5* (4). <https://doi.org/10.1208/pt050467>.
- (59) Roldo, M.; Hornof, M.; Caliceti, P.; Bernkop-Schnürch, A. Mucoadhesive Thiolated Chitosans as Platforms for Oral Controlled Drug Delivery: Synthesis and in Vitro Evaluation. *Eur. J. Pharm. Biopharm.* **2004**, *57* (1), 115–121. [https://doi.org/10.1016/S0939-6411\(03\)00157-7](https://doi.org/10.1016/S0939-6411(03)00157-7).
- (60) Kumar, A.; Vimal, A.; Kumar, A. Why Chitosan? From Properties to Perspective of Mucosal Drug Delivery. *Int. J. Biol. Macromol.* **2016**, *91*, 615–622. <https://doi.org/10.1016/J.IJBIOMAC.2016.05.054>.
- (61) Rodriguez-Emmenegger, C.; Preuss, C. M.; Yameen, B.; Pop-Georgievski, O.; Bachmann, M.; Mueller, J. O.; Bruns, M.; Goldmann, A. S.; Bastmeyer, M.; Barner-Kowollik, C. Controlled Cell Adhesion on Poly(Dopamine) Interfaces Photopatterned with Non-Fouling Brushes. *Adv. Mater.* **2013**, *25* (42), 6123–6127. <https://doi.org/10.1002/adma.201302492>.
- (62) Lefay, C.; Guillaneuf, Y.; Moreira, G.; Thevarajah, J. J.; Castignolles, P.; Ziarelli, F.; Bloch, E.; Major, M.; Charles, L.; Gaborieau, M.; et al. Heterogeneous Modification of Chitosan via Nitroxide-Mediated Polymerization. *Polym. Chem.* **2013**, *4* (2), 322–328. <https://doi.org/10.1039/c2py20544k>.
- (63) Gartner, C.; López, B. L.; Sierra, L.; Graf, R.; Spiess, H. W.; Gaborieau, M. Interplay between Structure and Dynamics in Chitosan Films Investigated with Solid-State NMR, Dynamic Mechanical Analysis, and X-Ray Diffraction. *Biomacromolecules* **2011**, *12* (4), 1380–1386. <https://doi.org/10.1021/bm200193u>.
- (64) Younes, I.; Hajji, S.; Frachet, V.; Rinaudo, M.; Jellouli, K.; Nasri, M. Chitin Extraction from Shrimp Shell Using Enzymatic Treatment. Antitumor, Antioxidant and Antimicrobial Activities of Chitosan. *Int. J. Biol. Macromol.* **2014**, *69*, 489–498. <https://doi.org/10.1016/j.ijbiomac.2014.06.013>.

- (65) Liu, N.; Ni, S.; Ragauskas, A. J.; Meng, X.; Hao, N.; Fu, Y. Laccase-Mediated Functionalization of Chitosan with 4-Hexyloxyphenol Enhances Antioxidant and Hydrophobic Properties of Copolymer. *J. Biotechnol.* **2018**, *269* (February), 8–15. <https://doi.org/10.1016/j.jbiotec.2018.01.015>.

CHAPTER IV

HYDROGELS FOR DRUG DELIVERY THROUGH THE DIELS–ALDER REACTION

IV.1. INTRODUCTION AND OBJECTIVE	127
IV.2. FURAN/MALEIMIDE CHITOSAN–BASED HYDROGEL FORMATION (CsFu/CsAMI)	129
IV.2.1. EXPERIMENTAL PART	129
IV.2.2. RESULTS AND DISCUSSION	130
IV.2.2.1. Physico–chemical characterization	130
IV.2.2.2. Rheological behaviour	131
IV.2.2.3. Morphological analysis	134
IV.2.2.4. Swelling and degradation studies	135
IV.2.2.5. Drug delivery study	139
IV.2.2.6. Antimicrobial activity	140
IV.2.2.7. Biocompatibility	141
IV.3. FURAN–FUNCTIONALIZED CHITOSAN AND POLYETHERAMINE–BASED BISMALIMIDE HYDROGELS FORMATION (CsFu/BMI)	143
IV.3.1. EXPERIMENTAL PART	143
IV.3.2. RESULTS AND DISCUSSION	145
IV.3.2.1. Physico–chemical characterization	145
IV.3.2.2. Rheological behaviour	147
IV.3.2.3. Morphological analysis	151
IV.3.2.4. Swelling and pH sensitivity studies	156
IV.3.2.5. Drug delivery study	161
IV.4. CONCLUSIONS	163
REFERENCES	166

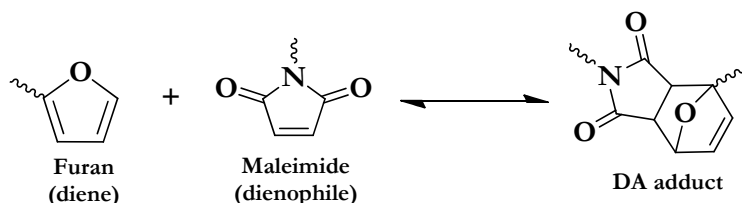
IV. HYDROGELS FOR DRUG DELIVERY THROUGH THE DIELS–ALDER REACTION

IV.1. INTRODUCTION AND OBJECTIVE

The Diels–Alder (DA) reaction is a powerful cross–linking strategy for biopolymer–based hydrogels as it is efficient, versatile and selective. Among all the click reactions, the Diels–Alder reaction has gained great importance since it usually takes place under mild reaction conditions and in absence of side reactions, being thermally reversible allowing the control of the reaction degree^{1,2} and additive–free, preserving the biocompatibility of the material³. While this reaction has previously been used for the synthesis of polymeric hydrogels via different strategies^{3–9}, few reports deal with its use for the preparation of chitosan–based hydrogels^{10,11}.

Many reactive pairs of dienes and alkenes (dienophiles) potentially lead to conjugation through carbon–carbon or carbon–heteroatom bond formation (hetero–Diels–Alder or HAD)¹², giving place to unsaturated rings. Since the Diels–Alder reaction is an electrocyclic reaction, which involves the formation of a cyclic product via a cyclic transition state, it is also referred to as a cycloaddition. One of the most commonly employed couple of functional groups for Diels–Alder cross–linking is the furan/maleimide, where furans act as electron–rich dienes and maleimides represent the dienophile groups¹³, resulting in Diels–Alder adducts (Scheme IV.1). Furan derivatives descend from renewable resources¹¹, whereas maleimides are biocompatible chemical compounds that have been recognized as promising molecules to prepare functional polymers, hydrogels and high performance thermosetting bismaleimide resins¹⁴, an important aspect regarding sustainable green chemistry and materials science. Adduct formation is predominant near 65 °C with reasonable reaction rates, whereas at higher temperature, typically above 90 °C, the corresponding retro–Diels–Alder reaction occurs and the conjugate splits in its original parts. This reversibility was quickly

recognized as an important characteristic of the furan–maleimide combination in cross–linking reactions as it provided paths to unprecedented dynamic systems¹².



Scheme IV.1. Diels–Alder reaction between furan and maleimide groups.

Hence, the main objective of this chapter was to design biopolymeric hydrogels towards the chemical cross–linking of chitosan through DA reaction in aqueous medium. The furan ring was introduced in the polymer structure using furfural, whereas dienophiles were incorporated in the form of maleimide moieties through two different strategies. To this end, the furan–modified chitosan (CsFu) synthesized as explained in the Section III.2 was used as a diene. Then, the cross–linking was carried out between the grafted furan groups in the chitosan macromolecule and i) maleimide–modified chitosan (CsAMI) as detailed in Section III.3 (described in Section IV.2) or ii) synthesized polyetherbismaleimide cross–linker (BMI) (described in Section IV.3). The networking occurred due to the formation of the Diels–Alder adduct after the reaction of both components at 65 °C. Both synthetic strategies for the hydrogels formation were developed in water, representing an interesting example of green click chemistry. Besides, in this case, medium molecular weight chitosan was used due to the need for developing high consistency 3D materials.

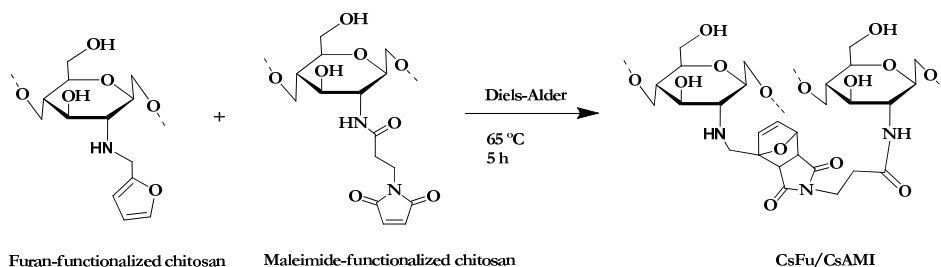
The Diels–Alder reaction was followed by UV–vis spectroscopy and the cross–linking reaction at 65 °C was monitored by dynamic rheological measurements in order to determine the gelation point. On the other hand, the as–prepared hydrogels were analysed in terms of microstructure and rheological behaviour.

The pH–sensitivity of the hydrogels was studied by conducting swelling studies in different media. Furthermore, the biodegradation of the final material based on complementary chitosans was assessed in the presence of lysozymes. Finally, the suitability of the DA hydrogels as possible drug carriers was evaluated using chloramphenicol as the model drug and simulating intestinal fluid conditions.

IV.2. FURAN/MALEIMIDE CHITOSAN–BASED HYDROGEL FORMATION (CsFu/CsAMI)

IV.2.1. Experimental part

The first chitosan–based DA cross–linked hydrogel was obtained by reacting two complementary chitosan–based derivatives. Namely, furan and maleimide–functionalized chitosan precursors were synthesized separately before the cross–linking reaction as detailed in Chapter III. CsFu and CsAMI were separately dissolved in 2 % v/v aqueous acetic acid solution and then mixed to a final volume of 2 mL. The reactive mixture was allowed to gel at 65 °C for 5 h (Scheme IV.2). The required concentration of both polymeric precursors was fixed to 5 % w/v since low concentrations resulted in non–gel like product whereas high concentrations led to a non–soluble starting solution. Additional experiments with different CsFu/CsAMI ratios led to non–stable materials so that a stoichiometric amount of CsFu and CsAMI was used.



Scheme IV.2. Hydrogel formation through DA reaction between CsFu and CsAMI.

Hydrogel samples before and after gelation are shown in Figure IV.1 along with a schematic representation of the hydrogel formation through Diels–Alder links. As it could be appreciated the resulting hydrogel presented elastic gel appearance maintaining the shape of the container.

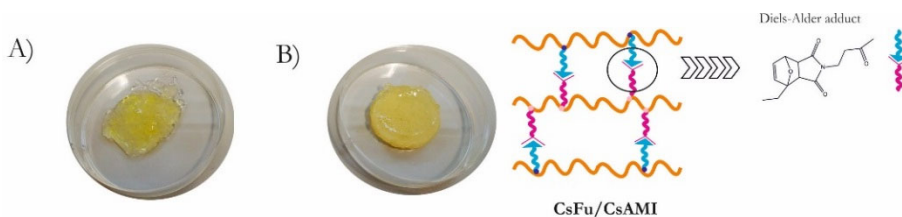


Figure IV.1. Images of A) complementary precursor's mixture in aqueous medium and B) hydrogel formed after 5 h at 65 °C.

IV.2.2. Results and discussion

Covalent networking of chitosan between the grafted furan and maleimide groups through the Diels–Alder cycloaddition was intended to improve the stability of the hydrogel and prevent its premature and uncontrolled solubilisation and, due to the intended applicability as drug carrier, the undesirable burst release of the entrapped drug. The resulting material was thus characterized in order to assess those hypotheses and test the suitability of the material as a drug delivery matrix. The sol–gel ratio of the hydrogel was calculated to be 60 % from Equation II.10.

IV.2.2.1. Physico–chemical characterization

The DA reaction was followed by UV–vis spectroscopy (Figure IV.2). The initial mixture containing both derivatives was placed in a cell inside the temperature–controlled spectrophotometer at 65 °C as described in Chapter II. During the reaction, the conjugation between the two carbonyl groups and the double bond of the maleimide ring is lost due to the formation of the DA adduct¹⁵ as shown in Scheme IV.1. Accordingly, the cross–linking reaction could be monitored by

the progressive decrease in the intensity of the absorption band near 275 nm, which corresponds to maleimide containing groups. Figure IV.2 represents the decrease in the absorption band related to the maleimide as the Diels–Alder reaction between the complementary diene and dienophile in the chitosan chains proceeded. As it could be observed, after 24 h of reaction the absorption band was hardly noticeable indicating the total maleimide consumption and the completeness of the cross–linking.

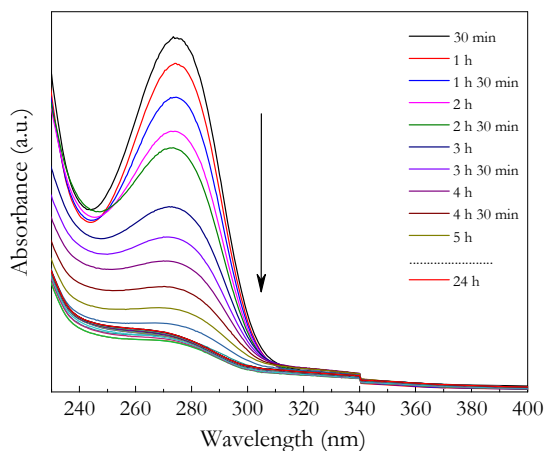


Figure IV.2. UV–vis spectra following the DA reaction of CsFu/CsAMI in HAc at 65 °C.

IV.2.2.2. Rheological behaviour

The cross–linking reaction at 65 °C was monitored by dynamic rheological measurements (Figure IV.3A). The gel time was considered as the time where both dynamic moduli crossover as described in Chapter II. It was found that the gelation time took place after 2 h being 120 Pa the value of both moduli. From this point onwards, the storage modulus (G') increased until a maximum value of 210 Pa at 65 °C.

Furthermore, the final elastic behaviour of the click cross-linked hydrogel at 37 °C was also studied by dynamic rheological analysis as shown in Figure IV.3B. As detailed in Chapter II, the as-prepared hydrogel was first submitted to a strain sweep test in order to establish the linear viscoelastic region where both moduli were independent of the applied strain. Afterwards, the frequency scan was conducted. The hydrogel presented a marked elastic character, being G' considerably higher than G'' in the whole range of measurement. The storage modulus was maintained constant over the whole range of applied angular frequency (ω), concluding the success of the Diels–Alder cross-linking between the two modified chitosan counterparts. The mean G' , G'' and damping factor ($\tan \delta$) values are reported in Table IV.1. The value of the damping factor represents the overall viscoelasticity of the material and was quite lower than 1, which was an indicative of the predominant elastic over viscous character.

It is worth noting that the used furan-functionalized chitosan was also used in our research group to design nanocomposite hydrogels by reacting with maleimide-coated gold nanoparticles. In this case, the storage moduli were observed to be lower, reaching a maximum value of 240 Pa when studying the viscoelastic properties of the sample with less amount of nanoparticles, which resulted to be the most appropriate formulation. Therefore, even if both data relayed on the same order of magnitude, using maleimide-containing chitosan derivative instead of gold nanoparticles as cross-linkers seemed to enhance the elastic properties of the final materials.

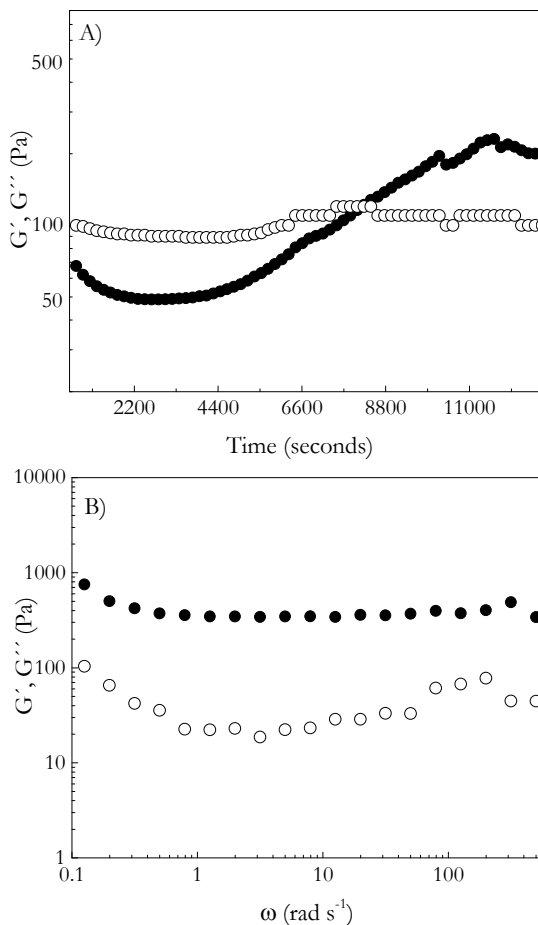


Figure IV.3. A) Storage modulus (G' , ●) and loss modulus (G'' , ○) versus time at 65 °C and B) frequency sweep at 37 °C of CsFu/CsAMI hydrogel.

Table IV.1. Mean storage and loss moduli and $\tan \delta$ values of cross-linked hydrogels at 37 °C (average \pm standard deviation, $n = 3$).

Hydrogel sample	G' (Pa)	G'' (Pa)	$\tan \delta$ (G''/G')
CsFu/CsAMI	399 ± 87	42 ± 10	0.10 ± 0.04

The ultrastructure and the architecture of the participant macromolecules plays a significant role in the control of properties of polymeric hydrogels. Hence, based

on the rheological results, the structural parameters of the developed chitosan-based hydrogel were determined. The average mesh size (ξ , nm), the cross-linking density (n_c , mol m⁻³) and the average molecular weight between neighbouring cross-links (M_c , kg mol⁻¹), were calculated based on the so-called rubber elastic theory (RET) from the Equation II.12, II.13 and II.14, respectively¹⁶, being the polymer concentration (c) 5 % w/v. The calculated parameters are presented in Table IV.2.

Table IV.2. Structural parameters of CsFu/CsAMI hydrogel based on the rheological frequency sweep analysis (average \pm standard deviation, n = 3).

Hydrogel	ξ (nm)	n_c (mol m ⁻³)	M_c (kg mol ⁻¹)
CsFu/CsAMI	10.3 \pm 0.8	0.15 \pm 0.03	329 \pm 71

The obtained structural values were similar to those reported previously for other polymeric hydrogels covalently cross-linked through different strategies; namely, hydrazone cross-linked polysaccharide-based hydrogels¹⁶ and poly(ethylene glycol)-based hydrogels cross-linked through thiol-ene reaction¹⁷. According with the data, it could be highlighted the great cross-linking efficiency and the potentiality of the developed furan:maleimide clicked system. Among the structural parameters, the mesh size is usually highlighted since it determines the diffusion of liquid and small solutes. As mentioned in Chapter I, it is defined as the open space between the polymer chains which are created in cross-linked hydrogel networks at the nanometric scale, where typical mesh sizes reported for hydrogels range from 5 to 100 nm, allowing the transport of small biomolecules through the networks.

IV.2.2.3. Morphological analysis

In order to examine the microstructure of the hydrogel, freeze-dried sample of the DA hydrogel was analysed by SEM. Figure IV.4 shows the SEM image of the synthesized material. An irregular microstructure can be appreciated, where compact zones and highly porous regions appeared in combination, leading to a

heterogeneous morphology. The smooth zones and intermediate regions alternated with pits and ruts defined the non-uniform surface of the material ($281 \pm 23 \mu\text{m}$).

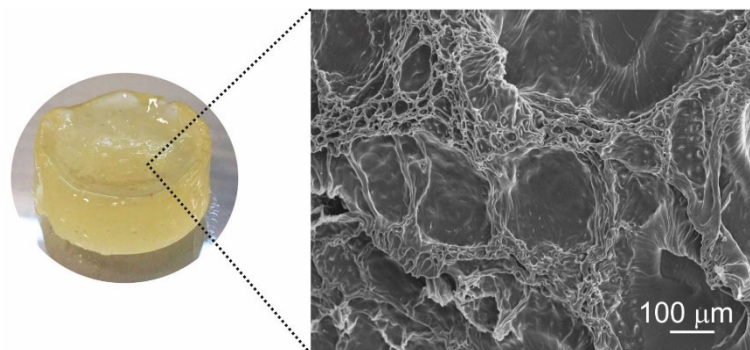


Figure IV.4. Image of the synthesized final hydrogel and SEM image of the freeze-dried sample.

IV.2.2.4. Swelling and degradation studies

The swelling kinetics of the hydrogel in different media provides relevant information about the suitability of the hydrogel to encapsulate both biomolecules and drugs that should be then released in a sustained manner, once in the gastrointestinal tract in oral administration or across the epidermis in case of dermatological applications, etc. Thus, the swelling properties of the DA cross-linked chitosan hydrogel were studied both in acidic solution simulating gastric fluids (0.1 M HCl) and simulated intestinal fluid (PBS, pH = 7.4) at 37 °C (Figure IV.5A) by a general gravimetric method detailed in Chapter II and using the Equation II.8. Figure IV.5B shows the equilibrium swelling values of the hydrogel in both media at 24 h.

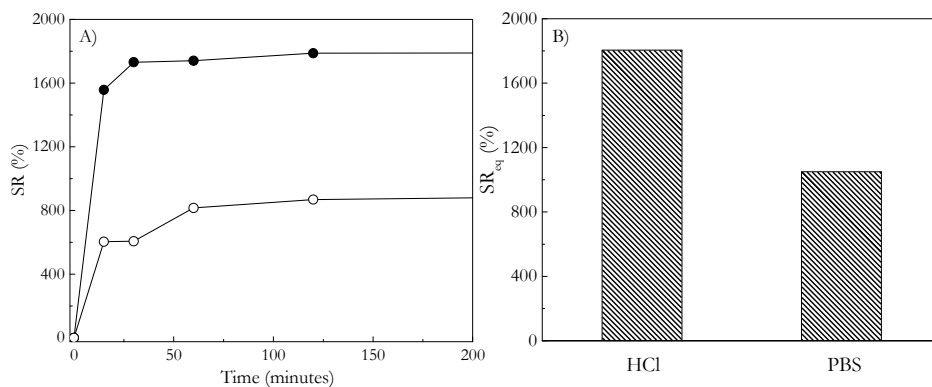


Figure IV.5. A) Swelling kinetics of CsFu/CsAMI hydrogel in HCl (●) and PBS (○) media and B) equilibrium swelling ratio of the hydrogel at 37 °C in both aqueous media at 24 h.

As it could be observed in the figure, at the first stages the swelling of the sample was quite fast in both media. However, over time, the sample in PBS reached a maximum value that slightly increased until equilibrium, whereas the swelling of the sample in acidic media grew up to values much higher than those for the neutral pH. Generally, the amino groups of chitosan are ionized in acidic solutions, which contribute to the electrostatic repulsion between adjacent ionized $-\text{NH}_2$ groups and lead to chain expansion and eventually increase the water absorption of the chitosan-based gels¹⁸. However, in occasions the pH-sensitivity of the chitosan has been observed to be lost or at least decreased when cross-linking the polymer covalently, due to the consumption of free $-\text{NH}_2$ groups within the polymer chain, responsible of the protonation and subsequent swelling in low pH presenting media¹⁹. Attending to the responsive behaviour of the CsFu/CsAMI hydrogel, it could be concluded that the substitution degrees of both chitosan derivatives were appropriated for the effective Diels–Alder cross-linking but not excessive, maintaining the distinctive pH-sensitive character of the original chitosan, which is highly desirable for specific applications. Since the composition of the hydrogel was held constant (5 % w/v), the pH of the medium and the type

of counterions present in the solution were the principal parameters that could influence the swelling capacity of CsFu/CsAMI.

For most of the pharmaceutical applications it is greatly relevant to know the swelling kinetics of the hydrogels that will be used as drug release agents, as this process will have a direct impact on drug release/delivery. Therefore, the swelling kinetics of the hydrogel was adjusted to Equation II.9. The swelling parameters (SR_{max} , k_s and r_0) of CsFu/CsAMI hydrogel at 37 °C are summarized in Table IV.3, where SR_{eq} is the value of the swelling degree in equilibrium (24 hours) obtained from the data of Figure IV.5B. As it can be observed, the absorption capacity of the hydrogel was higher in acidic medium, supporting the results on Figure IV.5. There was no difference between the SR_{eq} and SR_{max} values in neither media; however, a higher value of the initial swelling rate (r_0) in basic pH was observed, which could be related with a decrease in the swelling degree²⁰.

Table IV.3. Swelling parameters of CsFu/CsAMI hydrogel at 37 °C in different aqueous media.

Swelling media	SR_{eq} (%)	SR_{max} (%)	$k_s \cdot 10^4$ ($g_{hydrogel} g_{solution}^{-1} s^{-1}$)	$r_0 \cdot 10^3$ ($g_{solution} g_{hydrogel}^{-1} s^{-1}$)
HCl	1805	1810	2.87	1.06
PBS	1050	1060	1.02	8.72

One of the most important characteristics of the chitosan is its ability to degrade by the attack of several enzymes as chitosanases and lysozymes, which catalyzed the biodegradation of the polymer promoting the disruption of the glycosidic linkages in addition to hydrolysis^{21–23}. Namely, chitosan can be degraded by enzymes that hydrolyse those linkages between glucosamine–glucosamine, glucosamine–N–acetyl–glucosamine and N–acetyl–glucosamine–N–acetyl–glucosamine units. In human body, these enzymes are present in tears and saliva where they act as a barrier against infections. Lysozyme has been found in various human body fluids including serum with concentration of 0.004–0.013 mg mL⁻¹

and tears with 100-fold higher concentration²⁴. Thus, in order to mimic the *in vivo* degradation process of CsFu/CsAMI hydrogel, lysozymes were added to the medium following the procedure reported in Chapter II (Equation II.11). Hence, *in vitro* degradation of a dried hydrogel sample was monitored during four weeks of incubation at physiological conditions in 1 mg mL⁻¹ lysozyme containing PBS buffer solution, at 37 °C²⁵. Moreover, the hydrolytic degradation was also studied in enzyme-free PBS solution at the same temperature. The degradation profiles for the furan/maleimide chitosan-based hydrogel are shown in Figure IV.6. Neat chitosan was also tested as control reference sample.

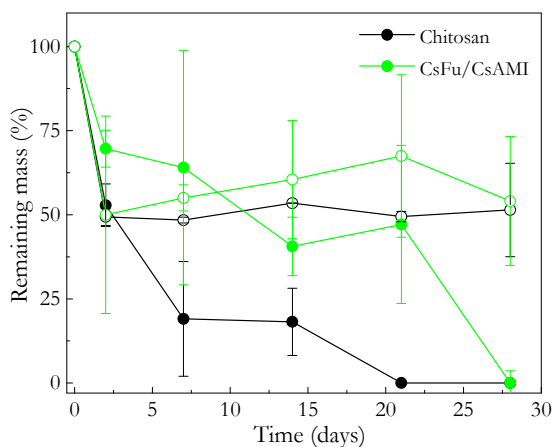


Figure IV.6. Dry weight remaining ratio of native chitosan and CsFu/CsAMI hydrogel in 1 mg mL⁻¹ lysozyme/PBS (filled symbols) and in PBS without lysozyme (empty symbols) at 37 °C as a function of time.

The results show a parallel degradation behaviour for native chitosan and CsFu/CsAMI hydrogel. The degradation of both materials was favoured by the presence of enzymes in the medium, being the latter more pronounced than the hydrolytic degradation. Namely, neat chitosan and hydrogel samples without lysozyme lost about 47 and 40 % mass, respectively, over 14 days (reaching a plateau), while the samples containing the enzymes lost 82 and 60 % of their mass,

respectively, after the same time, until there was nothing left. The plateau observed in PBS medium could be explained by the remaining stable chitosan network phase²⁶, which in the case of the hydrogel represented the sol–gel fraction previously mentioned. Therefore, the synthesized hydrogel still maintained the ability to biodegrade from the original polymer.

IV.2.2.5. Drug delivery study

Herein, it was highlighted a possible application of the Diels–Alder reaction in pharmaceuticals and biomedical engineering. Indeed, DA reaction have the potential to greatly facilitate the development of biomaterials as drug delivery systems², so the synthesized hydrogel was evaluated in terms of its ability as a drug delivery device. The complete study of the properties predicted a successful response from the CsFu/CsAMI hydrogel in the present test. Namely, the cumulative release of chloramphenicol (ClPh) was quantified at different time intervals using Equation II.15. Figure IV.7 shows the drug delivery profile of furan/maleimide chitosan-based hydrogel.

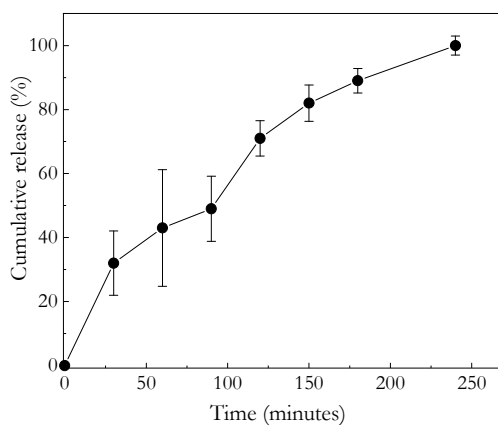


Figure IV.7. Release profile of Chloramphenicol from CsFu/CsAMI hydrogel in PBS at 37 °C.

As it could be observed, the hydrogel showed a sustained delivery of the drug and the concentration of ClPh increased with time in a controlled manner. Therefore, the often undesirable initial burst release was avoided, indicating that the drug was successfully encapsulated within the polymeric network. The total amount of drug loaded ($2.61 \pm 0.04 \text{ mg}_{\text{ClPh}} \text{ g}_{\text{hydrogel}}^{-1}$) was released after 4 h. The swelling capacity and the amount and rate of the drug released will be dependent on the hydrophilic/hydrophobic interactions and on the degree of cross-linking of the hydrogel. The recorded data were fitted to the Equation II.16 reported by Siepmann and Peppas²⁷ as described in Chapter II, where the n value resulted to be 0.60 for the CsFu/CsAMI hydrogel. Attending to this value, it could be concluded that the release of the drug to the surrounding environment was anomalous, where both the controlled diffusion mechanism and the controlled swelling phenomena were superposed. In view of these results, CsFu/CsAMI hydrogel will be a promising material for the encapsulation and release of biomolecules or drugs.

IV.2.2.6. Antimicrobial activity

The sustained drug administration is desirable not only in oral pharmacological treatments but also could be relevant in transdermal delivery or wound dressing, among others. Facing this kind of use for the hydrogel, the ability to constitute a barrier against external contaminating microorganisms offers additional skills to the product, as wounds often provide a favourable environment for the colonization of microorganisms which may both delay healing and cause infection²⁸. As mentioned in Chapter I, it is well known that chitosan exhibits antimicrobial activity against a large number of bacteria, apart from the most common ones (*Escherichia coli* and *Staphylococcus aureus*), its effectiveness against *Pseudomonas fluorescens*, *Pseudomonas aeruginosa*, *Salmonella typhimurium*, *Listeria monocytogenes* and *Bacillus cereus*, among others, has been also studied^{29,30}. Therefore, the bactericidal properties of the as-prepared hydrogel were tested using the disc-plate antibiogram technique by the evaluation

of the inhibition zone of bacterial growth as reported in Chapter II. The obtained results are presented in Table IV.4. The antimicrobial activity of CsFu/CsAMI was affected by the type of microorganism. Indeed, the activity of the hydrogel against *Escherichia coli* was found to be excellent, originating a clearly identifiable inhibition halo, while the effect against the *Staphylococcus aureus* bacteria was moderate. Hence, it was observed that the antimicrobial activity of the Gram–negative bacteria was much greater than to the Gram–positive one, being in accordance with several studies for pure chitosan^{29,31}. Various theories have been proposed to explain the way of action leading to the antimicrobial activity of chitosan. Although the exact mechanism has yet to be cleared out, the intracellular leakage hypothesis is widely accepted. In this mechanism, positively charged chitosan binds to the negatively charged bacterial surface and alters the membrane permeability, resulting in the leakage of intracellular constituents causing cell death^{32,33}. In the case of CsFu/CsAMI hydrogel, a good balance of cross–linking points based on Diels–Alder adducts and free amino groups seemed to have been achieved, leading to a highly stable hydrogel that maintained the antimicrobial activity of neat chitosan to a great extent.

Table IV.4. Antibacterial activity of CsFu/CsAMI hydrogel against bacterial test organism.

Microorganism	Inhibition zone diameter (mm)
<i>Escherichia coli</i>	20 ± 0
<i>Staphylococcus aureus</i>	14 ± 2

IV.2.2.7. Biocompatibility

In order to use the CsFu/CsAMI hydrogel as a sustained drug release system, it was necessary to verify the non–toxicity of the material. With that purpose, preliminary *in vitro* cytotoxicity assays were performed determining changes in cellular growth, incubating L929 murine fibroblasts cells over 24 and 48 h at 37 °C in CsFu/CsAMI, as explained in previous Chapter II. Figure IV.8A shows the

absorbance *versus* incubation time for positive and negative controls and the hydrogel sample. The positive control showed a notably toxic effect where the L929 murine fibroblasts were not able to proliferate, while CsFu/CsAMI displayed non-toxic cell growth, similar to the negative control. The cell viability with respect to that for the negative control as a function of incubation time is presented in Figure IV.8B. As expected, the positive control showed a toxic effect, as the L929 fibroblasts viability was drastically reduced below 20 % of the value of the negative control. In the case of cells cultured in extracted medium from CsFu/CsAMI hydrogel, cell viability was higher than the established acceptance limit of 70 % of the value of the negative control (87 % and 71 % for 24 and 48 h, respectively). These data indicate that the synthesized hydrogel could be considered as a valid candidate for biomedical uses.

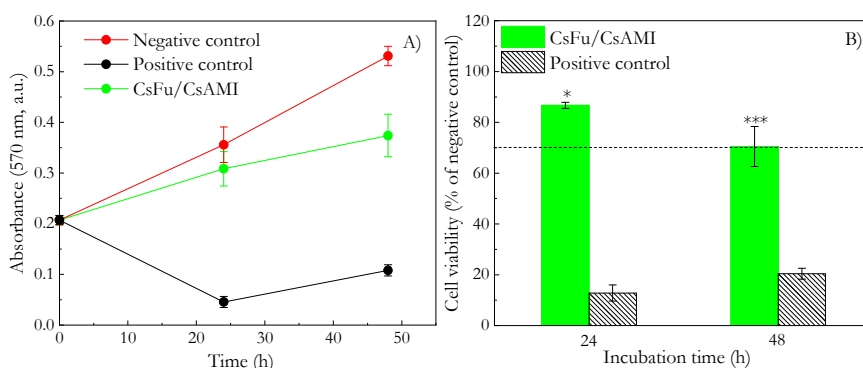


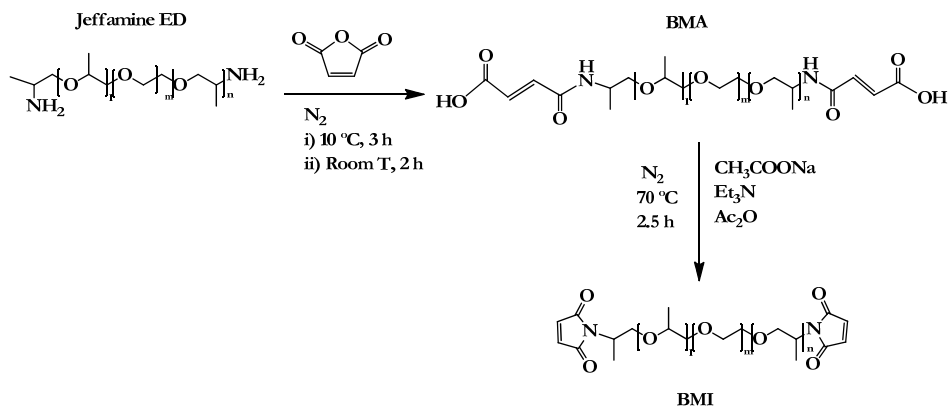
Figure IV.8. A) Absorbance at 570 nm *versus* incubation time of the positive control, negative control and CsFu/CsAMI hydrogel and B) *in vitro* cell viability of the positive control and CsFu/CsAMI hydrogel extract against L929 fibroblasts as a function of incubation time (* $p < 0.05$, *** $p < 0.001$).

IV.3. FURAN–FUNCTIONALIZED CHITOSAN AND POLYETHERAMINE–BASED BISMALLEIMIDE HYDROGELS FORMATION (CsFu/BMI)

IV.3.1. Experimental part

As explained above, the second type of DA hydrogels for drug delivery from furan–functionalized chitosan were developed using a previously synthesized water–soluble polyetheramine–based bismaleimide as a cross–linker. Namely, an aliphatic polyether diamine was used to prepare BMI, which acted as a dienophile in the Diels–Alder reaction and thiol–Michael addition reaction with the thiol–functionalized chitosan (Chapter V).

Thereby, the bismaleimide was prepared by the modification of Jeffamine® ED–900 Polyetheramine (Huntsman) with maleic anhydride following a method reported in the literature^{4,15}. This two–step procedure is depicted in Scheme IV.3. Bismaleimides, composed of two maleimide end groups, are attached through the nitrogen atoms via a linker (Jeffamine, in this case) and are often used as flexible linking agents in polymer click reactions^{4,15,34,35}.

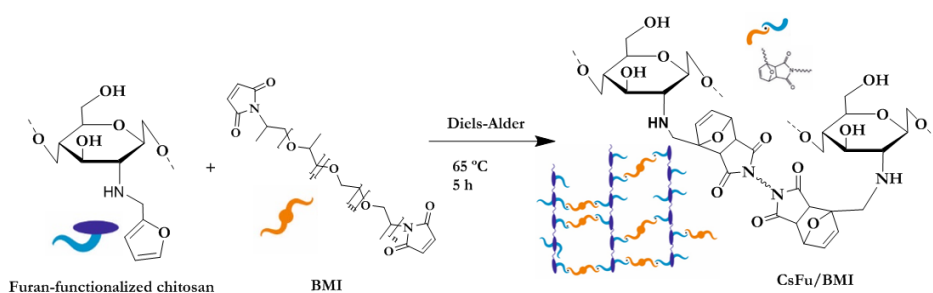


Scheme IV.3. Bismaleimide synthesis starting form Jeffamine® ED.

In the first step, a solution of maleic anhydride (51 mmol) in 50 mL of chloroform was kept under nitrogen at 10 °C until complete dissolution. The Jeffamine® ED (26 mmol) was added dropwise over a period of 3 h, turning the mixture to yellowish and then, it was allowed to warm up to room temperature under magnetic stirring for 2 h. The solution was finally dried under vacuum and the bismaleamic acid (BMA) was obtained as a yellow viscous liquid (96 % w/w yield).

The cyclation of the acid was carried out in the second step. Therefore, for 5 g of BMA (4.6 mmol), triethylamine (3 mmol) and sodium acetate trihydrate (3.5 mmol) were stirred in 10 mL of acetone under nitrogen for 10 minutes. Acetic anhydride (29 mmol) was added and the temperature was raised to 70 °C for 2.5 h. About 5 mL of acetone were rotatory evaporated and the viscous solution (BMI) was dried under vacuum maintaining the temperature below 60 °C for 24 h (55 % w/w yield).

Once the dienophile was synthesized, hydrogels were prepared by means of the Diels–Alder reaction between the furan–modified chitosan and the bismaleimide cross–linker (BMI). Different amounts of BMI were mixed with a solution of CsFu (3 % w/v) in 2 % v/v aqueous acetic acid solution. The mixtures were allowed to gel at 65 °C for 5 h (Scheme IV.4). Different furan–to–maleimide equivalent ratios (1:1, 1:2 and 1:3) were employed in order to study the influence of the amount of cross–linker on the final hydrogel properties. Hydrogels are referred hereafter as shown in Table IV.5.



Scheme IV.4. Hydrogel formation through DA reaction between CsFu and BMI.

Table IV.5. Composition of the different hydrogel formulations (furan–to–maleimide).

Hydrogel sample	Equivalent ratio	CsFu/BMI (% w/w)	CsFu (mg)	BMI (mg)
CsFu/BMI 1:1	1:1	55/45	60	49
CsFu/BMI 1:2	1:2	40/60	60	98
CsFu/BMI 1:3	1:3	30/70	60	147

IV.3.2. Results and discussion

Chitosan derived hydrogels were prepared by DA cycloaddition with tunable properties depending on the amount of cross–linker. Thus, the covalent networking occurred between the furanic dienes grafted in the chitosan chain and the maleimide ending groups of the cross–linking agent, resulting in stable insoluble hydrogels with pH–responsive properties. The sol–gel ratio of the hydrogels was calculated from Equation II.10, exceeding in all the formulations 55 %, being notable the obtained degree of cross–linking in the networks.

IV.3.2.1. Physico–chemical characterization

In the same way that for the previous hydrogel, the DA reaction was followed by UV–vis spectroscopy. Typically, a solution of CsFu in 3 % w/v HAc was mixed with the desired amount of BMI and was transferred to the 0.1 mm cell, which was left thereafter in the temperature–controlled spectrophotometer at 65 °C as explained in Chapter II. As it could be observed in Figure IV.9 the starting solution showed an absorbance maximum near 275 nm. After 24 h, the reaction was completed since no absorbance was detected in this region.

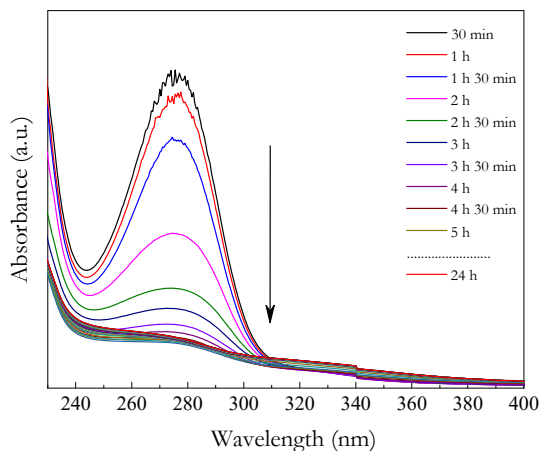


Figure IV.9. UV-vis spectra following the DA reaction of CsFu/BMI 1:1 in HAc at 65 °C.

FTIR spectroscopy was used for the comparison of the chemical structure before and after gelation (Figure IV.10). The composition of the initial mixture showed original bands of both furan (1454 cm^{-1}) and maleimide (1748 and 1473 cm^{-1}) rings, which disappeared in the spectrum of the DA hydrogel, giving place to the band at 1457 cm^{-1} corresponding to the stretching vibration of the -C=C- bond of the DA adduct^{3,8}. Some other bands, such as that at 1698 cm^{-1} (carbonyl groups (-C=O) of the grafted maleimide ring) and 1551 cm^{-1} (amide II of the modified chitosan), suffered slight alterations due to the cross-linking reaction.

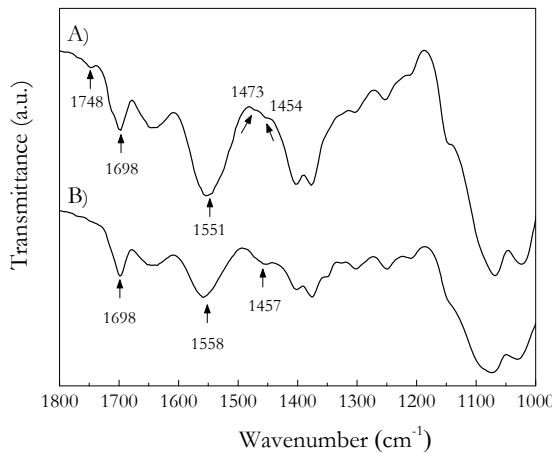


Figure IV.10. FTIR spectra A) before and B) after DA reaction of CsFu/BMI 1:1.

IV.3.2.2. Rheological behaviour

The rheological behaviour of the synthesized hydrogels was evaluated by dynamic experiments (Figure IV.11) according to the proposed methods in Chapter II. The gelation reaction was analysed by time sweep tests at 65 °C and 1 Hz. The variation of both moduli is shown in Figure IV.11A for the CsFu/BMI 1:1 hydrogel, as the three hydrogel formulations presented similar results.

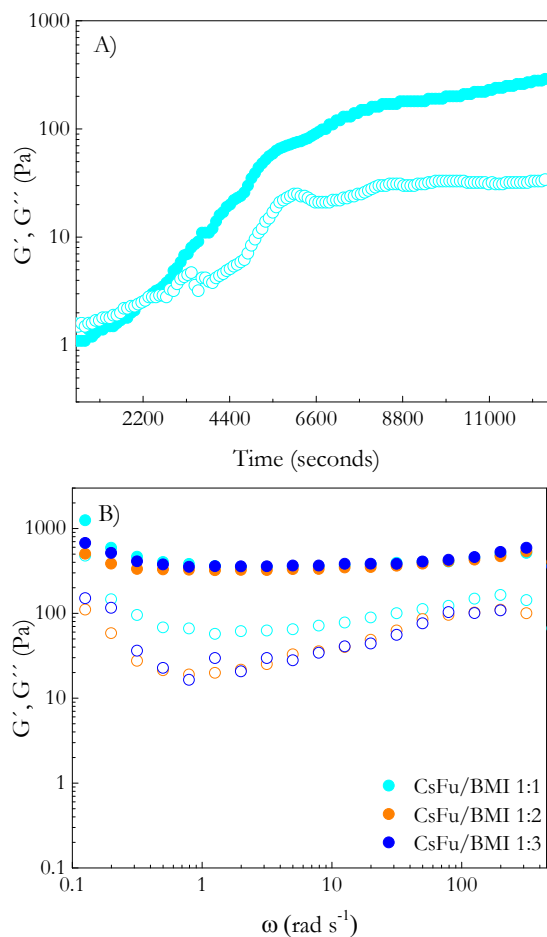


Figure IV.11. A) Storage modulus (G' , ●) and loss modulus (G'' , ○) *versus* time for CsFu/BMI 1:1 at 65 °C and B) frequency sweep of CsFu/BMI hydrogels at 37 °C.

The obtained curve in Figure IV.11A could be analysed in two sections. Namely, during the first 40 minutes approximately, G' was lower than G'' and both moduli increased gradually, following the typical behaviour of a viscoelastic fluid. From minute 50 onwards, G' increased faster than G'' , up to a maximum value of 280 Pa, revealing an elastic gel-like behaviour. Thus, after the first 40 minutes both dynamic moduli crossover, being that point the gelation time ($G' \approx G'' \approx$

2.6 Pa). The viscoelastic behaviour of these hydrogels is in agreement with reported literature, where chitosan–based hydrogels were obtained by ionic cross–linking³⁶. In terms of moduli, the improvement that implies the covalent cross–linking was observed, obtaining visibly higher values for G' . However, few reports could be found in the literature related to chitosan hydrogels cross–linked by click reactions, as they have been typically obtained by ionic or traditional covalent cross–linking. Montiel–Herrera et al. reported that the gelation time of a DA cross–linked chitosan hydrogel was close to 60 minutes at 85 °C¹¹. Besides, by comparing the two DA hydrogels developed, the gelation took more time in the CsFu/CsAMI hydrogel described in Section IV.2 (120 minutes), although similar maximum values of G' were recorded in both cases.

Additionally, rheological frequency sweep tests were performed at 37 °C to characterize the storage modulus of the cross–linked hydrogels (Figure IV.11B). Both moduli suffered a subtle descent at low frequencies reflecting viscoelasticity, which could be due to an unsuitable initial contact between these samples and the measuring equipment at the beginning of the test because of the gummy nature of the CsFu/BMI hydrogels. Nevertheless, all hydrogel compositions presented constant storage modulus values in the remaining measurement range and always higher than the loss modulus. The average values of G' are summarized in Table IV.6. As it can be appreciated, no significant differences were observed between the rheological values of the three formulations. It has to be taken into account that increasing amount of BMI could promote further cross–linking of the chitosan but also affect the G' value of the materials due to the flexible and hydrophilic character of low molecular mass cross–linker.

Table IV.6. Storage moduli (G') and loss moduli (G'') values of CsFu/BMI hydrogels at 37 °C (average \pm standard deviation, $n = 3$).

Hydrogel sample	G' (Pa)	G'' (Pa)	$\tan \delta (G''/G')$
CsFu/BMI 1:1	455 \pm 107	116 \pm 41	0.24 \pm 0.07
CsFu/BMI 1:2	379 \pm 95	50 \pm 23	0.33 \pm 0.69
CsFu/BMI 1:3	424 \pm 108	53 \pm 27	0.26 \pm 0.32

Indeed, the flexible nature of the cross-linker, along with the starting molecular weight of the biopolymer, resulted in G' values one order of magnitude lower than those reported by other authors¹¹. In conclusion, synthesized hydrogels presented rigidity values in between those obtained for physical hydrogels³⁷ and those synthesized by traditional covalent cross-linking with dialdehydes³⁸.

Furthermore, based on the rheological results, the structural parameters (ξ , n_c and M_c) of the developed hydrogels were determined from the Equation II.12, II.13 and II.14, as explained in the previous section (being the polymer concentration (c) of 3 % w/v). The calculated parameters are presented in Table IV.7.

Table IV.7. Structural parameters of CsFu/BMI hydrogels based on the rheological frequency sweep analysis (average \pm standard deviation, $n = 3$).

Hydrogel sample	ξ (nm)	n_c (mol m ⁻³)	M_c (kg mol ⁻¹)
CsFu/BMI 1:1	9.9 \pm 0.6	0.18 \pm 0.03	173 \pm 31
CsFu/BMI 1:2	10.5 \pm 1.0	0.15 \pm 0.04	211 \pm 61
CsFu/BMI 1:3	10.1 \pm 0.6	0.16 \pm 0.02	188 \pm 34

As in the previous case, the potentiality of the furan:maleimide systems and the effectiveness of the cross-linking reaction was confirmed. Similar values were observed for the three formulations, given the similarity of the hydrogels on the viscoelastic properties. Furthermore, the mesh size (ξ) and the cross-linking density (n_c) values were found to be similar to those calculated for the CsFu/CsAMI hydrogel.

IV.3.2.3. Morphological analysis

Hydrogels that swell in response to external stimuli, such as pH or temperature, open their pores to facilitate the diffusion of the encapsulated biomolecules or synthetic drugs under predetermined conditions³⁹. As it could be appreciated in Figure IV.12, hydrogel discs suffered drastic volume changes when exposed to different conditions, reducing their diameter almost to the half when it was allowed to air-dry and recovering the initial volume after the immersion in water.

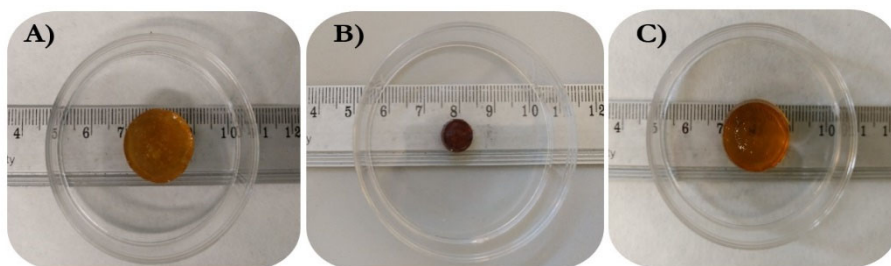


Figure IV.12. Transition of CsFu/BMI 1:2 hydrogel sample at different progressive stages: A) as-prepared, B) dried at room temperature and C) re-swelled in water.

Recent studies had shown that the morphology of hydrogels based on chitosan was closely connected to local pH gradient and salt concentration^{40,41}. Therefore, the 3D network microstructure of the freeze-dried hydrogels was studied by SEM, Figure IV.13, just after the gel formation and after swollen in different media for 24 h.

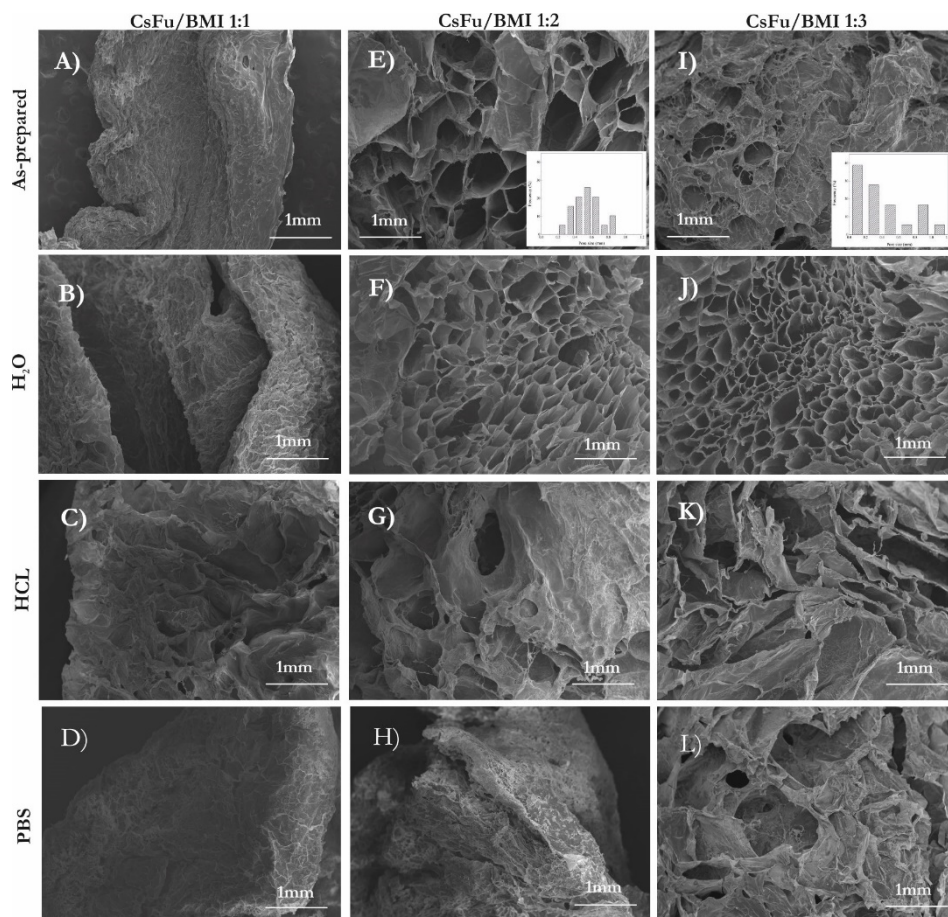


Figure IV.13. SEM images of the different hydrogel compositions: CsFu/BMI 1:1 A) as–prepared and after swollen in B) H₂O, C) HCl and D) PBS; CsFu/BMI 1:2 E) as–prepared and after swollen in F) H₂O, G) HCl and H) PBS; CsFu/BMI 1:3 I) as–prepared and after swollen in J) H₂O, K) HCl and L) PBS.

Chiefly, noticeable differences were appreciated between the different hydrogels in their initial state (Figure IV.13A, Figure IV.13E and Figure IV.13I). In all cases non–homogeneous surfaces were observed, where compact and porous regions appeared all together. This characteristic heterogeneous microstructure was quite similar to those observed in previous studies for other cross–linked chitosan–based

hydrogels⁴². Despite the heterogeneity of the samples, CsFu/BMI 1:1 showed a more compact and closed microstructure. Thereby, it was difficult to determine the size of the pits due to the irregular microstructure presented by the hydrogel. Nevertheless, CsFu/BMI 1:2 showed a homogeneous porosity with a mean pore size of about $500 \pm 130 \mu\text{m}$, whereas CsFu/BMI 1:3 presented more open areas with larger grooves, where water or any other fluid could get in more easily, with a random distribution of pores (pore diameter ranging from 100 to 1100 μm). Besides, a porous and regular surface with a higher number of junction points is generally associated to a higher cross-linking degree⁴³. According to the images, formulations with a high excess of cross-linker seemed not to result in more densely cross-linked networks.

Even if chitosan networks usually has been reported to be porous^{42,44–47}, whatever the type of cross-linking, the exhibited images showed great resemblance to the appearance observed for the CsFu/BMI 1:1 hydrogel, which was described as wrinkled and compact. Therefore, by the implementation of the Diels–Alder reaction in this thesis, improved microporous structures were achieved for the formulations with higher amount of cross-linker.

Moreover, the images revealed that the swelling media and the final microstructure were markedly related. In the same trend of previously reported results for other polymeric hydrogels, changes in the pH could have an impact on the behaviour of both the cross-linker and the polymeric matrix, revealing the intramolecular structure of the hydrogels^{48–50}.

Namely, the samples were allowed to swell in water (H_2O), acid (0.1 M HCl) and phosphate buffer (PBS) solutions until equilibrium was reached. In the case of CsFu/BMI 1:1, no large differences were observed in the morphology after swelling in the three different media, although the most compact structure appeared to obtain after immersion in PBS (Figure IV.13D). The initial highly interconnected porous

microstructure of CsFu/BMI 1:2 was maintained after swollen in water (Figure IV.13F), but the microstructure was notably different in the two other media. Indeed, after being swollen in PBS solution (Figure IV.13H), a more compact and wrinkled surface with larger cavities was observed. In the case of the CsFu/BMI 1:3 sample, the porosity increased considerably after swelling in water (Figure IV.13J) compared to the original sample (Figure IV.13I). More compact structures were observed for HCl and PBS swollen samples, although pits and grooves still appeared.

When comparing the three swelling media, it is worth noting that the hydrogels presented compact structures in PBS. As reported in literature, the electrostatic interactions between phosphate ions and the non-reacted amino groups remaining in the chitosan backbone could promote the shrinkage of the hydrogels in PBS solution⁵¹. This effect was less noticeable in the case of CsFu/BMI 1:3, probably due to the presence of a greater amount of mixed or grafted BMI in the hydrogel. Regarding the neutral medium (PBS solution), it could be observed that the hydrogels maintained their initial morphology, although for the 1:3 ratio a slight change in the microstructure was observed, probably as a consequence of the dissolution of the excess of BMI in the sample. In acid medium, the $-NH_2$ groups of the chitosan main chain will protonate, so that as expected, it resulted in more expanded networks due to the repulsion between the not reacted amino groups. Thus, given the remarkable variation of the microstructure of CsFu/BMI 1:2 and CsFu/BMI 1:3 at different pHs, it could be possible to tune their microstructures for specific applications.

On the other hand, with regard to the utilization of hydrogel materials for drug delivery systems, the analysis of the surface roughness is a key issue. Indeed, the roughness of hydrogels plays an important role regarding biomedical engineering applications, in particular, a hydrogel surface with a high degree of roughness can enable the dissociation of drug molecules⁵². Therefore, the topographic images of the surface section of the hydrogels examined by AFM are shown in Figure IV.14.

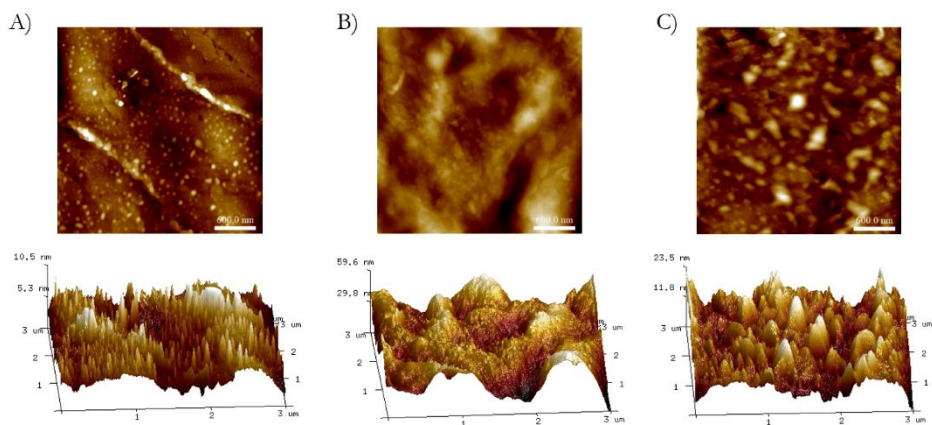


Figure IV.14. Height and 3D height topographic AFM images of the different hydrogel compositions: A) CsFu/BMI 1:1, B) CsFu/BMI 1:2 and C) CsFu/BMI 1:3.

In terms of height, the samples showed the characteristic appearance observed by other cross-linked chitosan hydrogels in previous studies^{53,54}. The images supported the rough surface of the hydrogels with different non-homogeneous areas. Furthermore, the roughness height parameters in terms of average roughness (R_a) and root mean square roughness (R_q) were obtained by AFM software at the nanometer scale (data shown in Table IV.8).

Table IV.8. Topographical parameters of the CsFu/BMI hydrogels.

Hydrogel sample	R_a (nm)	R_q (nm)
CsFu/BMI 1:1	0.8	1.0
CsFu/BMI 1:2	6.1	7.8
CsFu/BMI 1:3	2.7	3.5

The increase in roughness could be originated by the hydrogel cross-linking extent, due to the existing correlation between the cross-linking degree and the roughness. Namely, the hydrogels with higher cross-linking degree tend to have rougher structures^{54,55}. Higher roughness values were observed for the CsFu/BMI 1:2 sample, indicating a higher cross-linking degree for this formulation as suggested by the SEM images.

IV.3.2.4. Swelling and pH sensitivity studies

Whether the synthesized hydrogels would be used as wound dressings or drug carriers, it is particularly relevant to study the influence of the pH on their swelling properties. Indeed, chronic wound fluids are known to have a pH range of 7–8⁵⁶, while the pH value of intact skin is close to 6. Moreover, the pH value changes throughout the human body, from 3 in gastric fluids to 7 once in the intestinal tract. To evaluate the responsive capacity of the chitosan-based hydrogels in different media, their swelling behaviour was studied at 37 °C (Figure IV.15A) both in PBS and HCl (pH = 7.4 and pH = 1, respectively). Additionally, Figure IV.15B shows the equilibrium swelling values of the three hydrogel compositions in the two different media after 24 h, whereas the swelling/shrinking behaviour of the CsFu/BMI 1:2 hydrogel against abrupt changes in the pH is shown in Figure IV.15C.

The swelling degree is normally assumed to decrease with increasing cross-linking degree⁵⁷. In agreement with this statement and taking into account the results obtained in terms of microstructure and roughness for the CsFu/BMI systems, the 1:2 formulation presented a lower degree of swelling in both media (Figure IV.15A and B), which could be related to a more cross-linked network. Furthermore, the swelling capacity was observed to increase with further addition of BMI from 1:2 to 1:3, recording the latter the highest swelling ratio in both media. It is worth to note that the swelling capacity of covalently cross-linked hydrogels would be determined not only by the cross-linking degree but also by the hydrophilicity of the network. As the amount of CsFu was held constant in all the hydrogel formulations, the concentration of the hydrophilic cross-linker in the final material resulted crucial. Therefore, a higher concentration of BMI derived in a higher swelling capacity of the hydrogels, as it was previously reported in other studies with gelatin⁴ and methacrylate¹⁵-based hydrogels.

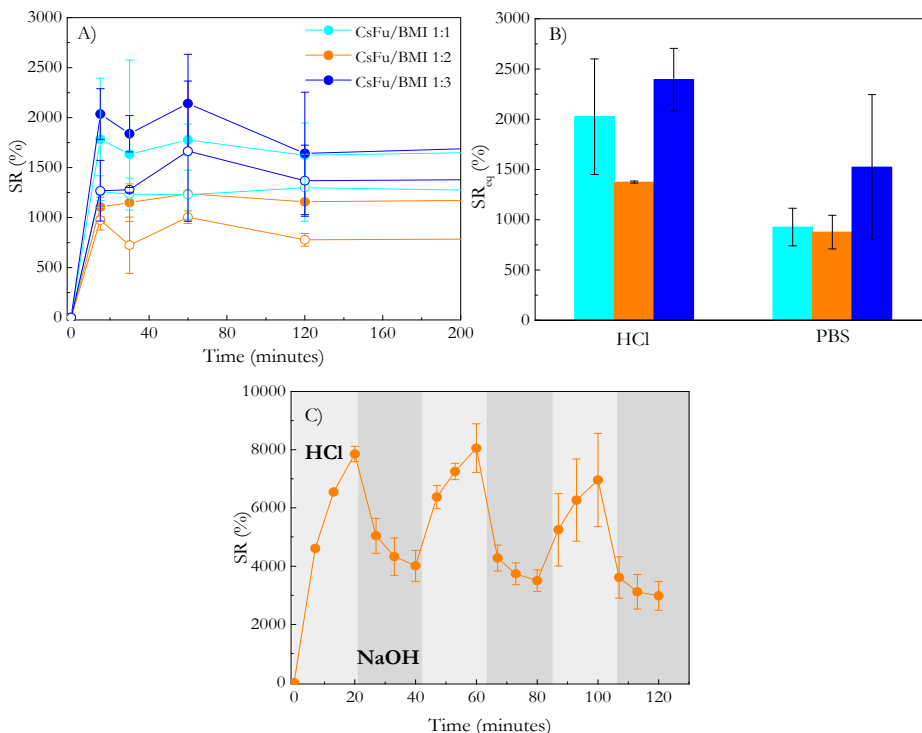


Figure IV.15. A) Swelling kinetics of CsFu/BMI hydrogels in HCl (filled symbols, ●) and PBS (empty symbols, ○) media, B) equilibrium swelling ratio of the hydrogels at 37 °C in both aqueous media after 24 h and C) swelling/shrinking pattern of CsFu/BMI 1:2 hydrogel as a function of time at successive cycles at different pHs.

Regarding the pH of the medium, hydrogels presented a marked responsive behaviour, being notable the higher swelling degrees measured for the samples in acidic solution. In the same way as in the case of the previous system (CsFu/CsAMI), the protonation of non-reacted amino groups which still remained in the chitosan backbone, promoting the repulsion forces between the polymeric chains and, thus, resulting in higher swelling values⁵⁸. The opposite effect was observed after incubating the samples in simulated intestinal fluid, where the presence of counterions could induce a screening effect, reducing the swelling capacity of the hydrogels due to a significant decrease in the number of repulsive forces between the polymer chains. Thus, CsFu/BMI hydrogels

maintained their characteristic pH-sensitiveness after the Diels–Alder cross-linking reaction, displaying a wide range of swelling degrees depending on the amount of cross-linker, indicating that the responsive of the hydrogels could be modulated by the initial concentration of reactants.

For certain *in vivo* applications, the knowledge of the swelling rate is important since it provides information on how quick a certain material can be filled during a surgical procedure. Therefore, the swelling kinetics of the hydrogels were adjusted to Equation II.9. The swelling parameters (SR_{max} , k_S and r_0) of CsFu/BMI hydrogels at 37 °C are summarized in Table IV.9, where SR_{eq} is the value of the swelling degree in equilibrium (24 hours) obtained from the data of Figure IV.15B. As already mentioned, it can be observed that the absorption capacity of the hydrogels was higher in acidic medium. Furthermore, there was no difference between the SR_{eq} and SR_{max} values in both media, where greatly close data were obtained. Moreover, similar values for the initial swelling rate (r_0) were obtained in both media for the CsFu/BMI hydrogels, suggesting an analogous initial behaviour once submerged in solution.

Table IV.9. Swelling parameters of CsFu/BMI at 37 °C in different aqueous media.

Swelling media	Hydrogel sample	SR_{eq} (%)	SR_{max} (%)	$k_S \cdot 10^4$ ($\frac{g_{hydrogel}}{g_{solution} \cdot s^{-1}}$)	$r_0 \cdot 10^3$ ($\frac{g_{solution}}{g_{hydrogel} \cdot s^{-1}}$)
HCl	CsFu/BMI 1:1	2025 ± 575	2050	0.45	5.29
	CsFu/BMI 1:2	1374 ± 11	1380	1.57	3.34
	CsFu/BMI 1:3	2395 ± 312	2420	0.47	3.63
PBS	CsFu/BMI 1:1	927 ± 187	1300	2.74	2.16
	CsFu/BMI 1:2	877 ± 168	880	7.83	1.65
	CsFu/BMI 1:3	1524 ± 721	1530	1.29	3.31

The pH sensitivity of chitosan-based hydrogels through the protonation of amino groups below the pK_a (6.2–6.5)⁵⁹ lead to volume changes on hydrogels (swell), whereas the opposite effect is normally observed when the pH increases (shrink)^{60–62}. Therefore, in order to assess the extent and the rate of this expected pH

responsiveness, samples were exposed to abrupt changes of pH following the pulsatile swelling procedure described in Chapter II.

According to the optimum results obtained for the CsFu/BMI 1:2 hydrogel, it was selected for the pulsatile measurements. Figure IV.15C shows the swelling/shrinking behaviour obtained for that hydrogel. The results evidenced that the hydrogel changed its ability to absorb solution when the environmental pH was altered. Namely, at strongly basic pH the minimum swelling ratio was measured and the highest values were recorded in acid environment, in agreement with the swelling profiles (Figure IV.15A and B). Results further demonstrated that the shrinking rates were higher than the swelling ones that seemed to be progressive.

In order to quantify the pH–sensitivity of the hydrogel, the degree of the response was calculated as the difference between the maximum and minimum swelling degrees achieved at both media related to the maximum value, which was found to be $52.0 \pm 0.6 \%$. The highly porous microstructure previously assessed by SEM (Figure IV.13) and the greater extent of cross–linking degree of CsFu/BMI 1:2, were likely to be the main factors affecting the pH responsiveness. This behaviour could be especially relevant for developing pH–sensitive controlled–release systems, due to the marked and quick response of the hydrogels to pH changes.

Additionally, in order to delve deeper into the obtained network structures of the CsFu/BMI hydrogels, samples were allowed to swell for 3 hours in PBS at 37 °C. Based on the gel content, the sol fraction over the total amount of BMI in each hydrogel was calculated (Table IV.10) following the Equation IV.1.

$$\text{Sol (\%)} = \frac{100 - \text{Gel}}{\text{BMI}_{\text{content}}} \cdot 100 \quad (\text{IV.1})$$

where Gel refers to the gel fraction (%) obtained from Equation II.10 and BMI_{content} was the initial percentage of cross-linker in the hydrogels expressed in terms of mass.

Table IV.10. Soluble fraction of the CsFu/BMI hydrogels.

Hydrogel sample	CsFu/BMI (w/w)	Gel/Sol fractions (%)	Sol. fraction ref. to BMI content (%)
CsFu/BMI 1:1	55/45	63 ± 2 / 37 ± 2	83 ± 4
CsFu/BMI 1:2	40/60	61 ± 1 / 39 ± 1	65 ± 2
CsFu/BMI 1:3	30/70	57 ± 6 / 43 ± 6	62 ± 8

Results revealed slight differences between the gel content values of the different formulations. Assuming that the sol fraction would be related to the non-reacted BMI (non-reacted furanic chitosan would not dissolve at neutral pH), the sol fraction was normalized by the amount of BMI in each hydrogel.

As it could be concluded from the data, from CsFu/BMI 1:1 to CsFu/BMI 1:2, the further addition of cross-linker turned out to be effective, promoting further cross-linking. Indeed, a larger amount of cross-linker in the gel fraction of the CsFu/BMI 1:2 resulted in the decrease of the final equilibrium swelling degree of the material (Figure IV.15A and B). On the contrary, when comparing the CsFu/BMI 1:2 and CsFu/BMI 1:3 hydrogels, the gel fraction decreased and the final swelling degree increased, indicating that, in this case, further increase of the bismaleimide content did not result in a higher cross-linked hydrogel whereas its hydrophilic character enhanced the swelling capacity. Indeed, some authors claimed that using a great excess of cross-linker led to reducing cross-linking degree, with higher amount of bismaleimide pendant from the main chain³⁴. Thus, it was deduced that a great excess of BMI in CsFu/BMI 1:3 seemed to be grafted (or even mixed) but did not increase the cross-linking degree of the hydrogel. A schematic representation of the hypothesized networks is shown in Figure IV.16.

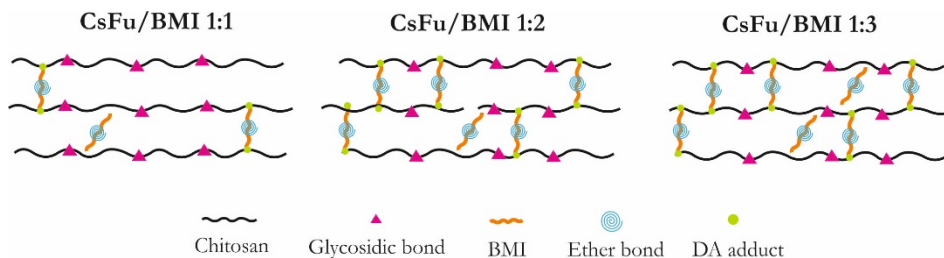


Figure IV.16. Scheme of the networked structures.

IV.3.2.5. Drug delivery study

As previously presented for the CsFu/CsAMI hydrogel, *in vitro* release studies in PBS at 37 °C using chloramphenicol as a model drug were carried out. The release profiles for the CsFu/BMI hydrogels are shown in Figure IV.17, whereas Table IV.11 collects the amounts of drug loaded in the hydrogels and the cumulative release of ClPh during the assay.

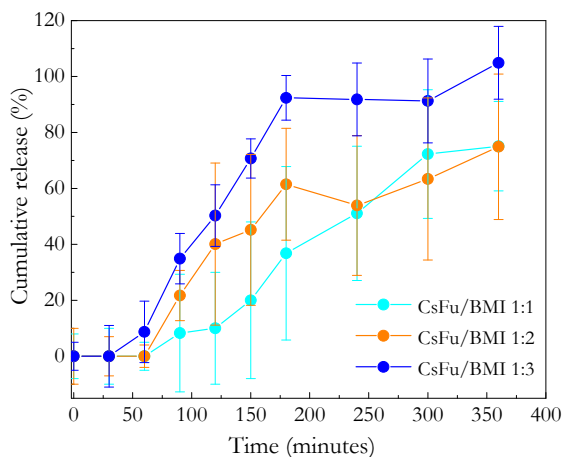


Figure IV.17. Release profile of Chloramphenicol from CsFu/BMI hydrogels in PBS at 37 °C.

Table IV.11. Loaded drug mass and cumulative drug release for CsFu/BMI hydrogels.

Hydrogel sample	Drug loaded ($\text{mg}_{\text{CIPh}} \text{g}_{\text{hydrogel}}^{-1}$)	Cumulative release (%)
CsFu/BMI 1:1	0.61 ± 0.01	75
CsFu/BMI 1:2	0.77 ± 0.15	75
CsFu/BMI 1:3	0.85 ± 0.01	100

As it could be observed, sustained drug delivery profiles were observed in all cases with some differences from one composition to another, not detecting initial sudden release of the drug. Similar values were obtained in terms of drug absorption in the three cases (Table IV.11). Namely, the drug loading process in 1:2 may be ruled by its porous structure, whereas in the case of 1:3 formulation its pronounced hydrophilic character might be the reason for the higher drug loading value.

Regarding the cumulative release profiles, CsFu/BMI 1:3 showed the highest total release, followed by CsFu/BMI 1:1 and CsFu/BMI 1:2, which released a similar amount of CIPh after 6 h. The drug release kinetics will be dependent on the swelling capacity, the diffusion of the drug in the media and the microstructure of each system. The swelling profiles in PBS supported the release results, as the swelling behaviour followed also the same trend for both hydrogels in this media (Figure IV.15). Namely, CsFu/BMI 1:3 displayed the highest swelling capacity, which was then reflected in a greater release of the drug. The spacious cavities and open areas presented by this sample could also facilitate the drug release, while the less hydrophilic nature of CsFu/BMI 1:1 and the higher cross-linking degree of CsFu/BMI 1:2 could delay the removal of the drug in those hydrogels. García-Astrain et al. investigated the release profile of the chloramphenicol for gelatin-based hydrogels cross-linked via Diels-Alder reaction with BMI⁴⁸. Even if higher drug loadings were recorded in this case, quite lower cumulative release values were reached. Namely, the highest release observed for gelatin-based hydrogels was found to be a 58 % of the total amount of drug loaded. In view of these data, it

seems clear that furan–functionalized chitosan enhanced the chloramphenicol release process.

Moreover, from the Equation II.16 in Chapter II the value of n was calculated to be 0.80, 0.75 and 0.74 for CsFu/BMI 1:1, CsFu/BMI 1:2 and CsFu/BMI 1:3, respectively. Similar results were obtained for the three formulations. Being the values close to 1 could suggest that the swelling was the predominant mechanism involved in the drug release in the case of CsFu/BMI hydrogels due to the incorporation of the hydrophilic cross–linker, although the drug release was a case of anomalous transport.

IV.4. CONCLUSIONS

In this chapter, it was demonstrated that Diels–Alder click chemistry is an efficient method for the preparation of biopolymer–based chemically cross–linked hydrogels from furan–modified chitosan. Hydrogels were covalently cross–linked following a clean one–step procedure in absence of any catalysts or initiators in aqueous environment. Indeed, two synthetic strategies for the development of chitosan–based novel biomaterials were described in this chapter. Namely, the networking occurred between furan–functionalized chitosan and maleimide containing compounds (maleimide–functionalized chitosan or maleimide–functionalized polyetheramines).

A biocompatible and biodegradable hydrogel was obtained after reacting both complementary chitosan derivatives (CsFu/CsAMI), whereas different hydrogel compositions were obtained by varying the furan to maleimide ratio when using BMI as a cross–linking agent (CsFu/BMI), in order to study the influence of the amount of cross–linker in the final properties of the hydrogels. The DA reaction at 65 °C for the formation of the hydrogels was followed by UV–vis spectroscopy and the gelation time was estimated by oscillatory viscoelastic measurements, confirming the success of both reactions under the studied conditions. After

studying the elastic properties of the different networks, it was found that the as-prepared hydrogels had a storage modulus similar to that of brain and nerve tissues (10^2 – 10^3 Pa)¹⁵. The microstructure of the different hydrogel compositions was studied by SEM, showing porous networks even if quite heterogeneous structures were observed. Additionally, the surrounding pH was found to have great impact in the microstructure of the as-prepared hydrogels.

On the other hand, the main hindrance that entails the cross-linking process is related to the loss of swelling capacity, due to the shortage of movement of the chains after the formation of new cross-linked points. Thus, one of the principle interests lied in finding the way to balance the advantages that carries the cross-linking without losing the main characteristic of the hydrogels, which was successfully overcome. The swelling was recorded for 24 hours in both fluids in order to ensure that the equilibrium was reached. The DA hydrogels presented responsive swelling capacity under acid and basic environments, where in the case of CsFu/BMI 1:2 hydrogel it was also found to be fast and was repeated at least for three consecutive cycles. The gel content of the hydrogels was calculated to be around 60 %, which made them highly stable, while maintaining the characteristic pH-sensitivity of the original biopolymer. Thus, the properties of the hydrogels could be successfully tuned according to the final application. Furthermore, as expected for chitosan derived materials, the degradation of the CsFu/CsAMI hydrogel was favoured by the presence of lysozymes in the medium.

Finally, in view of future biomedical applications, sustained delivery profiles of ClPh in simulated gastro-intestinal fluid suggested promising features for applications where delivery of therapeutics that can include different types of biomolecules and drugs are necessary. Outstanding values were obtained in terms of drug released for the DA hydrogels, varying the release time between 4 and 6 hours depending on the nature of the dienophile. Regarding drug loading values, the quantity of drug able to be loaded resulted to be within the expected values in

all the cases, based on previous investigations where the release of ClPh from different natural polymeric systems was studied^{5,48,63,64}. The value of the indicator n which represented the mechanism controlling the drug release was calculated to be $0.50 < n < 1$ for the DA hydrogels, indicating an anomalous transport and being in accordance with other authors results for different biopolymeric hydrogel/drug systems^{48,65,66}. However, as García–Astrain et al. claimed, even if the equation reported by Siepmann and Peppas (Equation II.16) can be useful to get a rough idea of the main release mechanisms governing drug release, the results are a limited insight into the release mechanism where different effects should also be taken into account to establish the exact mechanism governing the drug release⁶⁵. Indeed, along with the stimuli–responsive evolution of the hydrogel, the mesh size is also known to govern how drugs diffuse inside the networks⁶⁷. It is worth noting that this drug carrier approach, which was reproducible, could also be extended to different model drugs or compounds that can meet specific requirements.

REFERENCES

- (1) García-Astrain, C.; Gandini, A.; Coelho, D.; Mondragon, I.; Retegi, A.; Eceiza, A.; Corcuera, M. A.; Gabilondo, N. Green Chemistry for the Synthesis of Methacrylate-Based Hydrogels Crosslinked through Diels-Alder Reaction. *Eur. Polym. J.* **2013**, *49* (12), 3998–4007. <https://doi.org/10.1016/j.eurpolymj.2013.09.004>.
- (2) Gregoritza, M.; Brandl, F. P. The Diels–Alder Reaction: A Powerful Tool for the Design of Drug Delivery Systems and Biomaterials. *Eur. J. Pharm. Biopharm.* **2015**, *97*, 438–453. <https://doi.org/10.1016/j.EJPB.2015.06.007>.
- (3) Nimmo, C. M.; Owen, S. C.; Shoichet, M. S. Diels-Alder Click Cross-Linked Hyaluronic Acid Hydrogels for Tissue Engineering. *Biomacromolecules* **2011**, *12* (3), 824–830. <https://doi.org/10.1021/bm101446k>.
- (4) García-Astrain, C.; Gandini, A.; Peña, C.; Algar, I.; Eceiza, A.; Corcuera, M.; Gabilondo, N. Diels-Alder “Click” Chemistry for the Cross-Linking of Furfuryl-Gelatin-Polyetheramine Hydrogels. *RSC Adv.* **2014**, *4* (67), 35578–35587. <https://doi.org/10.1039/c4ra06122e>.
- (5) García-Astrain, C.; Chen, C.; Burón, M.; Palomares, T.; Eceiza, A.; Fruk, L.; Corcuera, M. Á.; Gabilondo, N. Biocompatible Hydrogel Nanocomposite with Covalently Embedded Silver Nanoparticles. *Biomacromolecules* **2015**, *16* (4), 1301–1310. <https://doi.org/10.1021/acs.biomac.5b00101>.
- (6) García-Astrain, C.; Peña-Rodríguez, C.; Retegi, A.; Eceiza, A.; Corcuera, M. A.; Gabilondo, N. Green Chemistry for the Cross-Linking of Photo-Sensitive Furan Modified Gelatin. *Mater. Lett.* **2015**, *160*, 142–145. <https://doi.org/10.1016/j.matlet.2015.07.096>.
- (7) Stewart, S. A.; Backholm, M.; Burke, N. A. D.; Stöver, H. D. H. Cross-Linked Hydrogels Formed through Diels-Alder Coupling of Furan- and Maleimide-Modified Poly(Methyl Vinyl Ether- Alt -Maleic Acid). *Langmuir* **2016**, *32* (7), 1863–1870. <https://doi.org/10.1021/acs.langmuir.5b04450>.
- (8) Fan, M.; Ma, Y.; Zhang, Z.; Mao, J.; Tan, H.; Hu, X. Biodegradable Hyaluronic Acid Hydrogels to Control Release of Dexamethasone through Aqueous Diels-Alder Chemistry for Adipose Tissue Engineering. *Mater. Sci. Eng. C* **2015**, *56*, 311–317. <https://doi.org/10.1016/j.msec.2015.04.004>.
- (9) Wei, H. L.; Yao, K.; Chu, H. J.; Li, Z. C.; Zhu, J.; Shen, Y. M.; Zhao, Z. X.; Feng, Y. L. Click Synthesis of the Thermo- and PH-Sensitive Hydrogels Containing β -Cyclodextrins. *J. Mater. Sci.* **2012**, *47* (1), 332–340. <https://doi.org/10.1007/s10853-011-5802-3>.

- (10) Gandini, A.; Hariri, S.; Le Nest, J. F. Furan-Polyether-Modified Chitosans as Photosensitive Polymer Electrolytes. *Polymer* **2003**, *44* (25), 7565–7572. <https://doi.org/10.1016/j.polymer.2003.09.061>.
- (11) Montiel-Herrera, M.; Gandini, A.; Goycoolea, F. M.; Jacobsen, N. E.; Lizardi-Mendoza, J.; Recillas-Mota, M.; Argüelles-Monal, W. M. N-(Furfural) Chitosan Hydrogels Based on Diels-Alder Cycloadditions and Application as Microspheres for Controlled Drug Release. *Carbohydr. Polym.* **2015**, *128*, 6–12. <https://doi.org/10.1016/j.carbpol.2015.03.052>.
- (12) Espeel, P.; Du Prez, F. E. “click”-Inspired Chemistry in Macromolecular Science: Matching Recent Progress and User Expectations. *Macromolecules* **2015**, *48* (1), 2–14. <https://doi.org/10.1021/ma501386v>.
- (13) Gandini, A. The Furan/Maleimide Diels-Alder Reaction: A Versatile Click-Unclick Tool in Macromolecular Synthesis. *Prog. Polym. Sci.* **2013**, *38* (1), 1–29. <https://doi.org/10.1016/j.progpolymsci.2012.04.002>.
- (14) Li, F.; Li, X.; Zhang, X. Dynamic Diels-Alder Reactions of Maleimide-Furan Amphiphiles and Their Fluorescence ON/OFF Behaviours. *Org. Biomol. Chem.* **2018**, *16* (42), 7871–7877. <https://doi.org/10.1039/c8ob01944d>.
- (15) García-Astrain, C.; Algar, I.; Gandini, A.; Eceiza, A.; Corcuera, M. Á.; Gabilondo, N. Hydrogel Synthesis by Aqueous Diels-Alder Reaction between Furan Modified Methacrylate and Polyetheramine-Based Bismaleimides. *J. Polym. Sci. Part A Polym. Chem.* **2015**, *53* (5), 699–708. <https://doi.org/10.1002/pola.27495>.
- (16) Karvinen, J.; Ihalainen, T. O.; Calejo, M. T.; Jönkkäri, I.; Kellomäki, M. Characterization of the Microstructure of Hydrazone Crosslinked Polysaccharide-Based Hydrogels through Rheological and Diffusion Studies. *Mater. Sci. Eng. C* **2019**, *94* (April 2018), 1056–1066. <https://doi.org/10.1016/j.msec.2018.10.048>.
- (17) Rehmann, M. S.; Skeens, K. M.; Kharkar, P. M.; Ford, E. M.; Maverakis, E.; Lee, K. H.; Kloxin, A. M. Tuning and Predicting Mesh Size and Protein Release from Step Growth Hydrogels. *Biomacromolecules* **2017**, *18* (10), 3131–3142. <https://doi.org/10.1021/acs.biomac.7b00781>.
- (18) Hamed, H.; Moradi, S.; Hudson, S. M.; Tonelli, A. E. Chitosan Based Hydrogels and Their Applications for Drug Delivery in Wound Dressings: A Review. *Carbohydr. Polym.* **2018**, *199*, 445–460. <https://doi.org/10.1016/j.CARBPOL.2018.06.114>.
- (19) Berger, J.; Reist, M.; Mayer, J. M.; Felt, O.; Peppas, N. A.; Gurny, R. Structure

- and Interactions in Covalently and Ionically Crosslinked Chitosan Hydrogels for Biomedical Applications. *Eur. J. Pharm. Biopharm.* **2004**, *57* (1), 19–34. [https://doi.org/10.1016/S0939-6411\(03\)00161-9](https://doi.org/10.1016/S0939-6411(03)00161-9).
- (20) Altinisik, A.; Yurdakoc, K. Chitosan/Poly(Vinyl Alcohol) Hydrogels for Amoxicillin Release. *Polym. Bull.* **2014**, *71* (3), 759–774. <https://doi.org/10.1007/s00289-013-1090-1>.
- (21) Kean, T.; Thanou, M. Biodegradation, Biodistribution and Toxicity of Chitosan. *Adv. Drug Deliv. Rev.* **2010**, *62* (1), 3–11. <https://doi.org/10.1016/j.addr.2009.09.004>.
- (22) Zakariassen, H.; Eijsink, V. G. H.; Sørlie, M. Signatures of Activation Parameters Reveal Substrate-Dependent Rate Determining Steps in Polysaccharide Turnover by a Family 18 Chitinase. *Carbohydr. Polym.* **2010**, *81* (1), 14–20. <https://doi.org/10.1016/J.CARBPOL.2010.01.048>.
- (23) Zakarlassen, H.; Aam, B. B.; Hom, S. J.; Vårum, K. M.; Sørlie, M.; Eijsink, V. G. H. Aromatic Residues in the Catalytic Center of Chitinase A from *Serratia Marcescens* Affect Processivity, Enzyme Activity, and Biomass Converting Efficiency. *J. Biol. Chem.* **2009**, *284* (16), 10610–10617. <https://doi.org/10.1074/jbc.M900092200>.
- (24) Lončarević, A.; Ivanković, M.; Rogina, A. Lysozyme-Induced Degradation of Chitosan: The Characterisation of Degraded Chitosan Scaffolds. *J. Tissue repair Regen.* **2017**, *1* (1), 12–22. <https://doi.org/10.14302/issn.2640>.
- (25) Hong, Y.; Song, H.; Gong, Y.; Mao, Z.; Gao, C.; Shen, J. Covalently Crosslinked Chitosan Hydrogel: Properties of in Vitro Degradation and Chondrocyte Encapsulation. *Acta Biomater.* **2007**, *3* (1), 23–31. <https://doi.org/10.1016/j.actbio.2006.06.007>.
- (26) Chou, H.-S.; Larsson, M.; Hsiao, M.-H.; Chen, Y.-C.; Röding, M.; Nydén, M.; Liu, D.-M. Injectable Insulin-Lysozyme-Loaded Nanogels with Enzymatically-Controlled Degradation and Release for Basal Insulin Treatment: In Vitro Characterization and in Vivo Observation. *J. Control. Release* **2016**, *224*, 33–42. <https://doi.org/10.1016/J.JCONREL.2015.12.036>.
- (27) Siepmann, J.; Peppas, N. . Modeling of Drug Release from Delivery Systems Based on Hydroxypropyl Methylcellulose (HPMC). *Adv. Drug Deliv. Rev.* **2001**, *48* (2–3), 139–157. [https://doi.org/10.1016/S0169-409X\(01\)00112-0](https://doi.org/10.1016/S0169-409X(01)00112-0).
- (28) Fan, L.; Yang, J.; Wu, H.; Hu, Z.; Yi, J.; Tong, J.; Zhu, X. Preparation and Characterization of Quaternary Ammonium Chitosan Hydrogel with

- Significant Antibacterial Activity. *Int. J. Biol. Macromol.* **2015**, *79*, 830–836. <https://doi.org/10.1016/j.ijbiomac.2015.04.013>.
- (29) Chung, Y. C.; Su, Y. P.; Chen, C. C.; Jia, G.; Wang, H. L.; Wu, J. C. G.; Lin, J. G. Relationship between Antibacterial Activity of Chitosan and Surface Characteristics of Cell Wall. *Acta Pharmacol. Sin.* **2004**, *25* (7), 932–936.
- (30) García, N. L.; Famá, L.; D’Accorso, N. B.; Goyanes, S. *Biodegradable Starch Nanocomposites*; 2015; Vol. 75. https://doi.org/10.1007/978-81-322-2470-9_2.
- (31) Chung, Y. C.; Chen, C. Y. Antibacterial Characteristics and Activity of Acid-Soluble Chitosan. *Bioresour. Technol.* **2008**, *99* (8), 2806–2814. <https://doi.org/10.1016/j.biortech.2007.06.044>.
- (32) Sajomsang, W.; Gonil, P.; Tantayanon, S. Antibacterial Activity of Quaternary Ammonium Chitosan Containing Mono or Disaccharide Moieties: Preparation and Characterization. *Int. J. Biol. Macromol.* **2009**, *44* (5), 419–427. <https://doi.org/10.1016/J.IJBIOMAC.2009.03.003>.
- (33) Sun, L.; Du, Y.; Fan, L.; Chen, X.; Yang, J. Preparation, Characterization and Antimicrobial Activity of Quaternized Carboxymethyl Chitosan and Application as Pulp-Cap. *Polymer* **2006**, *47* (6), 1796–1804. <https://doi.org/10.1016/J.POLYMER.2006.01.073>.
- (34) Shtenberg, Y.; Goldfeder, M.; Schroeder, A.; Bianco-Peled, H. Alginate Modified with Maleimide-Terminated PEG as Drug Carriers with Enhanced Mucoadhesion. *Carbohydr. Polym.* **2017**, *175*, 337–346. <https://doi.org/10.1016/j.carbpol.2017.07.076>.
- (35) González, K.; García-Astrain, C.; Santamaria-Echart, A.; Ugarte, L.; Avérous, L.; Eceiza, A.; Gabilondo, N. Starch/Graphene Hydrogels via Click Chemistry with Relevant Electrical and Antibacterial Properties. *Carbohydr. Polym.* **2018**, *202*, 372–381. <https://doi.org/10.1016/j.carbpol.2018.09.007>.
- (36) Yao, Y.; Xia, M.; Wang, H.; Li, G.; Shen, H.; Ji, G.; Meng, Q.; Xie, Y. Preparation and Evaluation of Chitosan-Based Nanogels/Gels for Oral Delivery of Myricetin. *Eur. J. Pharm. Sci.* **2016**, *91*, 144–153. <https://doi.org/10.1016/j.ejps.2016.06.014>.
- (37) Montembault, A.; Viton, C.; Domard, A. Rheometric Study of the Gelation of Chitosan in Aqueous Solution without Cross-Linking Agent. *Biomacromolecules* **2005**, *6* (2), 653–662. <https://doi.org/10.1021/bm049593m>.

- (38) Maity, S.; Datta, A.; Lahiri, S.; Ganguly, J. A Dynamic Chitosan-Based Self-Healing Hydrogel with Tunable Morphology and Its Application as an Isolating Agent. *RSC Adv.* **2016**, *6* (84), 81060–81068. <https://doi.org/10.1039/c6ra15138h>.
- (39) Salehi, S.; Moayedian, N. S.; Assaf, S. S.; Cid-Fuentes, R. G.; Solé-Pareta, J.; Alarcón, E. Releasing Rate Optimization in a Single and Multiple Transmitter Local Drug Delivery System with Limited Resources. *Nano Commun. Netw.* **2017**, *11*, 114–122. <https://doi.org/10.1016/J.NANCOM.2017.03.001>.
- (40) Bhattarai, N.; Gunn, J.; Zhang, M. Chitosan-Based Hydrogels for Controlled, Localized Drug Delivery. *Adv. Drug Deliv. Rev.* **2010**, *62* (1), 83–99. <https://doi.org/10.1016/j.addr.2009.07.019>.
- (41) Xu, H.; Matysiak, S. Effect of PH on Chitosan Hydrogel Polymer Network Structure. *Chem. Commun.* **2017**, *53* (53), 7373–7376. <https://doi.org/10.1039/c7cc01826f>.
- (42) Sohail, M.; Ahmad, M.; Minhas, M. U.; Rashid, H.; Khalid, I. Development and In Vitro Evaluation of High Molecular Weight Chitosan Based Polymeric Composites for Controlled Delivery of Valsartan. *Adv. Polym. Technol.* **2016**, *35* (4), 361–368. <https://doi.org/10.1002/adv.21558>.
- (43) Dash, R.; Foston, M.; Ragauskas, A. J. Improving the Mechanical and Thermal Properties of Gelatin Hydrogels Cross-Linked by Cellulose Nanowhiskers. *Carbohydr. Polym.* **2013**, *91* (2), 638–645. <https://doi.org/10.1016/J.CARBPOL.2012.08.080>.
- (44) Li, B.; Shan, C. L.; Zhou, Q.; Fang, Y.; Wang, Y. L.; Xu, F.; Han, L. R.; Ibrahim, M.; Guo, L. B.; Xie, G. L.; et al. Synthesis, Characterization, and Antibacterial Activity of Cross-Linked Chitosan-Glutaraldehyde. *Mar. Drugs* **2013**, *11* (5), 1534–1552. <https://doi.org/10.3390/md11051534>.
- (45) Piątkowski, M.; Kitala, D.; Radwan-Pragłowska, J.; Janus; Klama-Baryła, A.; Łabuś, W.; Tomanek, E.; Glik, J.; Matýsek, D.; Kawecki, M. Chitosan/Aminoacid Hydrogels with Antimicrobial and Bioactive Properties as New Scaffolds for Human Mesenchymal Stem Cells Culture Applicable in Wound Healing. *Express Polym. Lett.* **2018**, *12* (1), 100–112. <https://doi.org/10.3144/expresspolymlett.2018.8>.
- (46) Piątkowski, M.; Janus; Radwan-Pragłowska, J.; Raclavsky, K. Microwave-Enhanced Synthesis of Biodegradable Multifunctional Chitosan Hydrogels for Wastewater Treatment. *Express Polym. Lett.* **2017**, *11* (10), 809–919. <https://doi.org/10.3144/expresspolymlett.2017.77>.

- (47) Mighri, N.; Mao, J.; Mighri, F.; Ajjj, A.; Rouabhia, M. Chitosan-Coated Collagen Membranes Promote Chondrocyte Adhesion, Growth, and Interleukin-6 Secretion. *Materials* **2015**, *8* (11), 7673–7689. <https://doi.org/10.3390/ma8115413>.
- (48) García-Astrain, C.; Guaresti, O.; González, K.; Santamaria-Echart, A.; Eceiza, A.; Corcuera, M. A.; Gabilondo, N. Click Gelatin Hydrogels: Characterization and Drug Release Behaviour. *Mater. Lett.* **2016**, *182*. <https://doi.org/10.1016/j.matlet.2016.06.115>.
- (49) Rui-Hong, X.; Peng-Gang, R.; Jian, H.; Fang, R.; Lian-Zhen, R.; Zhen-Feng, S. Preparation and Properties of Graphene Oxide-Regenerated Cellulose/Polyvinyl Alcohol Hydrogel with PH-Sensitive Behavior. *Carbohydr. Polym.* **2016**, *138*, 222–228. <https://doi.org/10.1016/J.CARBPOL.2015.11.042>.
- (50) Bao, Z.; Jiang, C.; Wang, Z.; Ji, Q.; Sun, G.; Bi, S.; Liu, Y.; Chen, X. The Influence of Solvent Formulations on Thermosensitive Hydroxybutyl Chitosan Hydrogel as a Potential Delivery Matrix for Cell Therapy. *Carbohydr. Polym.* **2017**, *170*, 80–88. <https://doi.org/10.1016/J.CARBPOL.2017.04.038>.
- (51) Fukushima, T.; Hayakawa, T.; Okamura, K.; Takeda, S.; Inoue, Y.; Miyazaki, K.; Okahata, Y. Buffer Solution Can Control the Porosity of DNA-Chitosan Complexes. *J. Biomed. Mater. Res. - Part B Appl. Biomater.* **2006**, *76* (1), 121–129. <https://doi.org/10.1002/jbm.b.30334>.
- (52) Treesuppharat, W.; Rojanapanthu, P.; Siangsano, C.; Manuspiya, H.; Ummartyotin, S. Synthesis and Characterization of Bacterial Cellulose and Gelatin-Based Hydrogel Composites for Drug-Delivery Systems. *Biotechnol. Reports* **2017**, *15*, 84–91. <https://doi.org/10.1016/J.BTRE.2017.07.002>.
- (53) Milosavljević, N. B.; Ristić, M. D.; Perić-Grujić, A. A.; Filipović, J. M.; Štrbac, S. B.; Rakočević, Z. L.; Krušić, M. T. K. Removal of Cu²⁺ Ions Using Hydrogels of Chitosan, Itaconic and Methacrylic Acid: FTIR, SEM/EDX, AFM, Kinetic and Equilibrium Study. *Colloids Surfaces A Physicochem. Eng. Asp.* **2011**, *388* (1–3), 59–69. <https://doi.org/10.1016/j.colsurfa.2011.08.011>.
- (54) Belali, S.; Emandi, G.; Cafolla, A. A.; O'Connell, B.; Haffner, B.; Möbius, M. E.; Karimi, A.; Senge, M. O. Water-Soluble, Neutral 3,5-Diformyl-BODIPY with Extended Fluorescence Lifetime in a Self-Healable Chitosan Hydrogel. *Photochem. Photobiol. Sci.* **2017**, *16* (11), 1700–1708. <https://doi.org/10.1039/c7pp00316a>.
- (55) Naghizadeh, Z.; Karkhaneh, A.; Khojasteh, A. Self-Crosslinking Effect of

- Chitosan and Gelatin on Alginate Based Hydrogels: Injectable in Situ Forming Scaffolds. *Mater. Sci. Eng. C* **2018**, *89* (November 2017), 256–264. <https://doi.org/10.1016/j.msec.2018.04.018>.
- (56) Jones, E. M.; Cochrane, C. A.; Percival, S. L. The Effect of PH on the Extracellular Matrix and Biofilms. *Adv. Wound Care* **2015**, *4* (7), 431–439. <https://doi.org/10.1089/wound.2014.0538>.
- (57) Khan, S.; Ranjha, N. M. Effect of Degree of Cross-Linking on Swelling and on Drug Release of Low Viscous Chitosan/Poly(Vinyl Alcohol) Hydrogels. *Polym. Bull.* **2014**, *71* (8), 2133–2158. <https://doi.org/10.1007/s00289-014-1178-2>.
- (58) Qu, X.; Wirsén, A.; Albertsson, A. C. Novel PH-Sensitive Chitosan Hydrogels: Swelling Behavior and States of Water. *Polymer* **2000**, *41* (12), 4589–4598. [https://doi.org/10.1016/S0032-3861\(99\)00685-0](https://doi.org/10.1016/S0032-3861(99)00685-0).
- (59) Maciel, V. B. V.; Yoshida, C. M. P.; Franco, T. T. Chitosan/Pectin Polyelectrolyte Complex as a PH Indicator. *Carbohydr. Polym.* **2015**, *132*, 537–545. <https://doi.org/10.1016/J.CARBPOL.2015.06.047>.
- (60) Rizwan, M.; Yahya, R.; Hassan, A.; Yar, M.; Azzahari, A. D.; Selvanathan, V.; Sonsudin, F.; Abouloula, C. N. PH Sensitive Hydrogels in Drug Delivery: Brief History, Properties, Swelling, and Release Mechanism, Material Selection and Applications. *Polymers* **2017**, *9* (4). <https://doi.org/10.3390/polym9040137>.
- (61) Gunasekaran, S.; Tao, W.; Chunxiang, C. Swelling of PH-Sensitive Chitosan-Poly(Vinyl Alcohol) Hydrogels. *J. Appl. Polym. Sci.* **2006**, *102* (5), 4665–4671. <https://doi.org/10.1002/app.24825>.
- (62) Julkapli, N. M.; Ahmad, Z.; Akil, H. M. Effects of Different PH Medium on Swelling Properties of 1, 2, 4, 5-Benzenetetracarboxylic-Chitosan-Filled Chitosan Bio-Composites. *Polym. Bull.* **2011**, *67* (2), 291–320. <https://doi.org/10.1007/s00289-010-0424-5>.
- (63) González, K.; Guaresti, O.; Palomares, T.; Alonso-Varona, A.; Eceiza, A.; Gabilondo, N. The Role of Cellulose Nanocrystals in Biocompatible Starch-Based Clicked Nanocomposite Hydrogels. *Int. J. Biol. Macromol.* **2020**, *143*, 265–272. <https://doi.org/10.1016/j.ijbiomac.2019.12.050>.
- (64) Buhus, G.; Popa, M.; Desbrieres, J. Hydrogels Based on Carboxymethylcellulose and Gelatin for Inclusion and Release of Chloramphenicol. *J. Bioact. Compat. Polym.* **2009**, *24* (6), 525–545. <https://doi.org/10.1177/0883911509349687>.

- (65) García-Astrain, C.; Avérous, L. Synthesis and Behavior of Click Cross-Linked Alginate Hydrogels: Effect of Cross-Linker Length and Functionality. *Int. J. Biol. Macromol.* **2019**, *137*, 612–619. <https://doi.org/10.1016/J.IJBIOMAC.2019.07.010>.
- (66) Martínez-Ruvalcaba, A.; Sánchez-Díaz, J. C.; Becerra, F.; Cruz-Barba, L. E.; González-Álvarez, A. Swelling Characterization and Drug Delivery Kinetics of Polyacrylamide-Co-Itaconic Acid/Chitosan Hydrogels. *Express Polym. Lett.* **2009**, *3* (1), 25–32. <https://doi.org/10.3144/expresspolymlett.2009.5>.
- (67) Li, J.; Mooney, D. J. Designing Hydrogels for Controlled Drug Delivery. *Nat. Rev. Mater.* **2016**, *1* (12), 1–38. <https://doi.org/10.1038/natrevmats.2016.71>.

CHAPTER V

THE THIOL–MICHAEL ADDITION FOR *IN SITU* FORMING HYDROGELS

V.1. INTRODUCTION AND OBJECTIVE	177
V.2. THIOL–FUNCTIONALIZED CHITOSAN AND POLYETHERAMINE–BASED BISMALLEIMIDE HYDROGELS FORMATION (CsSH/BMI)	179
V.2.1. EXPERIMENTAL PART	179
V.2.2. RESULTS AND DISCUSSION	180
V.2.2.1. Rheological behaviour	181
V.2.2.2. Morphological analysis	184
V.2.2.3. Swelling study	185
V.2.2.4. Biocompatibility	187
V.3. CONCLUSIONS	188
REFERENCES	191

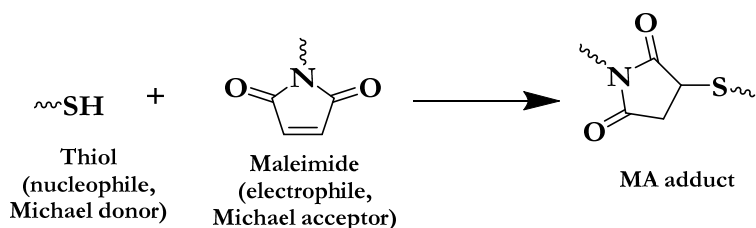
V. THE THIOL–MICHAEL ADDITION FOR *IN SITU* FORMING HYDROGELS

V.1. INTRODUCTION AND OBJECTIVE

In recent years, *in situ* forming biomaterials from natural sources have been widely investigated as artificial 3D scaffolds given their hydrophilic nature and matrix complexation that can provide structural integrity to tissue constructions, drug control and protein delivery to tissues and cultures, and serve as adhesives or barriers between tissue and material surfaces since they resemble to the extracellular matrix (ECM)^{1–8}.

Selective and rapid chemical reaction under physiological conditions is indispensable for *in situ* formation of hydrogels. The Michael addition (MA) reaction, a highly regioselective and efficient click reaction, holds great potential to address these challenges and hence, it has recently gained increased attention as a polymer synthesis strategy for tailored macromolecular architectures⁹. The reaction occurs rapidly at human body temperature under mild reaction conditions, quantitatively, tolerates most functional groups and proceeds in biologically friendly solvents including water, with no heat or light needed and displaying high conversions and favourable reaction rates¹⁰. The Michael addition chemistry involves the addition of a nucleophile (known as the Michael donor) to a α – β –unsaturated carbonyl containing molecule (electron–deficient alkene, known as Michael acceptor) to create a new carbon–carbon single bond^{11,12}. Among this specific chemistry, thiol–click reaction holds great potential and it is widely applied in the synthesis of new compounds and hydrogels formation^{11,13–15}. Indeed, hydrogel synthesis with natural precursors and synthetic materials¹⁰ based on thiol–Michael addition reaction finds significant application in drug delivery, tissue engineering and tissue repair^{16–18}.

Although most of the research on thiol–Michael reaction is focused on the addition of thiol groups to acrylic compounds^{9,10,12,19–22}, many other groups such as vinyl sulfones, maleimides, fumarates, crotonate, ynones or propiolates can also act as Michael acceptors^{11,23,24}. Moreover, it is common knowledge the reduced reactivity of acrylates compared to maleimides^{11,24,25}, which can be reflected on the high number of research works dedicated to the thiol–maleimide reaction for the formation of hydrogels in recent years^{25–33}. Thereby, thiol groups attack the double bond of the maleimide moieties in thiol–Michael addition to generate a covalent and durable thioether bond³¹ (Scheme V.1).



Scheme V.1. Thiol–Michael reaction between thiol and maleimide groups.

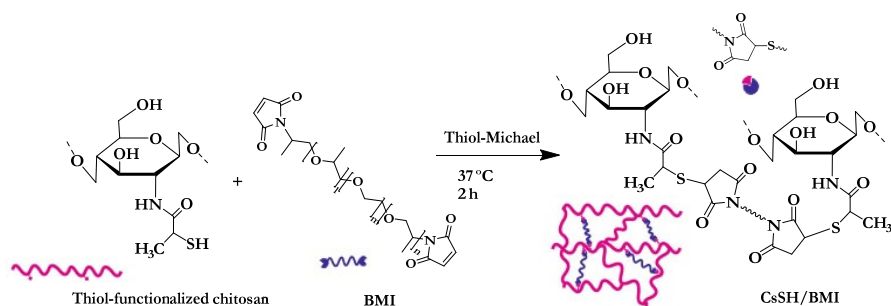
Therefore, this chapter consists on the design of *in situ* forming biomaterials through thiol–Michael addition reaction in aqueous medium. The thiol moieties were incorporated into the chitosan backbone (CsSH) as described in Section III.4, whereas the maleimide rings found on the modified Jeffamine (bismaleimide) were synthesized as explained in Section IV.3.1, acted as the electrophile groups. Until the date, research focused on the formation of biocompatible hydrogels from these singular tailored precursors is unknown. The networking occurred due to the formation of the Michael adduct after the reaction of both components at 37 °C in PBS buffer solution (pH 7.4). In this case, medium molecular weight chitosan was used contributing to the formation of robust hydrogels starting from water–soluble precursors.

Accordingly, *in situ* gelation of the synthesized hydrogels was demonstrated through oscillatory rheology measurements. Furthermore, the effectiveness of the cross–linking was proved to be influenced by the thiol/maleimide ratio, so that different cross–linker amounts were used in order to analyse its influence on the properties of the ensuing materials. The covalently cross–linked networks presented notably different properties in terms of swelling capacity and viscoelastic properties, depending on the cross–linking degree. Besides, based on the rheological study, the microstructural parameters of the polymeric networks were calculated. Finally, the non–toxicity of the hydrogels using L929 murine fibroblast cells was confirmed. Thereby, the efficiency of the reaction along with the favourable conditions evidenced the formation of tailored materials with propitious characteristics for their use in tissue engineering.

V.2. THIOL–FUNCTIONALIZED CHITOSAN AND POLYETHERAMINE–BASED BISMALIMIDE HYDROGELS FORMATION (CsSH/BMI)

V.2.1. Experimental part

In situ formed hydrogels were prepared by the cross–linking of the thiolated chitosan with the bismaleimide (BMI) under physiological conditions. Both water–soluble precursors were synthesized following the procedures described in Chapter III and IV. CsSH derivative and BMI were mixed in PBS buffer solution (pH 7.4) at different equivalent ratios of 1:2 and 1:3 thiol–to–maleimide in 0.7 mL total volume. The reaction for hydrogels synthesis from CsSH and BMI is shown in Scheme V.2. Mixtures were allowed to gel at 37 °C for 2 h to ensure complete conjugation²⁶ (Figure V.1). Maleimide groups were added in excess in both cases to avoid the formation of disulphide bonds between the thiol groups as far as possible. All hydrogels were formed at a polymer concentration of 7 % w/v. Hydrogels will be referred hereafter as shown in Table V.1.



Scheme V.2. Hydrogel formation through MA addition reaction between CsSH and BMI.

Table V.1. Composition of the different hydrogel formulations (thiol-to-maleimide).

Hydrogel sample	Equivalent ratio	CsSH/BMI (% w/w)	CsSH (mg)	BMI (mg)
CsSH/BMI 1:2	1:2	43/57	50	66
CsSH/BMI 1:3	1:3	34/66	50	100

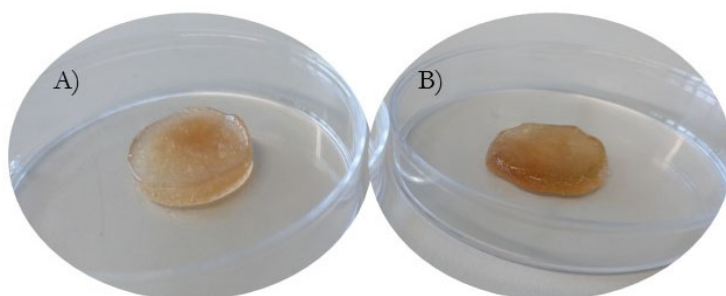


Figure V.1. Hydrogel pictures of A) CsSH/BMI 1:2 and B) CsSH/BMI 1:3.

V.2.2. Results and discussion

Even if it has been studied that maleimides can act as Michael acceptors for primary amine donors²⁵, they react approximately 1000 times faster with thiols than with amines at neutral pH and below²⁸. Therefore, covalent networking took place

between the grafted thiol groups on the chitosan backbone and the maleimide groups of BMI in different ratios, giving place to different hydrogels that were subsequently characterized in order to evaluate the effect of the cross–linker amount. The sol–gel ratio of the hydrogels was calculated to be around 35 % from Equation II.10 for both hydrogels. Even being a relatively low value, the remaining cross–linked gel fractions were observed to be consistent and stable enough in solution for been used as potential scaffolds for tissue engineering.

V.2.2.1. Rheological behaviour

Oscillatory rheology measurements were performed to study the evolution of the rheological parameters during the *in situ* gelation of CsSH/BMI hydrogels (Figure V.2A). As it has been previously explained throughout this thesis and according to the proposed method in Chapter II, the point where the storage (G') and the loss (G'') moduli crossover is generally assumed to reflect the transition from liquid– to solid–like behaviour, namely, the gel point⁹. In accordance with the results presented by other authors^{29,30,34,35}, very fast gelation times were observed for both compositions at 37 °C and 1 Hz. A further increase in the amount of cross–linker from 1:2 to 1:3 resulted in longer gelation time, which could be related to possible steric impediments and/or dilution effects due to the presence of long bismaleimide chains involved in the reaction. Furthermore, the initial mixing of both precursors and the proper conditions of the reaction itself made the cross–point in CsSH/BMI 1:2 not observable, being intuited by the trend of the moduli, whereas in the case of CsSH/BMI 1:3, the gel point could be established after 95 seconds. Therefore, the final materials presented the desirable property of being formed *in situ*, which is essential for injectable hydrogels.

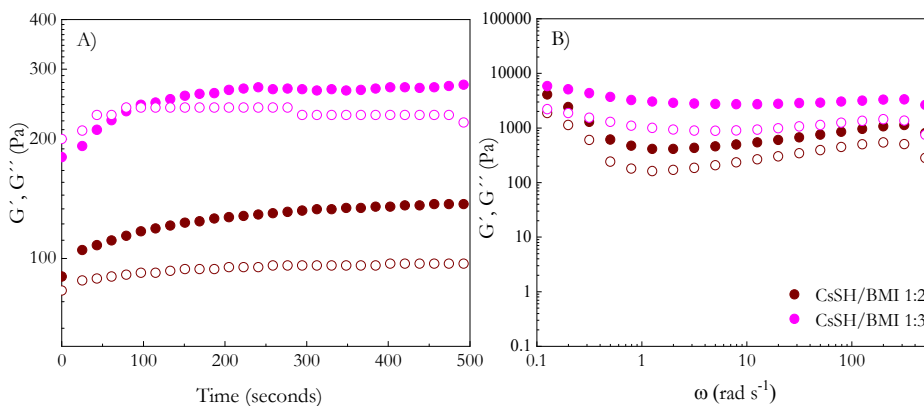


Figure V.2. A) Dynamic moduli (G' (●) and G'' (○)) as a function of time at 37 °C and B) frequency sweep of CsSH/BMI hydrogels at 37 °C.

Table V.2. Mean storage and loss moduli and $\tan \delta$ values of CsSH/BMI hydrogels at 37 °C (average \pm standard deviation, $n = 3$).

Hydrogel sample	G' (Pa)	G'' (Pa)	$\tan \delta$ (G''/G')
CsSH/BMI 1:2	975 ± 106	452 ± 128	0.46 ± 0.1
CsSH/BMI 1:3	3332 ± 502	1207 ± 388	0.36 ± 0.0

Dynamic rheological analysis was also performed to study the final viscoelastic properties of the as-prepared hydrogels at 37 °C (Figure V.2B). As it could be observed, the samples showed an initial drop at low frequency values as observed in Chapter IV for the CsFu/BMI hydrogels, recovering the desirable solid-like gel behaviour afterwards, represented by an elastic character in the studied frequency range, where G' was maintained constant and always higher than G'' . Namely, after reacting for 2h, the moduli considerably increased due to the formation of stable networks. The main G' , G'' and damping ($\tan \delta$) values for both hydrogels are shown in Table V.2. The values obtained for the storage moduli were in accordance with those previously reported by other authors for different chitosan–based hydrogels cross-linked via Michael addition^{36,37}. Additionally, the value of the damping factor, which represents the overall viscoelasticity of the materials, was much lower than 1 in both systems, indicating

a predominant elastic behaviour over viscous conduct. Therefore, the networks were considered to be strongly cross–linked, being slightly more noticeable the case of CsSH/BMI 1:3 indicating greater amount of effective intermolecular cross–links^{38,39}. Furthermore, the influence of the molecular weight of the starting chitosan should not be neglected. In fact, the high M_w value of the neat biopolymer used in this case (680 kDa) could interfere in the final data, resulting in higher values of both moduli.

The architecture of the final polymeric network formed could determine the applicability of the hydrogels as scaffolds for tissue engineering. Thus, based on rheological results, the structural parameters (ξ , n_c and M_c) of the developed hydrogels were determined from the Equation II.12, II.13 and II.14, being the polymer concentration (c) of 7 % w/v. The calculated parameters are summarized in Table V.3.

Table V.3. Structural parameters of CsSH/BMI hydrogels based on the rheological frequency sweep analysis (average \pm standard deviation, $n = 3$).

Hydrogel sample	ξ (nm)	n_c (mol m ⁻³)	M_c (kg mol ⁻¹)
CsSH/BMI 1:2	7.6 \pm 0.2	0.38 \pm 0.03	184 \pm 13
CsSH/BMI 1:3	5.1 \pm 0.6	1.29 \pm 0.46	58 \pm 21

According to the data, it was found that CsSH/BMI hydrogels displayed a mesh size (ξ) of 7.6 and 5.1 nm for CsSH/BMI 1:2 and CsSH/BMI 1:3, respectively, resulting in interesting biological scaffolds which could allow the transport of small molecules through the networks⁴⁰. Furthermore, the consequent values for the cross–linking density (n_c) suggested a higher cross–linked network for the hydrogel containing a higher amount of cross–linker, increasing from 0.38 to 1.29 mol m⁻³, with similar range values in accordance with what stated by other authors⁴¹. Finally, the average molecular weight between neighbouring cross–link points (M_c) took values of 184 and 58 kg mol⁻¹ for CsSH/BMI 1:2 and CsSH/BMI 1:3, respectively. These results were in accordance with those obtained for other

cross-linked polysaccharide-based hydrogels, even if lower values for n_e were observed⁴². As can be noted, ξ and M_c values decreased while n_e value increased when the amount of BMI in the hydrogel increased. Namely, the results were in line with the expected behaviour explained by the higher the G' , the lower the mesh size and M_c and higher the cross-linking density⁴², highlighting the great cross-linking efficiency and the potentiality of the developed thiol/maleimide system.

V.2.2.2. Morphological analysis

The obtention of porous microstructure is crucial concerning materials design for tissue engineering. Therefore, the internal morphology of the hydrogels was studied by SEM. As it can be observed in Figure V.3, the structure of the hydrogels seemed to be affected by the composition, particularly by the amount of cross-linker in the samples. Even if porous microstructures were obtained with both compositions, differences in the networks were apparent. While CsSH/BMI 1:2 presented pores homogeneously distributed ($318 \pm 98 \mu\text{m}$), increasing the BMI amount to 1:3 ratio led to a heterogeneous microstructure with less sum of large pores ($343 \pm 124 \mu\text{m}$) in combination with smaller ones ($56 \pm 25 \mu\text{m}$). Indeed, the use of greater amounts of cross-linking agent in the formulations is normally related with a decrease in the pore size due to higher cross-linking densities³⁸. Therefore, the above findings were in agreement with the viscoelastic behaviour and the structural parameters obtained for the CsSH/BMI networks.

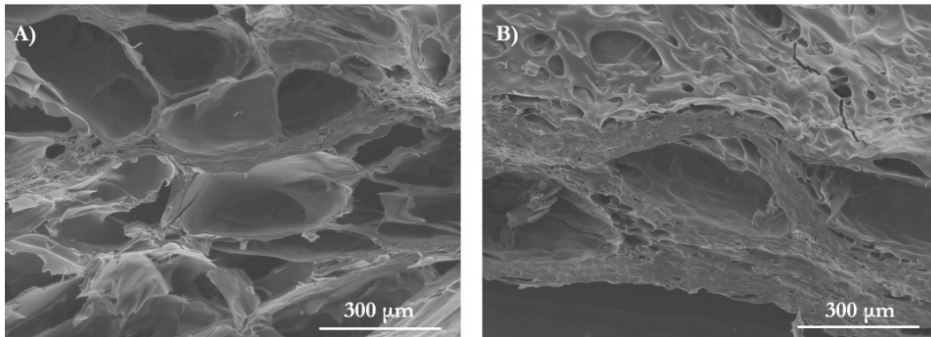


Figure V.3. SEM images of the freeze-dried hydrogels: A) CsSH/BMI 1:2 and B) CsSH/BMI 1:3.

V.2.2.3. Swelling study

Similarly to the DA hydrogels designed for drug delivery applications in Chapter IV, the present hydrogels prepared for being applied in tissue engineering should also present important swelling capacity. Therefore, in order to evaluate the responsive capacity of the as-prepared hydrogels, the swelling behaviour was studied at 37 °C in HCl (pH 1) and PBS (pH 7.4) by a general gravimetric method detailed in Chapter II and using the Equation II.8. The swelling kinetics and the equilibrium swelling values after 48 h in both media for both CsSH/BMI hydrogels are shown in Figure V.4A and B, respectively. As expected, the swelling capacity of the hydrogels was found to be highly sensitive to the surrounding pH being notably higher the swelling degree in acidic medium as a result of the repulsive forces between the chitosan chains as previously stated.

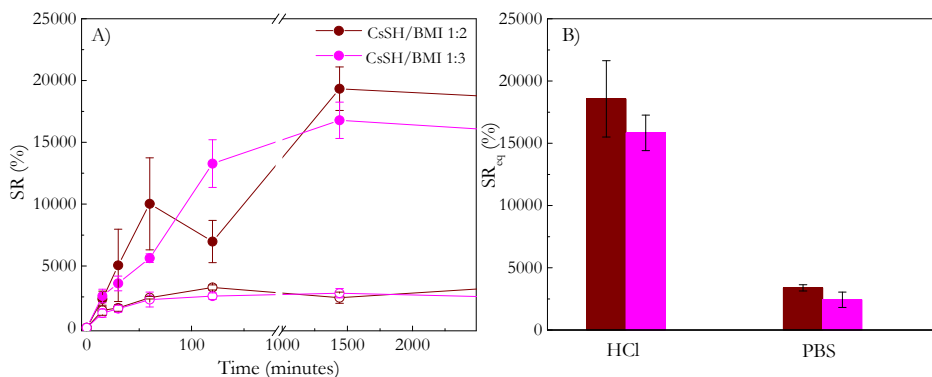


Figure V.4. A) Swelling kinetics of CsSH/BMI hydrogels in HCl (●) and PBS (○) media and B) equilibrium swelling ratio of the hydrogels at 37 °C in both aqueous media at 48 h.

The equilibrium properties, the viscoelastic modulus and the maximum swelling ratio could be controlled by varying the dosage of cross-linker⁴³. Moreover, the swelling degree is normally assumed to decrease with increasing cross-linking degree as it has been already discussed in Chapter IV for the CsFu/BMI hydrogels. As expected, the addition of a higher amount of bifunctional cross-linker in the 1:3 ratio led to the subsequent decrease in the swelling ratio of the hydrogel in both media, following the same trend of the rheological behaviour and confirming the relation between the 3D microstructure (Section V.2.2.2) and the swelling conduct.

The swelling kinetics of the hydrogels were adjusted to Equation II.9 and the obtained parameters (SR_{max} , k_S and r_0) are presented in Table V.4, where SR_{eq} is the value of the swelling degree in equilibrium (48 hours) obtained from the data of Figure V.4B. As expected, the obtained SR_{eq} and SR_{max} values were similar in both media for each of the formulations.

Table V.4. Swelling parameters of CsSH/BMI hydrogels at 37 °C in different aqueous media.

Swelling media	Hydrogel sample	SR _{eq} (%)	SR _{max} (%)	$k_s \cdot 10^4$ ($\frac{\text{g}_{\text{hydrogel}}}{\text{g}_{\text{solution}} \cdot \text{s}^{-1}}$)	$r_0 \cdot 10^3$ ($\frac{\text{g}_{\text{solution}}}{\text{g}_{\text{hydrogel}} \cdot \text{s}^{-1}}$)
HCl	CsSH/BMI	18564 ±	19230	0.01	2.70
	1:2	3069			
	CsSH/BMI	15834 ±	16390	0.08	0.47
	1:3	1421			
PBS	CsSH/BMI	3392 ± 250	3270	0.11	8.50
	1:2				
	CsSH/BMI	2430 ± 624	2490	0.85	1.90
	1:3				

Regarding the effect of the pH, as already mentioned, the absorption and retention capability of the hydrogels was notably higher in acid medium. Furthermore, the initial swelling rate values shown by the CsSH/BMI hydrogels were quite similar in both media.

V.2.2.4. Biocompatibility

To further test the potential of these materials for future biomedical applications, *in vitro* cell viability and proliferation was studied by short–term preliminary cytotoxicity assays evaluating changes in cellular growth, incubating L929 murine fibroblast cells for 24 and 48 hours in the CsSH/BMI hydrogel following the procedure reported in Chapter II. Due to the remarkable properties of CsSH/BMI using the lowest amount of cross–linker for its synthesis, CsSH/BMI 1:2 sample was chosen to perform these tests. As expected, these preliminary studies confirmed the favourable cytocompatibility of MA hydrogels since samples presented non–toxic behaviour and allowed cell growth.

Figure V.5A shows the absorbance versus incubation time for positive and negative controls, as well as for CsSH/BMI 1:2 hydrogel sample. The proliferation curve of the hydrogel showed similar increasing pattern of the negative control, whereas the positive control showed a notably toxic effect where the L929 murine fibroblasts were not able to proliferate. Furthermore, the cell viability was evaluated at 24 and 48 hours in cells cultured in extracted medium from the hydrogel. The cell proliferation with respect to the negative control as a function of the incubation time is represented in Figure V.5B. The cell viability values were much higher than the acceptance limit of 70 %. Therefore, these data indicate that the synthesized hydrogels could be considered as valid candidates for biomedical uses.

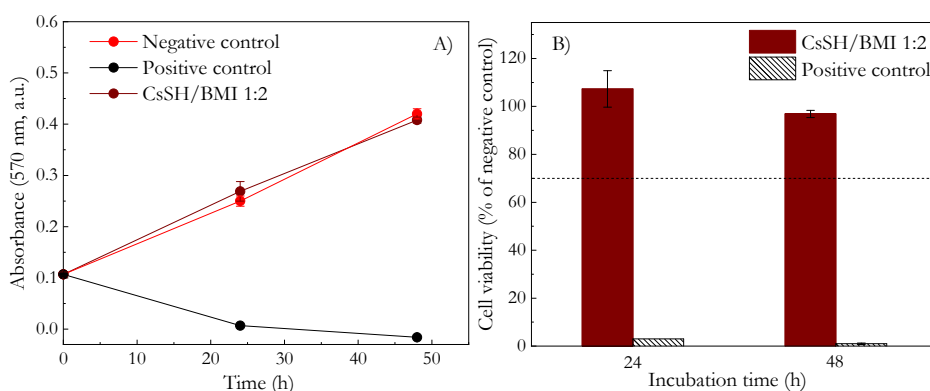


Figure V.5. A) Absorbance at 570 nm *versus* incubation time of the positive control, negative control and CsSH/BMI 1:2 hydrogel and B) *in vitro* cell viability of the positive control and CsSH/BMI 1:2 hydrogel extract against L929 fibroblasts as a function of incubation time.

V.3. CONCLUSIONS

In this chapter, biocompatible hydrogels based on thiol–Michael addition reaction were prepared. The chemical cross–linking between the thiol–modified chitosan and the maleimide–containing linker was satisfactorily carried out according to

the results obtained for the synthesized materials. Moreover, the selectivity of the thiol–maleimide reaction in aqueous environments, the rapid kinetics associated with the reaction and the stability of the thiol–maleimide product were fundamental for this work. Therefore, given the water solubility of both precursors and the favourable reaction conditions, porous networks were obtained through thiol/maleimide coupling under mild physiological conditions. For the sake of improvement, the amount of cross–linker was increased when forming the hydrogels, achieving materials with highly enhanced properties.

In terms of results, the success of the reaction was confirmed by very fast gelation times by oscillatory rheology measurements, supporting the *in situ* forming property. Indeed, the transition from liquid to gel–like behaviour was measured in a time interval of seconds, highlighting the high reactivity between both functional groups. On the other hand, the viscoelastic properties expressed in terms of storage and loss moduli gave a broad perspective of the permanent elastic character of the synthesized materials. Furthermore, the efficiency of the cross–linking resulted in a solid–like gels with a G' value, constant in the whole range of frequency, and similar to that of liver, fat, relaxed muscle or breast gland tissue (10^3 – 10^4 Pa), being interesting candidates for tissue engineering applications⁴⁵. Increasing the amount of bismaleimide in the hydrogels notably improved the storage modulus value, which was related with an increase in effective cross–linking density and simultaneous decrease in average molecular weight between cross–linking points.

The pH–sensitivity and the architecture of the final polymeric networks of the final hydrogels were also evaluated, especially relevant properties in biomedical applications. On the one hand, the microstructure of the different hydrogel compositions was studied by SEM, showing heterogeneous porous networks with a decrease in the pore size when increasing the cross–linking density. Besides, the

swelling was recorded for 48 hours in both fluids in order to ensure that the equilibrium was reached.

Finally, short-term cytotoxicity assays for the CsSH/BMI 1:2 sample revealed that the cross-linked hydrogels were non-toxic, showing a great potential for biomedical applications. Therefore, the properties of the CsSH/BMI hydrogels could be tailored to the needs of the biomaterial, tuning the nature of the products to properly suit the biology of cells and tissues.

REFERENCES

- (1) Slaughter, B. V.; Khurshid, S. S.; Fisher, O. Z.; Khademhosseini, A.; Peppas, N. A. Hydrogels in Regenerative Medicine. *Adv. Mater.* **2009**, *21*, 3307–3329. <https://doi.org/10.1002/adma.200802106>.
- (2) Yang, J.-A.; Yeom, J.; Hwang, B. W.; Hoffman, A. S.; Hahn, S. K. In Situ-Forming Injectable Hydrogels for Regenerative Medicine. *Prog. Polym. Sci.* **2014**, *39* (12), 1973–1986. <https://doi.org/10.1016/J.PROGPOLYMSCI.2014.07.006>.
- (3) Annaka, M.; Mortensen, K.; Vigild, M. E.; Matsuura, T.; Tsuji, S.; Ueda, T.; Tsujinaka, H. Design of an Injectable in Situ Gelation Biomaterials for Vitreous Substitute. *Biomacromolecules* **2011**, *12* (11), 4011–4021. <https://doi.org/10.1021/bm201012f>.
- (4) Śmiga-Matuszowicz, M.; Korytkowska-Walach, A.; Nowak, B.; Pilawka, R.; Lesiak, M.; Sieroń, A. L. Poly(Isosorbide Succinate)-Based in Situ Forming Implants as Potential Systems for Local Drug Delivery: Preliminary Studies. *Mater. Sci. Eng. C* **2018**, *91*, 311–317. <https://doi.org/10.1016/J.MSEC.2018.05.046>.
- (5) Rydholm, A. E.; Bowman, C. N.; Anseth, K. S. Degradable Thiol-Acrylate Photopolymers: Polymerization and Degradation Behavior of an in Situ Forming Biomaterial. *Biomaterials* **2005**, *26* (22), 4495–4506. <https://doi.org/10.1016/J.BIOMATERIALS.2004.11.046>.
- (6) Balakrishnan, B.; Jayakrishnan, A. Self-Cross-Linking Biopolymers as Injectable in Situ Forming Biodegradable Scaffolds. *Biomaterials* **2005**, *26* (18), 3941–3951. <https://doi.org/10.1016/J.BIOMATERIALS.2004.10.005>.
- (7) Tan, H.; Chu, C. R.; Payne, K. A.; Marra, K. G. Injectable in Situ Forming Biodegradable Chitosan–Hyaluronic Acid Based Hydrogels for Cartilage Tissue Engineering. *Biomaterials* **2009**, *30* (13), 2499–2506. <https://doi.org/10.1016/J.BIOMATERIALS.2008.12.080>.
- (8) Balakrishnan, B.; Mohanty, M.; Umashankar, P. R.; Jayakrishnan, A. Evaluation of an in Situ Forming Hydrogel Wound Dressing Based on Oxidized Alginate and Gelatin. *Biomaterials* **2005**, *26* (32), 6335–6342. <https://doi.org/10.1016/J.BIOMATERIALS.2005.04.012>.
- (9) Liu, Z. Q.; Wei, Z.; Zhu, X. L.; Huang, G. Y.; Xu, F.; Yang, J. H.; Osada, Y.; Zrínyi, M.; Li, J. H.; Chen, Y. M. Dextran-Based Hydrogel Formed by Thiol–Michael Addition Reaction for 3D Cell Encapsulation. *Colloids Surfaces B Biointerfaces* **2015**, *128*, 140–148.

- <https://doi.org/10.1016/J.COLSURFB.2015.02.005>.
- (10) Moon, N. G.; Pekkanen, A. M.; Long, T. E.; Showalter, T. N.; Libby, B. Thiol-Michael ‘Click’ Hydrogels as an Imageable Packing Material for Cancer Therapy. *Polymer* **2017**, *125*, 66–75. <https://doi.org/10.1016/j.polymer.2017.07.078>.
- (11) Nair, D. P.; Podgórski, M.; Chatani, S.; Gong, T.; Xi, W.; Fenoli, C. R.; Bowman, C. N. The Thiol-Michael Addition Click Reaction: A Powerful and Widely Used Tool in Materials Chemistry. *Chem. Mater.* **2014**, *26* (1), 724–744. <https://doi.org/10.1021/cm402180t>.
- (12) Sonnenschein, M. F.; Werness, J. B.; Patankar, K. A.; Jin, X.; Larive, M. Z. From Rigid and Flexible Foams to Elastomers via Michael Addition Chemistry. *Polymer* **2016**, *106*, 128–139. <https://doi.org/10.1016/j.polymer.2016.10.054>.
- (13) Fu, R.; Fu, G. D. Polymeric Nanomaterials from Combined Click Chemistry and Controlled Radical Polymerization. *Polym. Chem.* **2011**, *2* (3), 465–475. <https://doi.org/10.1039/c0py00174k>.
- (14) Wang, Z.; Dai, Z.; Wu, J.; Zhao, N.; Xu, J. Vacuum-Dried Robust Bridged Silsesquioxane Aerogels. *Adv. Mater.* **2013**, *25* (32), 4494–4497. <https://doi.org/10.1002/adma.201301617>.
- (15) Chatani, S.; Sheridan, R. J.; Podgórski, M.; Nair, D. P.; Bowman, C. N. Temporal Control of Thiol-Click Chemistry. *Chem. Mater.* **2013**, *25* (19), 3897–3901. <https://doi.org/10.1021/cm402229j>.
- (16) Fu, Y.; Kao, W. J. In Situ Forming Poly(Ethylene Glycol)-Based Hydrogels via Thiol-Maleimide Michael-Type Addition. *J. Biomed. Mater. Res. - Part A* **2011**, *98 A* (2), 201–211. <https://doi.org/10.1002/jbm.a.33106>.
- (17) Hiemstra, C.; Van Der Aa, L. J.; Zhong, Z.; Dijkstra, P. J.; Feijen, J. Novel in Situ Forming, Degradable Dextran Hydrogels by Michael Addition Chemistry: Synthesis, Rheology, and Degradation. *Macromolecules* **2007**, *40* (4), 1165–1173. <https://doi.org/10.1021/ma062468d>.
- (18) Zustiak, S. P.; Leach, J. B. Hydrolytically Degradable Poly(Ethylene Glycol) Hydrogel Scaffolds with Tunable Degradation and Mechanical Properties. *Biomacromolecules* **2010**, *11* (5), 1348–1357. <https://doi.org/10.1021/bm100137q>.
- (19) Lin, H.; Ou, J.; Liu, Z.; Wang, H.; Dong, J.; Zou, H. Facile Construction of Macroporous Hybrid Monoliths via Thiol-Methacrylate Michael Addition

- Click Reaction for Capillary Liquid Chromatography. *J. Chromatogr. A* **2015**, *1379*, 34–42. <https://doi.org/10.1016/j.chroma.2014.12.031>.
- (20) Çakmakçi, E.; Yuce-Dursun, B.; Demir, S. Maleic Anhydride Functionalization of OSTe Based Coatings via Thiol-Ene “Click” Reaction for the Covalent Immobilization of Xylanase. *React. Funct. Polym.* **2017**, *111*, 38–43. <https://doi.org/10.1016/j.reactfunctpolym.2016.11.006>.
- (21) Kröger, A. P. P.; Boonen, R. J. E. A.; Paulusse, J. M. J. Well-Defined Single-Chain Polymer Nanoparticles via Thiol-Michael Addition. *Polymer* **2017**, *120*, 119–128. <https://doi.org/10.1016/j.polymer.2017.05.040>.
- (22) Grover, G. N.; Alconcel, S. N. S.; Matsumoto, N. M.; Maynard, H. D. Trapping of Thiol-Terminated Acrylate Polymers with Divinyl Sulfone to Generate Well-Defined Semitelechelic Michael Acceptor Polymers. *Macromolecules* **2009**, *42* (20), 7657–7663. <https://doi.org/10.1021/ma901036x>.
- (23) Mather, B. D.; Viswanathan, K.; Miller, K. M.; Long, T. E. Michael Addition Reactions in Macromolecular Design for Emerging Technologies. *Prog. Polym. Sci.* **2006**, *31* (5), 487–531. <https://doi.org/10.1016/j.progpolymsci.2006.03.001>.
- (24) Stolz, R. M.; Northrop, B. H. Experimental and Theoretical Studies of Selective Thiol-Ene and Thiol-Yne Click Reactions Involving N -Substituted Maleimides. *J. Org. Chem.* **2013**, *78* (16), 8105–8116. <https://doi.org/10.1021/jo4014436>.
- (25) Baldwin, A. D.; Kiick, K. L. Tunable Degradation of Maleimide-Thiol Adducts in Reducing Environments. *Bioconjug. Chem.* **2011**, *22* (10), 1946–1953. <https://doi.org/10.1021/bc200148v>.
- (26) Arslan, M.; Gevrek, T. N.; Sanyal, A.; Sanyal, R. Cyclodextrin Mediated Polymer Coupling via Thiol-Maleimide Conjugation: Facile Access to Functionalizable Hydrogels. *RSC Adv.* **2014**, *4* (101), 57834–57841. <https://doi.org/10.1039/c4ra12408a>.
- (27) Belbekhouche, S.; Guerrouache, M.; Carbonnier, B. Thiol-Maleimide Michael Addition Click Reaction: A New Route to Surface Modification of Porous Polymeric Monolith. *Macromol. Chem. Phys.* **2016**, *217* (8), 997–1006. <https://doi.org/10.1002/macp.201500427>.
- (28) Ravi, S.; Krishnamurthy, V. R.; Caves, J. M.; Haller, C. A.; Chaikof, E. L. Maleimide-Thiol Coupling of a Bioactive Peptide to an Elastin-like Protein Polymer. *Acta Biomater.* **2012**, *8* (2), 627–635.

- <https://doi.org/10.1016/j.actbio.2011.10.027>.
- (29) Jansen, L. E.; Negrón-Piñeiro, L. J.; Galarza, S.; Peyton, S. R. Control of Thiol-Maleimide Reaction Kinetics in PEG Hydrogel Networks. *Acta Biomater.* **2018**, *70*, 120–128. <https://doi.org/10.1016/j.actbio.2018.01.043>.
- (30) Darling, N. J.; Hung, Y. S.; Sharma, S.; Segura, T. Controlling the Kinetics of Thiol-Maleimide Michael-Type Addition Gelation Kinetics for the Generation of Homogenous Poly(Ethylene Glycol) Hydrogels. *Biomaterials* **2016**, *101*, 199–206. <https://doi.org/10.1016/j.biomaterials.2016.05.053>.
- (31) Shtenberg, Y.; Goldfeder, M.; Schroeder, A.; Bianco-Peled, H. Alginate Modified with Maleimide-Terminated PEG as Drug Carriers with Enhanced Mucoadhesion. *Carbohydr. Polym.* **2017**, *175*, 337–346. <https://doi.org/10.1016/j.carbpol.2017.07.076>.
- (32) Buono, P.; Duval, A.; Averous, L.; Habibi, Y. Lignin-Based Materials Through Thiol–Maleimide “Click” Polymerization. *ChemSusChem* **2017**, *10* (5), 984–992. <https://doi.org/10.1002/cssc.201601738>.
- (33) Billiet, L.; Gok, O.; Dove, A. P.; Sanyal, A.; Nguyen, L. T. T.; Du Prez, F. E. Metal-Free Functionalization of Linear Polyurethanes by Thiol-Maleimide Coupling Reactions. *Macromolecules* **2011**, *44* (20), 7874–7878. <https://doi.org/10.1021/ma201323g>.
- (34) Qu, J.; Zhao, X.; Ma, P. X.; Guo, B. PH-Responsive Self-Healing Injectable Hydrogel Based on N-Carboxyethyl Chitosan for Hepatocellular Carcinoma Therapy. *Acta Biomater.* **2017**, *58*, 168–180. <https://doi.org/10.1016/j.actbio.2017.06.001>.
- (35) Phelps, E. ; Enemchukwu, N. ; Fiore, V. ; Sy, J. ; Murthy, N.; Sulchek, T. ; Barker, T. ; Garcia, A. . Maleimide Cross-Linked Bioactive PEG Hydrogel Exhibits Improved Reaction Kinetics and Cross-Linking for Cell Encapsulation and in-Situ Delivery. *Adv. Mater.* **2012**, *24* (1), 64–72. <https://doi.org/10.1002/adma.201103574>.Maleimide.
- (36) Yu, Y.; Deng, C.; Meng, F.; Shi, Q.; Feijen, J.; Zhong, Z. Novel Injectable Biodegradable Glycol Chitosan-Based Hydrogels Crosslinked by Michael-Type Addition Reaction with Oligo(Acryloyl Carbonate)-b-Poly(Ethylene Glycol)-b-Oligo(Acryloyl Carbonate) Copolymers. *J. Biomed. Mater. Res. - Part A* **2011**, *99 A* (2), 316–326. <https://doi.org/10.1002/jbm.a.33199>.
- (37) Kim, M.; Choi, Y.; Noh, I.; Tae, G. Synthesis and Characterization of in Situ Chitosan-Based Hydrogel via Grafting of Carboxyethyl Acrylate. *J. Biomed. Mater. Res. Part A* **2007**, *83* (3), 674–682. <https://doi.org/10.1002/jbm.a>.

- (38) González, K.; García-Astrain, C.; Santamaria-Echart, A.; Ugarte, L.; Avérous, L.; Eceiza, A.; Gabilondo, N. Starch/Graphene Hydrogels via Click Chemistry with Relevant Electrical and Antibacterial Properties. *Carbohydr. Polym.* **2018**, *202*, 372–381. <https://doi.org/10.1016/j.carbpol.2018.09.007>.
- (39) Teng, D. yong; Wu, Z. ming; Zhang, X. ge; Wang, Y. xia; Zheng, C.; Wang, Z.; Li, C. xing. Synthesis and Characterization of *in Situ* Cross-Linked Hydrogel Based on Self-Assembly of Thiol-Modified Chitosan with PEG Diacrylate Using Michael Type Addition. *Polymer* **2010**, *51* (3), 639–646. <https://doi.org/10.1016/j.polymer.2009.12.003>.
- (40) Li, J.; Mooney, D. J. Designing Hydrogels for Controlled Drug Delivery. *Nat. Rev. Mater.* **2016**, *1* (12), 1–38. <https://doi.org/10.1038/natrevmats.2016.71>.
- (41) Liu, Y.; Huglin, M. B. Effective Crosslinking Densities and Elastic Moduli of Some Physically Crosslinked Hydrogels. *Polymer* **1995**, *36* (8), 1715–1718. [https://doi.org/10.1016/0032-3861\(95\)99018-P](https://doi.org/10.1016/0032-3861(95)99018-P).
- (42) Karvinen, J.; Ihalainen, T. O.; Calejo, M. T.; Jönkkäri, I.; Kellomäki, M. Characterization of the Microstructure of Hydrazone Crosslinked Polysaccharide-Based Hydrogels through Rheological and Diffusion Studies. *Mater. Sci. Eng. C* **2019**, *94* (April 2018), 1056–1066. <https://doi.org/10.1016/j.msec.2018.10.048>.
- (43) Tang, S.; Olsen, B. D. Controlling Topological Entanglement in Engineered Protein Hydrogels with a Variety of Thiol Coupling Chemistries. *Front. Chem.* **2014**, *2*, 1–11. <https://doi.org/10.3389/fchem.2014.00023>.
- (44) Altinisik, A.; Yurdakoc, K. Chitosan/Poly(Vinyl Alcohol) Hydrogels for Amoxicillin Release. *Polym. Bull.* **2014**, *71* (3), 759–774. <https://doi.org/10.1007/s00289-013-1090-1>.
- (45) Vanderhooft, J. L.; Alcoutlabi, M.; Magda, J. J.; Prestwich, G. D. Rheological Properties of Cross-Linked Hyaluronan-Gelatin Hydrogels for Tissue Engineering. *Macromol. Biosci.* **2009**, *9* (1), 20–28. <https://doi.org/10.1002/mabi.200800141>.

CHAPTER VI

DEVELOPING FLUORESCENT HYDROGELS BY THE NITEC REACTION

VI.1. INTRODUCTION AND OBJECTIVE	199
VI.2. TETRAZOLE/MALEIMIDE CHITOSAN-BASED HYDROGELS FORMATION (CsTZ/CsAMI)	201
VI.2.1. EXPERIMENTAL PART	201
VI.2.2. RESULTS AND DISCUSSION	203
VI.2.2.1. Physico-chemical characterization	204
VI.2.2.2. Rheological behaviour	207
VI.2.2.3. Morphological analysis	214
VI.2.2.4. Swelling, pH sensitivity and degradation studies	216
VI.2.2.5. Biocompatibility	220
VI.3. CONCLUSIONS	221
REFERENCES	223

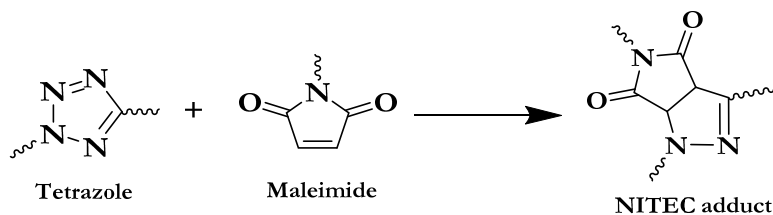
VI. DEVELOPING FLUORESCENT HYDROGELS BY THE NITEC REACTION

VI.1. INTRODUCTION AND OBJECTIVE

Light-driven reactions have become a synthetic tool in several fields of chemistry¹. Indeed, current developments in biomedicine², materials science^{3,4} and polymer chemistry⁵ benefit from the advantages of using light as a trigger to chemically modify the structure of some (bio)macromolecules. Light-triggered reactions proceed relatively fast at ambient temperature and provide unique spatiotemporal control over the chemical process⁵. In this way, a fine-tuning of the physical and chemical properties of a given material can be readily achieved. One of the strategies that comprise the photo triggered cross-linking involves nitrile imine groups that undergo 1,3-dipolar cycloaddition with different activated alkenes after UV-irradiation of tetrazole species, producing a fluorescent adduct. Thereby, tetrazole moieties release a nitrogen molecule forming a reactive nitrile-imine dipole intermediate, which can undergo a [3 + 2] cycloaddition with reactive dipolarphiles, resulting in the formation of pyrazoline units⁶. Due to this fluorescent behaviour, the nitrile imine-mediated tetrazole-ene cycloaddition (NITEC) is mainly focused on enabling on-demand control of polymerization and conjugation reactions⁷, as well as surface modification^{3,8,9}. However, photo-click reactions such as NITEC can also be particularly interesting for applications in hydrogel cross-linking as they can be controlled on-demand, do not involve the use of toxic catalysts being environmentally friendly and are bioorthogonal, giving place to excellent candidates for biomedical treatments. Moreover, the resulting fluorescent polymeric hydrogels will find advanced applications in chemical and environmental sensing, photonics, bioimaging, and electrofluorochromic devices¹⁰.

Thus, tetrazoles act as photo reactive groups that react after ultraviolet (UV) activation with dipolarphiles. One of the most common and promising

candidates for this reaction is based on the tetrazole/maleimide coupling, where maleimides act as photo-complementary functional moieties. The excellent chemoselectivity of this particular NITEC reactive groups leads to a fluorescent adduct, allowing monitoring of the reaction progress (Scheme VI.1).



Scheme VI.1. NITEC reaction between tetrazole and maleimide groups.

Hence, the objective of this chapter was to develop stable hydrogels by UV-triggered photo cross-linking at 320 nm based on novel chitosan precursors through the variation of their initial concentration. To this end, the tetrazole-modified chitosan (CsTZ) synthesized as explained in the Section III.5 in Chapter III was used for the cross-linking of the maleimide-modified chitosan (CsAMI) as detailed in Section III.3 in Chapter III. The possible limitations that could arise after the functionalization of the polymer, mostly related with insolubility problems, were tried to reduce by using a low molecular weight chitosan for both precursors. Moreover, the synthetic strategy for the hydrogels formation was developed in aqueous environment, representing an interesting novel example of green click chemistry. The photochemical ligation proceeded smoothly in all the formulations, obtaining elastic networks with fluorescent properties, even at the lowest concentration of polymer.

The NITEC reaction was verified by fluorescence spectroscopy at an excitation wavelength of 396 nm. The pH-sensitivity of the hydrogels was studied by conducting swelling studies in different media. The capacity of the materials to absorb fluids was also corroborated with the SEM images, which showed an

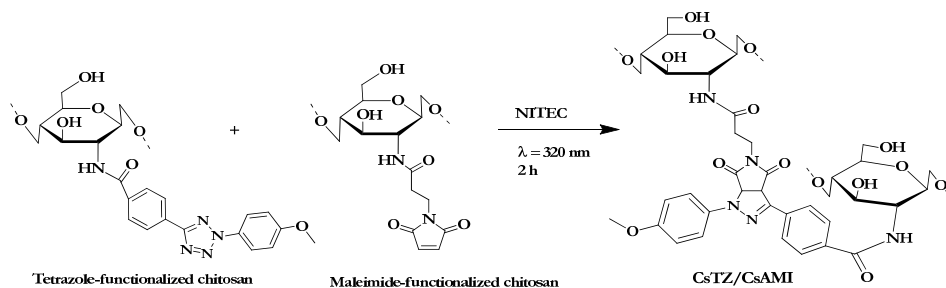
increase in the pore size of the materials after swollen in water. Furthermore, the as-prepared hydrogels were analysed in terms of rheological behaviour, resulting in materials with tunable sol/gel transition behaviour largely interesting for injectable or 3D printable applications. Finally, the biodegradation of the final materials was assessed under lysozymes whereas the non-toxicity of the hydrogels was tested by a short-term cytotoxicity assay. Therefore, the studied photo-induced hydrogelation could be relevant for the development of highly tuneable biomaterials.

VI.2. TETRAZOLE/MALEIMIDE CHITOSAN-BASED HYDROGELS FORMATION (CsTZ/CsAMI)

VI.2.1. Experimental part

Chitosan-based cross-linked hydrogels were obtained by photochemical cross-linking in the presence of UV light reacting two complementary chitosan-based derivatives as shown in Scheme VI.2. Namely, tetrazole and maleimide-functionalized chitosan precursors were synthesized separately as detailed in Chapter III. The maleimide-functionalized chitosan derivative under appropriate conditions and concentration forms a physical hydrogel due to effective intra and inter-macromolecular secondary interactions. Taking advantage of this property, the tetrazole-functionalized chitosan was added in order not only to act as cross-linker and improve the stability of the hydrogel, but also to attribute fluorescence to the maleimide-functionalized chitosan matrix. At the same time, the effect of adding different amounts of CsTZ into the maleimide-containing matrix was evaluated. Indeed, two different hydrogels with tetrazole-to-maleimide equivalent ratios of 1:50 and 1:15 were synthesized adding desired amounts of CsTZ aqueous solution ($1.5 \cdot 10^{-3}$ % w/v) to a constant mass of CsAMI matrix (54 mg). As calculated from NMR spectroscopy in Chapter III, degrees of substitution were found to be 29 (Equation II.5) and 12 % (Equation II.4) for CsTZ and CsAMI, respectively. Finally, the precursors were irradiated for 2 h in

a custom-built photoreactor using a lamp with an emission maximum at 320 nm to promote the photo cross-linking of the hydrogels, which are referred hereafter as CsTZ/CsAMI 1:50 and CsTZ/CsAMI 1:15.



Scheme VI.2. Hydrogel formation through NITEC reaction between CsTZ and CsAMI.

Hydrogel samples before and after gelation are shown in Figure VI.1 along with a schematic representation of the hydrogel formation through NITEC links, giving place to fluorescent materials under UV light.

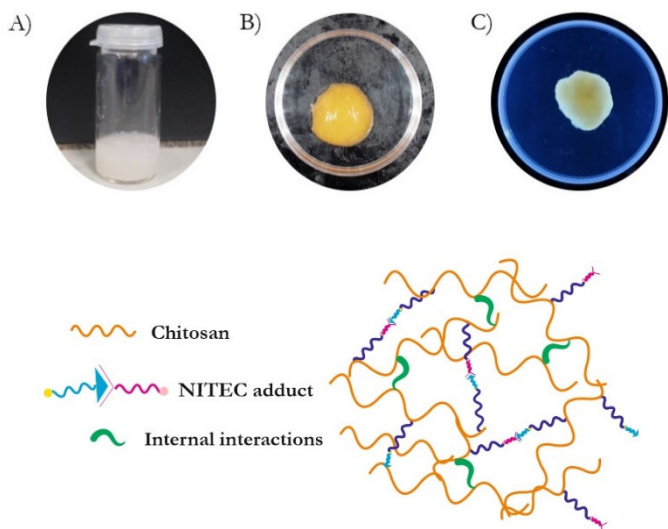


Figure VI.1. Schematic representation of the networked structure and images of A) mixture of chitosan precursors in aqueous medium, B) CsTZ/CsAMI hydrogel formed after 2 h at $\lambda = 320$ nm under daylight and C) CsTZ/CsAMI hydrogel under UV light at $\lambda_{\max} = 365$ nm.

VI.2.2. Results and discussion

As previously has been mentioned, covalent networking of chitosan between the grafted tetrazole and maleimide groups through NITEC reaction was intended to improve the stability of the maleimide-containing physical gel, preventing its premature degradation and, at the same time, conferring fluorescent property. Therefore, NITEC reaction was performed using 320 nm irradiation over 2 hours. As a consequence of the covalent click bonding between the tetrazole and maleimide units, stable cross-linked 3D networks were obtained, which remained insoluble and maintained their integrity after 3 h, presenting a sol-gel ratio of 93 % from Equation II.10.

It has to be mentioned that, as it has been reported elsewhere, nitrile imines of the tetrazole-containing acid can undergo dimerization reaction forming

dihydropyridazines in the absence of suitable dipolarophiles⁶. In order to minimize this undesired side reaction, maleimide groups were added in excess (50 and 15 times more), obtaining dark orange solid products (Figure VI.1).

VI.2.2.1. Physico-chemical characterization

The occurrence of the intermolecular cross-linking process could be readily monitored by fluorescence spectroscopy using an excitation wavelength of 396 nm in order to verify the NITEC reaction (Figure VI.2A). As it could be observed, CsTZ/CsAMI hydrogels showed a broad and intense emission peak in the green/yellow region (left image in Figure VI.2), demonstrating the success of the reaction and the formation of fluorescent pyrazoline adducts. Furthermore, the degree of cross-linking clearly was influenced by the UV irradiation time, increasing with the increase of exposure time. Namely, higher fluorescence emission signals were obtained when the samples were irradiated for a longer time and at the same time, peaks were slightly displaced to higher wavelengths, which could be related to a higher number and better stability of the formed adducts between chitosan derivatives. On the other hand, with increasing the CsTZ content (1:15 formulation) the probability of pyrazoline adduct formation during the intramolecular cross-linking also increased, leading to increased fluorescence intensity, indicating higher cross-linking degree in this case. Table VI.1 collects the maximum of the broad fluorescence emission band, which lied at around 500 nm for both formulations, being in the biocompatible visible range¹¹.

In the sake of comparison, control samples of both chitosan derivatives (CsTZ and CsAMI) were separately tested after 2 h of irradiation (Figure VI.2B). In this case, the control samples containing CsTZ and CsAMI presented their fluorescence emission peaks shifted towards lower wavelengths, which correspond to the blue/violet region (right image in Figure VI.2). These results

confirmed that the desired NITEC reaction among the reactive groups prevailed and the dimerization reaction occurred in a residual extent.

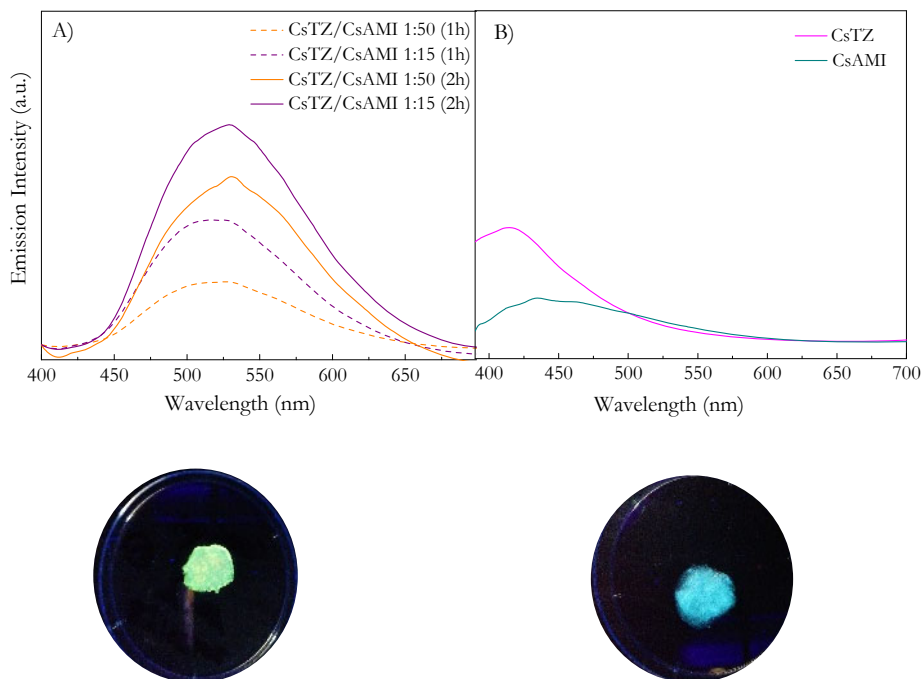


Figure VI.2. Images under irradiation light at $\lambda_{\text{max}} = 365 \text{ nm}$ and fluorescence emission spectra at an excitation wavelength of 396 nm for: A) CsTZ/CsAMI hydrogels after 1 and 2 hours of irradiation and B) CsTZ and CsAMI precursors after 2 hours of irradiation.

Table VI.1. Wavelength values for the fluorescence emission signals of NITEC hydrogels and chitosan derivatives as a function of time.

Sample	Wavelength at 1 h irradiation (nm)	Wavelength at 2 h irradiation (nm)
CsTZ/CsAMI 1:50	518	530
CsTZ/CsAMI 1:15	518	530
CsTZ	-	415
CsAMI	-	432

It is known that the electronic spectrum of molecules is influenced by their immediate environment, where one of the main environmental factors affecting

the electronic spectra is the solvent effect. Indeed, a change of solvent is accompanied by a change in polarity, dielectric constant and change in polarizability of the surrounding medium, influencing the electronic state behaviour of the compounds¹². As these interactions could affect the fluorescence, the fluorescent properties of the as-prepared CsTZ/CsAMI hydrogels were observed to change when varying the solution media where they were immersed in. Thereby, as explained in Chapter II, in order to check the effect on the fluorescent properties and the stability of the formed adduct, dried samples were immersed in HCl and PBS (pH = 1 and pH = 7.4, respectively) for 48 h and the fluorescence was measured after drying the samples again at room temperature. Figure VI.3 illustrates the emission spectra of the fluorescent hydrogels excited at 390 nm, where single peaks could be observed in all cases, being again higher the fluorescence intensity for 1:15 formulation as previously shown just after cross-linking (Figure VI.2). However, a dependency on the solvent was noticeable. Namely, a strong enhancement of the fluorescence signal happened after suspending the samples in PBS, suggesting higher stability and larger amount of the tetrazole/maleimide adduct. Without any other prior reference on which to base, this behaviour could be explained given the preference of the NITEC reaction to take place in phosphate buffer solutions¹³, basic aqueous solutions¹⁴ or organic solvents⁶, being the most convenient solvent. In contrast, initially unreacted chitosan moieties could be dissolving in HCl, showing lower emission intensities than in PBS due to an alteration of the tetrazole/maleimide system. Furthermore, a slight emission spectral shift ($\Delta\lambda$ about 14–17 nm) was remarked in HCl (Table VI.2). This effect could be attributable to the transition energy becomes higher based on a hypsochromic shift, giving place to a subtle blue shift of the emitted fluorescence with increasing solvent polarity^{12,15}.

In addition, along with the polarity of the solvent, the pH of the medium can also induce fluorescence fluctuations in the hydrogels^{10,16,17}. As observed, the

fluorescent activity of CsTZ/CsAMI hydrogels was more intense in neutral pH, confirming the stability of the NITEC adduct under physiological conditions.

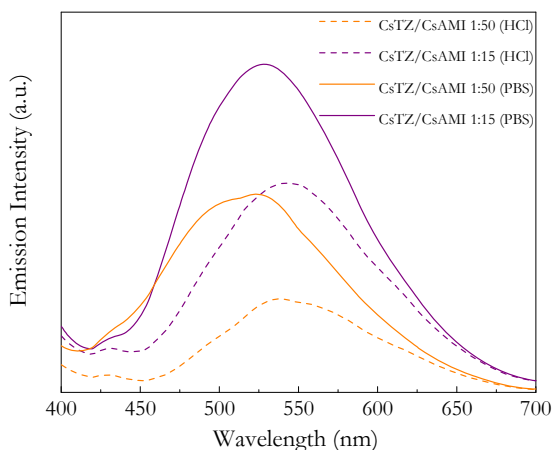


Figure VI.3. Fluorescence emission spectra at an excitation wavelength of 396 nm for CsTZ/CsAMI hydrogels after being immersed in HCl and PBS for 48 h.

Table VI.2. Wavelength values for the fluorescence emission signals of NITEC hydrogels as a function of solvent.

Sample	Wavelength after HCl immersion (nm)	Wavelength after PBS immersion (nm)
CsTZ/CsAMI 1:50	542	525
CsTZ/CsAMI 1:15	544	530

VI.2.2.2. Rheological behaviour

Similar to the previous hydrogels, dynamic rheological analysis was performed once the hydrogels were synthesized with the aim of studying the viscoelastic properties of the synthesized clicked hydrogels at 37 °C (Figure VI.4). The influence of the amount of tetrazole–functionalized chitosan in the stiffness of the hydrogels was evaluated. As evidenced by the frequency sweep, the incorporation of tetrazole containing chitosan into the maleimide–functionalized chitosan matrix resulted

in the formation of robust stable networks, since both formulations showed a marked solid-like behaviour independent of the applied frequency and supported by the fact that G' was always constant, even at lower frequencies, and higher than G'' .

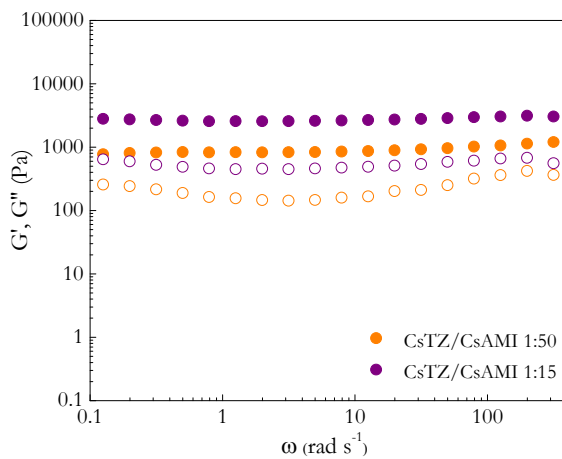


Figure VI.4. Frequency sweep of CsTZ/CsAMI hydrogels at 37 °C (G' (●) and G'' (○)).

Table VI.3. Mean storage and loss moduli and $\tan \delta$ values of CsTZ/CsAMI hydrogels at 37 °C (average \pm standard deviation, $n = 3$).

Hydrogel sample	G' (Pa)	G'' (Pa)	$\tan \delta$ (G''/G')
CsTZ/CsAMI 1:50	902 ± 320	226 ± 29	0.26 ± 0.08
CsTZ/CsAMI 1:15	2716 ± 1253	515 ± 203	0.19 ± 0.01

The mean G' , G'' and damping factor ($\tan \delta$) values for the final hydrogels are summarized in Table VI.3. As it could be appreciated, for CsTZ/CsAMI 1:15, the damping factor value was lower, indicating an even more pronounced elastic character in this case. Moreover, significant differences were observed between the G' values of both hydrogels. In fact, an increasing amount of tetrazole-functionalized chitosan could promote further cross-linking of the network, giving a higher value of storage moduli even though the total polymer

concentration was lower. The storage moduli of the hydrogels, as indicator of rigidity, would be directly related to the final application of the material, influencing its final performance. Furthermore, the power of the proposed NITEC cross-linking reaction was highly manifested, since visibly higher values of storage modulus were obtained for CsTZ/CsAMI hydrogels regardless the molecular weight of the starting chitosan in this case, which was similar to that used in Chapter IV for DA hydrogels.

To gain deeper insights, the structural parameters (ξ , n_c and M_c) of the developed chitosan-based hydrogels were determined based on the rheological results from the Equation II.12, II.13 and II.14, being the polymer concentration (c) in the samples of 18 and 6 % w/v for CsTZ/CsAMI 1:50 and CsTZ/CsAMI 1:15, respectively. The calculated parameters are summarized in Table VI.4.

Table VI.4. Structural parameters of CsTZ/CsAMI hydrogels based on the rheological frequency sweep analysis (average \pm standard deviation, $n = 3$).

Hydrogel sample	ξ (nm)	n_c (mol m ⁻³)	M_c (kg mol ⁻¹)
CsTZ/CsAMI 1:50	7.9 \pm 1.0	0.35 \pm 0.12	545 \pm 193
CsTZ/CsAMI 1:15	5.5 \pm 1.0	1.05 \pm 0.49	53 \pm 24

According with this data, both the ξ and M_c values of CsTZ/CsAMI hydrogels decreased as the amount of tetrazole-functionalized chitosan increased, and therefore, the resulting values for the cross-linking density (n_c) increased from 0.35 to 1.05 mol m⁻³ suggesting a higher cross-linked network for CsTZ/CsAMI 1:15 hydrogel. As mentioned in previous chapters, results were in line with the expected behaviour that the higher the G' , the lower the mesh size and M_c and higher the cross-linking density¹⁸, highlighting the great cross-linking efficiency. Moreover, the obtained structural values were similar to those reported in previous chapters for the other chitosan-based clicked systems as well as to the results for other polymeric hydrogels covalently cross-linked through different

strategies; namely, hydrazine cross-linked polysaccharide-based hydrogels¹⁸ and poly(ethylene glycol)-based hydrogels cross-linked through thiol-ene reaction¹⁹.

Nevertheless, regarding the polymer concentration (c), a characteristic behaviour could be highlighted for this particular tetrazole/maleimide system. The use of different c values derived in the possibility of studying the influence of this parameter in this case. Indeed, lower values for ξ and M_c and a higher value for n_c were obtained for the lowest polymer concentration (6 % w/v). In contrast, Karvinen et al. claimed the opposite trend¹⁸; whereas, Rehmann et al. also observed a decrease in the mesh size value when increasing the polymer concentration¹⁹. The explanation to this particular finding may be related to the fact that when increasing the volume of aqueous solution, the amount CsTZ was also increased, enhancing the cross-linking between the two complementary derivatives. Therefore, even if the total polymer concentration was lower in CsTZ/CsAMI 1:15 hydrogel, the formation of the network was improved and gave rise to a smaller mesh size being consistent with the theory. Thereby, the potentiality of the NITEC reaction was reflected in the structural properties over the polymer concentration.

As explained before, fluorescent hydrogels have great applicability in the biomedical field. At the same time, increasing investigations are focusing on the development of injectable or 3D printable biomaterials, since printing gives the possibility to create complex morphological structures similar to tissues and organs. The printability of hydrogels is subjected to the shear-thinning property, defined as the continuous decrease in the viscosity (η) with an increasing shear rate, allowing them to be extruded through a needle²⁰. In order to assess the injectability of the developed NITEC hydrogels, shear thinning and yield stress rheological measurements were performed. Figure VI.5A shows the evolution of η for the two hydrogels during the shear-thinning test. As it could be observed, in both cases their viscosity sharply decreased with increasing the shear rate,

which represented the above mentioned shear–thinning behaviour in the range of interest (0.1 to 1000 s^{-1}) and indicated that the tetrazole/maleimide clicked chitosan hydrogels described a typical non–Newtonian pseudoplastic fluid behaviour^{21,22}. According to Alghoonch et al., during the application of high shear rates, shear forces promote the alignment of the polymer chains in the flow direction losing many of their intra and inter–chain interactions²³.

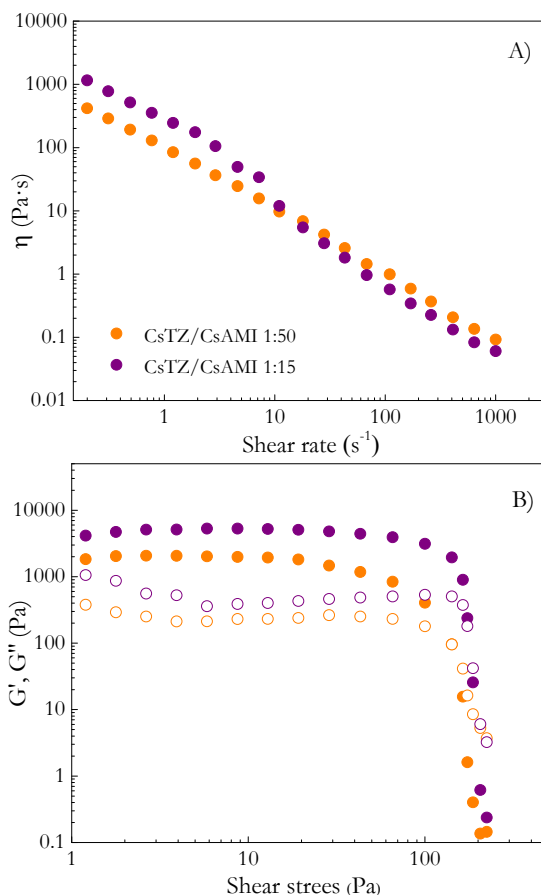


Figure VI.5. A) Evolution of the viscosity (η) as a function of shear rate ($\dot{\gamma}$) and B) G' (\bullet) and G'' (\circ) moduli versus shear stress (τ) for CsTZ/CsAMI hydrogels.

On the other hand, oscillatory stress sweep experiments were carried out in order to estimate the yield point of the as-prepared hydrogels (Figure VI.5B), i.e. the shear stress at which the material first started to flow. The transition between solid and liquid-like behaviour was clearly observed as a sharp decrease of the dynamic moduli, requiring similar yield stress (100 Pa) for both tetrazole/maleimide chitosan hydrogels close to that reported for other polymeric cross-linked hydrogels²⁴.

Based on the rheological results, the as-prepared hydrogels could be classified as so-called second-generation self-healing materials with hybrid architectures involving both reversible and irreversible interactions. Namely, upon application of the shear force, the ensemble of weak reversible interactions preferably yields providing deformability, while the stronger irreversible bonds remain intact, providing scaffolding. Ideally, when the force is removed, the scaffold of irreversible interactions guides the reassembly of the reversible interactions, restoring the material to its original undeformed state²⁵. This self-healing phenomenon is a result of the presence of both the covalent bonds achieved through NITEC reaction between tetrazole and maleimide groups, and the secondary reactions involving the reversible non-covalent interactions such as hydrogen bonding or hydrophobic interactions in the complementary chitosan derivatives²⁶.

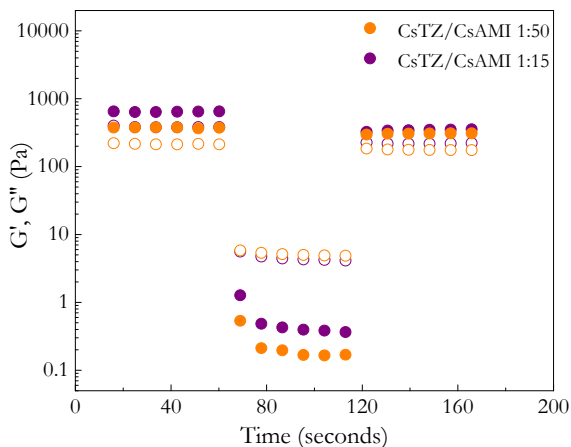


Figure VI.6. Variation of G' (●) and G'' (○) moduli during the continuous step-strain measurement at alternate 0.1 % and 50 % strain (frequency = 1 Hz) versus time for CsTZ/CsAMI hydrogels.

In order to further understand the ability of NITEC hydrogels to self-restore, step-strain measurements (strain = 0.1 to 50 % at 20 °C) were conducted following the methodology described in Chapter II. Figure VI.6 displayed the results for the recovery of the CsTZ/CsAMI hydrogels. As described earlier, NITEC hydrogels had solid-like elastic properties at low strain values, where higher G' modulus values were recorded in comparison with G'' . When the strain was increased above the critical region, the hydrogels collapsed to form fluid or quasi-liquid state, losing their mechanical stability which was indicated by a complete inversion of the G' and G'' moduli values. Finally, with the reduction of the strain, the broken hydrogel networks were transformed into stable gels and quickly recovered their mechanical strength. These results confirmed the reversible sol-gel transition of the networks and demonstrated the *in situ* recovery of the materials, confirming their self-healing capacity.

The particular rheological response presented by the CsTZ/CsAMI hydrogels would be largely interesting for injectable or 3D printable applications. Both the

shear-thinning trend and the reasonable value obtained for the yield point could be reliable indicatives of the printability of the materials. Besides, the high storage modulus and the low $\tan \delta$ values could confirm the shape fidelity of the tetrazole/maleimide systems after the printing process, which was also supported by the self-healing ability²⁷.

VI.2.2.3. Morphological analysis

The microstructure of the hydrogels was studied by scanning electron microscopy (SEM). Regular and homogeneous porous microstructures for both hydrogel samples were obtained in Figure VI.7A and B in their initial state (freeze-dried just after the gel formation) and in Figure VI.7C and D after swollen in water for 48 h, based on the equilibrium data from the swelling studies (described in the following section). In view of the SEM images, highly porous networks were obtained.

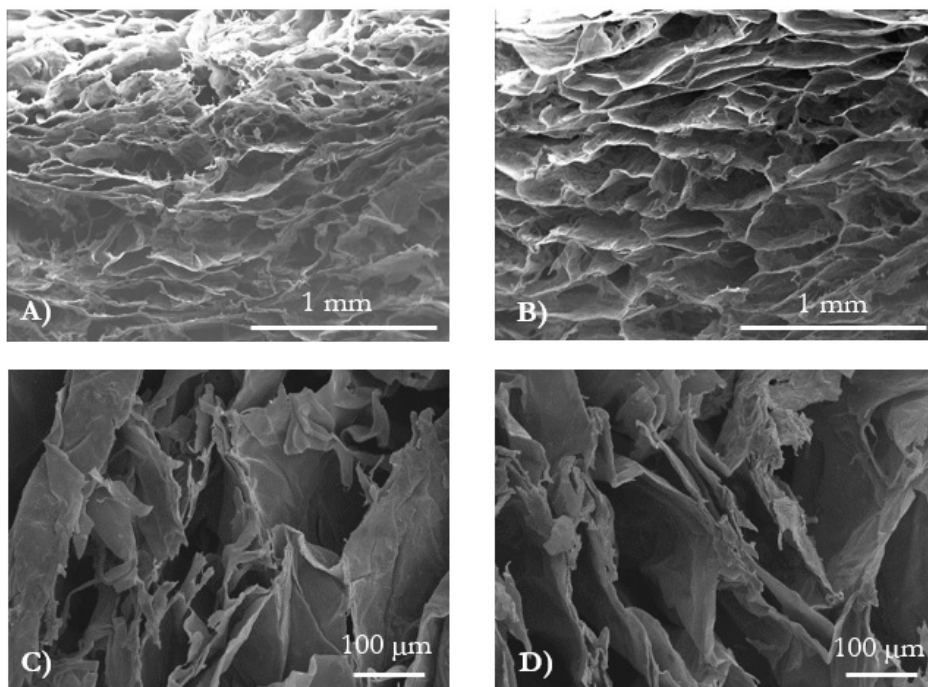


Figure VI.7. SEM images of the freeze-dried CsTZ/CsAMI hydrogels: A) as-prepared and C) after swollen in H₂O for CsTZ/CsAMI 1:50; B) as-prepared and D) after swollen in H₂O for CsTZ/CsAMI 1:15.

A homogeneous distribution of porous within the hydrogels was expected to directly influence the response-rate of the materials. Accordingly, the resulting 3D microstructure of the hydrogels could be a determining factor for the control of the swelling ability of the materials as previously was observed in Chapter IV for the CsFu/BMI hydrogels. Thus, the dimensions of the pores present in the interconnected networks were determined (Figure VI.8A and B for CsTZ/CsAMI 1:50 and CsTZ/CsAMI 1:15 samples, respectively). Based on the pore size distribution, a significant increase in the pore size after the hydrogels were swelled in water was observed. The mean pore diameter for CsTZ/CsAMI 1:50 hydrogel increased from $267 \pm 113 \mu\text{m}$ just after its formation to 884 ± 216

μm after swelling, whereas for CsTZ/CsAMI 1:15 hydrogel the mean pore diameter increased from $398 \pm 98 \mu\text{m}$ to $1217 \pm 155 \mu\text{m}$.

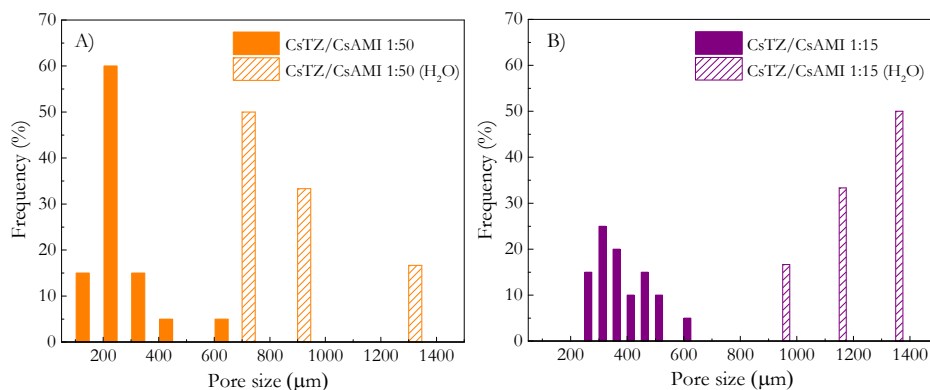


Figure VI.8. Pore size distribution for A) CsTZ/CsAMI 1:50 hydrogel and B) CsTZ/CsAMI 1:15 hydrogel.

Analysing the pore size distribution in 3D matrices is very useful when studying changes and modifications produced as a result of *in vitro* behaviour of materials under simulated human body conditions. Namely, pore size distribution plays an important role in the signalling and microenvironment stimuli imparted to cells when studying cellular growth and proliferation within the matrix²⁸ as well as in drug delivery applications, where *in vitro* drug release studies have shown that an increase in porosity results in the improved drug release²⁹. Therefore, the tuning of pore size distribution clearly made this tetrazole/maleimide system competent for biomedical applications. The results were in total agreement with the data obtained in previous chapters for DA and MA hydrogels.

VI.2.2.4. Swelling, pH sensitivity and degradation studies

In order to assess the applicability of CsTZ/CsAMI hydrogels for biomedical applications that might be accompanied by changes of pH, their behaviour at different pHs under simulated gastric (HCl, pH 1) and intestinal (PBS, pH 7.4)

conditions at 37 °C was explored (Figure VI.9) by a general gravimetric method detailed in Chapter II and using the Equation II.8.

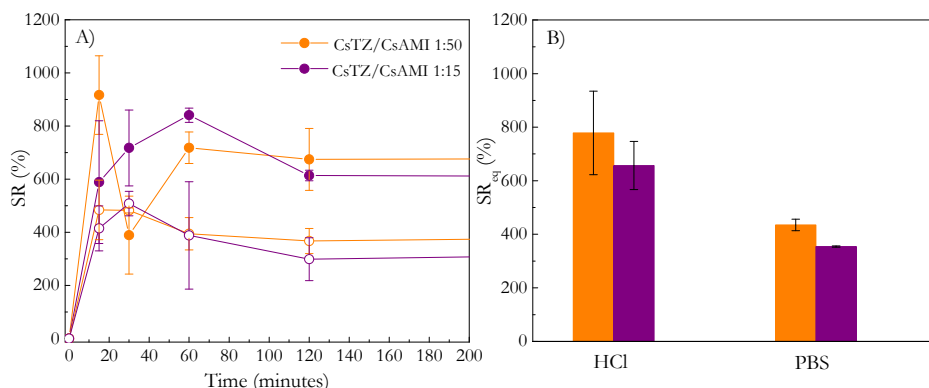


Figure VI.9. A) Swelling kinetics of CsTZ/CsAMI hydrogels in HCl (●) and PBS (○) media and B) equilibrium swelling ratio of the hydrogels at 37 °C in both aqueous media at 48 h.

As expected, the swelling capacity of the hydrogels was again greater under acidic environment. As already has been commented in previous chapters for DA and MA hydrogels, this effect was due to the cationic nature of chitosan, which generated repulsive forces between the protonated free amines causing the hydrogel expansion. Under buffered conditions of the intestine fluids, swelling was lower due to the decrease of repulsions between the chains at this pH.

As reported in Chapters IV and V, further cross-linking degree could be related with lower swelling ratio values. Following this trend, the addition of a higher amount of tetrazole-functionalized chitosan seemed to be contributing to the formation of a higher interconnected network, since lower swelling ratios were presented in both media, even when the total concentration of polymer was lower, highlighting the potential of the NITEC reaction. Moreover, the present behaviour was in accordance with the observed rheological one.

The swelling kinetics of the hydrogels were adjusted to Equation II.9 and the obtained parameters (SR_{max} , k_S and r_o) are presented in Table VI.5, where SR_{eq} is the value of the swelling degree in equilibrium (48 hours) obtained from the data of Figure VI.9B. Greatly close values for SR_{eq} and SR_{max} in both media were obtained.

Table VI.5. Swelling parameters of CsTZ/CsAMI hydrogels at 37 °C in different aqueous media.

Swelling media	Hydrogel sample	SR_{eq} (%)	SR_{max} (%)	$k_S \cdot 10^4$ ($\frac{g_{hydrogel}}{g_{solution} \cdot s^{-1}}$)	$r_o \cdot 10^3$ ($\frac{g_{solution} \cdot g}{hydrogel \cdot s^{-1}}$)
HCl	CsTZ/CsAMI 1:50	778 ± 156	770	0.84	20
	CsTZ/CsAMI 1:15	657 ± 90	640	0.21	116
PBS	CsTZ/CsAMI 1:50	435 ± 21	440	0.50	103
	CsTZ/CsAMI 1:15	354 ± 2	370	0.22	332

As observed in Figure VI.9, regarding the pH, the absorption capacity of the hydrogels was higher in acidic medium. Therefore, the lower swelling ratio values presented by the hydrogels in basic medium were related with higher r_o values as stated by Altinisik and Yurdakoc³⁰.

With the aim of applying the synthesized hydrogels as possible bioink materials for the 3D printing of tissue structures, particular requirements apart from printability (confirmed above in Section VI.2.2.2) need to be satisfied, which mainly include biodegradability and biocompatibility (explained below in Section VI.2.2.5). As reported in previous chapters, chitosan biodegrades in human body due to the activity of lysozyme and bacterial enzymes present in the colon³¹. In order to estimate the behaviour of the final materials *in vivo*, *in vitro* degradation studies were carried out. Therefore, the degradation of CsTZ/CsAMI hydrogels was monitored for 4 weeks following the method described in Chapter II. The degradation profiles for the NITEC hydrogels at physiological conditions, both in 1 mg mL⁻¹ lysozyme and enzyme-free solutions, are shown in Figure VI.10.

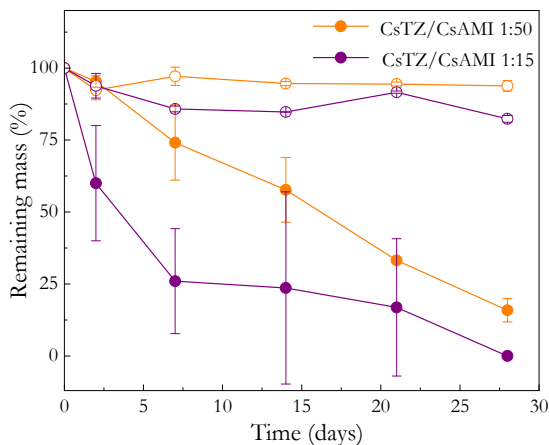


Figure VI.10. Dry weight remaining percent of CsTZ/CsAMI hydrogels in 1 mg mL⁻¹ lysozyme/PBS (●) and in PBS without lysozyme (○) at 37 °C as a function of time.

The degradation behaviour of the hydrogels in lysozyme containing environment showed that the samples were sensitive to enzymes. Their highly porous microstructures and the good pore interconnectivity facilitate the enzyme transport and diffusion of the degradation products from the material, which is essential for tissue restoration³¹. Furthermore, when the breakage of the glycosidic bonds and the amide bonds reach a critical value, the whole cross-linked network will disjoin, resulting in the disappearance of the hydrogel³². Herein, NITEC hydrogels suffered a sharp decrease in their remaining mass ratio from the beginning of the study and completely degraded after 28 days of incubation in lysozyme solution, being even more pronounced in the case of CsTZ/CsAMI 1:15 hydrogel probably related with its higher pore size. The ability of the hydrogels to be biodegradable brings numerous advantages to these materials towards being used in the field of biomedicine. On the other hand, the control samples incubated in PBS without enzymes showed the opposite trend. The loss of weight remained constant during the degradation study, as was already observed when calculating the gel content of the NITEC hydrogels, where values

around 93 % were obtained. This behaviour suggested the excellent stability of the tetrazole/maleimide hydrogels in the medium due to the presence of the covalent bonds generated after the NITEC reaction.

VI.2.2.5. Biocompatibility

In order to evaluate the suitability of the new hydrogels as potential biomaterials, the biocompatibility was assessed following ISO 10993 standard, using cytotoxicity assessment employing L929 murine fibroblast cells, as explained in Chapter II. Figure VI.11 shows the cell viability (in % with respect to the negative control) at 24 and 48 hours for the CsTZ/CsAMI 1:50 hydrogel and the positive control. As the nature of the hydrogels in terms of toxicity could be analysed in the same way, CsTZ/CsAMI 1:50 was used as reference. According to the results, the cell viability was demonstrated as the obtained value was higher than the established acceptance limit of 70 % with respect to the negative control, indicating the potential biomedical applicability of the new hydrogels.

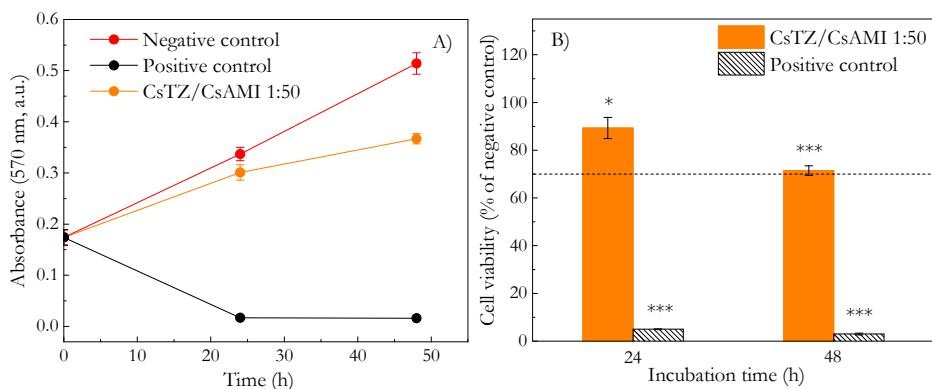


Figure VI.11. A) Absorbance at 570 nm *versus* incubation time of the positive control, negative control and CsTZ/CsAMI 1:50 hydrogel and B) *in vitro* cell viability of the positive control and CsTZ/CsAMI 1:50 hydrogel extract against L929 fibroblasts as a function of incubation time (* $p < 0.05$, *** $p < 0.001$).

VI.3. CONCLUSIONS

In this chapter, a novel synthetic strategy involving the synthesis of totally renewable materials from tetrazole/maleimide-functionalized chitosan precursors was proposed. Accordingly, covalently cross-linked hydrogels were successfully synthesized through light induced click strategy. The photo-triggered NITEC reaction was confirmed by fluorescence spectroscopy, resulting in broad and intense emission peaks in the green/yellow region, originated from the cross-links in the networks. With increasing the tetrazole content, the fluorescent signal became more intense. Moreover, the degree of cross-linking depended on the UV irradiation time, i.e. it increased as exposure time increases, leading to hydrogels with higher elastic solid-like properties and lower swelling ratio³³.

The formation of stable networks after the cross-linking reaction was confirmed by rheology. Increasing the amount of CsTZ in the hydrogel notably improved the storage modulus value, which was related with an increase in effective cross-linking density and simultaneous decrease in the mesh size and the average molecular weight between cross-linking points. Furthermore, the G' value of CsTZ/CsAMI 1:15 hydrogel was measured to be comparable to those of that of liver, fat, relaxed muscle or breast gland tissue, which are found in the range between 10^3 – 10^4 Pa³⁴. On the other hand, NITEC hydrogels presented shear-thinning property and a reasonable value of yield point, making them interesting candidates for injectable or 3D printable applications. In addition, hydrogels were proved to present self-healing ability, which could occur autonomously without any external intervention based on supramolecular chemistry.

Spongy-like microstructures were obtained for the freeze-dried samples both before and after swelling in water, where it was noteworthy that all of the hydrogels were highly porous. Analysis of the SEM image revealed that the hydrogels displayed a continuous and porous structure by virtue of the NITEC reaction, resembling other natural macromolecular hydrogel system structures,

with mean diameter pore size in the range of 267–398 μm for the original hydrogels. When hydrogels were not swollen, the samples only contained the water used during their synthesis. On the contrary, after being swollen in water, their liquid content was significantly higher and the amount of solvent embedded in the hydrogels influenced the microstructure of the network. Thus, after swelling in water the mean diameter pore size of the hydrogels increased to 884–1217 μm . This finding confirmed the hypothesis that CsTZ/CsAMI hydrogels could be highly promising materials as structural scaffolds, allowing cellular growth or encapsulating cells or biomolecules for delivery that need relatively large dimensions.

The swelling was recorded for 48 hours in both fluids in order to ensure equilibrium was reached. The swelling study revealed the pH-sensitiveness of the synthesized hydrogels, being more pronounced in acidic medium given the cationic nature of the chitosan. Furthermore, the swelling capacity was influenced by the degree of cross-linking as was evidenced by the lower values obtained for the CsTZ/CsAMI 1:1 5 hydrogel. Additionally, the fluorescence signal of the synthesized hydrogels was markedly influenced by the surrounding media, being more affected by neutral pH.

Finally, even if the developed tetrazole/maleimide clicked systems were observed to remain stable and insoluble under physiological conditions due to the formed cross-linked networks, CsTZ/CsAMI hydrogels were susceptible to degradation during the *in vitro* culture with lysozymes. In contrast to the common cross-linking strategies to fabricate hydrogels, which include the Diels–Alder reaction and the Michael addition described in previous chapters, the use of the NITEC reaction for developing green 3D networks resulted to be highly novel.

REFERENCES

- (1) Estupiñán, D.; Gegenhuber, T.; Blinco, J. P.; Barner-Kowollik, C.; Barner, L. Self-Reporting Fluorescent Step-Growth Raft Polymers Based on Nitrile Imine-Mediated Tetrazole-Ene Cycloaddition Chemistry. *ACS Macro Lett.* **2017**, *6* (3), 229–234. <https://doi.org/10.1021/acsmacrolett.7b00024>.
- (2) Bao, C.; Zhu, L.; Lin, Q.; Tian, H. Building Biomedical Materials Using Photochemical Bond Cleavage. *Adv. Mater.* **2015**, *27* (10), 1647–1662. <https://doi.org/10.1002/adma.201403783>.
- (3) Delaittre, G.; Goldmann, A. S.; Mueller, J. O.; Barner-Kowollik, C. Efficient Photochemical Approaches for Spatially Resolved Surface Functionalization. *Angew. Chemie - Int. Ed.* **2015**, *54* (39), 11388–11403. <https://doi.org/10.1002/anie.201504920>.
- (4) Russev, M. M.; Hecht, S. Photoswitches: From Molecules to Materials. *Adv. Mater.* **2010**, *22* (31), 3348–3360. <https://doi.org/10.1002/adma.200904102>.
- (5) Chatani, S.; Kloxin, C. J.; Bowman, C. N. The Power of Light in Polymer Science: Photochemical Processes to Manipulate Polymer Formation, Structure, and Properties. *Polym. Chem.* **2014**, *5* (7), 2187–2201. <https://doi.org/10.1039/c3py01334k>.
- (6) Hufendiek, A.; Carlmark, A.; Meier, M. A. R.; Barner-Kowollik, C. Fluorescent Covalently Cross-Linked Cellulose Networks via Light-Induced Ligation. *ACS Macro Lett.* **2016**, *5* (1), 139–143. <https://doi.org/10.1021/acsmacrolett.5b00806>.
- (7) Junkers, T. [2+2] Photo-Cycloadditions for Polymer Modification and Surface Decoration. *Eur. Polym. J.* **2015**, *62*, 273–280. <https://doi.org/10.1016/j.eurpolymj.2014.08.005>.
- (8) Kerbs, A.; Mueller, P.; Kaupp, M.; Ahmed, I.; Quick, A. S.; Abt, D.; Wegener, M.; Niemeyer, C. M.; Barner-Kowollik, C.; Fruk, L. Photo-Induced Click Chemistry for DNA Surface Structuring by Direct Laser Writing. *Chem. - A Eur. J.* **2017**, *23* (21), 4990–4994. <https://doi.org/10.1002/chem.201700673>.
- (9) Dietrich, M.; Delaittre, G.; Blinco, J. P.; Inglis, A. J.; Bruns, M.; Barner-Kowollik, C. Photoclickable Surfaces for Profluorescent Covalent Polymer Coatings. *Adv. Funct. Mater.* **2012**, *22* (2), 304–312. <https://doi.org/10.1002/adfm.201102068>.
- (10) Li, Y.; Young, D. J.; Loh, X. J. Fluorescent Gels: A Review of Synthesis, Properties, Applications and Challenges. *Mater. Chem. Front.* **2019**, *3* (8),

- 1489–1502. <https://doi.org/10.1039/c9qm00127a>.
- (11) Willenbacher, J.; Wuest, K. N. R.; Mueller, J. O.; Kaupp, M.; Wagenknecht, H. A.; Barner-Kowollik, C. Photochemical Design of Functional Fluorescent Single-Chain Nanoparticles. *ACS Macro Lett.* **2014**, *3* (6), 574–579. <https://doi.org/10.1021/mz500292e>.
- (12) Mannekutla, J. R.; Mulimani, B. G.; Inamdar, S. R. Solvent Effect on Absorption and Fluorescence Spectra of Coumarin Laser Dyes: Evaluation of Ground and Excited State Dipole Moments. *Spectrochim. Acta Part A Mol. Biomol. Spectrosc.* **2008**, *69* (2), 419–426. <https://doi.org/10.1016/J.SAA.2007.04.016>.
- (13) Fan, Y.; Deng, C.; Cheng, R.; Meng, F.; Zhong, Z. In Situ Forming Hydrogels via Catalyst-Free and Bioorthogonal “Tetrazole-Alkene” Photo-Click Chemistry. *Biomacromolecules* **2013**, *14* (8), 2814–2821. <https://doi.org/10.1021/bm400637s>.
- (14) Stolzer, L.; Vigovskaya, A.; Barner-Kowollik, C.; Fruk, L. A Self-Reporting Tetrazole-Based Linker for the Biofunctionalization of Gold Nanorods. *Chem. - A Eur. J.* **2015**, *21* (41), 14309–14313. <https://doi.org/10.1002/chem.201502070>.
- (15) Piatkevich, K. D.; Malashkevich, V. N.; Morozova, K. S.; Nemkovich, N. A.; Almo, S. C.; Verkhusha, V. V. Extended Stokes Shift in Fluorescent Proteins: Chromophore-Protein Interactions in a near-Infrared TagRFP675 Variant. *Sci. Rep.* **2013**, *3*, 1–11. <https://doi.org/10.1038/srep01847>.
- (16) Tóth, V.; Hermann, P.; Végh, D.; Zelles, T.; Géczi, Z. Study of the Intrinsic Fluorescence of a Highly Branched Cationic Dendrimer, Poly (Ethyleneimine) (PEI). *Molecules* **2019**, *24* (20). <https://doi.org/10.3390/molecules24203690>.
- (17) Liu, S. G.; Li, N.; Ling, Y.; Kang, B. H.; Geng, S.; Li, N. B.; Luo, H. Q. PH-Mediated Fluorescent Polymer Particles and Gel from Hyperbranched Polyethylenimine and the Mechanism of Intrinsic Fluorescence. *Langmuir* **2016**, *32* (7), 1881–1889. <https://doi.org/10.1021/acs.langmuir.6b00201>.
- (18) Karvinen, J.; Ihalainen, T. O.; Calejo, M. T.; Jönkkäri, I.; Kellomäki, M. Characterization of the Microstructure of Hydrazone Crosslinked Polysaccharide-Based Hydrogels through Rheological and Diffusion Studies. *Mater. Sci. Eng. C* **2019**, *94* (April 2018), 1056–1066. <https://doi.org/10.1016/j.msec.2018.10.048>.
- (19) Rehmann, M. S.; Skeens, K. M.; Kharkar, P. M.; Ford, E. M.; Maverakis, E.;

- Lee, K. H.; Kloxin, A. M. Tuning and Predicting Mesh Size and Protein Release from Step Growth Hydrogels. *Biomacromolecules* **2017**, *18* (10), 3131–3142. <https://doi.org/10.1021/acs.biomac.7b00781>.
- (20) Qu, J.; Zhao, X.; Ma, P. X.; Guo, B. PH-Responsive Self-Healing Injectable Hydrogel Based on N-Carboxyethyl Chitosan for Hepatocellular Carcinoma Therapy. *Acta Biomater.* **2017**, *58*, 168–180. <https://doi.org/10.1016/j.actbio.2017.06.001>.
- (21) Gong, J.; Wang, L.; Wu, J.; Yuan, Y.; Mu, R. J.; Du, Y.; Wu, C.; Pang, J. The Rheological and Physicochemical Properties of a Novel Thermosensitive Hydrogel Based on Konjac Glucomannan/Gum Tragacanth. *Lwt* **2019**, *100* (August 2018), 271–277. <https://doi.org/10.1016/j.lwt.2018.10.080>.
- (22) Chaves, L. L.; Silveri, A.; Vieira, A. C. C.; Ferreira, D.; Cristiano, M. C.; Paolino, D.; Di Marzio, L.; Lima, S. C.; Reis, S.; Sarmiento, B.; et al. PH-Responsive Chitosan Based Hydrogels Affect the Release of Dapsone: Design, Set-up, and Physicochemical Characterization. *Int. J. Biol. Macromol.* **2019**, *133*, 1268–1279. <https://doi.org/10.1016/J.IJBIOMAC.2019.04.178>.
- (23) Alghooneh, A.; Razavi, S. M. A.; Behrouzian, F. Rheological Characterization of Hydrocolloids Interaction: A Case Study on Sage Seed Gum-Xanthan Blends. *Food Hydrocoll.* **2017**, *66*, 206–215. <https://doi.org/10.1016/J.FOODHYD.2016.11.022>.
- (24) Kim, J. Y.; Song, J. Y.; Lee, E. J.; Park, S. K. Rheological Properties and Microstructures of Carbopol Gel Network System. *Colloid Polym. Sci.* **2003**, *281* (7), 614–623. <https://doi.org/10.1007/s00396-002-0808-7>.
- (25) Brochu, A. B. W.; Craig, S. L.; Reichert, W. M. Self-Healing Biomaterials. *J. Biomed. Mater. Res. - Part A* **2011**, *96 A* (2), 492–506. <https://doi.org/10.1002/jbm.a.32987>.
- (26) Lehn, J. M. Supramolecular Chemistry: From Molecular Information towards Self-Organization and Complex Matter. *Reports Prog. Phys.* **2004**, *67* (3), 249–265. <https://doi.org/10.1088/0034-4885/67/3/R02>.
- (27) Liu, Z.; Zhang, M.; Yang, C. Impact of Rheological Properties of Mashed Potatoes on 3D Printing. *J. Food Eng.* **2018**, *220*, 76–82. <https://doi.org/10.1016/J.JFOODENG.2017.04.017>.
- (28) Leal-Egaña, A.; Dietrich-Braumann, U.; Díaz-Cuenca, A.; Nowicki, M.; Bader, A. Determination of Pore Size Distribution at the Cell-Hydrogel Interface. *J. Nanobiotechnology* **2011**, *9* (1), 24. <https://doi.org/10.1186/1477-3155-9-24>.

- (29) Varghese, J. S.; Chellappa, N.; Fathima, N. N. Gelatin-Carrageenan Hydrogels: Role of Pore Size Distribution on Drug Delivery Process. *Colloids Surfaces B Biointerfaces* **2014**, *113*, 346–351. <https://doi.org/10.1016/j.colsurfb.2013.08.049>.
- (30) Altinisik, A.; Yurdakoc, K. Chitosan/Poly(Vinyl Alcohol) Hydrogels for Amoxicillin Release. *Polym. Bull.* **2014**, *71* (3), 759–774. <https://doi.org/10.1007/s00289-013-1090-1>.
- (31) Lončarević, A.; Ivanković, M.; Rogina, A. Lysozyme-Induced Degradation of Chitosan: The Characterisation of Degraded Chitosan Scaffolds. *J. Tissue repair Regen.* **2017**, *1* (1), 12–22. <https://doi.org/10.14302/issn.2640>.
- (32) Hong, Y.; Song, H.; Gong, Y.; Mao, Z.; Gao, C.; Shen, J. Covalently Crosslinked Chitosan Hydrogel: Properties of in Vitro Degradation and Chondrocyte Encapsulation. *Acta Biomater.* **2007**, *3* (1), 23–31. <https://doi.org/10.1016/j.actbio.2006.06.007>.
- (33) Cho, I. S.; Cho, M. O.; Li, Z.; Nurunnabi, M.; Park, S. Y.; Kang, S.-W.; Huh, K. M. Synthesis and Characterization of a New Photo-Crosslinkable Glycol Chitosan Thermogel for Biomedical Applications. *Carbohydr. Polym.* **2016**, *144*, 59–67. <https://doi.org/10.1016/J.CARBPOL.2016.02.029>.
- (34) Vanderhooft, J. L.; Alcoutlabi, M.; Magda, J. J.; Prestwich, G. D. Rheological Properties of Cross-Linked Hyaluronan-Gelatin Hydrogels for Tissue Engineering. *Macromol. Biosci.* **2009**, *9* (1), 20–28. <https://doi.org/10.1002/mabi.200800141>.

CHAPTER VII

NANOGELES DESIGN FOR TARGETED DELIVERY

VII.1. INTRODUCTION AND OBJECTIVE	229
VII.2. THIOLATED CHITOSAN-BASED NANOGELES FORMATION (C_sSH/PEGBCOOH)	233
VII.2.1. EXPERIMENTAL PART	233
VII.2.2. RESULTS AND DISCUSSION	235
VII.2.2.1. Physico-chemical characterization	236
VII.2.2.2. Thermal behaviour	238
VII.2.2.3. pH-responsive swelling properties	239
VII.2.2.4. Size and morphological analysis	243
VII.2.2.5. Mucoadhesion property	245
VII.2.2.6. Assessment as potential nanocarriers for drug delivery by click chemistry	250
VII.2.2.6.1. Experimental part	251
VII.2.2.6.2. Results and discussion	251
VII.3. CONCLUSIONS	254
REFERENCES	257

VII. NANOGELS DESIGN FOR TARGETED DELIVERY

VII.1. INTRODUCTION AND OBJECTIVE

In the research field of hydrogels, a great number of studies are focused on the development of nanoscaled new alternatives. Indeed, given their small size, nanogels have shown advantages over their macroscopic analogs and have been recently envisaged as an alternative solution to obtain less invasive delivery carriers than hydrogels¹. Nanogels present larger surface area and can enhance penetration through tissue barriers. Therefore, the diameter of nanogels is approximately of 1 to 100 nm², being their size much smaller than the inner diameter of most needles (~ 1 mm). At the same time, nano-sized gels respond more rapidly to changes in the environment and therefore, can be used more efficiently in biomedical applications³.

In fact, the size of the hydrogels determines how they transport and adhere once introduced into blood vessels, airways or the gastro-intestinal tract. In addition to transepithelial and local injection (such as intraperitoneal and intrabony injection), nanogels also enable other routes for penetration. Nanogels of size 10–100 nm are suitable for systemic drug administration, because they can leave small blood vessels through fenestrations in the endothelial lining, allowing for extravasation into tissues. Furthermore, hydrogels below 10 nm in diameter can be cleared by kidney filtration, while those of 500–10000 nm can be phatogocytized by macrophages⁴.

The synthesis of nanogels by emulsion methods is currently an area of considerable interest⁵. The emulsion technique promises to be one of the versatile preparation methods, which enables to control the particle properties such as mechanisms of particle size control, geometry, morphology, homogeneity and surface area. Emulsions are isotropic, macroscopically homogeneous and

thermodynamically stable solutions containing at least three components: a polar phase (usually water), a non-polar phase (usually oil) and a surfactant. On a molecular level, the surfactant molecules form an interfacial film separating the polar and the non-polar domains, where water droplets are dispersed in a continuous oil phase, i.e. water in oil (W/O) emulsion. Indeed, W/O emulsions, which are also called as reverse emulsions, can be used as nanoreactors for the synthesis of nanoparticles with low polydispersity^{6,7}. Especially, nanoemulsions ($d < 100$ nm) are particularly suitable in low to high viscosity products where high optical clarity, high physical stability and rapid release are required⁵. Figure VII.1 shows a graphical depiction of the formation of a reverse micelle by nanoemulsion.

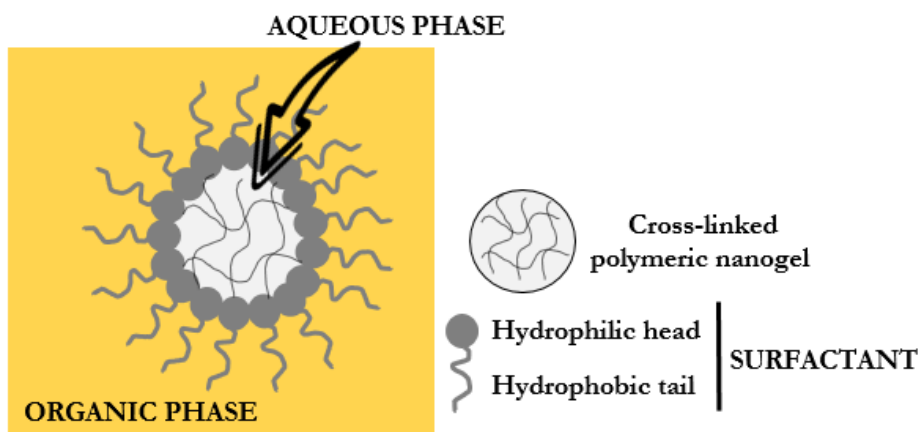


Figure VII.1. Schematic representation of a nanoemulsion where a reverse micelle is formed.

In accordance with the general purpose of this thesis focused on applying specific click reactions as a powerful tool for developing novel biomaterials, the greatest contribution of this chemistry in nanogels relies on the surface-functionalization of the nanogels with different purposes. One of the research areas where the use of functionalized nanogels is of great interest is that focused on targeted drug

administration for cancer therapies. Namely, since some specific antigens or receptors are overexpressed on the membranes of cancer cells, the selectivity to tumor tissues of the nanoparticles can be improved by coupling with specific targeting agents. Among them, folic acid derivatives have demonstrated high specificity for tumor cells and are currently promising in the vectorization of anti-cancer systems, since its receptors have been identified as tumor markers^{8,9}. Therefore, folic acid derivatives has been extensively employed as a targeting moiety for various anti-cancer drugs through covalent conjugation with liposomes, radio imaging agents, gene transfer vectors and microgels, which have shown to be efficiently internalized within tumor cells via folate receptor-mediated endocytosis¹⁰. For that reason, folate was used to functionalize the synthesized nanogels on its surface via thiol-Michael addition. Namely, commercially available maleimide and folate heterofunctionalized polyethyleneglycol (PEG) derivative was reacted with the vacant thiol groups on the surface of the previously modified nanogels.

As it has been reported throughout this thesis, one of the main drawbacks of the chitosan is that it is only water-soluble at acid pHs, which could limit in some cases its biomedical applications. In order to overcome this drawback and achieve well-dispersed chitosan-based nanogels in water, thiolated chitosan (CsSH) was employed as precursor, which has been confirmed to be soluble in neutral aqueous solution in Chapter III and V. Namely, aqueous solutions of the starting materials are indispensable for the implementation of reverse emulsion method. On the other hand, in this case, low molecular weight chitosan was used for the formation of the nanogels based on the synthesis requirements. Indeed, it is considered that the increased solubility of the low M_w chitosan may aid in the colloidal stability of nanoparticles in solution¹¹.

Thereby, the possibility to modify chitosan provides the opportunity to create novel cross-linked nanogels, with a high versatility of their architecture that

allows stimuli-responsive behaviour and the accommodation of several molecules¹². Moreover, the presence of covalent cross-linked points in nanogels enable the stability of these type of soft networks. Commonly, chitosan nanogels have been synthesized through amide coupling reaction with a wide range of bifunctional agents¹³. Nevertheless, it has been reported that some of these cross-linkers could display certain toxicity obstructing the final purpose of their existence. Bearing this in mind, biocompatible and non-toxic poly(ethylene glycol)bis(carboxymethyl)ether (PEGBCOOH) was used for the cross-linking and formation of chitosan nanoparticles via W/O reverse nanoemulsion method in this chapter. As reported by several authors, PEG is one of the most popular polymers used to covalently cross-link chitosan chains in order to form 3D networks^{14–16}. It shows exceptional physicochemical and biological properties, such as high solubility in water, biocompatibility and ease for chemical modification¹⁷.

Furthermore, the mucoadhesive nature of chitosan is a valuable property, which makes it a great candidate for the controlled release in oral delivery¹⁸. As expressed in Chapter III, mucoadhesion is defined as the ability of materials to adhere to the soft mucosal surface that lines the gastrointestinal, tracheobronchial, reproductive and ocular systems, varying the thickness of the mucus layer depending on the area¹⁹. The mucus layer is primarily composed of the mucin glycoprotein, water, inorganic salts and lipids. Specifically, the natural mucoadhesion of chitosan is achieved by a strong electrostatic adhesion force between the positively charged chitosan molecules and negatively charged mucosal surface¹⁹, enabling the development of carriers for transmucosal drug delivery that achieve a localized and prolonged effect of active ingredients ($\sim 12\text{--}24\text{ h}$)²⁰. In addition, thiolation or addition of thiol carrying moiety to chitosan greatly improve its mucoadhesion by creating a strong interaction between the thiol group on the chitosan surface and the cysteine rich region of the mucus glycoprotein (disulphide bond)²¹ as pioneered by Bernkop-

Schnurch et al. by modifying different polysaccharides after grafting thiol groups with encouraging outcomes^{22–25}. These covalent bonds are much stronger than the original mucoadhesive interaction between the positively charged chitosan and negatively charged mucin as it was corroborated after turbidimetric assays in Chapter III.

Thus, thiolated nanogels with uniform particle size distribution were obtained in this chapter. The morphology and topography of the nanogels were studied by TEM and AFM, respectively. Besides, the dispersion of the nanogels in aqueous solution and their pH-sensitive swelling along with the interaction with mucin proteins of mucosa were improved by the presence of thiol groups, highlighting this novel incorporation even more. The nanogels were further labelled with folate as an example of simple and easy functionalization pathway via Michael-addition (MA) reaction for future studies of tumor targeting efficiency.

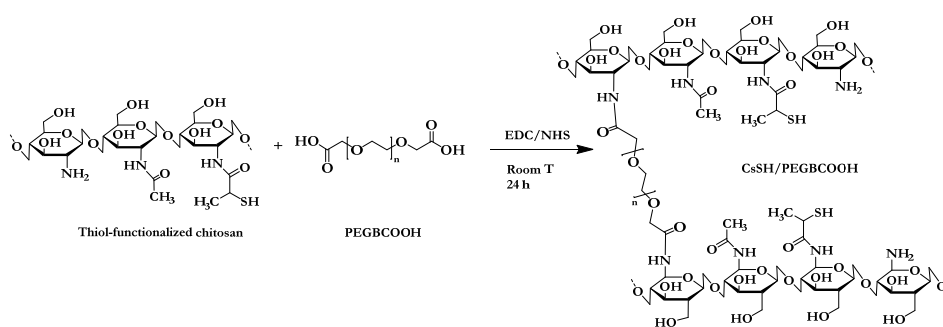
VII.2. THIOLATED CHITOSAN-BASED NANOGELS FORMATION (CsSH/PEGBCOOH)

VII.2.1. Experimental part

Thiol-functionalized chitosan (CsSH) nanogels were cross-linked with PEGBCOOH following a previously reported method based on reverse W/O emulsion^{17,26}, where chitosan/cross-linker equivalent ratio was fixed to 1:1 (Scheme VII.1). The degree of substitution of the CsSH used for the nanogels synthesis via ninhydrin assay (Equation II.7) was calculated to be 11 %.

The cross-linked nanoparticles were obtained by mixing separately prepared thiolated chitosan and cross-linking agent emulsions. Firstly, a solution of 0.01 g mL⁻¹ of thiolated chitosan in 1% v/v aqueous acetic acid solution was prepared. Cyclohexane (organic phase), 2-hexanol (co-surfactant) and chitosan solution were mixed in a fixed ratio of 5.5:2:2 (v/v) at room temperature. The thiolated chitosan emulsion was formed by adding Triton X-100 (surfactant) drop by drop

into the mixture under vigorous stirring until the mixture became transparent and left for 1 hour. The W/O emulsion of the cross-linker was prepared following the same procedure but prior to it, the carboxylic acid groups were activated by reaction with EDC and NHS following the synthetic pathway represented in Scheme III.1 (Chapter III). In order to ensure the efficient activation, 242 μL of PEGBCOOH and 220 mg of NHS were first mixed in 20 mL of water for 15 minutes. The pH of the mixture was adjusted to 5.4 by the addition of 1 M NaOH solution. Afterwards, 750 mg of EDC were gradually added and the mixture was stirred at room temperature during 4 hours. The ratio between COOH, NHS and EDC was 1:4:10 (v/v).



Scheme VII.1. Nanogels formation through the cross-linking reaction between CsSH and PEGBCOOH.

The cross-linking reaction took place during 24 hours at room temperature after the addition of the cross-linker nanoemulsion into the thiolated chitosan nanoemulsion (Figure VII.2). The nanoparticles were isolated by precipitation in ethanol. After decantation, the nanogels were washed by dispersion in ethanol followed by centrifugation for successive cycles (6500 rpm, 15 °C and 20 minutes per cycle). This step was repeated four times and the obtained nanogels were then dispersed in 1 % v/v aqueous acetic acid solution. The samples were dialyzed in tubings of cellulose membranes (molecular weight cut-off of 3.5 kDa) alternating between aqueous acetic acid solution and water by purification for 15 days. Finally,

the nanoparticles were lyophilized (30 % w/w yield) and stored at 4 °C in dark until needed for further use.

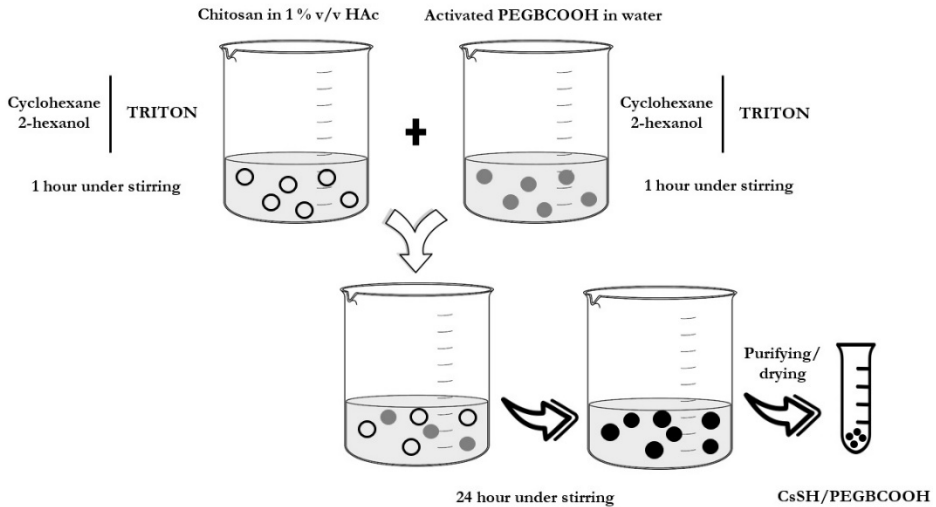


Figure VII.2. Schematic representation of the experimental procedure for obtaining CsSH/PEGBCOOH nanogels.

VII.2.2. Results and discussion

Nanometric gel particles were successfully synthesized through covalent cross-linking between the remaining free amines of the chitosan after the thiolation and the carboxylic acid groups of the cross-linker. Thus, the amidation reaction led to the formation of stable nanosized networks which were positively or negatively charged depending on the pH of the medium due to the presence of both amines and thiols. Not being the number of charged groups of both natures very high given the purpose of amines for reacting, this behaviour was markedly observed during the characterization of the nanogels, concluding the high impact that could suppose this nanoparticles, which have not been studied before.

VII.2.2.1. Physico-chemical characterization

The success of the cross-linking reaction was confirmed and quantitatively evaluated by ^1H NMR spectroscopy. Figure VII.3 displays the spectra of thiolated chitosan and CsSH/PEGBCOOH nanogels. As has been repeatedly shown in Chapter III, the spectrum for pure chitosan shows a peak at 1.90 ppm corresponding to the three protons of *N*-acetyl glucosamine (GlcNAc) and a peak at 3.0 ppm related with the proton of the C₂ (H₂) of glucosamine residues (GlcN), which represent the primary amino group content of the chitosan^{27,28}. The same signals appeared in the corresponding spectra of thiolated chitosan and CsSH/PEGBCOOH nanogels. However, the signal corresponding to the presence of the carbonated polymeric chain of the diacid (PEGBCOOH) in the nanogels could be appreciated by the new prominent signal at 3.6 ppm. Moreover, a clear decrease of the signal at 3.0 ppm was observed for the CsSH/PEGBCOOH sample, indicating the loss of amine groups by the reaction with the PEG-based diacid in order to develop the cross-linked nanogels as detailed below. Consequently, the formation of nanoparticles was successfully carried out.

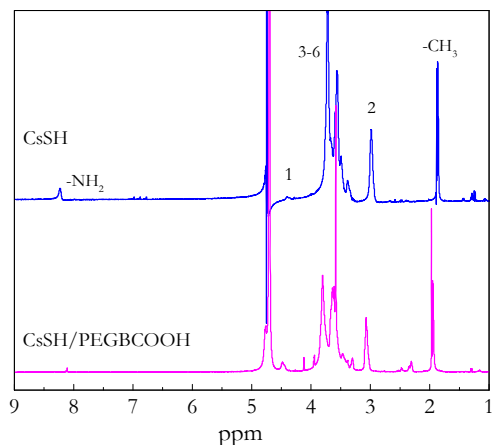


Figure VII.3. Liquid-state ^1H NMR spectra of thiolated chitosan and CsSH/PEGBCOOH nanogels.

Since the cross-linking involves the formation of new amide groups, the protons of C_2 were displaced to lower positions. Therefore, the cross-linking degree was determined by quantifying the protons that were not shifted. Briefly, the peak of the ^1H NMR spectra corresponding to the methyl protons at 1.90 ppm (A_{CH_3}) was used as reference for the quantitative determination of the composition of the nanogels, by means of the integration of the resonance of the proton of the C_2 (A_{H_2}) at 3.0 ppm following the procedure reported by Arteché Pujana et al. in several works^{8,13,17,26}. Firstly, the modification degree of the cross-linking reaction was evaluated by the decrease of the glucosamine signal (3.0 ppm), followed by the calculation of the overall degree of cross-linking, assuming that no intramolecular cross-linkings were formed (cross-linking degree = (modification degree) $_{\text{CsSH}}$ – (modification degree) $_{\text{CsSH/PEGBCOOH}}/2$, as it was assumed that the reaction occurred on both reaction sites of the diacid cross-linker molecule). Thus, the modification degree (MD) for the thiolated chitosan (CsSH) and the nanogels (CsSH/PEGBCOOH) was calculated the same way by comparing the

new signal ratio of the nanogels spectrum (Equation VII.1)²⁹ and were found to be 79 and 74 %, respectively.

$$\text{MD (\%)} = \left[1 - \frac{\frac{1}{3} A_{\text{CH}_3}}{\frac{1}{3} A_{\text{CH}_3} + A_{\text{H}_2}} \right] \cdot 100 \quad (\text{VII.1})$$

For the formation of thiolated chitosan-based nanogels, which involved the cross-linking by amide coupling reaction, the degree of cross-linking was estimated to be 3 %. Although it may be considered a humble value in comparison with the results obtained by Arteché Pujana et al.^{8,13,26}, the cross-linking reaction widely demonstrated that allowed the generation of stable and well-formed nanogels with novel properties as it is shown below.

VII.2.2.2. Thermal behaviour

The thermal behaviour of CsSH/PEGBOOH nanogels could be evaluated by TGA experiments as described in Chapter II. The corresponding thermograms for neat and thiolated chitosan were previously analysed in Chapter III (Section III.4), whereas the thermal behaviour for CsSH/PEGBOOH nanogels is shown in Figure VII.4. Following the same trend as its precursors, when exposing the material to high temperatures, the thermal degradation was observed to be the principal process. In Figure III.12 the incorporation of thiol groups was observed to reduce the decomposition temperature of the biopolymer, while in the thermogram of the nanogels shown in Figure VII.4, a gradual degradation that started long before was observed. The cross-linking by the PEG-based diacid was noticeable by the shift on the thermogram of the nanogels, where the stability of the final materials in terms of thermal behaviour was enhanced. While a new peak appeared at 147 °C, the main degradation of the biopolymer was displaced to 295 °C and took place in two-stages just as the modified sample, represented by the small shoulder in

the dTGA curve. Furthermore, the content of water was significantly higher in the case of the nanogel samples, being represented by the peak at 56 °C.

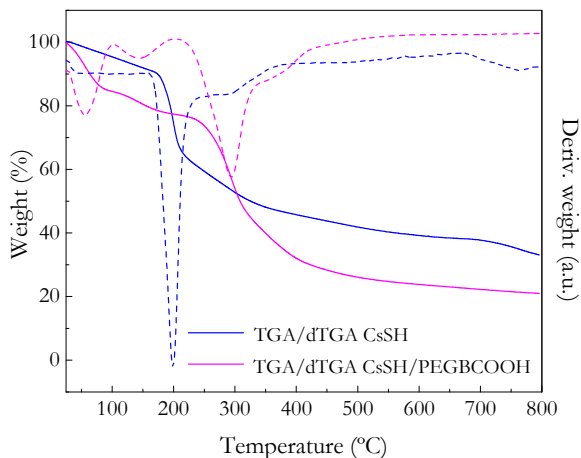


Figure VII.4. TGA (left axis, solid line) and dTGA (right axis, dash line) curves of CsSH and CsSH/PEGBCOOH nanogels under inert atmosphere.

VII.2.2.3. pH–responsive swelling properties

The particle size and zeta potential of the swollen nanogels was determined after the progressive dilution of the nanoparticle dispersions, which has been reported as an effective way to reduce the inter–particle interaction and the presence of large aggregates of chitosan³⁰, following the method reported in Chapter II.

The swelling behaviour of thiolated chitosan nanogels was studied by dynamic light scattering (DLS) as a function of the external pH. Figure VII.5 shows the hydrodynamic mean diameter (D_H) and the evolution of the zeta potential (ζ –potential) of CsSH/PEGBCOOH nanogels measured at different pHs. Chitosan cross–linked nanogels showed a pH–responsive volume transition, where the average size increased both at acid and basic pH being consistent with the pKa

value of linear chitosan chains¹⁷ since tended to show a minimum in that pH range. It should be noted that the developed nanoparticles possessed free primary amines and thiol pending groups, both sensitive to the surrounding pH changes. In fact, the primary amines will be protonated in acid media and thus, the hydrodynamic diameter increased because of the repulsive interactions³¹. At the same time, the presence of negatively charged ions at higher pH values due to the deprotonation of the thiol group was also noticeable, where the hydrodynamic diameter of the nanogels again increased. Supporting this approach, Figure VII.6 shows a schematic representation of the behaviour that the as-prepared nanogels would follow when varying the pH of the medium. Therefore, depending on the surrounding environment, the nature of the charged groups located on the surface that would determine the swelling of the nanogels would vary. In general, when referring to pH-responsive hydrogels, the final materials are supposed to swell mostly at some pH levels rather than others, depending on the nature of the starting polymer. Nevertheless, the dual response to pH achieved by the present system included extreme pHs, covering the whole pH range.

All those findings were opposite to the results observed by other authors when studying the pH-response of cross-linked chitosan nanogels, where a decreased in the hydrodynamic diameter was observed as the pH rised^{17,26}. Moreover, the potential of this system was not only evident by the presence of thiol groups and the distinctive pH-responsive behaviour, but also because of the large volume of solvent absorbed by the nanogels. Therefore, it could be concluded that the synthesized nanogels displayed a strong swelling capacity which could be also related with the hydrophilic nature of the employed cross-linker, in contrast with other authors which did not observe the expected pH-responsive swelling behaviour due to the limitations caused by the cross-linking³² and the hydrophobic nature of the cross-linker^{8,17} or the reaction conditions themselves³³.

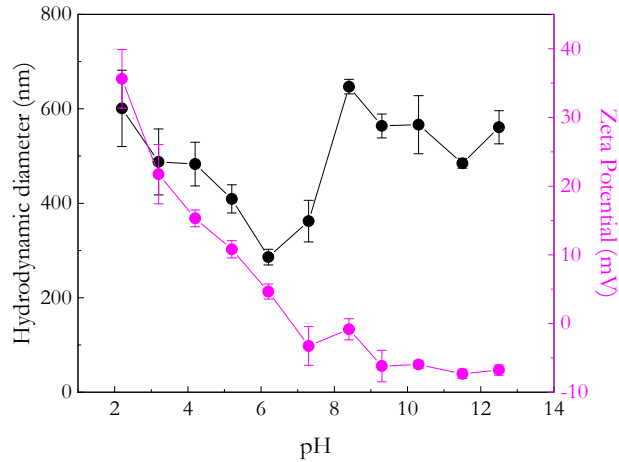


Figure VII.5. Average hydrodynamic diameter and zeta potential of CsSH/PEGBCOOH nanogels as a function of external pH.

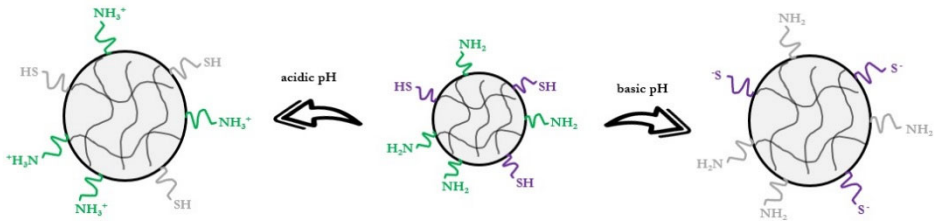


Figure VII.6. Schematic representation of the variation of the superficial charges of thiolated chitosan nanoparticles depending on the pH.

On the other hand, results obtained from the study of the electrophoretic mobility of the nanogels displayed both positive and negative values of ζ -potential depending on the surrounding environment conditions. Indeed, the most important factor that affects the measurement of the particles ζ -potential is pH. A ζ -potential value on its own without a quoted pH is a virtually meaningless number³². Namely, by measuring the electrokinetic potential of the nanogels, it was confirmed the progressive protonation of amino groups when the pH decreases and the presence of anionic groups in the nanogels at higher pH values, decreasing the ζ -potential

value from $+36 \pm 4$ to -7 ± 1 mV in the range of pH from 2 to 12. An inflexion point could be appreciated at pH around 6.5 (pKa value of chitosan), since at this pH the transition between positive and negative values of ζ -potential occurred. The decrease of the ζ -potential before that value was observed to be more pronounced, whereas after this point, the drop was less sharp, reaching a plateau from pH 9 onwards. Therefore, the cationic nature of the biopolymer prevailed, given place to a reasonable behaviour despite the chemical modifications conducted on chitosan. Although the ζ -potential measurements characterizes the surface charge of the particles, it could be assumed that the charged groups inside the nanogel behave in a similar way to the surface ones¹⁷.

The positive value of ζ -potential is clearly related to the presence of chitosan in the nanoparticles and the free amino groups of the polysaccharide^{34,35}. Nevertheless, different approaches have been made in the last decade concerning the ζ -potential value of chitosan-based nanoparticles. Namely, Bravo-Osuna et al. observed a decrease in the positive charges onto chitosan particles in the presence of superficially localized thiol groups when increasing the pH, especially at pH higher than the chitosan pKa value (around 6.5), which was influenced by the emulsion polymerization technique but never reached negative ζ -potential values³². On the other hand, Arteché Pujana et al. carried out several studies where they observed a similar ζ -potential tendency to the one in Figure VII.5 for chitosan nanogels cross-linked with a dicarboxylic acid linker, even without the presence of other negatively charged molecules than the $-\text{COO}^-$ of the acid that could remain unreacted, but did not notice an increase in the size of the nanogels at high pH values^{17,26}.

These data supported the theory that the synthesized nanogels swell both at low and high pH values due to the presence of cationic ($-\text{NH}_3^+$) and anionic groups (S^-) that create repulsive interactions in the whole measurement range, not being all necessarily in the surface. Results extracted from Figure VII.5 are summarized

in Table VII.1. Additionally, the polydispersity index (Pdl) was observed to be < 0.50 for the entire pH measuring range, which indicated that adequate monodisperse nanoemulsions were obtained³⁶.

Table VII.1. Hydrodynamic mean diameter (D_H), polydispersity index (Pdl) and ζ -potential for CsSH/PEGBCOOH nanogels as a function of pH.

pH	D_H (nm)	Pdl	ζ -potential (mV)
2	601 ± 81	0.51 ± 0.15	+36 ± 4
3	488 ± 70	0.54 ± 0.17	+22 ± 4
4	483 ± 46	0.52 ± 0.15	+15 ± 1
5	409 ± 30	0.55 ± 0.12	+11 ± 1
6	286 ± 17	0.49 ± 0.10	+5 ± 1
7	362 ± 44	0.46 ± 0.12	-3 ± 3
8	647 ± 15	0.34 ± 0.04	-1 ± 2
9	564 ± 25	0.44 ± 0.04	-6 ± 2
10	566 ± 61	0.37 ± 0.17	-6 ± 1
11	485 ± 10	0.32 ± 0.04	-7 ± 1
12	561 ± 35	0.27 ± 0.03	-7 ± 1

VII.2.2.4. Size and morphological analysis

TEM technique allowed the isolation and observation of very well individualized particles. TEM micrograph (Figure VII.7A) showed that spherical particles were obtained in the nano-size range, where nanogels seemed to be non-agglomerated and highly monodispersed. Figure VII.7B confirmed that the size distribution of CsSH/PEGBCOOH nanogels ranged from 5 to 12 nm, in that, more than 60 % of the nanogels were between 6.5–7.5 nm in size. Therefore, the cross-linking technique used for the formation of the nanogels allowed obtaining chitosan particles with small size, in great agreement with different studies based on reverse emulsion method for the cross-linking of chitosan nanogels, where diameter sizes ranged from 3 to 20 nm¹³, 11 to 15 nm¹⁷ or 4 to 15 nm³¹ guided by TEM images.

Besides, as observed before by many other authors when analysing chitosan particles, smaller particle diameters were obtained by TEM or AFM techniques, while these methods are based on the dry state of the materials, DLS shows the hydrodynamic particle diameter^{32,37,38}. In agreement with the definition of hydrogels which states that gel type materials are mainly constituted by water and content high percentages of liquid, the synthesized nanoparticles showed a mean hydrodynamic diameter 50 times higher than the observed by TEM/AFM for the dried samples.

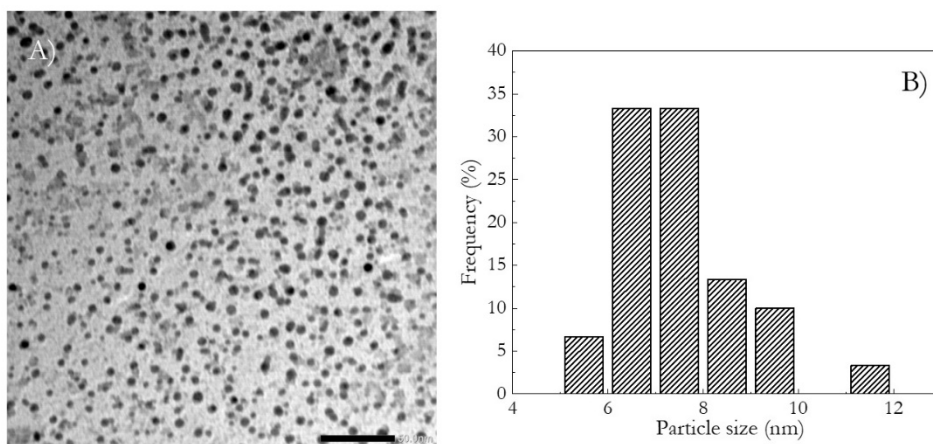


Figure VII.7. A) TEM micrograph and B) particle size distribution of CsSH/PEGBCOOH nanogels.

The AFM technique allowed to examine the surface morphology and the size of the synthesized nanoparticles. The obtained height images are presented in Figures VII.8A and VII.8B. As it could be observed quite elliptic shaped nanoparticles were detected probably due to the haul of the tip and the operating tapping mode that provoked slightly the elongation and orientation of the nanoparticles in the same direction (vertical), partially distorting the real image in this plane. However, the average diameter of the nanogels (horizontal) (Figure

VII.7C) was in good agreement with the sizes obtained previously by TEM (Figure VII.7B), where more than 50 % of the nanogels were 12.5 nm in size.

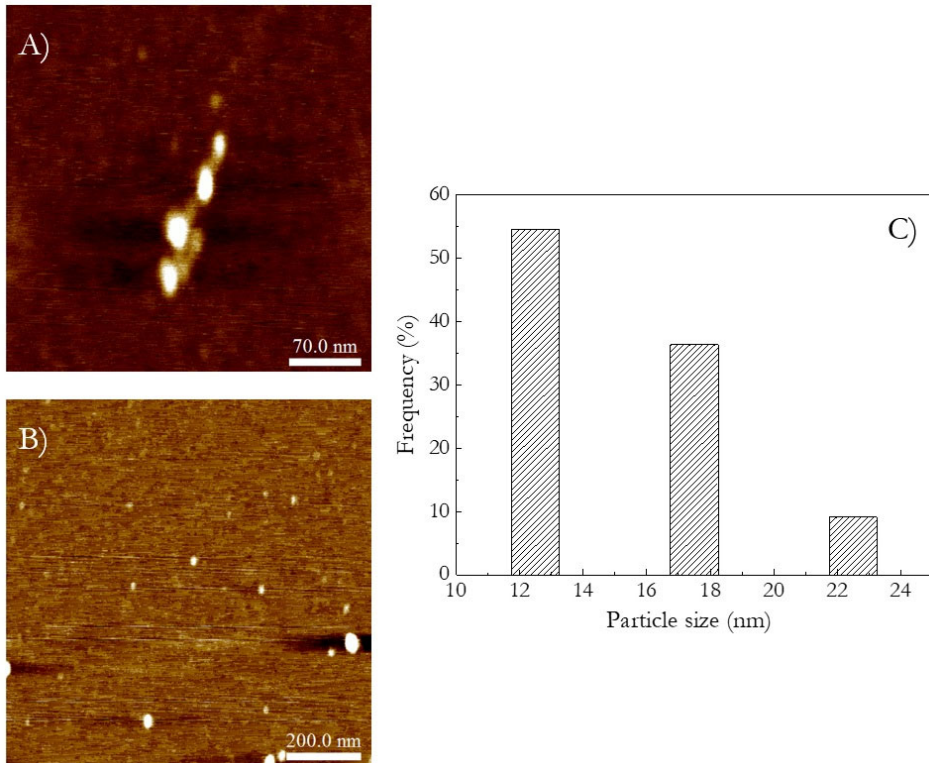


Figure VII.8. Height topographic AFM images at different scan area (A and B) and C) particle size distribution of CsSH/PEGBCOOH nanogels.

VII.2.2.5. Mucoadhesion property

The body protects its cavities from the external environment by utilizing the goblet cells of the mucosal tissues, which cover all body cavities and secrete mucus onto the epithelial surfaces. Mucins, the main component of mucus, are responsible for the adhesion phenomena and are known as soluble, heterogeneous, have a high molecular weight and are cysteine rich glycoproteins^{39,40}. Furthermore,

mucoadhesion is a condition where macromolecules of different nature adhere to these mucosal surfaces in the body (buccal, intestinal, vaginal, rectal, etc.)⁴⁰.

In order to assess the mucoadhesion capacity of the developed nanoparticles, the influence of the pH and the concentration of mucin was studied for different polymer/mucin mixtures after 1, 2, and 5 h of interaction under magnetic stirring at room temperature. In the same way as in Chapter III for chitosan and its thiolated derivative and following the methodology described in Chapter II, thiol-functionalized chitosan samples were compared with the resulting thiolated nanogels. The polymeric samples concentration was kept constant (0.25 mg mL^{-1}) in all the cases while the mucin concentration was varied (0.25 , 0.50 , 1.25 and 1.50 mg mL^{-1}) both in water (pH 6) and acid aqueous environment (0.5% v/v HAc, pH 3). The response derived from the interaction between the polymeric samples and the mucin in both media was obtained by applying the Equation II.17 and II.18 and is represented in Figure VII.9 and VII.10.

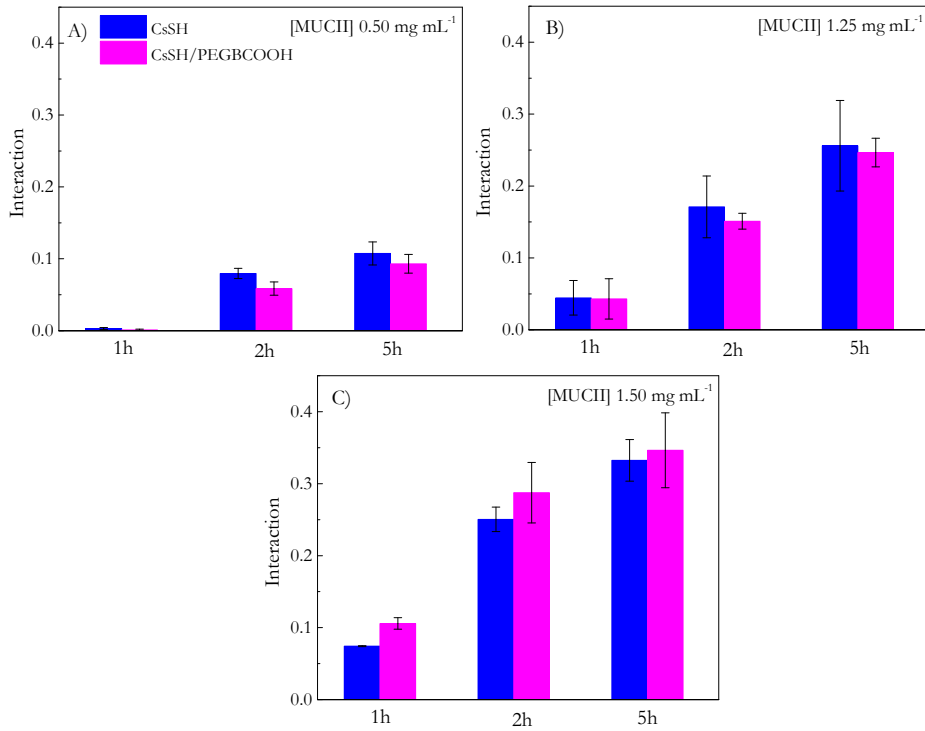


Figure VII.9. Influence of mucin concentration on CsSH and CsSH/PEGBCOOH nanogels as a function of interaction time for: A) 0.50, B) 1.25 and C) 1.50 mg mL⁻¹ mucin concentrations at pH 3.

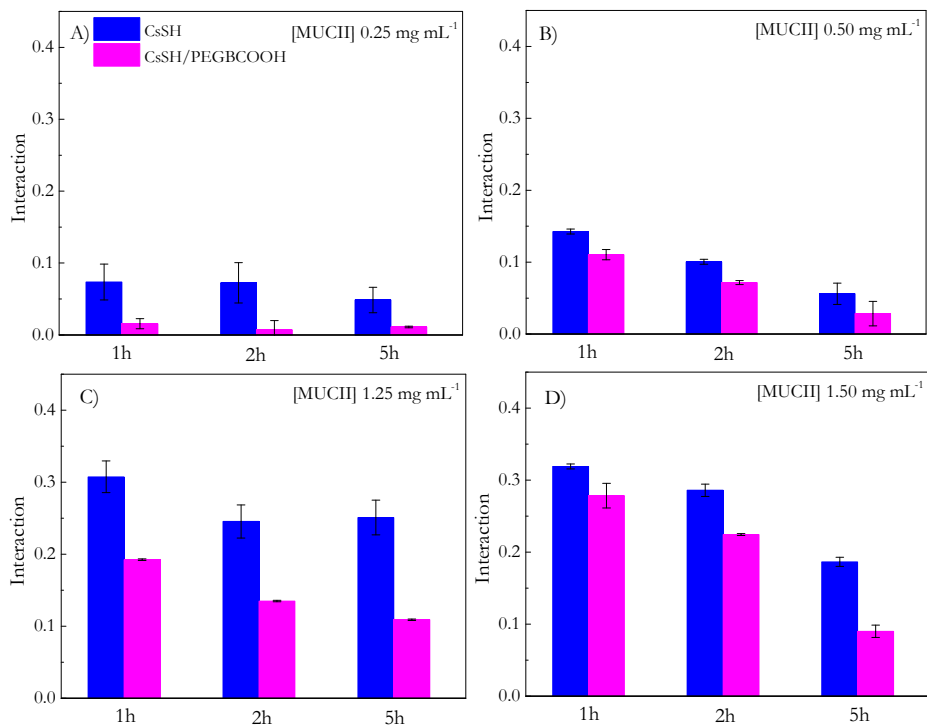


Figure VII.10. Influence of mucin concentration on CsSH and CsSH/PEGBCOOH nanogels as a function of interaction time for: A) 0.25, B) 0.50, C) 1.25 and D) 1.50 mg mL⁻¹ mucin concentrations at pH 6.

In view of the results, the polymer/mucin interactions greatly depend on the mucin concentration and the interaction time. Moreover, the nature and conformation of the polymers in study were also highly significant in order to achieve spotlighted values of mucoadhesion. First, as the concentration of mucin increases, both in acid and neutral medium, the interactions between the mucus layer and the chitosan-based materials increased (in a greater extent under acid environment) independently to conformation of the materials. Indeed, higher concentrations favoured bioadhesion because higher number of molecules can interpenetrate and more functional groups are available to develop electrostatic or chemical bonds⁴¹. Moreover, as in Chapter III, no adhesion was detected for none of the materials in

stomachal conditions (pH 3) for 0.25 mg mL^{-1} mucin concentration, which indicated that this concentration was not enough for the creation of detectable interactions under these conditions.

Mucoadhesion results varied with the contact time depending on the pH of the medium. At neutral pH, the interactions remained equal or lost force as the time went by. On the contrary, time acted in favour under acid conditions, where all samples showed improved interactions with all concentrations of mucin as the contact time increased. This trend could be explained by the decrease in the thiol group content as a function of time at pH 6, which was previously studied by Kast and Bernkop-Schnürch⁴². Indeed, they observed that thiols were susceptible to oxidation and turned to negative thiolate anions (S^-) at this pH values, being this tendency even more pronounced as the contact time increased. Thus, the probability of forming intramolecular disulphide bonds within the nanogels could increase in the present case, decreasing the amount of connections with the mucus layer.

As reported in literature, the mucoadhesion increases with the degree of deacetylation and decreases with an increase in the cross-linking⁴³. Therefore, in accordance with this statement, when cross-linking the thiolated chitosan to develop CsSH/PEGBCOOH nanogels, the mucoadhesion was maintained slightly below the levels presented by the thiolated chitosan. This effect could be explained by the reduction of available reactive groups once the nanogels are formed, namely i) the number of amines in the chitosan main chain, which created the electrostatic bonds with the mucus layer, decreased due to cross-linking reaction with the cross-linker and ii) the amount of thiol groups grafted into the chitosan main chain, which were not implicated in the cross-linking remaining free and were responsible for the formation of covalent disulphide bonds, may not be so accessible due to the new conformation of the material. Nevertheless, the mucoadhesion values for the CsSH/PEGBCOOH nanogels at pH 3 (Figure VII.9) were similar to the ones obtained for CsSH for all the mucin concentrations.

In general, the final CsSH/PEGBCOOH nanogels displayed a significant mucoadhesive behaviour in either medium, being highly influenced by the contact time with the mucus layer. Indeed, similar interaction values were obtained for 1.50 mg mL⁻¹ mucin concentration after 5 h of contact time in pH 3 (Figure VII.9C) and after 1 h of contact time in pH 6 (Figure VII.10D), revealing the great potential of the CsSH/PEGBCOOH nanogels which showed a dual behaviour given their charged nature. This behaviour could be explained by the *in situ* disulphide exchange reaction between the cysteine rich domains of the mucus layer and the thiolate anions of the nanogels at pH 6 or the progressive creation of electrostatic linkages with the amines at pH 3, which are less stable and could need more time to generate similar strong bonds.

Therefore, the additional mucoadhesive property presented by the synthesized nanogels could promote the use of these nanodevices as drug delivery systems. Namely, the nanogels could extend the retention period of the dosage form at the absorption site, enhancing absorption and consequently, the therapeutic effectiveness of the drug both in stomach and intestine environment.

VII.2.2.6. Assessment as potential nanocarriers for targeted drug delivery by click chemistry

Folate ligand was clicked into chitosan nanogels by *in situ* functionalization procedure by means of thiol/maleimide reaction (Figure VII.11). Therefore, instead of the traditionally employed direct amide link between folic acid and chitosan, a modified folate compound containing maleimide (each at one end of a PEG spacer) was employed in order to provide the linkage of this ligand to the thiol molecules grafted to the chitosan backbone and presumably located in the surface of the nanogels that also could be found inside the particles. Figure VII.11 represents the CsSH/PEGBCOOH nanogels after applying the thiol–Michael addition reaction for folate insertion.

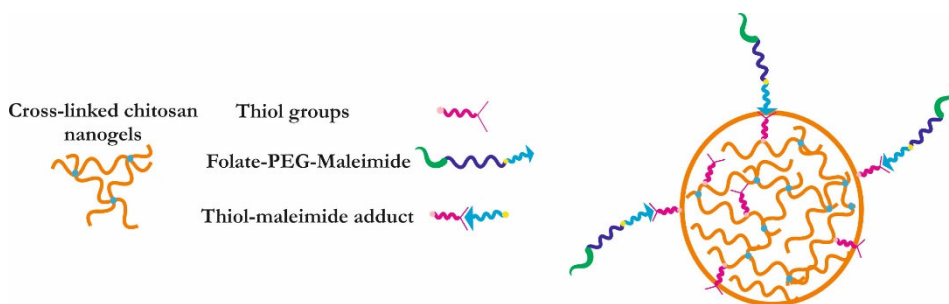


Figure VII.11. Schematic representation of the chitosan nanoparticles after the folate receptor incorporation.

VII.2.2.6.1. Experimental part

In situ functionalization of the thiolated nanogels was carried out by mixing 300 μL of a dispersion of CsSH/PEGBCOOH nanogels in 2 % v/v aqueous acetic acid solution (0.002 g mL^{-1}) to a final volume of 0.9 mL of PBS solution containing Folate-PEG-Mal ($3.5 \cdot 10^{-4} \text{ g mL}^{-1}$) in an equivalent ratio of 2:1 thiol-to-maleimide. The reaction was carried out at $37 \text{ }^\circ\text{C}$ under continuous magnetic stirring for 24 h. Finally, a clear yellowish nanodispersion was obtained as a result of the addition of folate moieties.

VII.2.2.6.2. Results and discussion

The MA reaction between the maleimide containing folate derivative and the thiolated nanoparticles was followed by UV-vis spectroscopy as the reaction proceeded and the adduct was formed due to the progressive disappearance of the absorbance signal associated to the maleimide moiety. The reaction was monitored for 24 h after placing aliquots in a 1 mL quartz cuvette inside the spectrophotometer at specific time intervals as described in Chapter II.

During the reaction, the loss of conjugation between the two carbonyl groups and the double bond of the maleimide ring took place due to the formation of the MA adduct when reacting with the thiol group as described in Chapter V (Scheme

V.1). Therefore, the folate receptor coupling to the nanogels could be monitored by the progressive decrease in the intensity of the absorption signal (Figure VII.12). Thus, in a very equal way that in the cases reported in Chapter IV for the DA cross-linking reaction, as the reaction proceeded, the absorption band associated to the maleimide groups near 278 nm decreased. Besides, the folate moiety also presented a maximum absorption peak close to this wavelength⁴⁴. The particular profile of the folate conjugates was clearly observed for the as-prepared derivatives characterized by a principal signal with various shoulders²⁶, which could also be influenced by the presence of maleimide groups in this case. Given the possibility that part of the thiol groups could be found inside the nanogels making the access somehow more complicated, the reaction took place during 24 h and the thiol groups were found in excess. Considering these particular conditions, the absorption signal did not disappear completely, which did not have to mean that maleimide remain without attaching, since the signal corresponding to the folate moiety will always remain visible.

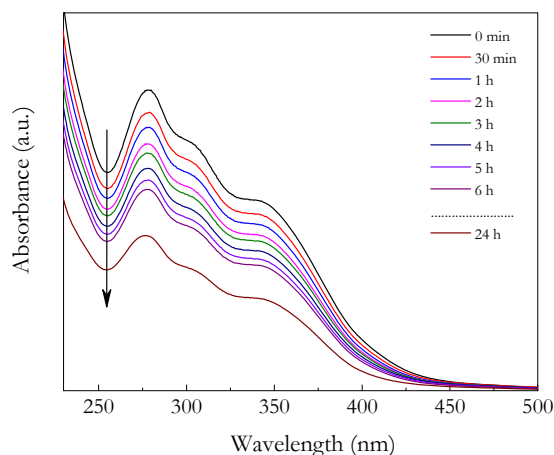


Figure VII.12. UV-vis spectra following the MA reaction between CsSH/PEGBCOOH nanogels and Folate-PEG-Mal in PBS.

FTIR was employed as an efficient technique to determine the incorporation of folate moieties into the nanogels (Figure VII.13). As shown in the spectrum of CsSH/PEGBCOOH, the structure of the chitosan main chain could be clearly identified as the principal compound in the nanogels CsSH/PEGBCOOH, where the distinctive bands for neat and thiolated chitosan were identified in Chapter III (Section III.4). On the other hand, in the Folate–CsSH/PEGBCOOH nanogels spectrum the characteristic bands related to both chitosan and Folate–PEG–Mal were displayed, which confirmed the successful immobilization of the new compound into the chitosan nanocarriers. Indeed, the folate containing compound was evidenced by the presence of several new bands which were characteristic of the Folate–PEG–Mal (Figure VII.13A) at 856 and 660 cm^{-1} ⁴⁵. Moreover, the addition of new C–H and C=O groups into the final nanomaterials was also relevant. Namely, the bands at 2936 and 2851 cm^{-1} and the one corresponding to the amide I band at 1648 cm^{-1} were affected by the incorporation of Folate–PEG–Mal⁴⁵, resulting in more intense and pronounced bands.

The resulting data evidenced that as-prepared nanoparticles still had the potential to undergo further modifications, as demonstrated by the functionalization with folate containing ligand. Therefore, the prepared folate–nanogels enhance the potential use of the prepared particles as biomaterial nanodevices for antitumor targeted drug delivery.

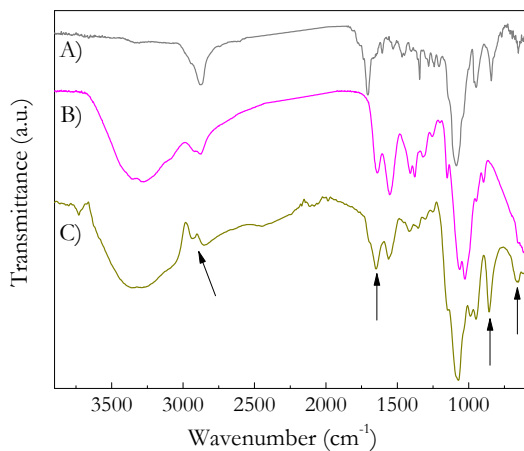


Figure VII.13. FTIR spectra of A) Folate-PEG-Mal, B) thiolated chitosan nanogels (CsSH/PEGBCOOH) and C) folate containing thiolated chitosan nanogels (Folate-CsSH/PEGBCOOH).

VII.3. CONCLUSIONS

In this chapter, novel chitosan-based nanogels were synthesized by applying a commonly employed synthetic strategy. Indeed, nanogels were obtained after the well-established reverse emulsion method based on cyclohexane/Triton X-100/n-hexane/water systems. Previously synthesized water-soluble thiolated chitosan (Chapter III) was cross-linked with a commercially available PEG-based diacid, involving the creation of materials at the nanometric scale. The cross-linking degree was assumed to be adequate to obtain well-dispersed and stable nanoparticles, whereas the thermal behaviour of the final materials was observed to be influenced by the formation of the nanogels.

Swelling results suggested that CsSH/PEGBCOOH nanogels were completely swollen in aqueous solutions due to their high liquid absorption ability over the entire pH range. The particle size of nanogels dispersion decreased from 601 to 286 nm by increasing the pH from 2 to 6, while increased from 362 nm to 561

nm by increasing the pH from 7 to 12. Therefore, the synthesized nanogels showed a pH-responsive swelling behaviour that corresponds to the pKa of the neat chitosan. Regarding the zeta potential values, the charge of the protonated network suffered a progressive decrease until pH 9, where it reached a plateau. The swelling capacity and surface charge were influenced in great extent by the functional groups grafted to the polymeric chains and the flexibility and the hydrophilic character of the cross-linker.

The use of reverse emulsion method allowed obtaining small size nanogels, which are better carriers for biologically active molecules than those of bigger size. AFM images of nanoparticles confirmed TEM observations, showing spherical shapes and similar average diameter size ranging from 5 to 23 nm when analysing dry samples.

For the purpose of using the synthesized nanogels as mucosal drug delivery nanocarriers, the importance of their mucoadhesive property was reported. Chitosan has an inherent mucoadhesive and permeation enhancer activity¹⁹, which was shown to increase after its thiolation. CsSH/PEGBCOOH nanogels maintained the mucoadhesion values presented by the thiolated chitosan, being significant both in acid and neutral pH, even if the contact time with the mucus layer played an important role. Namely, at 1.50 mg mL⁻¹ mucin concentration 5 hours were required to reach the highest values of interaction under stomachal conditions, while similar results were obtained after 1 hour at intestinal environment.

Finally, the synthesized nanoparticles were further functionalized in order to assess their applicability in the highly demanded targeted drug delivery field. Namely, chemical modification of the nanogels allowed the incorporation of targeting ligands for guided drug delivery, which would help to control the drug release in a specific site through external stimulus. Therefore, the prepared

chitosan nanogels were potential candidates for new cancer treatments, based on a targeted therapy.

REFERENCES

- (1) Li, J.; Mooney, D. J. Designing Hydrogels for Controlled Drug Delivery. *Nat. Rev. Mater.* **2016**, *1* (12), 1–38. <https://doi.org/10.1038/natrevmats.2016.71>.
- (2) Sanson, N.; Rieger, J. Synthesis of Nanogels/Microgels by Conventional and Controlled Radical Crosslinking Copolymerization. *Polym. Chem.* **2010**, *1* (7), 965–977. <https://doi.org/10.1039/c0py00010h>.
- (3) Norton, L. W.; Tegnell, E.; Toporek, S. S.; Reichert, W. M. In Vitro Characterization of Vascular Endothelial Growth Factor and Dexamethasone Releasing Hydrogels for Implantable Probe Coatings. *Biomaterials* **2005**, *26* (16), 3285–3297. <https://doi.org/10.1016/J.BIOMATERIALS.2004.07.069>.
- (4) Alexis, F.; Pridgen, E.; Molnar, L. K.; Farokhzad, O. C. Factors Affecting the Clearance and Biodistribution Of. *Mol. Pharm.* **2008**, *5* (4), 505–515.
- (5) Saberi, A. H.; Fang, Y.; McClements, D. J. Formation of Thermally Reversible Optically Transparent Emulsion-Based Delivery Systems Using Spontaneous Emulsification. *Soft Matter* **2015**, *11* (48), 9321–9329. <https://doi.org/10.1039/c5sm02221e>.
- (6) Destrée, C.; George, S.; Champagne, B.; Guillaume, M.; Ghijsen, J.; Nagy, J. B. J-Complexes of Retinol Formed within the Nanoparticles Prepared from Microemulsions. *Colloid Polym. Sci.* **2008**, *286* (1), 15–30. <https://doi.org/10.1007/s00396-007-1679-8>.
- (7) Ou, Z.; Yao, H.; Kimura, K. Preparation and Optical Properties of Organic Nanoparticles of Porphyrin without Self-Aggregation. *J. Photochem. Photobiol. A Chem.* **2007**, *189* (1), 7–14. <https://doi.org/10.1016/J.JPHOTOCHEM.2006.12.042>.
- (8) Pujana, M. A.; Pérez-Álvarez, L.; Iturbe, L. C. C.; Katime, I. Water Soluble Folate-Chitosan Nanogels Crosslinked by Genipin. *Carbohydr. Polym.* **2014**, *101* (1), 113–120. <https://doi.org/10.1016/j.carbpol.2013.09.014>.
- (9) Yu, L.; Zhou, L.; Ding, M.; Li, J.; Tan, H.; Fu, Q.; He, X. Synthesis and Characterization of Novel Biodegradable Folate Conjugated Polyurethanes. *J. Colloid Interface Sci.* **2011**, *358* (2), 376–383. <https://doi.org/10.1016/J.JCIS.2011.03.007>.
- (10) Blanco, M. D.; Guerrero, S.; Benito, M.; Teijón, C.; Olmo, R.; Muñiz, E.; Katime, I.; Teijón, J. M. Tamoxifen-Loaded Folate-Conjugate Poly[(p-Nitrophenyl Acrylate)-Co-(N- Isopropylacrylamide)] Sub-Microgel as

- Antitumoral Drug Delivery System. *J. Biomed. Mater. Res. - Part A* **2010**, *95* (4), 1028–1040. <https://doi.org/10.1002/jbm.a.32929>.
- (11) Wu, Y.; Yang, W.; Wang, C.; Hu, J.; Fu, S. Chitosan Nanoparticles as a Novel Delivery System for Ammonium Glycyrrhizinate. *Int. J. Pharm.* **2005**, *295* (1–2), 235–245. <https://doi.org/10.1016/J.IJPHARM.2005.01.042>.
- (12) Soni, K. S.; Desale, S. S.; Bronich, T. K. Nanogels: An Overview of Properties, Biomedical Applications and Obstacles to Clinical Translation. *J. Control. Release* **2016**, *240*, 109–126. <https://doi.org/10.1016/J.JCONREL.2015.11.009>.
- (13) Arteche Pujana, M.; Pérez-Álvarez, L.; Cesteros Iturbe, L. C.; Katime, I. Biodegradable Chitosan Nanogels Crosslinked with Genipin. *Carbohydr. Polym.* **2013**, *94* (2), 836–842. <https://doi.org/10.1016/j.carbpol.2013.01.082>.
- (14) Kulkarni, A. R.; Hukkeri, V. I.; Sung, H. W.; Liang, H. F. A Novel Method for the Synthesis of the PEG-Crosslinked Chitosan with a PH-Independent Swelling Behavior. *Macromol. Biosci.* **2005**, *5* (10), 925–928. <https://doi.org/10.1002/mabi.200500048>.
- (15) Bodnar, M.; Hartmann, J. F.; Borbely, J. Synthesis and Study of Cross-Linked Chitosan-N-Poly (Ethylene Glycol) Nanoparticles. **2006**, 3030–3036.
- (16) Fukushima, T.; Hayakawa, T.; Okamura, K.; Takeda, S.; Inoue, Y.; Miyazaki, K.; Okahata, Y. Buffer Solution Can Control the Porosity of DNA-Chitosan Complexes. *J. Biomed. Mater. Res. - Part B Appl. Biomater.* **2006**, *76* (1), 121–129. <https://doi.org/10.1002/jbm.b.30334>.
- (17) Pujana, M. A.; Pérez-Álvarez, L.; Iturbe, L. C. C.; Katime, I. Water Dispersible PH-Responsive Chitosan Nanogels Modified with Biocompatible Crosslinking-Agents. *Polymer* **2012**, *53* (15), 3107–3116. <https://doi.org/10.1016/j.polymer.2012.05.027>.
- (18) Wittaya-Areekul, S.; Kruenate, J.; Prahsarn, C. Preparation and in Vitro Evaluation of Mucoadhesive Properties of Alginate/Chitosan Microparticles Containing Prednisolone. *Int. J. Pharm.* **2006**, *312* (1–2), 113–118. <https://doi.org/10.1016/j.ijpharm.2006.01.003>.
- (19) Kumar, A.; Vimal, A.; Kumar, A. Why Chitosan? From Properties to Perspective of Mucosal Drug Delivery. *Int. J. Biol. Macromol.* **2016**, *91*, 615–622. <https://doi.org/10.1016/J.IJBIOMAC.2016.05.054>.
- (20) Menchicchi, B.; Fuenzalida, J. P.; Bobbili, K. B.; Hensel, A.; Swamy, M. J.;

- Goycoolea, F. M. Structure of Chitosan Determines Its Interactions with Mucin. *Biomacromolecules* **2014**, *15* (10), 3550–3558. <https://doi.org/10.1021/bm5007954>.
- (21) Dhawan, S.; Singla, A. K.; Sinha, V. R. Evaluation of Mucoadhesive Properties of Chitosan Microspheres Prepared by Different Methods. *AAPS PharmSciTech* **2004**, *5* (4). <https://doi.org/10.1208/pt050467>.
- (22) Bernkop-Schnürch, A.; Guggi, D.; Pinter, Y. Thiolated Chitosans: Development and in Vitro Evaluation of a Mucoadhesive, Permeation Enhancing Oral Drug Delivery System. *J. Control. Release* **2004**, *94* (1), 177–186. <https://doi.org/10.1016/J.JCONREL.2003.10.005>.
- (23) Bernkop-Schnürch, A.; Kast, C. E.; Richter, M. F. Improvement in the Mucoadhesive Properties of Alginate by the Covalent Attachment of Cysteine. *J. Control. Release* **2001**, *71* (3), 277–285. [https://doi.org/10.1016/S0168-3659\(01\)00227-9](https://doi.org/10.1016/S0168-3659(01)00227-9).
- (24) Bernkop-Schnürch, A. Thiomers: A New Generation of Mucoadhesive Polymers. *Adv. Drug Deliv. Rev.* **2005**, *57* (11), 1569–1582. <https://doi.org/10.1016/J.ADDR.2005.07.002>.
- (25) Leitner, V. M.; Walker, G. F.; Bernkop-Schnürch, A. Thiolated Polymers: Evidence for the Formation of Disulphide Bonds with Mucus Glycoproteins. *Eur. J. Pharm. Biopharm.* **2003**, *56* (2), 207–214. [https://doi.org/10.1016/S0939-6411\(03\)00061-4](https://doi.org/10.1016/S0939-6411(03)00061-4).
- (26) Artech Pujana, M.; Perez-Alvarez, L.; Cesteros Iturbe, L. C.; Katime, I. PH-Sensitive Chitosan-Folate Nanogels Crosslinked with Biocompatible Dicarboxylic Acids. *Eur. Polym. J.* **2014**, *61*, 215–225. <https://doi.org/10.1016/j.eurpolymj.2014.10.007>.
- (27) Pereira, A. G. B.; Muniz, E. C.; Hsieh, Y. Lo. ¹H NMR and ¹H-¹³C HSQC Surface Characterization of Chitosan-Chitin Sheath-Core Nanowhiskers. *Carbohydr. Polym.* **2015**, *123*, 46–52. <https://doi.org/10.1016/j.carbpol.2015.01.017>.
- (28) Ramasamy, P.; Subhapradha, N.; Thinesh, T.; Selvin, J.; Selvan, K. M.; Shanmugam, V.; Shanmugam, A. Characterization of Bioactive Chitosan and Sulfated Chitosan from *Doryteuthis Singhalensis* (Ortmann, 1891). *Int. J. Biol. Macromol.* **2017**, *99*, 682–691. <https://doi.org/10.1016/J.IJBIOMAC.2017.03.041>.
- (29) Kasaa, M. R. Determination of the Degree of N-Acetylation for Chitin and Chitosan by Various NMR Spectroscopy Techniques: A Review. *Carbohydr.*

- Polym.* **2010**, *79* (4), 801–810. <https://doi.org/10.1016/J.CARBPOL.2009.10.051>.
- (30) Sorlier, P.; Rochas, C.; Morfin, I.; Viton, C.; Domard, A. Light Scattering Studies of the Solution Properties of Chitosans of Varying Degrees of Acetylation. *Biomacromolecules* **2003**, *4* (4), 1034–1040. <https://doi.org/10.1021/bm034054n>.
- (31) Pérez-Álvarez, L.; Ruiz-Rubio, L.; Artetxe, B.; Vivanco, M. d. M.; Gutiérrez-Zorrilla, J. M.; Vilas-Vilela, J. L. Chitosan Nanogels as Nanocarriers of Polyoxometalates for Breast Cancer Therapies. *Carbohydr. Polym.* **2019**, *213* (January), 159–167. <https://doi.org/10.1016/j.carbpol.2019.02.091>.
- (32) Bravo-Osuna, I.; Ponchel, G.; Vauthier, C. Tuning of Shell and Core Characteristics of Chitosan-Decorated Acrylic Nanoparticles. *Eur. J. Pharm. Sci.* **2007**, *30* (2), 143–154. <https://doi.org/10.1016/J.EJPS.2006.10.007>.
- (33) Hu, Y.; Jiang, X.; Ding, Y.; Ge, H.; Yuan, Y.; Yang, C. Synthesis and Characterization of Chitosan-Poly(Acrylic Acid) Nanoparticles. *Biomaterials* **2002**, *23* (15), 3193–3201. [https://doi.org/10.1016/S0142-9612\(02\)00071-6](https://doi.org/10.1016/S0142-9612(02)00071-6).
- (34) Bravo-Osuna, I.; Teutonico, D.; Arpicco, S.; Vauthier, C.; Ponchel, G. Characterization of Chitosan Thiolation and Application to Thiol Quantification onto Nanoparticle Surface. *Int. J. Pharm.* **2007**, *340* (1–2), 173–181. <https://doi.org/10.1016/j.ijpharm.2007.03.019>.
- (35) Bertholon-Rajot, I.; Labarre, D.; Vauthier, C. Influence of the Initiator System, Cerium–Polysaccharide, on the Surface Properties of Poly(Isobutylcyanoacrylate) Nanoparticles. *Polymer* **2005**, *46* (4), 1407–1415. <https://doi.org/10.1016/J.POLYMER.2004.11.067>.
- (36) Danaei, M.; Dehghankhold, M.; Ataei, S.; Hasanzadeh Davarani, F.; Javanmard, R.; Dokhani, A.; Khorasani, S.; Mozafari, M. R. Impact of Particle Size and Polydispersity Index on the Clinical Applications of Lipidic Nanocarrier Systems. *Pharmaceutics* **2018**, *10* (2), 1–17. <https://doi.org/10.3390/pharmaceutics10020057>.
- (37) Li, X. W.; Lee, D. K. L.; Chan, A. S. C.; Alpar, H. O. Sustained Expression in Mammalian Cells with DNA Complexed with Chitosan Nanoparticles. *Biochim. Biophys. Acta - Gene Struct. Expr.* **2003**, *1630* (1), 7–18. <https://doi.org/10.1016/J.BBAEXP.2003.08.011>.
- (38) Aktaş, Y.; Andrieux, K.; Alonso, M. J.; Calvo, P.; Gürsoy, R. N.; Couvreur, P.; Çapan, Y. Preparation and in Vitro Evaluation of Chitosan Nanoparticles

- Containing a Caspase Inhibitor. *Int. J. Pharm.* **2005**, *298* (2), 378–383. <https://doi.org/10.1016/J.IJPHARM.2005.03.027>.
- (39) Sosnik, A.; das Neves, J.; Sarmento, B. Mucoadhesive Polymers in the Design of Nano-Drug Delivery Systems for Administration by Non-Parenteral Routes: A Review. *Prog. Polym. Sci.* **2014**, *39* (12), 2030–2075. <https://doi.org/10.1016/J.PROGPOLYMSCI.2014.07.010>.
- (40) Shtenberg, Y.; Goldfeder, M.; Schroeder, A.; Bianco-Peled, H. Alginate Modified with Maleimide-Terminated PEG as Drug Carriers with Enhanced Mucoadhesion. *Carbohydr. Polym.* **2017**, *175*, 337–346. <https://doi.org/10.1016/j.carbpol.2017.07.076>.
- (41) Hsein, H.; Garrait, G.; Beyssac, E.; Hoffart, V. Whey Protein Mucoadhesive Properties for Oral Drug Delivery: Mucin-Whey Protein Interaction and Mucoadhesive Bond Strength. *Colloids Surfaces B Biointerfaces* **2015**, *136*, 799–808. <https://doi.org/10.1016/j.colsurfb.2015.10.016>.
- (42) Kast, C. E.; Bernkop-Schnürch, A. Thiolated Polymers - Thiomers: Development and in Vitro Evaluation of Chitosan-Thioglycolic Acid Conjugates. *Biomaterials* **2001**, *22* (17), 2345–2352. [https://doi.org/10.1016/S0142-9612\(00\)00421-X](https://doi.org/10.1016/S0142-9612(00)00421-X).
- (43) George, M.; Abraham, T. E. Polyionic Hydrocolloids for the Intestinal Delivery of Protein Drugs: Alginate and Chitosan — a Review. *J. Control. Release* **2006**, *114* (1), 1–14. <https://doi.org/10.1016/J.JCONREL.2006.04.017>.
- (44) Fu, F. F.; Zhou, B. Q.; Ouyang, Z. J.; Wu, Y. L.; Zhu, J. Y.; Shen, M. W.; Xia, J. D.; Shi, X. Y. Multifunctional Cholesterol-Modified Dendrimers for Targeted Drug Delivery to Cancer Cells Expressing Folate Receptors. *Chinese J. Polym. Sci.* **2019**, *37* (2), 129–135. <https://doi.org/10.1007/s10118-019-2172-9>.
- (45) Chanphai, P.; Konka, V.; Tajmir-Riahi, H. A. Folic Acid–Chitosan Conjugation: A New Drug Delivery Tool. *J. Mol. Liq.* **2017**, *238*, 155–159. <https://doi.org/10.1016/J.MOLLIQ.2017.04.132>.

CHAPTER VIII

GENERAL CONCLUSIONS, FUTURE WORK AND PUBLICATIONS

VIII.1. GENERAL CONCLUSIONS	265
VIII.2. FUTURE WORK	271
VIII.3. LIST OF PUBLICATIONS AND COMMUNICATIONS	273
VIII.3.1. LIST OF PUBLICATIONS	274
VIII.3.2. LIST OF COMMUNICATIONS	278
REFERENCES	287

VIII. GENERAL CONCLUSIONS, FUTURE WORK AND PUBLICATIONS

VIII.1. GENERAL CONCLUSIONS

The main objective of this thesis was to design novel biopolymeric hydrogels starting from chitosan and appropriately using click synthetic strategies and reactions based on green chemistry, mainly for drug delivery and tissue engineering applications. The present study could be the promoter of this interesting and relevant line of research, which implies the development of stable materials with outstanding properties that were acquired not only after the cross-linking reaction (fluorescence, great porosity and swelling capacity, pH-sensitivity or self-healing ability, among others) but also by presenting a natural origin (biodegradability, biocompatibility, mucoadhesion or non-toxicity).

Therefore, throughout this thesis the versatility and sustainability of using chitosan for a variety of click reactions were declared in order to develop a wide range of chitosan-based 3D networks. Final results confirmed the high potential of this biopolymer, mainly due its great capacity to adapt under different environments and its high reactivity towards different molecules.

Nevertheless, one of the main drawbacks of neat chitosan is related to solubility limitations, merely possible in aqueous acid pHs, which restricts its biomedical applications. As it has been extensively studied, the main explanation of chitosan insolubility is the structured network of intra/intermacromolecular hydrogen bonds that lead to the chitosan chains to be held together. The disruption of these intra/intermacromolecular hydrogen bonding interactions leads to a decrease in chitosan crystallinity and results in an improvement of its water solubility. In this way, the crystallinity and solubility of the synthesized chitosan derivatives in this thesis were affected by the modification of the biopolymer. Indeed, chitosan was chemically modified obtaining more accessible and versatile chitosan. With the

purpose of achieving this goal, furan, maleimide, thiol or tetrazole groups were covalently grafted into the chitosan main chain conferring a high reactive character to the biopolymer (Chapter III). Certainly, X-ray diffraction patterns of the functionalized chitosan precursors demonstrated the loss of crystallinity in all cases. However, the solubility in neutral aqueous solutions was only achieved when thiol groups were grafted, resulting in totally water-soluble derivative at neutral pHs. Additionally, thiolated chitosan presented improved mucoadhesivity both at acid and neutral pHs.

As a result of the combination of complementary chitosan derivatives (CsFu, CsAMI, CsSH and CsTZ) or the reaction with a properly synthesized cross-linking agent (BMI), stimuli-responsive covalently cross-linked hydrogels were developed based on Diels-Alder (furan/maleimide), thiol-Michael addition (thiol/maleimide) or NITEC (tetrazole/maleimide) click reactions. The simple reaction conditions, the use of biocompatible molecules and the aqueous environment, made the synthesized products mimic natural systems to be widely applied in biomedicine. Therefore, different final soft materials with tailored properties were obtained depending on the specific characteristics that provide each of the reactions. Namely, the hydrogels obtained by Diels-Alder reaction proved to be great candidates as drug delivery devices (Chapter IV); while *in situ* hydrogels were synthesized by thiol-Michael addition reaction under physiological conditions with potential applications in the field of tissue engineering (Chapter V); whereas the fluorescent hydrogels synthesized by light-driven NITEC reaction presented excellent rheological properties, highlighting their self-healing ability, which turned them into possible bioinks to be used in 3D printing (Chapter VI).

Resulting hydrogels also presented common properties independent of the peculiarities acquired after each reaction. Indeed, synthesized hydrogels were characterized by remarkable stability and porous microstructures. Furthermore,

all hydrogels displayed interesting viscoelastic behaviour with storage moduli resembling that of liver, fat, relaxed muscle or breast gland tissue (10^3 – 10^4 Pa) or brain and nerve tissues (10^2 – 10^3 Pa). Based on these values, the internal architecture of the materials was modelled in order to determine the average mesh size (ξ , nm), the cross-linking density (n_c , mol m⁻³) and the average molecular weight between neighbouring cross-links (M_c , kg mol⁻¹) in the nanometric scale. On the other hand, the pH responsive swelling presented by the hydrogels under different environments was also studied. Great amounts of fluid were absorbed by the resulting materials. However, the characteristic cationic character of the chitosan at acid medium, the cross-linking degree and the hydrophilic nature of the cross-linker (when used) determined the swelling behaviour of the final materials. In addition, the synthesized all-chitosan hydrogels (CsFu/CsAMI and CsTZ/CsAMI hydrogels) were found to interact with the human system properly and degrade by certain human enzymes as lysozymes at physiological conditions. Preliminary short-term cytotoxicity studies revealed that the synthesized hydrogels showed a non-toxic profile arising as suitable materials for biomedical applications.

Table VIII.1 summarizes the principal characteristics collected throughout this thesis for the four types of hydrogels obtained via different click reactions, i. e. CsFu/CsAMI (Chapter IV), CsFu/BMI (Chapter IV), CsSH/BMI (Chapter V) and CsTZ/CsAMI (Chapter VI). After a deep analysis where the behaviour of the hydrogels in different areas was studied, the optimum formulations for each of the systems were selected, which are the ones specified in Table VIII.1.

Table VIII.1. Main properties of the clicked hydrogels.

Properties	HYDROGELS			
	CsFu/CsAMI (58 kDa)	CsFu/BMI 1:2 (58 kDa)	CsSH/BMI 1:3 (680 kDa)	CsTZ/CsAMI 1:15 (67 kDa)
Pore size (μm)	281 ± 23	500 ± 130	343 ± 124	398 ± 98
Swelling time (h)	24	24	48	48
SR_{eq} (%)	1050	877 ± 168	2430 ± 624	354 ± 2
$r_o \cdot 10^3$ ($\text{g}_{\text{sol}}\text{g}_{\text{hyd}}^{-1}\text{s}^{-1}$)	8.72	1.65	1.90	332
Gel content (%)	60	61	35	93
G' (Pa)	399 ± 87	379 ± 95	3332 ± 502	2716 ± 1253
ξ (nm)	10.3 ± 0.8	10.5 ± 1.0	5.1 ± 0.6	5.5 ± 1.0
n_c (mol m^{-3})	0.15 ± 0.0	0.15 ± 0.0	1.3 ± 0.5	1.1 ± 0.5
M_c (kg mol^{-1})	329 ± 71	211 ± 61	58 ± 21	53 ± 24
c (% w/v)	5	3	7	6

According to the results in Table VIII.1, several concepts have to be highlighted. Even if it would not be correct to compare the four samples between them, since a great deal of concepts would have to be taken into account, certain similarities and differences were obvious among the clicked hydrogels. While keeping in mind that the starting chitosan was different in every system, with particular average molecular weight (M_w) and degree of deacetylation (DDc) that influence the final properties, the type of reaction chosen seemed to be decisive. At first glance, both furan/maleimide systems based on Diels–Alder reaction presented analogous features, while the thiol/maleimide and tetrazole/maleimide coupling systems behaved similarly in terms of general characteristics. As it could be observed, regarding elastic properties, the mean G' values for the two latest were one order of magnitude higher than those of DA hydrogels, which is crucial in terms of tissue engineering applications as has been emphasized by the *in situ* formation of MA hydrogels and the self-healing behaviour of NITEC hydrogels. The structural parameters proceeded in parallel to the increase observed in the storage modulus, i.e. the cross-linking density (n_c) was observed to be higher while the average mesh size (ξ) and the average molecular weight between neighbouring cross-links (M_c) decreased¹, regardless the polymer concentration. Typical mesh

sizes reported for hydrogels range from 5 to 100 nm². Due to network heterogeneity and polymer polydispersity, a wide distribution of mesh sizes is normally common, as the mesh size depends on polymer and cross-linker concentration, as well as external stimuli such as temperature and pH². To put into context the obtained mesh size value for the clicked hydrogels, the widely used lysozyme and immunoglobulin G model proteins have hydrodynamic diameters of 4.1 and 10.7 nm, respectively³, in the range of the obtained mesh size values, and, thus, indicating that the as-prepared hydrogels would allow the transport of small molecules through the networks, resulting in interesting biological scaffolds.

Moreover, the microstructure of the synthesized hydrogels gives an opportunity to get an overview of the conformation and morphology of the final products in terms of porosity, pore size or interconnectivity between pores, relevant parameters for future final applications. Furthermore, one of the most important characteristics that defines this type of materials, as the swelling capacity which directly affects the pH-sensitivity, is ruled by the porosity of the hydrogel. Moura et al. reported that covalently cross-linked chitosan-based hydrogels presented a size distribution curve shifted towards higher values compared to ionically cross-linked ones⁴. Furthermore, previously reported investigations studied the pore size of chemically cross-linked chitosan-based hydrogels; namely, the pore diameter when using glutaraldehyde ranged from 20 to 100 μm^{5,6}, while employing genipin from 30 to 170 μm⁷. Indeed, genipin and glutaraldehyde are characterized for being small size cross-linkers, where the cross-linking reaction with the amines of chitosan is highly accessible, giving rise to smaller pores. In the case of the clicked hydrogels in study, the possibilities were reduced since the functional groups capable of the cross-linking were randomly distributed, resulting in larger pore sizes in all the cases ranged from 300 to 500 μm.

Additionally, the pore size distribution in 3D matrices is also greatly useful when studying changes and modifications produced as a result of using the as-prepared

materials as cellular growth and proliferation containers, as pore size distribution plays an important role in the signalling and microenvironment stimuli imparted to the cells⁸. Indeed, the tissue engineering scaffolds should have a interconnected porous structure and high porosity, necessary to provide sufficient space for growth, attachment and proliferation of cells and secretion of extracellular matrix^{9,10}. The size of a human cell range from 6 to 100 μm in diameter, being the red blood cell and the oocyte the smallest and largest cells of the human body, respectively. For instance, Janik and Marzec reported that the optimum pore size of a cartilage scaffold should be about 200 μm ¹¹, whereas Wang et al. designed 3D tumour models based on chitosan with a mean pore size of approximately 180 μm for growing breast cancer MCF-7 cells¹². Therefore, the obtained materials in this thesis could be considered as interesting biomaterials for cell growth according to the previous statement.

In addition to porosity and mesh size, as it has been already discussed, the swelling process could also be affected by specific relations between the swelling medium and the polymer pendant groups, where many kinds of polymer/solution interactions could be expected giving place to complex kinetics. Regarding swelling capacity, the MA hydrogels were observed to absorb higher amounts of fluid, probably related to the water affinity presented by these hydrogels due to the hydrophilic nature of the precursors. Nevertheless, solubility could also influence the low gel content value of these hydrogels. Furthermore, the initial swelling rate that was calculated from the swelling parameters could help understanding the behaviour of the designed networks. Thereby, as stated by Altinisik and Yurdakoc an increase of r_0 was related with the decrease in the swelling ratio¹³. Namely, NITEC hydrogels showed the lowest swelling capacity exhibiting the highest values of initial swelling ratio and gel content. It is observed that the lowest values of r_0 were presented by the systems containing BMI, which may be related with the presence of hydrophilic chains that could be water-soluble and affect swelling

beyond cross-linking, resulting in greater swelling ratio values, as already discussed in this thesis.

On the other hand, nanogels show advantages similar to those from bulk hydrogels and can be targeted to specific sites of action in the organism. Therefore, hydrogel nanoparticles with uniform particle size distribution were obtained after covalently cross-linking with a commercial biocompatible cross-linking agent via reverse emulsion method (Chapter VII). Nanogels were extremely swollen in aqueous solutions due to their high liquid absorption ability over the entire pH range. Besides, nanogels maintained the enhanced mucoadhesion properties shown by the thiolated chitosan precursor, which turned them into excellent bioadhesive materials. In order to develop potential anticancer drug delivery nanodevices with specific targeting properties, folate receptor was attached into the nanogels surface by thiol-Michael addition linkage.

Therefore, smart materials as stimuli-responsive hydrogels and nanogels based on chitosan were successfully developed in this thesis. The whole set of analysed properties made them of particular interest for application in tissue engineering or design of drug delivery platforms, opening a new line of research that could enable the creation of heterogeneous gel-type scaffolds of different sizes applying a great variety of green click cross-linking reactions.

All these results motivated the proposals for future research routes.

VIII.2. FUTURE WORK

Based on this work and with the aim of following with the research in this field, different challenges are proposed, which would complete this work and provide suitable outlines for future frameworks:

- i. The selection of photo-initiated chitosan derivatives in hybrid hydrogels introduces the exciting possibility of an additional level of spatial control over

- these materials. Therefore, the synthesized NITEC hydrogels can be tuned by controlling the photocleavage reaction sites within the networks. It is proposed the photo-irradiation of the hydrogels through a mask, enabling to pattern specific regions of the networks by controlling the site of irradiation.
- ii. Given the excellent rheological response shown by the NITEC hydrogels in terms of being used as injectable materials, it is suggested the 3D printing technology for the development of tridimensional scaffolds. Thus, the main parameters involved in the printing process have to be optimized in order to obtain biocompatible materials with a final applicability in the area of biomedicine concerning tissue engineering.
 - iii. The use of DNA as a structural element to build novel architectures. Namely, hydrogels based on pure DNA have shown to be expensive and exhibit low sensitivity¹⁴; therefore, sensing hydrogels combining polymers and DNA have attracted great attention lately. Among others, DNA-conjugated hydrogels have shown to be useful in bioanalytics and biosensing, new material design and surface modification¹⁵. In this context, the development of novel chitosan-DNA hybrid hydrogels is proposed. The preparation of chitosan containing clickable functional groups that allow the incorporation of modified DNA strands into the biopolymer backbone through click reactions for the subsequent formation of chitosan-DNA conjugates by hybridisation. Being the DNA strands complementary sequences, they are expected to hybridise into double helix when mixed together, cross-linking the polymer chains and resulting in the desired hydrogel.
 - iv. Tissues are dynamic structures constituted by multiple cell types, an extracellular matrix (ECM) and a variety of signalling molecules, where the extracellular matrix is a crucial component of the cellular microenvironment and forms a complex 3D network¹⁶. The development of tissue specific scaffolds that possess the complex hierarchy of natural tissues remains deficient in tissue engineering applications; therefore, it is proposed the

suitability of the synthesized chitosan-based hydrogels as sustainable containers for cell growth. Previous studies performed in this thesis revealed that functionalized chitosan matrixes displayed excellent properties and short-term cytotoxicity assays confirmed the biocompatibility of the materials; thus, cells could be seeded onto these scaffolds after fabrication, penetrating the depths of the structure due to their microporous morphology, simulating the extracellular matrix of human tissues. In addition, enzymatic degradation of the hydrogels loaded with cells could also be performed in order to study the action of the lysozymes on the cells once the hydrogels are degraded. So that the *in vivo* situation could be mimic, different human cell lines could be cultured into the hydrogels to discover new therapies, namely, breast cancer MCF-7 cells or lung fibroblasts WI-38 cells.

- v. Due to their size, nanogels can enter areas which are not easily accessed by bulk compounds or drugs and have the capacity to deliver therapeutic nucleoside analogs (siRNA/DNA) into the cytoplasm for intracellular delivery. Therefore, gene delivery involves the loading of genetic materials like DNA, RNA, oligonucleotides or combinations of these in the nanogels that provide protection and act as nanocarriers for direct and localized administration of genes to tissues. Chitosan can self-assemble with DNA or RNA by electrostatic attraction to form complexes due to its cationic nature¹⁷. Thus, applying the reverse emulsion technique described in this thesis, the design of hybrid chitosan-based nanogels for gene delivery is proposed.

VIII.3. LIST OF PUBLICATIONS AND COMMUNICATIONS

The results obtained from this work have led to several scientific publications and have also been presented at various conferences. The mentioned contributions are listed below.

VIII.3.1. List of publications

Authors Olatz Guaresti, Sheila Maiz, Teodoro Palomares, Ana Alonso-Varona, Arantxa Eceiza, Leyre Pérez-Álvarez, Nagore Gabilondo

Title Design of biocompatible folate functionalized chitosan nanogels through inverse microemulsion method with enhanced mucoadhesive properties

Journal Under preparation

Year 2020

Authors Olatz Guaresti, Leander Crocker, Teodoro Palomares, Ana Alonso-Varona, Arantxa Eceiza, Ljiljana Fruk, Nagore Gabilondo

Title Light-driven assembly of biocompatible fluorescent chitosan hydrogels with self-healing ability

Journal Under preparation

Year 2020

Authors Olatz Guaresti, Senda Basasoro, Kizkitza González, Arantxa Eceiza, Nagore Gabilondo

Title *In situ* cross-linked chitosan hydrogels via Michael addition reaction based on water-soluble thiol-maleimide precursors

Journal European Polymer Journal, 119, 376–384

Year 2019

Impact factor 3.621 (JCR 2018)

Rank 14/87 (Polymer Science) (JCR 2018)

Authors Olatz Guaresti, Clara García-Astrain, Leire Urbina, Arantxa Eceiza, Nagore Gabilondo

Title Reversible swelling behaviour of Diels-Alder clicked chitosan hydrogels in response to pH changes

Journal eXPRESS Polymer Letters, 13, 27–36

Year 2019

Impact factor 2.875 (JCR 2018)

Rank 22/87 (Polymer Science) (JCR 2018)

Authors Olatz Guaresti, Clara García–Astrain, Roberto Hernandez Aguirresarobe, Arantxa Eceiza, Nagore Gabilondo

Title Synthesis of stimuli–responsive chitosan–based hydrogels by Diels–Alder cross–linking ‘click’ reaction as potential carriers for drug administration

Journal Carbohydrate Polymers, 183, 278–286

Year 2018

Impact factor 6.044 (JCR 2018)

Rank 4/87 (Polymer Science), 2/71 (Applied Chemistry), 3/57 (Organic Chemistry) (JCR 2018)

Authors Olatz Guaresti, Clara García–Astrain, Teodoro Palomares, Ana Alonso–Varona, Arantxa Eceiza, Nagore Gabilondo

Title Synthesis and characterization of a biocompatible chitosan–based hydrogel cross–linked via ‘click’ chemistry for controlled drug release

Journal International Journal of Biological Macromolecules, 102, 1–9

Year 2017

Impact factor 4.784 (JCR 2018)

Rank 8/87 (Polymer Science), 52/299 (Biochemistry & Molecular Biology), 9/71 (Applied Chemistry) (JCR 2018)

Authors Clara García–Astrain, Rebeca Hernández, Olatz Guaresti, Ljiljana Fruk, Carmen Mijangos, Arantxa Eceiza, Nagore Gabilondo

Title Click crosslinked chitosan/gold nanocomposite hydrogels

Journal Macromolecular Materials and Engineering, 301, 1295–1300

Year 2016

Impact factor 3.038 (JCR 2018)

Rank 19/87 (Polymer Science), 99/293 (Multidisciplinary Materials Science) (JCR 2018)

Authors Clara García-Astrain, Kizkitza González, Tania Gurrea, Olatz Guaresti, Itxaso Algar, Arantxa Eceiza, Nagore Gabilondo

Title Maleimide-grafted cellulose nanocrystals as cross-linkers for bionanocomposite hydrogels

Journal Carbohydrate Polymers, 149, 94–101

Year 2016

Impact factor 6.044 (JCR 2018)

Rank 4/87 (Polymer Science), 2/71 (Applied Chemistry), 3/57 (Organic Chemistry) (JCR 2018)

COLLABORATIONS:

Authors Kizkitza González, Olatz Guaresti, Teodoro Palomares, Ana Alonso-Varona, Arantxa Eceiza, Nagore Gabilondo

Title The role of cellulose nanocrystals in biocompatible starch-based clicked nanocomposite hydrogels

Journal International Journal of Biological Macromolecules, 143, 265–272

Year 2020

Impact factor 4.784 (JCR 2018)

Rank 8/87 (Polymer Science), 52/299 (Biochemistry & Molecular Biology), 9/71 (Applied Chemistry) (JCR 2018)

Authors Nagore Barroso, Olatz Guaresti, Leyre Pérez-Álvarez, Leire Ruiz-Rubio, Nagore Gabilondo, José Luis Vilas-Vilela

Title Self-healable hyaluronic acid/chitosan polyelectrolyte complex hydrogels and multilayers

Journal European Polymer Journal, 120, 109268

Year 2019

Impact factor 3.621 (JCR 2018)

Rank 14/87 (Polymer Science) (JCR 2018)

Authors Leire Urbina, Olatz Guaresti, Jesús Requires, Nagore Gabilondo, Arantxa Eceiza, María Ángeles Corcuera, Aloña Retegi

Title Design of reusable novel membranes based on bacterial cellulose and chitosan for the filtration of copper in wastewaters

Journal Carbohydrate Polymers, 193, 362–372

Year 2018

Impact factor 6.044 (JCR 2018)

Rank 4/87 (Polymer Science), 2/71 (Applied Chemistry), 3/57 (Organic Chemistry) (JCR 2018)

Authors Clara García–Astrain, Olatz Guaresti, Kizkitza González, Arantzazu Santamaria–Echart, Arantxa Eceiza, María Ángeles Corcuera, Nagore Gabilondo

Title Click gelatin hydrogels: Characterization and drug release behaviour

Journal Materials Letters, 182, 134–137

Year 2016

Impact factor 3.019 (JCR 2018)

Rank 44/148 (Applied Physics), 101/293 (Multidisciplinary Materials Science) (JCR 2018)

Authors Clara García–Astrain, Ishtiaq Ahmed, Dania Kendziora, Olatz Guaresti, Arantxa Eceiza, Ljiljana Fruk, María Ángeles Corcuera, Nagore Gabilondo

Title Effect of maleimide–functionalized gold nanoparticles on hybrid biohydrogels properties

Journal RSC Advances, 5, 50268–50277

Year 2015

Impact factor 3.049 (JCR 2018)

Rank 68/172 (Multidisciplinary Chemistry)

VIII.3.2. List of communications

Authors Olatz Guaresti

Title Desarrollo de nuevos hidrogeles a partir de quitosano aplicando los fundamentos de la química 'clíc' con propiedades de estímulo—respuesta mejoradas

Conference II Jornadas Doctorales de la UPV/EHU

Contribution Poster

Year 2019

Place Bilbao, Spain

Authors Olatz Guaresti, Leander Crocker, Arantxa Eceiza, Ljiljana Fruk, Nagore Gabilondo

Title Light induced cycloaddition for chitosan-based 3D fluorescent networks formation

Conference 7th International Conference on Biobased and Biodegradable Polymers (BIOPOL 2019)

Contribution Oral Communication

Year 2019

Place Stockholm, Sweden

Authors Olatz Guaresti, Arantxa Eceiza, Nagore Gabilondo

Title *In situ* cross-linked chitosan hydrogels by Michael addition reaction based on water soluble thiol-maleimide precursors

Conference Sixth International Symposium Frontiers in Polymer Science

Contribution Poster

Year 2019

Place Budapest, Hungary

Authors Olatz Guaresti, Kizkitza González, Arantxa Eceiza, Nagore Gabilondo

Title Thiolated chitosan–based hydrogels using Michael addition and by controlling the macromolecular architecture

Conference 10th ECNP International Conference on Nanostructured Polymers and Nanocomposites

Contribution Poster

Year 2018

Place Donostia–San Sebastián, Spain

Authors Olatz Guaresti, Kizkitza González, Arantxa Eceiza, Nagore Gabilondo

Title Design of thiol–modified chitosan hydrogels with different maleimide-based cross–linkers

Conference Polymer Networks and Gels 2018

Contribution Oral Communication

Year 2018

Place Prague, Czech Republic

Authors Olatz Guaresti, Clara García–Astrain, Leire Urbina, Arantxa Eceiza, Nagore Gabilondo

Title *In situ* cross–linked chitosan-based hydrogels via thiol–maleimide Michael addition

Conference 6th International Conference on Biobased and Biodegradable Polymers (BIOPOL 2017)

Contribution Poster

Year 2017

Place Mons, Belgium

Authors Olatz Guaresti, Clara García–Astrain, Arantxa Eceiza, Nagore Gabilondo

Title Covalently cross–linked chitosan–based hydrogels via ‘click’ chemistry for sustained antibiotic release

Conference International Conference on Biobased Materials and Composites (ICBMC 2017)

Contribution Oral Communication

Year 2017

Place Nantes, France

Authors Olatz Guaresti, Clara García-Astrain, Arantxa Eceiza, Nagore Gabilondo

Title Síntesis de hidrogeles de quitosano reticulados mediante química 'click' para aplicaciones biomédicas

Conference I Seminario de Jóvenes Investigadores en Polímeros (ICTP-CSIC)

Contribution Oral Communication

Year 2016

Place Madrid, Spain

Authors Olatz Guaresti, Clara García-Astrain, Aloña Retegi, Arantxa Eceiza, Nagore Gabilondo

Title A renewable synthesis strategy for the development of cross-linked chitosan-based hydrogel for biomedical applications

Conference 15th International Symposium on Biopolymers (ISBP 2016)

Contribution Poster

Year 2016

Place Madrid, Spain

Authors Olatz Guaresti, Clara García-Astrain, Arantxa Eceiza, Nagore Gabilondo

Title Characterization of cross-linked chitosan based hydrogels

Conference 9th International Conference on Modification, Degradation and Stabilization of Polymers (MoDeSt 2016)

Contribution Poster

Year 2016

Place Krakow, Poland

Authors Olatz Guaresti, Clara García–Astrain, Arantxa Eceiza, Nagore Gabilondo

Title Diseño de un hidrogel de quitosano químicamente entrecruzado por reacción de Diels–Alder

Conference I Jornadas Doctorales de la UPV/EHU

Contribution Poster

Year 2016

Place Bilbao, Spain

Authors Olatz Guaresti, Clara García–Astrain, Arantxa Eceiza, Nagore Gabilondo

Title Design and applications of a chemical hydrogel network of chitosan synthesized via Diels–Alder reaction

Conference International Conference on Macromolecular Materials (Polymat Spotlight 2016)

Contribution Poster + Flash presentation

Year 2016

Place Donostia–San Sebastián, Spain

Authors Olatz Guaresti, Clara García–Astrain, Arantxa Eceiza, Maria Ángeles Corcuera, Nagore Gabilondo

Title Cross–linked biopolymer–based hydrogels via aqueous Diels–Alder ‘click’ chemistry

Conference 5th International Conference on Biobased and Biodegradable Polymers (BIOPOL 2015)

Contribution Poster

Year 2015

Place Donostia–San Sebastián, Spain

Authors Olatz Guaresti, Clara García–Astrain, Arantxa Eceiza, Maria Ángeles Corcuera, Nagore Gabilondo

Title Diels–Alder cross–linked gelatin–based hydrogels for controlled drug delivery

Conference 5th Workshop Green Chemistry and Nanotechnologies in Polymer Chemistry, ECLIPSE Workshop, BIOPURFIL Workshop

Contribution Poster

Year 2014

Place Donostia–San Sebastián, Spain

Authors Olatz Guaresti, Clara García–Astrain, Arantxa Eceiza, Maria Ángeles Corcuera, Nagore Gabilondo

Title Diels–Alder erreakzioz saretutako gelatina hidrogelen ebaluaketa botiken askapenean

Conference Materialen Zientzia eta Teknologia II. Kongresua (MZTII 2014)

Contribution Poster

Year 2014

Place Donostia–San Sebastián, Spain

COLLABORATIONS:

Authors Leire Urbina, Olatz Guaresti, Arantxa Eceiza, Maria Ángeles Corcuera, Aloña Retegi

Title Stiff bacterial cellulose nanopapers with improved hydrophobicity and antioxidant properties

Conference 7th International Conference on Biobased and Biodegradable Polymers (BIOPOL 2019)

Contribution Poster

Year 2019

Place Stockholm, Sweden

Authors Gabriel Arner, Olatz Guaresti, Leire Urbina, Aloña Retegi, Tamara Calvo–Correas, Arantxa Eceiza, Nagore Gabilondo

Title Biosynthesis of bacterial cellulose/chitosan/alginate hybrid particles

Conference 9th Conference Green Chemistry and Nanotechnologies in Polymeric Materials

Contribution Poster

Year 2018

Place Krakow, Poland

Authors Izaskun Larraza, Gabriel Arner, Olatz Guaresti, Leire Urbina, Aloña Retegi, Arantxa Eceiza, Nagore Gabilondo

Title Bacterial cellulose nanofibrils embedded *in situ* formed chitosan/alginate particles

Conference 10th ECNP International Conference on Nanostructured Polymers and Nanocomposites

Contribution Poster

Year 2018

Place Donostia–San Sebastián, Spain

Authors Kizkitza González, Olatz Guaresti, Clara García–Astrain, Arantxa Eceiza, Nagore Gabilondo

Title Diels–Alder reaction for the cross–linking of maize starch based materials

Conference International Conference on Biobased Materials and Composites (ICBMC 2017)

Contribution Oral Communication

Year 2017

Place Nantes, France

Authors Leire Urbina, Olatz Guaresti, Nagore Gabilondo, Arantxa Eceiza, Maria Ángeles Corcuera, Aloña Retegi

Title Design of new membranes based on bacterial cellulose and chitosan for the filtration of heavy metals in water wastes

Conference International Conference on Biobased Materials and Composites (ICBMC 2017)

Contribution Poster + Flash presentation

Year 2017

Place Nantes, France

Authors Kizkitza González, Clara García–Astrain, Olatz Guaresti, Arantxa Eceiza, Nagore Gabilondo

Title Functionalized polysaccharides ready for the Diels–Alder reaction

Conference 3rd International Conference on Bioinspired and Biobased Chemistry & Materials (N.I.C.E. 2016)

Contribution Poster

Year 2016

Place Nice, France

Authors Clara García–Astrain, Olatz Guaresti, Tania Gurrea, Arantxa Eceiza, Maria Ángeles Corcuera, Nagore Gabilondo

Title Bionanocomposite hydrogels with various covalently bound nanospecies

Conference 5th International Conference on Biobased and Biodegradable Polymers (BIOPOL 2015)

Contribution Oral Communication

Year 2015

Place Donostia–San Sebastián, Spain

Authors Itxaso Algar, Clara García–Astrain, Alba González, Loli Martin, Olatz Guaresti, Nagore Gabilondo, Aloña Retegi, Arantxa Eceiza

Title Hybrid bionanocomposites by in-situ assembling of bacterial cellulose/montmorillonite clay

Conference 6th Workshop on Green Chemistry and Nanotechnologies in Polymer Chemistry (GCNPC)

Contribution Poster

Year 2015

Place Bragança, Portugal

* Best Poster Award

Authors Clara García–Astrain, Olatz Guaresti, Tania Gurrea, Arantxa Eceiza, Ljiljana Fruk, María Ángeles Corcuera, Nagore Gabilondo

Title Bionanocomposite hydrogels effectively cross–linked with functionalized nanoparticles

Conference Imaginenano 2015

Contribution Poster

Year 2015

Place Bilbao, Spain

Authors Clara García–Astrain, Ljiljana Fruk, Alessandro Gandini, Ana Alonso–Varona, Teodoro Palomares, María Burón, Olatz Guaresti, María Ángeles Corcuera, Nagore Gabilondo

Title Silver nanoparticles as cross–linkers for gelatin–based bionanocomposite hydrogel via Diels–Alder ‘click’ chemistry

Conference 5th Workshop Green Chemistry and Nanotechnologies in Polymer Chemistry, ECLIPSE Workshop, BIOPURFIL Workshop

Contribution Oral Communication

Year 2014

Place Donostia–San Sebastián, Spain

Authors Clara García–Astrain, Alessandro Gandini, Olatz Guaresti, Arantxa Eceiza, María Ángeles Corcuera, Nagore Gabilondo

Title Diels–Alder bitartez saretutako hidrogelak eta bere nanokonpositoak

Conference Materialen Zientzia eta Teknologia II. Kongresua (MZTII 2014)

Contribution Poster

Year 2014

Place Donostia-San Sebastián, Spain

REFERENCES

- (1) Karvinen, J.; Ihalainen, T. O.; Calejo, M. T.; Jönkkäri, I.; Kellomäki, M. Characterization of the Microstructure of Hydrazone Crosslinked Polysaccharide-Based Hydrogels through Rheological and Diffusion Studies. *Mater. Sci. Eng. C* **2019**, *94* (April 2018), 1056–1066. <https://doi.org/10.1016/j.msec.2018.10.048>.
- (2) Li, J.; Mooney, D. J. Designing Hydrogels for Controlled Drug Delivery. *Nat. Rev. Mater.* **2016**, *1* (12), 1–38. <https://doi.org/10.1038/natrevmats.2016.71>.
- (3) Burczak, K.; Fujisato, T.; Hatada, M.; Ikada, Y. Protein Permeation through Poly(Vinyl Alcohol) Hydrogel Membranes. *Biomaterials* **1994**, *15* (3), 231–238. [https://doi.org/10.1016/0142-9612\(94\)90072-8](https://doi.org/10.1016/0142-9612(94)90072-8).
- (4) Moura, M. J.; Faneca, H.; Lima, M. P.; Gil, M. H.; Figueiredo, M. M. In Situ Forming Chitosan Hydrogels Prepared via Ionic/Covalent Co-Cross-Linking. *Biomacromolecules* **2011**, *12* (9), 3275–3284. <https://doi.org/10.1021/bm200731x>.
- (5) Zou, W.; Chen, Y.; Zhang, X.; Li, J.; Sun, L.; Gui, Z.; Du, B.; Chen, S. Cytocompatible Chitosan Based Multi-Network Hydrogels with Antimicrobial, Cell Anti-Adhesive and Mechanical Properties. *Carbohydr. Polym.* **2018**, *202*, 246–257. <https://doi.org/10.1016/J.CARBPOL.2018.08.124>.
- (6) Martínez-Mejía, G.; Vázquez-Torres, N. A.; Castell-Rodríguez, A.; del Río, J. M.; Corea, M.; Jiménez-Juárez, R. Synthesis of New Chitosan-Glutaraldehyde Scaffolds for Tissue Engineering Using Schiff Reactions. *Colloids Surfaces A Physicochem. Eng. Asp.* **2019**, *579*, 123658. <https://doi.org/10.1016/J.COLSURFA.2019.123658>.

- (7) Silva, S. S.; Motta, A.; Rodrigues, M. T.; Pinheiro, A. F. M.; Gomes, M. E.; Mano, J. F.; Reis, R. L.; Migliaresi, C. Novel Genipin-Cross-Linked Chitosan/Silk Fibroin Sponges for Cartilage Engineering Strategies. *Biomacromolecules* **2008**, *9* (10), 2764–2774. <https://doi.org/10.1021/bm800874q>.
- (8) Leal-Egaña, A.; Dietrich-Braumann, U.; Díaz-Cuenca, A.; Nowicki, M.; Bader, A. Determination of Pore Size Distribution at the Cell-Hydrogel Interface. *J. Nanobiotechnology* **2011**, *9* (1), 24. <https://doi.org/10.1186/1477-3155-9-24>.
- (9) Song, X.; Zhu, C.; Fan, D.; Mi, Y.; Li, X.; Fu, R. Z.; Duan, Z.; Wang, Y.; Feng, R. R. A Novel Human-like Collagen Hydrogel Scaffold with Porous Structure and Sponge-like Properties. *Polymers* **2017**, *9* (12), 1–16. <https://doi.org/10.3390/polym9120638>.
- (10) Krishnamoorthy, S.; Noorani, B.; Xu, C. Effects of Encapsulated Cells on the Physical–Mechanical Properties and Microstructure of Gelatin Methacrylate Hydrogels. *Int. J. Mol. Sci.* **2019**, *20* (20), 5061. <https://doi.org/10.3390/ijms20205061>.
- (11) Janik, H.; Marzec, M. A Review: Fabrication of Porous Polyurethane Scaffolds. *Mater. Sci. Eng. C* **2015**, *48*, 586–591. <https://doi.org/10.1016/j.msec.2014.12.037>.
- (12) Wang, H.; Qian, J.; Zhang, Y.; Xu, W.; Xiao, J.; Suo, A. Growth of MCF-7 Breast Cancer Cells and Efficacy of Anti-Angiogenic Agents in a Hydroxyethyl Chitosan/Glycidyl Methacrylate Hydrogel. *Cancer Cell Int.* **2017**, *17* (1), 1–14. <https://doi.org/10.1186/s12935-017-0424-8>.
- (13) Altinisik, A.; Yurdakoc, K. Chitosan/Poly(Vinyl Alcohol) Hydrogels for Amoxicillin Release. *Polym. Bull.* **2014**, *71* (3), 759–774.

<https://doi.org/10.1007/s00289-013-1090-1>.

- (14) Xing, Y.; Cheng, E.; Yang, Y.; Chen, P.; Zhang, T.; Sun, Y.; Yang, Z.; Liu, D. Self-Assembled DNA Hydrogels with Designable Thermal and Enzymatic Responsiveness. *Adv. Mater.* **2011**, *23* (9), 1117–1121. <https://doi.org/10.1002/adma.201003343>.
- (15) Bauer, D. M.; Ahmed, I.; Vigovskaya, A.; Fruk, L. Clickable Tyrosine Binding Bifunctional Linkers for Preparation of DNA-Protein Conjugates. *Bioconjug. Chem.* **2013**, *24* (6), 1094–1101. <https://doi.org/10.1021/bc4001799>.
- (16) Tamay, D. G.; Usal, T. D.; Alagoz, A. S.; Yucel, D.; Hasirci, N.; Hasirci, V. 3D and 4D Printing of Polymers for Tissue Engineering Applications. *Front. Bioeng. Biotechnol.* **2019**, *7* (JUL). <https://doi.org/10.3389/fbioe.2019.00164>.
- (17) Wang, H.; Qian, J.; Ding, F. Recent Advances in Engineered Chitosan-Based Nanogels for Biomedical Applications. *J. Mater. Chem. B* **2017**, *5* (34), 6986–7007. <https://doi.org/10.1039/c7tb01624g>.

ANNEXES

LIST OF FIGURES

293

LIST OF SCHEMES

302

LIST OF TABLES

304

LIST OF ABBREVIATIONS

308

LIST OF SYMBOLS

311

LIST OF FIGURES

CHAPTER I

- Figure I.1.** Schematic disposal of chitin chains in α , β and γ -chitin. 6
- Figure I.2.** Chemical structure of chitin and chitosan as integral structural components of different living organisms. 8
- Figure I.3.** Chitosan-based systems and their preparation techniques⁵⁶. 12
- Figure I.4.** Multiscale properties of hydrogels. 15
- Figure I.5.** Implantation route for hydrogels of different size. 17
- Figure I.6.** Structure of polyelectrolyte complexes (PEC). 19
- Figure I.7.** Schematic representation of this thesis. 26

CHAPTER III

- Figure III.1.** FTIR spectra of A) chitosan and B) furan-functionalized chitosan (CsFu). 86
- Figure III.2.** Liquid-state ^1H NMR spectra and chemical structure of chitosan and furan-functionalized chitosan (CsFu). 87
- Figure III.3.** X-ray diffractograms of chitosan and furan-functionalized chitosan (CsFu). 88
- Figure III.4.** TGA (left axis, solid line) and dTGA (right axis, dash line) curves of chitosan and furan-functionalized chitosan (CsFu) under inert atmosphere. 89

Figure III.5. FTIR spectra of A) chitosan and B) maleimide-functionalized chitosan (CsAMI). 92

Figure III.6. Liquid-state ^1H NMR spectra and chemical structure of chitosan and maleimide-functionalized chitosan (CsAMI). 93

Figure III.7. X-ray patterns of chitosan and maleimide-functionalized chitosan (CsAMI). 94

Figure III.8. TGA (left axis, solid line) and dTGA (right axis, dash line) curves of chitosan and maleimide-functionalized chitosan (CsAMI) under inert atmosphere. 95

Figure III.9. A) Cell proliferation of murine fibroblasts L929 in contact with the CsAMI material as a function of time (the viability data represented were obtained from PrestoBlue[®] at 570 nm), B) viability of L929 murine fibroblast cell line with respect to the negative control at 24 and 48 h and C) adhesion and viability of L929 cells on CsAMI at 3 (A) and 7 (B) days of incubation, where live cells appear in green and dead cells in red (images obtained by confocal microscopy (100x)). 97

Figure III.10. FTIR spectra of A) chitosan and B) thiol-functionalized chitosan (CsSH). 100

Figure III.11. X-ray patterns of chitosan and thiol-functionalized chitosan (CsSH). 101

Figure III.12. TGA (left axis, solid line) and dTGA (right axis, dash line) curves of chitosan and thiolated chitosan (CsSH) under inert atmosphere. 102

- Figure III.13.** Influence of mucin concentration on chitosan and thiolated chitosan as a function of interaction time for: A) 0.50, B) 1.25 and C) 1.50 mg mL⁻¹ mucin concentrations at pH 3. 103
- Figure III.14.** Influence of mucin concentration on chitosan and thiolated chitosan as a function of interaction time for: A) 0.25, B) 0.50, C) 1.25 and D) 1.50 mg mL⁻¹ mucin concentrations at pH 6. 104
- Figure III.15.** A) Cell proliferation of murine fibroblasts L929 in contact with the CsSH material as a function of time (the viability data represented were obtained from PrestoBlue® at 570 nm) and B) viability of L929 murine fibroblast cell line with respect to the negative control at 24 and 48 h. 106
- Figure III.14.** FTIR spectra of A) chitosan and B) tetrazole-functionalized chitosan (CsTZ). 110
- Figure III.15.** Solid-state ¹³C NMR spectra and chemical structure of chitosan and tetrazole-functionalized chitosan (CsTZ). 111
- Figure III.16.** X-ray patterns of chitosan and tetrazole-functionalized chitosan (CsTZ). 112
- Figure III.17.** TGA (left axis, solid line) and dTGA (right axis, dash line) curves of chitosan and tetrazole-functionalized chitosan (CsTZ) under inert atmosphere. 113

CHAPTER IV

- Figure IV.1.** Images of A) complementary precursors mixture in aqueous medium and B) hydrogel formed after 5 h at 65 °C. 130
- Figure IV.2.** UV-vis spectra following the DA reaction of CsFu/CsAMI in HAc at 65 °C. 131
- Figure IV.3.** A) Storage modulus (G' , ●) and loss modulus (G'' , ○) *versus* time at 65 °C and B) frequency sweep at 37 °C of CsFu/CsAMI. 133
- Figure IV.4.** Image of the synthesized final hydrogel and SEM image of the freeze-dried sample. 135
- Figure IV.5.** A) Swelling kinetics of CsFu/CsAMI hydrogel in HCl (●) and PBS (○) media and B) equilibrium swelling ratio of the hydrogel at 37 °C in both aqueous media at 24 h. 136
- Figure IV.6.** Dry weight remaining ratio of native chitosan and CsFu/CsAMI hydrogel in 1 mg mL⁻¹ lysozyme/PBS (filled symbols) and in PBS without lysozyme (empty symbols) at 37 °C as a function of time. 138
- Figure IV.7.** Release profile of Chloramphenicol from CsFu/CsAMI hydrogel in PBS at 37 °C. 139
- Figure IV.8.** A) Absorbance at 570 nm *versus* incubation time of the positive control, negative control and CsFu/CsAMI hydrogel and B) *in vitro* cell viability of the positive control and CsFu/CsAMI hydrogel extract against L929 fibroblasts as a function of incubation time (* $p < 0.05$, *** $p < 0.001$). 142

- Figure IV.9.** UV-vis spectra following the DA reaction of CsFu/BMI 1:1 in HAc at 65 °C. 146
- Figure IV.10.** FTIR spectra A) before and B) after DA reaction of CsFu/BMI 1:1. 147
- Figure IV.11.** A) Storage modulus (G' , ●) and loss modulus (G'' , ○) *versus* time for CsFu/BMI 1:1 at 65 °C and B) frequency sweep of CsFu/BMI hydrogels at 37 °C. 148
- Figure IV.12.** Transition of CsFu/BMI 1:2 hydrogel sample at different progressive stages: A) as-prepared, B) dried at room temperature and C) re-swelled in water. 151
- Figure IV.13.** SEM images of the different hydrogel compositions: CsFu/BMI 1:1 A) as-prepared and after swollen in B) H₂O, C) HCl and D) PBS; CsFu/BMI 1:2 E) as-prepared and after swollen in F) H₂O, G) HCl and H) PBS; CsFu/BMI 1:3 I) as-prepared and after swollen in J) H₂O, K) HCl and L) PBS. 152
- Figure IV.14.** Height and 3D height topographic AFM images of the different hydrogel compositions: A) CsFu/BMI 1:1, B) CsFu/BMI 1:2 and C) CsFu/BMI 1:3. 155
- Figure IV.15.** A) Swelling kinetics of CsFu/BMI hydrogels in HCl (filled symbols, ●) and PBS (empty symbols, ○) media, B) equilibrium swelling ratio of the hydrogels at 37 °C in both aqueous media after 24 h and C) swelling/shrinking pattern of CsFu/BMI 1:2 hydrogel as a function of time at successive cycles at different pHs. 157
- Figure IV.16.** Scheme of the networked structures. 161

Figure IV.17. Release profile of Chloramphenicol from CsFu/BMI hydrogels in PBS at 37 °C. 161

CHAPTER V

Figure V.1. Hydrogel pictures of A) CsSH/BMI 1:2 and B) CsSH/BMI 1:3. 180

Figure V.2. A) Dynamic moduli (G' (●) and G'' (○)) as a function of time at 37 °C and B) frequency sweep of CsSH/BMI hydrogels at 37 °C. 182

Figure V.3. SEM images of the freeze-dried hydrogels: A) CsSH/BMI 1:2 and B) CsSH/BMI 1:3. 185

Figure V.4. A) Swelling kinetics of CsSH/BMI hydrogels in HCl (●) and PBS (○) media and B) equilibrium swelling ratio of the hydrogels at 37 °C in both aqueous media at 48 h. 186

Figure V.5. A) Absorbance at 570 nm *versus* incubation time of the positive control, negative control and CsSH/BMI 1:2 hydrogel and B) *in vitro* cell viability of the positive control and CsSH/BMI 1:2 hydrogel extract against L929 fibroblasts as a function of incubation time. 188

CHAPTER VI

Figure VI.1. Schematic representation of the networked structures and images of A) mixture of chitosan precursors in aqueous medium, B) CsTZ/CsAMI hydrogel formed after 2 h at $\lambda = 320$ nm under daylight and C) CsTZ/CsAMI hydrogel under UV light at $\lambda_{\max} = 365$ nm. 203

- Figure VI.2.** Images under irradiation light at $\lambda_{\max} = 365$ nm and fluorescence emission spectra at an excitation wavelength of 396 nm for: A) CsTZ/CsAMI hydrogels after 1 and 2 hours of irradiation and B) CsTZ and CsAMI precursors after 2 hours of irradiation. 205
- Figure VI.3.** Fluorescence emission spectra at an excitation wavelength of 396 nm for CsTZ/CsAMI hydrogels after being immersed in HCl and PBS for 48 h. 207
- Figure VI.4.** Frequency sweep of CsTZ/CsAMI hydrogels at 37 °C (G' (●) and G'' (○)). 208
- Figure VI.5.** A) Evolution of the viscosity (η) as a function of shear rate ($\dot{\gamma}$) and B) G' (●) and G'' (○) moduli versus shear stress (τ) for CsTZ/CsAMI hydrogels. 211
- Figure VI.6.** Variation of G' (●) and G'' (○) moduli during the continuous step–strain measurement at alternate 0.1 % and 50 % strain (frequency = 1 Hz) versus time for CsTZ/CsAMI hydrogels. 213
- Figure VI.7.** SEM images of the freeze–dried CsTZ/CsAMI hydrogels: A) as–prepared and C) after swollen in H₂O for CsTZ/CsAMI 1:50; B) as–prepared and D) after swollen in H₂O for CsTZ/CsAMI 1:15. 215
- Figure VI.8.** Pore size distribution for A) CsTZ/CsAMI 1:50 hydrogel and B) CsTZ/CsAMI 1:15 hydrogel. 216

Figure VI.9. A) Swelling kinetics of CsTZ/CsAMI hydrogels in HCl (●) and PBS (○) media and B) equilibrium swelling ratio of the hydrogels at 37 °C in both aqueous media at 48 h. 217

Figure VI.10. Dry weight remaining percent of CsTZ/CsAMI hydrogels in 1 mg mL⁻¹ lysozyme/PBS (●) and in PBS without lysozyme (○) at 37 °C as a function of time. 219

Figure VI.11. A) Absorbance at 570 nm *versus* incubation time of the positive control, negative control and CsTZ/CsAMI 1:50 hydrogel and B) *in vitro* cell viability of the positive control and CsTZ/CsAMI 1:50 hydrogel extract against L929 fibroblasts as a function of incubation time (*p < 0.05, ***p < 0.001). 220

CHAPTER VII

Figure VII.1. Schematic representation of a nanoemulsion where a reverse micelle is formed. 230

Figure VII.2. Schematic representation of the experimental procedure for obtaining CsSH/PEGBCOOH nanogels. 235

Figure VII.3. Liquid-state ¹H NMR spectra of thiolated chitosan and CsSH/PEGBCOOH nanogels. 237

Figure VII.4. TGA (left axis, solid line) and dTGA (right axis, dash line) curves of CsSH and CsSH/PEGBCOOH nanogels under inert atmosphere. 239

Figure VII.5. Average hydrodynamic diameter and zeta potential of CsSH/PEGBCOOH nanogels as a function of external pH. 241

- Figure VII.6.** Schematic representation of the variation of the superficial charges of thiolated chitosan nanoparticles depending on the pH. 241
- Figure VII.7.** A) TEM micrograph and B) particle size distribution of CsSH/PEGBCOOH nanogels. 244
- Figure VII.8.** Height topographic AFM images at different scan area (A and B) and C) particle size distribution of CsSH/PEGBCOOH nanogels. 245
- Figure VII.9.** Influence of mucin concentration on thiolated chitosan and CsSH/PEGBCOOH nanogels as a function of interaction time for: A) 0.50, B) 1.25 and C) 1.50 mg mL⁻¹ mucin concentrations at pH 3. 247
- Figure VII.10.** Influence of mucin concentration on thiolated chitosan and CsSH/PEGBCOOH nanogels as a function of interaction time for: A) 0.25, B) 0.50, C) 1.25 and D) 1.50 mg mL⁻¹ mucin concentrations at pH 6. 248
- Figure VII.11.** Schematic representation of the chitosan nanoparticles after the folate receptor incorporation. 251
- Figure VII.12.** UV–vis spectra following the MA reaction between CsSH/PEGBCOOH nanogels and Folate–PEG–Mal in PBS. 252
- Figure VII.13.** FTIR spectra of A) Folate–PEG–Mal, B) thiolated chitosan nanogels (CsSH/PEGBCOOH) and C) folate containing thiolated chitosan nanogels (Folate–CsSH/PEGBCOOH). 254

LIST OF SCHEMES

CHAPTER III

- Scheme III.1.** General representation for the acid activation mechanism prior to the amide coupling cross-linking reaction. 83
- Scheme III.2.** Synthesis of CsFu through the reaction between chitosan and furfural. 84
- Scheme III.3.** AMI synthesis from β -alanine and maleic anhydride. 90
- Scheme III.4.** Synthesis of CsAMI through the reaction between chitosan and AMI modifier. 91
- Scheme III.5.** Synthesis of CsSH through the reaction between chitosan and thiolactic acid. 98
- Scheme III.6.** Synthesis of 4-(2-(4-methoxyphenyl)-2H-tetrazol-5-yl)benzoic acid. 108
- Scheme III.7.** Synthesis of CsTZ through the reaction between chitosan and TBA modifier. 109

CHAPTER IV

- Scheme IV.1.** Diels-Alder reaction between furan and maleimide groups. 128
- Scheme IV.2.** Hydrogel formation through DA reaction between CsFu and CsAMI. 129
- Scheme IV.3.** Bismaleimide synthesis starting from Jeffamine® ED. 143

Scheme IV.4. Hydrogel formation through DA reaction between CsFu and BMI.	144
--	-----

CHAPTER V

Scheme V.1. Thiol–Michael reaction between thiol and maleimide groups.	178
---	-----

Scheme V.2. Hydrogel formation through MA addition reaction between CsSH and BMI.	180
--	-----

CHAPTER VI

Scheme VI.1. NITEC reaction between tetrazole and maleimide groups.	200
--	-----

Scheme VI.2. Hydrogel formation through NITEC reaction between CsTZ and CsAMI.	202
---	-----

CHAPTER VII

Scheme VII.1. Nanogels formation through the cross–linking reaction between CsSH and PEGBCOOH.	234
---	-----

LIST OF TABLES

CHAPTER I

- Table I.1.** Influence of the degree of deacetylation (DDc) and molecular weight (M_w) on the physico-chemical and biological properties of chitosan samples (\uparrow directly proportional to the property; \downarrow inversely proportional to the property). 11
- Table I.2.** Main applications of chitosan as a biomaterial³⁸. 13
- Table I.3.** Schemes of the click chemistry reactions. 24

CHAPTER II

- Table II.1.** Chemical structure of some of the compounds used in this thesis. 51
- Table II.2.** Physico-chemical properties (molecular weight (M_w) and degree of deacetylation (DDc)) of the employed chitosan batches. 54

CHAPTER III

- Table III.1.** Main properties of the synthesized chitosan derivatives. 114

CHAPTER IV

- Table IV.1.** Mean storage and loss moduli and $\tan \delta$ values of cross-linked hydrogels at 37 °C (average \pm standard deviation, $n = 3$). 133

Table IV.2. Structural parameters of CsFu/CsAMI hydrogel based on the rheological frequency sweep analysis (average \pm standard deviation, n = 3).	134
Table IV.3. Swelling parameters of CsFu/CsAMI hydrogel at 37 °C in different aqueous media.	137
Table IV.4. Antibacterial activity of CsFu/CsAMI hydrogel against bacterial test organism.	141
Table IV.5. Composition of the different hydrogel formulations (furan-to-maleimide).	145
Table IV.6. Storage moduli (G') and loss moduli (G'') values of CsFu/BMI hydrogels at 37 °C (average \pm standard deviation, n = 3).	150
Table IV.7. Structural parameters of CsFu/BMI hydrogels based on the rheological frequency sweep analysis (average \pm standard deviation, n = 3).	150
Table IV.8. Topographical parameters of the CsFu/BMI hydrogels.	155
Table IV.9. Swelling parameters of CsFu/BMI at 37 °C in different aqueous media.	158
Table IV.10. Soluble fraction of the CsFu/BMI hydrogels.	160
Table IV.11. Loaded drug mass and cumulative drug release for CsFu/BMI hydrogels.	162

CHAPTER V

Table V.1. Composition of the different hydrogel formulations (thiol-to-maleimide).	180
Table V.2. Mean storage and loss modulus and $\tan \delta$ values of CsSH/BMI hydrogels at 37 °C (average \pm standard deviation, $n = 3$).	182
Table V.3. Structural parameters of CsSH/BMI hydrogels based on the rheological frequency sweep analysis (average \pm standard deviation, $n = 3$).	183
Table V.4. Swelling parameters of CsSH/BMI hydrogels at 37 °C in different aqueous media.	187

CHAPTER VI

Table VI.1. Wavelength values for the fluorescence emission signals of NITEC hydrogels and chitosan derivatives as a function of time.	205
Table VI.2. Wavelength values for the fluorescence emission signals of NITEC hydrogels as a function of solvent.	207
Table VI.3. Mean storage and loss moduli and $\tan \delta$ values of CsTZ/CsAMI hydrogels at 37 °C (average \pm standard deviation, $n = 3$).	208
Table VI.4. Structural parameters of CsTZ/CsAMI hydrogels based on the rheological frequency sweep analysis (average \pm standard deviation, $n = 3$).	209

Table VI.5. Swelling parameters of CsTZ/CsAMI hydrogels at 37 °C in different aqueous media.	218
---	-----

CHAPTER VII

Table VII.1. Hydrodynamic mean diameter (D_H), polydispersity index (PdI) and ζ -potential for CsSH/PEGBCOOH nanogels as a function of pH.	243
---	-----

CHAPTER VIII

Table VIII.1. Main properties of the clicked hydrogels.	268
--	-----

LIST OF ABBREVIATIONS

^1H NMR	Proton nuclear magnetic resonance
^{13}C NMR	Carbon nuclear magnetic resonance
3D	Three-dimensional
AFM	Atomic force microscopy
AMI	Maleimide-based acid
ARES	Advanced Rheometric Expansion System
BMA	Bismaleamic acid
BMI	Bismaleimide
CI^{XRD}	Crystallinity index
ClPh	Chloramphenicol
Cs	Chitosan
CsAMI	Maleimide-functionalized chitosan
CsFu	Furan-functionalized chitosan
CsSH	Thiol-functionalized chitosan
CsTZ	Tetrazole-functionalized chitosan
CuAAC	Cu^{I} -catalysed azide/alkyne cycloaddition
DA	Diels-Alder
DAc	Degree of acetylation
DCM	Dichloromethane
DDc	Degree of deacetylation
DLS	Dynamic light scattering
DMEM	Dulbecco's modified Eagle's medium
DMF	Anhydrous N,N-dimethylformamide

DMSO	Dimethyl sulfoxide
DNA	Deoxyribonucleic acid
DS	Degree of substitution
dTGA	Derivative thermogravimetric curve
ECM	Extracellular matrix
EDC	N-(3-dimethylaminopropyl)-N'-ethylcarbodiimide hydrochloride
EDTA	Ethylenediaminetetraacetic acid
EGDE	Ethylene glycol di-glycidyl ether
Folate-PEG-Mal	Folate-poly(ethylene glycol)-Maleimide
FTIR	Fourier transformed infrared spectroscopy
Fu	Furfural
Gel	Gel fraction
GlcN	D-glucosamine
GlcNAc	N-acetyl-D-glucosamine
HAc	Acetic acid
HDA	Hetero-Diels-Alder
LVR	Linear viscoelastic region
MA	Michael addition
Mal	Maleimide
MD	Modification degree
MWCO	Molecular weight-cutoff
NHS	N-hydroxysuccinimide
NITEC	Nitrile imine-mediated tetrazole-ene cycloaddition
PBS	Phosphate buffer solution

PdI	Polydispersity index
PEC	Polyelectrolyte complexes
PEG	Poly(ethylene glycol)
PEGBCOOH	Poly(ethylene glycol)bis(carboxymethyl)ether
PEO	Poly(ethylene oxide)
PPO	Poly(propylene oxide)
RET	Rubber elastic theory
RNA	Ribonucleic acid
SEM	Scanning electron microscopy
SR	Swelling ratio
Sol	Soluble fraction
SPAAC	Strain-promoted azide/alkyne cycloaddition
TEM	Transmission electron microscopy
TBA	Tetrazole-based acid
TGA	Thermogravimetric analysis
TLA	Thiolactic acid
TPP	Tripolyphosphate
UV	Ultraviolet
UV-vis	Ultraviolet-visible
W/O	Water in oil
XRD	X-ray diffraction

LIST OF SYMBOLS

$\Delta[\text{Abs}]$	Absorbance difference
α	Polymer–solvent constant
A	Area of the NMR signal (proton/carbon)
[Abs]	Absorbance
C	Carbon of the chitosan structure
c	Polymer concentration
D_H	Average hydrodynamic diameter
$\dot{\gamma}$	Shear rate
G'	Storage modulus
G''	Loss modulus
G_e	Plateau value of storage modulus
H	Proton assigned to the carbons of the chitosan structure
I	Maximum intensity of the diffraction peak
K	Polymer–solvent constant
k	Structural and geometrical constant
k_s	Swelling constant rate
λ	Wavelength
M	Amount of ClPh loaded/released
m	Slope
M_c	Average molecular weight between neighbouring cross–links
M_w	Average molecular weight

η	Viscosity
$[\eta]$	Intrinsic viscosity
N_A	Avogadro constant
n	Release exponent
n_c	Cross-linking density
ξ	Average mesh size
θ	Angle of incidence of the X-ray
ρ	Density
R	Gas constant
R_a	Average roughness
R_q	Root mean square roughness
r_o	Swelling rate
τ	Shear stress
T	Temperature
$\tan \delta$	Damping factor
v	Volume fraction to express concentration
ω	Angular frequency
w	Weight fraction to express concentration
W	Weight of the hydrogels
ζ -potential	Zeta potential

